University of Alberta

Fundamentals and Applications of Solvent Effects in Capillary Electrophoresis

by

Kimberly Irene Roy ©

A thesis submitted to the Faculty of Graduate Studies and Research in partial fulfillment of the requirements for the degree of Doctor of Philosophy.

Department of Chemistry

Edmonton, Alberta

Spring 2003

National Library
of Canada

Acquisitions and
Bibliographic Services

395 Wellington Street
Ottawa ON K1A 0N4
Canada

Bibliothèque nationale
du Canada

Acquisisitons et
services bibliographiques

395, rue Wellington
Ottawa ON K1A 0N4
Canada

Your file Votre référence
ISBN: 0-612-82162-5
Our file Notre référence
ISBN: 0-612-82162-5

The author has granted a non-exclusive licence allowing the National Library of Canada to reproduce, loan, distribute or sell copies of this thesis in microform, paper or electronic formats.

The author retains ownership of the copyright in this thesis. Neither the thesis nor substantial extracts from it may be printed or otherwise reproduced without the author's permission.

L'auteur a accordé une licence non exclusive permettant à la Bibliothèque nationale du Canada de reproduire, prêter, distribuer ou vendre des copies de cette thèse sous la forme de microfiche/film, de reproduction sur papier ou sur format électronique.

L'auteur conserve la propriété du droit d'auteur qui protège cette thèse. Ni la thèse ni des extraits substantiels de celle-ci ne doivent être imprimés ou aturement reproduits sans son autorisation.

Canada

University of Alberta

Library Release Form

Name of Author: Kimberly Irene Roy

Title of Thesis: Fundamentals and Applications of Solvent Effects in Capillary Electrophoresis

Degree: Doctor of Philosophy

Year this Degree Granted: 2003

Permission is hereby granted to the University of Alberta Library to reproduce single copies of this thesis and to lend or sell such copies for private, scholarly or scientific research purposes only.

The author reserves all other publication and other rights in association with the copyright in the thesis, and except as herein before provided, neither the thesis nor any substantial portion thereof may be printed or otherwise reproduced in any material form whatever without the author's prior written permission.

7409 172nd Street
Edmonton, Alberta
T5T 2P7
CANADA

Jan. 20, 2003
Date

University of Alberta

Faculty of Graduate Studies and Research

The undersigned certify that they have read, and recommend to the Faculty of Graduate Studies and Research for acceptance, a thesis entitled "Fundamentals and Applications of Solvent Effects in Capillary Electrophoresis" submitted by Kimberly Irene Roy in partial fulfillment of the requirements for the degree of Doctor of Philosophy.

Supervisor, Dr. Charles Lucy, Dept. of Chemistry

Fred Cantwell

Dr. Frederick Cantwell, Dept. of Chemistry

Dr. Liang Li, Dept. of Chemistry

Dr. Jacob Masliyah, Dept. of Chemical & Materials Engineering

Dr. Pierre-Nicholas Roy, Dept. of Chemistry

External Examiner, Dr. Edgar Arriaga, Dept. of Chemistry, University of Minnesota

Jan 16/03

Date

This thesis is dedicated to my husband and family.

ABSTRACT

Capillary electrophoresis (CE) is a separation technique in which charged molecules are separated from one another in an electric field. The use of organic solvents in CE offers different separation characteristics compared to purely aqueous media. However, the mechanism responsible for solvent-induced selectivity changes was not well understood. The most commonly used mobility model, the Hückel equation, does not predict the different separation characteristics observed in organic or aqueous-organic media. This model only considers the viscous drag, or hydrodynamic friction, experienced by an ion.

This thesis demonstrates that a theoretical mobility model accounting for charge-induced friction can explain solvent-induced selectivity changes in CE. The Hubbard-Onsager *dielectric friction* model successfully predicts the mobility behavior of organic anions and cations in methanol-water, acetonitrile-water, ethanol-water and 2-propanol-water media. As predicted by this model, the changes in ion mobility correlate with the corresponding changes in solvent viscosity (η), dielectric constant (ε) and dielectric relaxation time (τ). Dielectric friction is thus used to explain the solvent-induced selectivity changes observed herein and elsewhere. This is the first report showing the importance of solvent τ on mobility in CE.

Despite its success in aqueous-organic media, the Hubbard-Onsager model does not explain mobility behavior in nonaqueous methanol-acetonitrile media. This is explained by the continuum nature of the model, whereby the different ion-solvent interactions in acetonitrile and methanol are not taken into account. Further, no evidence is seen for temperature-induced selectivity changes resulting from dielectric friction.

Consistent with a theoretical model, the ionic strength effects generally vary with ion charge (z), solvent content and temperature as a function of $z/\eta\varepsilon^{1/2}$. Departures from this trend in nonaqeuous media are attributed to ion association.

Finally, in an alternate project, polyamines are derivatized with 1-pyrenebutanoic acid succinimidyl ester (PSE) and analyzed using micellar electrokinetic chromatography with laser-induced fluorescence detection. This derivatization allows for sensitive and selective detection of the polyamines. Detection limits for PSE-labeled putrescine, cadaverine, spermidine and spermine are 2, 2, 4 and 5 nM, respectively.

ACKNOWLEDGEMENTS

I would like to thank my supervisor, Dr. Charles Lucy, for his guidance, encouragement and support throughout the past two and a half years. Thank you for your kind advice when Dr. Norm Dovichi announced his move to Seattle, and for welcoming me into your group when I made the difficult decision to remain at the University of Alberta. Dr. Dovichi's support and guidance during my first two years in graduate school are also greatly appreciated.

Past and present members of the Lucy group are gratefully acknowledged for their helpful ideas, discussions and friendship. In particular I would like to thank Richard Paproski, whose competence in the lab made my 4-month role as supervisor enjoyable. Also, many members of the chemistry department have provided me with support during my graduate career. Especial thanks are extended to Dr. Rik Tykwinski and Trent Rankin for the synthesis of one of my analytes.

Drs. Fred Cantwell, Liang Li, Pierre-Nicholas Roy, Jacob Masliyah and Edgar Arriaga are greatfully acknowledged for their comments and critique of this thesis.

Financial support for this research was provided by the Natural Sciences and Engineering Research Council of Canada (NSERC) and the University of Alberta. I would like to thank NSERC for a postgraduate scholarship, and the American Chemical Society Division of Analytical Chemistry for a graduate fellowship sponsored by DuPont.

I am grateful to my parents and brother for their continued enthusiasm and support. Warm thanks are also expressed to my husband Brent, who quit his job in Montreal to move to Edmonton with me. Your love and encouragement have helped me overcome all obstacles. Thank you for your unconditional support.

TABLE OF CONTENTS

CHAPTER ONE. Introduction

1.1 History of Capillary Electrophoresis (CE)....1

1.2 Principles of Capillary Electrophoresis....2
  1.2.1 Instrumentation....2
  1.2.2 Electrophoretic Mobility....3
  1.2.3 Electroosmotic Flow (EOF)....5
  1.2.4 Modes of Capillary Electrophoresis....7
    1.2.4.1 Capillary Zone Electrophoresis (CZE)....8
    1.2.4.2 Micellar Electrokinetic Chromatography (MEKC)....9
  1.2.5 Detection....13
    1.2.5.1 Absorbance Detection....13
    1.2.5.2 Fluorescence Detection....14
    1.2.5.3 Sample Stacking....16

1.3 Factors Affecting Migration in CE....18
  1.3.1 Buffer pH....18
  1.3.2 Buffer Ionic Strength....19
  1.3.3 Organic Solvents....20
  1.3.4 Temperature....21
  1.3.5 Other Buffer Additives....21

1.4 Thesis Overview....22

1.5 References....23

CHAPTER TWO. Selective Fluorometric Detection of Polyamines Using Micellar Electrokinetic Chromatography with Laser-Induced Fluorescence Detection

2.1 Introduction....27

2.2 Preliminary Work....32
  2.2.1 Capillary Electrophoresis System....32
  2.2.2 Derivatization Procedure with FQ....33
  2.2.3 Separation of FQ-Labeled Polyamines by MEKC....34
  2.2.4 Analysis of Real Samples....36
  2.2.5 Motivation for an Improved Method for Polyamine Analysis....40

2.3 Experimental....41
  2.3.1 Apparatus....41
  2.3.2 Chemicals....41
  2.3.3 Derivatization Procedure with PSE....42
  2.3.4 Capillary Electrophoresis....43

2.4 Results and Discussion 44
  2.4.1 Separation of PSE-Labeled Polyamines by MEKC 44
  2.4.2 Characterization of Labeled Polyamines 46
  2.4.3 Precision and Limits of Detection 51
  2.4.4 Selectivity of the Method 53

2.5 Concluding Remarks 54

2.6 References 55

CHAPTER THREE. Theory of Ion Mobility

3.1 Introduction 60

3.2 Models Accounting for Hydrodynamic Friction 60
  3.2.1 Hückel Model 60
  3.2.2 Perrin's and Elworthy's Shape Models 64
  3.2.3 Gurney-Frank-Wen Model 66

3.3 Empirical and Semi-Empirical Models 68
  3.3.1 Mobility Prediction in Aqueous Media 69
  3.3.2 Mobility Prediction in Aqueous-Organic Media 74

3.4 Models Accounting for Charge-Induced Friction 78
  3.4.1 What is Charge-Induced Friction? 78
  3.4.2 Solvent-Berg Model 79
  3.4.3 Dielectric Friction Model 81
    3.4.3.1 Theory of Dielectric Friction 81
    3.4.3.2 Continuum Dielectric Friction Models 82
      3.4.3.2.1 The Evolution of Continuum Dielectric Friction Models 83
      3.4.3.2.2 Hubbard-Onsager Dielectric Friction Model 86
      3.4.3.2.3 Other Advances in Continuum Dielectric Friction Models 91
      3.4.3.2.4 Limitations of the Continuum Models 93
    3.4.3.3 Molecular Dielectric Friction Models 94
    3.4.3.4 Why Choose Continuum Models Over Molecular Models? 98

3.5 Effects of Ionic Strength on Mobility 98
  3.5.1 The Debye-Hückel Ionic Cloud Model of Ion-Ion Interactions 99
  3.5.2 The Debye-Hückel-Onsager Equation 101
  3.5.3 Empirical and Semi-Empirical Expressions 104
  3.5.4 Pitts' Equation 105
    3.5.4.1 Extension of the Pitts Treatment to Mobility Prediction in CE 107

3.6 Summary 108

3.7 References 108

CHAPTER FOUR. Dielectric Friction in Capillary Electrophoresis: Mobility of Organic Anions and Cations in Mixed Methanol-Water Media

4.1 Introduction 115

4.2 Experimental 117
  4.2.1 Apparatus 117
  4.2.2 Chemicals 118
  4.2.3 Determination of Absolute Mobilities 120
  4.2.4 Measurement of Relative Viscosity 123

4.3 Results and Discussion 124
  4.3.1 Ionic Strength Effects 124
    4.3.1.1 Influence of Analyte Charge on Ionic Strength Effect 130
    4.3.1.2 Dominance of the Electrophoretic Term in the Onsager Slope 133
    4.3.1.3 Variations in Onsager Slope for Ions of Similar Charge: The Importance of the Relaxation Effect 136
  4.3.2 Dielectric Friction 137
  4.3.3 Correlation Between Mobility and Solvent Parameters 142
  4.3.4 Comparison of Dielectric Friction Effects for Cations and Anions 145

4.4 Concluding Remarks 147

4.5 References 148

CHAPTER FIVE. Mobility of Anions in Aqueous-Organic Media Containing Acetonitrile, Ethanol and 2-Propanol

5.1 Introduction 153

5.2 Experimental 155
  5.2.1 Apparatus 155
  5.2.2 Chemicals 155
  5.2.3 Determination of Absolute Mobilities 156
  5.2.4 Measurement of Relative Viscosity 157

5.3 Results and Discussion 157
  5.3.1 Ionic Strength Effects 157
    5.3.1.1 Influence of Analyte Charge on Ionic Strength Effect 158
    5.3.1.2 Influence of Solvent Composition and Type on Ionic Strength Effects 165

5.3.2 Dielectric Friction 169
5.3.3 Correlation Between Mobility and Solvent Parameters....174
5.3.4 Influence of Solvent Type on Dielectric Friction 177

5.4 Concluding Remarks....182

5.5 References....183

CHAPTER SIX. Nonaqueous Capillary Electrophoresis

6.1 Introduction....187

6.2 Experimental....189
6.2.1 Apparatus 189
6.2.2 Chemicals....190
6.2.3 Determination of Absolute Mobilities 191
6.2.4 Measurement of Relative Viscosity 192

6.3 Results and Discussion 192
6.3.1 Ionic Strength Effects 192
6.3.1.1 Influence of Analyte Charge on Ionic Strength Effect 196
6.3.1.2 Variations in Onsager Slope for Monocharged Ammonium Ions....198
6.3.1.3 Correlation Between Onsager Slope and $z/\eta\varepsilon^{1/2}$ 201
6.3.2 Dielectric Friction 203
6.3.3 Correlation Between Mobility and Solvent Parameters....207
6.3.4 Comparison of Cation Mobilities in 100% MeOH and MeOH/H_2O Media 208

6.4 Concluding Remarks....211

6.5 References....212

CHAPTER SEVEN. The Influence of Temperature on Selectivity in Capillary Electrophoresis

7.1 Introduction....216

7.2 Experimental....218
7.2.1 Apparatus 218
7.2.2 Chemicals....218
7.2.3 Determination of Mobility 220

7.3 Results and Discussion 221
7.3.1 Ionic Strength Effects 221
7.3.2 Influence of Dielectric Friction....226

7.4 Concluding Remarks....231

7.5 References....231

CHAPTER EIGHT. Conclusions and Future Work

8.1 Conclusions....234

8.2 Future Work....237
    8.2.1 Measurement of Conductivity Spectra....237
    8.2.2 Determination of Peptide Charge by Ionic Strength Effects....238
    8.2.3 Ion-Ion and Ion-Solvent Interactions....240

8.3 References....243

LIST OF TABLES

Table 3.1: Dependence of the Empirical Correction Factor *n* on the van der Waals Radii (r_w), as Determined by Edward from the Solid Curve in Figure 3.5.....70

Table 3.2: Hydration Numbers in Pure Water for Simple Ions Obtained by Different Methods.....81

Table 4.1: Effect of Buffer Methanol Content on Solvent Parameters.....116

Table 4.2: pK_a Values for the Analyte Anions and Cations.....119

Table 4.3: Ionic Strength Effects on the Mobility of Anions in MeOH/H_2O Media.....126

Table 4.4: Ionic Strength Effects on the Mobility of Cations in MeOH/H_2O Media.....128

Table 4.5: Correlation Between the Cation Mobilities Measured on Coated and Uncoated Capillaries.....129

Table 4.6: Ionic Strength Effects on the Mobility of Phthalate Isomers.....130

Table 4.7: Regression Data for the Plots of $1/\mu_o\eta$ versus $\tau/\varepsilon\eta$ (Figure 4.5) Constructed for the Anions and Cations in Methanol-Water Media.....144

Table 5.1: Effect of Buffer Organic Solvent Content on Solvent Parameters.....154

Table 5.2: Ionic Strength Effects on the Mobility of Anions in ACN/H_2O, EtOH/H_2O and 2-PrOH/H_2O Media.....162

Table 5.3: Regression Data for the Plots of $1/\mu_o\eta$ versus $\tau/\varepsilon\eta$ (Figure 5.8) Constructed for the Anions in Acetonitrile-Water, Ethanol-Water and 2-Propanol-Water Media.....176

Table 6.1: Variation of Solvent Parameters with MeOH/ACN Content.....188

Table 6.2: Ionic Strength Effects on the Mobility of Cations in Nonaqueous Media.....195

Table 6.3: Correlation Coefficients (R^2) for the Plot of Onsager Slope versus $1/\eta\varepsilon^{1/2}$ (Figure 6.3b) Constructed for the Cations in Methanol-Acetonitrile Media.....203

Table 6.4: Regression Data for the Plots of $1/\mu_o\eta$ versus $\tau/\varepsilon\eta$ (Figure 6.8) Constructed for the Cations in Media Consisting of 0-100% Methanol in Water.....210

Table 7.1: Effect of Buffer Temperature on Solvent Parameters.....217

Table 7.2: Ionic Strength Effects as a Function of Temperature.....223

LIST OF FIGURES

Figure 1.1: Schematic of a capillary electrophoresis system 3

Figure 1.2: Schematic illustration of the electric double layer and the potential variation with the distance from the capillary wall, according to the Gouy-Chapman model refined by Stern and Grahame 6

Figure 1.3: Illustration of the flat profile of the electroosmotic flow 7

Figure 1.4: Illustration of A) a CZE separation inside a capillary and B) the resulting electropherogram 9

Figure 1.5: Structure of sodium cholate 10

Figure 1.6: Illustration of A) an MEKC separation of neutral analytes in a capillary using sodium cholate as surfactant, and B) the resulting electropherogram 11

Figure 1.7: Partial energy diagram for a fluorescence system 14

Figure 1.8: Schematic of a sheath flow cuvette 16

Figure 1.9: A) Conventional field-amplified stacking for ionic solutes in CZE. B) High-salt stacking for neutral analytes in MEKC 17

Figure 2.1: Reaction scheme for the derivatization of polyamines with PSE 31

Figure 2.2: Reaction scheme for the derivatization of primary amines with FQ 32

Figure 2.3: Separation of FQ-labeled Put, Cad and Spd 35

Figure 2.4: Separation by MEKC of a rat brain microdialysate sample derivatized with FQ 37

Figure 2.5: Separation by MEKC of a rat liver homogenate sample derivatized with FQ 38

Figure 2.6: Optimization of the separation of PSE-labeled Put and Cad 45

Figure 2.7: Separation of PSE-labeled Put, Cad, Spd and Spm in under 10 min 47

Figure 2.8: Variation in the intensities of the PSE-labeled Spm peaks (peaks 1-5) as a function of PSE concentration 48

Figure 2.9: Pictorial representation of the difference between *inter*molecular and *intra*molecular excimer formation 49

Figure 2.10: Comparison of the fluorescence profiles of PSE-labeled Spm at 400 nm and 490 nm 50

Figure 2.11: Improvement of the method's sensitivity for Spd and Spm by sample stacking 53

Figure 2.12: Illustration of the selectivity of the method towards polyamines 54

Figure 3.1: Plot of Walden product ($\lambda_o\eta$) versus reciprocal radius ($1/r$) for alkali metal, halide and tetraalkylammonium ions in water at 25°C 62

Figure 3.2: Inability of the Hückel equation to predict solvent- and temperature-induced selectivity changes....................63

Figure 3.3: Illustration of an ellipsoid showing the different semi-axes 65

Figure 3.4: The different solvent regions surrounding an ion, according to the Gurney-Frank-Wen model....................66

Figure 3.5: Empirical constants of *n* in the Stokes-Einstein equation (eqn 3.8), as determined by Edwards....................70

Figure 3.6: Pictorial representation of a solvent-berg....................80

Figure 3.7: Pictorial representation of the retarding force (dielectric friction) experienced by an ion due to the non-instantaneous relaxation of solvent dipoles 82

Figure 3.8: Agreement between the revised Zwanzig model (eqn 3.24) and the experimental Walden products, in methanol at 298 K....................86

Figure 3.9: Agreement between the Hubbard-Onsager model (eqn 3.25) and the experimental Walden products, in methanol at 298 K....................88

Figure 3.10: Agreement between the Wolynes model (eqn 3.31) and experimental data, in methanol at 298 K 96

Figure 3.11: Illustration of the excellent agreement between experimental data and the molecular model developed by Bagchi and coworkers, in methanol at 298 K....................97

Figure 3.12: Debye-Hückel ionic cloud model of ion-ion interactions 99

Figure 3.13: The asymmetrical egg-shaped ionic cloud around a moving ion....................102

Figure 4.1: Ionic strength effects on the mobilities of organic anions for buffers containing A) 0% MeOH, B) 30% MeOH, C) 60% MeOH and D) 75% MeOH 125

Figure 4.2: Ionic strength effects on the mobilities of organic cations for buffers containing A) 0% MeOH, B) 30% MeOH, C) 60% MeOH and D) 75% v/v MeOH 127

Figure 4.3: Dependence of Onsager slope on the electrophoretic effect for A) anions and B) cations in methanol-water media 135

Figure 4.4: Dependence of the Walden product on the methanol content of the buffer for A) anions and B) cations 138

Figure 4.5: Correlation between change in ion mobility and solvent τ, ε and η for A) anions and B) cations in methanol-water media, according to the Hubbard-Onsager equation (eqn 3.27)....143

Figure 4.6: Comparison of dielectric friction effects experienced by cations and anions in methanol-water media....146

Figure 5.1: Ionic strength effects on the mobilities of organic anions for buffers containing A) 0% ACN, B) 30% ACN, C) 60% ACN and D) 75% ACN....159

Figure 5.2: Ionic strength effects on the mobilities of organic anions for buffers containing A) 0% EtOH, B) 30% EtOH, C) 60% EtOH and D) 75% EtOH....160

Figure 5.3: Ionic strength effects on the mobilities of organic anions for buffers containing A) 0% 2-PrOH, B) 30% 2-PrOH, C) 60% 2-PrOH and D) 75% 2-PrOH....161

Figure 5.4: Dependence of Onsager slope on the electrophoretic effect for anions in A) ACN/H_2O, B) EtOH/H_2O and C) 2-PrOH/H_2O media....166

Figure 5.5: Ionic strength effects on 1,3,(6 or 7)-naphthalenetrisulfonate in media containing A) 30% and B) 75% organic solvent, as a function of organic modifier....167

Figure 5.6: Correlation plot showing the influence of solvent content and type on the ionic strength effects for the –1, –2 and –3 sulfonates....168

Figure 5.7: Dependence of Walden product on the organic content of the buffer for A) ACN, B) EtOH and C) 2-PrOH....170

Figure 5.8: Correlation between change in ion mobility and solvent τ, ε and η for aqueous-organic media containing A) ACN, B) EtOH and C) 2-PrOH....175

Figure 5.9: Influence of solvent type on the dielectric friction experienced by A) the –2 sulfonate and B) the –3 sulfonate....178

Figure 6.1: Ionic strength effects on the mobilities of organic cations differing in charge for nonaqueous buffers containing A) 100% MeOH, B) 25% (v/v) ACN in MeOH, C) 50% (v/v) ACN in MeOH, D) 75% (v/v) ACN in MeOH, and E) 100% ACN....193

Figure 6.2: Ionic strength effects on the mobilities of singly-charged organic cations for nonaqueous buffers containing A) 100% MeOH, B) 25% (v/v) ACN in MeOH, C) 50% (v/v) ACN in MeOH, D) 75% (v/v) ACN in MeOH, and E) 100% ACN....194

Figure 6.3: Dependence of the Onsager slope on the electrophoretic effect for cations in methanol-acetonitrile media. A) All analytes are considered together. B) Each analyte is considered individually....202

Figure 6.4: Dependence of the Walden product on the MeOH/ACN content of the buffer 205

Figure 6.5: Dependence of Walden product on the MeOH/ACN content of the buffer for a series of anilinium ions, as determined by Kenndler and coworkers 207

Figure 6.6: Correlation between change in cation mobility and solvent τ, ε and η in methanol-acetonitrile media 208

Figure 6.7: Variation in the Walden products of cations in media consisting of 0-100% (v/v) methanol........ 209

Figure 6.8: Correlation between change in cation mobility and solvent τ, ε and η for media conisting of 0-100% methanol in water........ 210

Figure 7.1: Influence of temperature on ionic strength effects for A) 1,3,(6 or 7)-naphthalenetrisulfonate and B) 1,2,4,5-benzenetetracarboxylate 222

Figure 7.2: Dependence of Onsager slope on temperature, viscosity and dielectric constant 224

Figure 7.3: Influence of temperature on the ionic strength (I_c) at which migration order reversal occurs between the –3 and –4 ions 225

Figure 7.4: Walden plots as a function of temperature using A) literature viscosities (Table 7.1) and B) measured viscosities 227

Figure 7.5: Correlation between absolute mobility and viscosity according to the Hückel equation 230

LIST OF SYMBOLS AND ABBREVIATIONS

Symbol	**Parameter**
ω	circular frequency of electric field (s^{-1})
$\langle (F^{S})^{2} \rangle$	mean squared fluctuation in the soft long-range attractive force acting on the ion
Ψ_d	potential at the outer Helmholtz plane (V)
Φ_F	quantum efficiency
Ψ_o	potential at the capillary wall (V)
A	absorbance (absorbance units, AU)
a	ion size parameter (Å)
a_{H+}	hydrogen ion activity (mol/L)
b	optical path length (cm)
B	solvent-dependent constant in the Pitts' equation ($L^{1/2}Å^{-1}mol^{-1/2}$)
c	molar concentration (mol/L)
C_{H3BO3}	initial added concentration of boric acid (mol/L)
D^{o}	diffusion coefficient (cm^2/s)
E	electric field (V/cm)
e	elementary charge (1.602×10^{-19} Coul)
F	power of fluorescent radiation (arbitrary fluorescence units)
$F(\theta,\phi)$	elliptic integral of the first kind
f_b	hydrodynamic friction coefficient of solute backbone ($Coul\cdot V\cdot s/cm^2$)
f_c	volume fraction of organic modifier
F_{CI}	charge-induced friction term approximated by pK_a, pK_b or z^2/volume
f_d	dielectric (charge-induced) friction coefficient of an ion ($Coul\cdot V\cdot s/cm^2$)
F_E	electric force ($Coul\cdot V/cm$)
F_F	frictional drag force ($Coul\cdot V/cm$)
f_h	hydrodynamic friction coefficient of an ion ($Coul\cdot V\cdot s/cm^2$)
$f_{h,o}$	frictional coefficient of an idealized spherical molecule ($Coul\cdot V\cdot s/cm^2$)
f_{HH}	friction coefficient due to the hard collisions of solvent molecules with the reference ion ($Coul\cdot V\cdot s/cm^2$)

$f_{\mathrm{HH}}, f_{\mathrm{SS}}$	cross terms resulting from the reciprocal effect of the soft force on the hard force, and vice versa (Coul·V·s/cm^2)
F_{R}	random force exerted on an ion by the solvent molecules (N)
f_{SS}	friction coefficient due to the weak long-range attractive force between the reference ion and the solvent molecules (Coul·V·s/cm^2)
f_{t}	total friction coefficient of an ion (Coul·V·s/cm^2)
f_{w}	volume fraction of water
g	electrolyte parameter
H	McGowan waters of hydration increments
I	ionic strength (mol/L)
I_{C}	ionic strength at which two Onsager slopes intersect (mol/L)
k	constant in Grossman's model
k'	retention factor
K_{a}	acid dissociation constant
K_{A}	ion association constant
k_{B}	Boltzmann's constant (1.381×10^{-23} JK^{-1})
L_{d}	length of the capillary to the detector (cm)
L_{t}	total capillary length (cm)
m	slope of linear calibration curve (signal·L/mol)
M	molecular mass (g/mol)
M_{c}	molecular weight of organic modifier (g/mol)
M_{w}	molecular weight of water (g/mol)
n	constant in the Hückel equation
n_a	number of amino acids in a peptide chain
N_{A}	Avogadro's number (6.022×10^{23} mol^{-1})
n_{o}	number of identical moieties attached to solute backbone
P	radiation power after having passed through the sample
P_{o}	incident radiation power
q	ion charge (Coul)
r	radius of ion (m)

r_∞	hydrodynamic ion radius in a solvent of infinite dielectric constant (m)
r_i	inertial radius (m)
r_rot	rotational radius (m)
r_s	ion radius calculated from Stokes' law (m)
r_w	van der Waals' radius (m)
S_b	standard deviation of the baseline (signal)
T	temperature (K)
T_R	transmittance
t_A	migration time of the analyte (s)
t_d	delay time (s)
t_eof	migration time of electroosmotic flow (s)
t_inj	injection time (s)
t_m	migration time (s)
t_mc	migration time of the micelle (s)
t_migr	time for which the run potential is applied (s)
t_N1	migration time of the first EOF marker (s)
t_N3	migration time of the second EOF marker (s)
$t_\mathrm{ramp\text{-}down}$	time for the voltage to decrease from V to 0 kV (s)
$t_\mathrm{ramp\text{-}up}$	time for the voltage to increase from 0 kV to V (s)
v	ion velocity (cm/s)
V	applied voltage (V)
V_o	solute volume (m^3)
y	activity coefficient
$y_\pm$	mean activity coefficient
z	charge number of ion
z_-	anion integer charge
z_+	cation integer charge
$Z_{x=0}$	charge of the native protein
Δ	desolvation function
ΔZ_n	charge difference between native protein and protein with x derivatives

α	solvatochromic parameter for solvent or solute hydrogen bond donor acidity
α_i, i=0,1,2	fraction of acid dissocation
α_{IP}	degree of dissociation of ion pair
β	solvatochromic parameter for solvent or solute hydrogen bond acceptor basicity
$\delta f^{\neq}$	friction coefficient due to the charge of each moiety
δf_o	hydrodynamic friction coefficient for an uncharged moiety
ε	static (low frequency) dielectric constant of solvent
ε'	molar absorptivity ($L \cdot mol^{-1} \cdot cm^{-1}$)
ε_∞	high frequency dielectric constant of solvent
η	solvent viscosity (P)
η_{eff}	local viscosity in the first solvation shell of the ion (P)
η_R	rotational viscosity (P)
κ^{-1}	Debye-Hückel length (Å)
λ	effective ion conductivity ($cm^2\Omega^{-1}mol^{-1}$)
λ_-	effective anion conductivity ($cm^2\Omega^{-1}mol^{-1}$)
$\lambda_{-,o}$	absolute anion conductivity ($cm^2\Omega^{-1}mol^{-1}$)
λ_+	effective cation conductivity ($cm^2\Omega^{-1}mol^{-1}$)
$\lambda_{+,o}$	absolute cation conductivity ($cm^2\Omega^{-1}mol^{-1}$)
λ_o	absolute ion conductivity ($cm^2\Omega^{-1}mol^{-1}$)
μ	electrophoretic mobility (cm^2/Vs)
μ'	apparent mobility in the presence of ion association effects (cm^2/Vs)
μ_-	effective anion mobility (cm^2/Vs)
$\mu_{-,o}$	absolute anion mobility (cm^2/Vs)
μ_+	effective cation mobility (cm^2/Vs)
$\mu_{+,o}$	absolute cation mobility (cm^2/Vs)
μ_a	apparent mobility (cm^2/Vs)
μ_c	mobility in organic modifier (cm^2/Vs)
μ_e	effective ion mobility (cm^2/Vs)

μ_{eof}	electroosmotic mobility (cm^2/Vs)
μ_o	absolute ion mobility (cm^2/Vs)
μ_w	mobility in water (cm^2/Vs)
μ_x	mobility of protein with *x* derivatives (cm^2/Vs)
$\mu_{x=0}$	mobility of protein with 0 derivatives (cm^2/Vs)
π^*	solvatochromic parameter for solvent or solute dipolarity.polarizability
ρ	bulk solvent density (g/cm^3)
ρ_{loc}	local density in the first solvation shell of the ion (g/cm^3)
τ	solvent dielectric relaxation time (s)
τ_F	characteristic relaxation time of the long-range attractive force between the reference ion and the solvent molecules (s)
ζ	zeta potential (potential at plane of shear) (V)
2-PrOH	isopropanol (2-propanol)
AccQ	6-aminoquinolyl-N-hydroxysuccinimidyl carbamate
ACN	acetonitrile
Ala	alanine
Cad	cadaverine
CE	capillary electrophoresis
CEC	capillary electrochromatography
CGE	capillary gel electrophoresis
CIEF	capillary isoelectric focussing
CITP	capillary isotachophoresis
cmc	critical micelle concentration
CZE	capillary zone electrophoresis
DMSO	dimethyl sulfoxide
ELISA	competitive enzyme-linked immunosorbent assay
EOF	electroosmotic flow
EtOH	ethanol
FITC	fluorescein isothiocyanate
FQ	5-furoylquinoline-3-carboxaldehyde

Glu	glutamine
HPLC	high performance liquid chromatography
HQS	8-hydroxyquinoline-5-sulfonic acid
IHP	inner Helmholtz plane
LIF	laser-induced fluorescence
LOD	limit of detection
MEKC	micellar electrokinetic chromatography
MeOH	methanol
MS	mass spectrometry
NDA	naphthalene-2,3-dicarboxaldehyde
OHP	outer Helmholtz plane
OPA	*o*-phthalaldehyde
PEO	polyethylene oxide
PSE	1-pyrenebutanoic acid succinimidyl ester
PTFE	polytetrafluoroethylene
Put	putrescine
RSD	relative standard deviation
SDS	sodium dodecyl sulfate
SPC/E	simple point charge model
Spd	spermidine
Spm	spermine
Taur	taurine
TDR	time domain reflectometry
THF	tetrahydrofuran
UV	ultraviolet

CHAPTER ONE. Introduction

Capillary electrophoresis (CE) is a relatively new separation technique. As it matures, a more fundamental understanding of the parameters affecting analyte migration is essential. Indeed, before the full potential of the technique can be exploited, insight must be gained into what variables affect mobility, and how they interrelate with one another to govern the overall ion mobility. The primary objective of this thesis is to investigate the mechanisms governing analyte migration in CE. Chapter 3 is entirely devoted to a discussion of the fundamentals of ion mobility. Here, the basic fundamentals of CE will be introduced.

1.1 History of Capillary Electrophoresis (CE)

Electrophoresis is the differential migration of charged species in an electric field. It's first use as a separation technique dates back to 1937, when Tiselius [1] separated proteins under an electric field in free solution. For his pioneering work in separation science, Tiselius was awarded the Nobel Prize in chemistry in 1948. Unfortunately, these initial electrophoresis studies in free solution were limited by convective mixing. For this reason, electrophoresis has typically been performed in non-convective media, such as agarose and polyacrylamide gels. Polyacrylamide gel electrophoresis (PAGE), first introduced by Raymond and Weintraub [2], has become a widely used separation technique for biological macromolecules. However, because of the viscous media and the low applied voltages, slab gel electrophoresis generally suffers from long analysis times and low efficiencies.

An alternate solution to using non-convective gels is to use narrow-bore capillaries. The most significant advantage of using capillaries in electrophoresis is that their large surface area-to-volume ratios allow efficient dissipation of the electrically-generated heat (Joule heat). This reduces band broadening arising from thermal convective mixing. Consequently, high electric field strengths can be applied, resulting in short analysis times and high efficiencies. The first demonstration of capillary electrophoresis came in 1967, when Hjertén [3] separated small inorganic anions and macromolecules in 3-mm capillary tubes. These capillaries were rotated along their longitudinal axes to minimize convective mixing. In 1981, Jorgenson and Lukacs [4] reported high separation efficiencies by using high field strengths in narrow 75-μm I.D. capillaries. This report is generally accepted as the first real demonstration of the power of capillary electrophoresis. In the two decades since, capillary electrophoresis has continued to grow as a separation technique and has been proven useful for a wide variety of applications.

1.2 Principles of Capillary Electrophoresis

1.2.1 Instrumentation

A schematic of a capillary electrophoresis system is shown in Figure 1.1. Polyimide-coated fused silica capillaries with inner diameters of 10-100 μm and lengths of 20-100 cm are typically used. To perform a CE separation, the inlet and outlet ends of the capillary are placed in buffer reservoirs, and the capillary is filled with the electrolyte solution by applying an external pressure. The inlet buffer reservoir is then replaced by a sample reservoir, and a sample plug (1-10 nL) is injected either electrokinetically (with

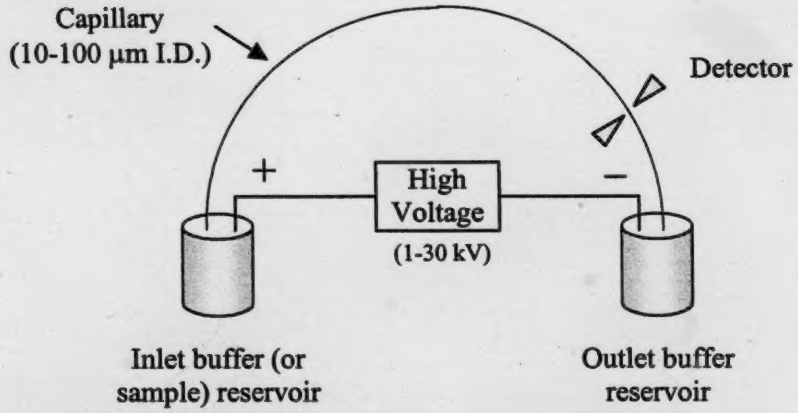
Capillary
(10-100 μm I.D.)
Detector
+
High
Voltage
(1-30 kV)
−
Inlet buffer (or
sample) reservoir
Outlet buffer
reservoir

Figure 1.1: Schematic of a capillary electrophoresis system.

voltage) or hydrodynamically (with pressure) onto the end of the capillary. The inlet buffer reservoir is then reintroduced, and separation is initiated by applying a voltage (1-30 kV). The high voltage power supply is connected to the buffer reservoirs via platinum electrodes. Under the applied electric field, the analytes migrate towards the detector according to their charge-to-size ratios. Detection is performed either on-column (Figure 1.1) or post-column; the former method requires that a section of polyimide coating be removed to create a detection window. The detector output is then sent to a computer for processing.

1.2.2 Electrophoretic Mobility

An ion migrating in the presence of an electric field (E) experiences two opposing forces [5]: an electric force (F_E) and a frictional drag force (F_F). These forces are defined by:

$$F_E = qE \tag{1.1}$$

and

$$F_F = f_t v \tag{1.2}$$

where q is the ion charge, f_t is the total frictional drag coefficient, and v is the ion's velocity. During electrophoresis, the electric force and the frictional drag force are exactly counter-balanced, resulting in a steady ion migration velocity. By equating eqns 1.1 and 1.2, the steady-state ion velocity can be expressed as:

$$v = \frac{qE}{f_t} \tag{1.3}$$

The electrophoretic mobility of an ion (μ) is defined as the ion velocity per unit field strength, and is therefore given by:

$$\mu = \frac{v}{E} = \frac{q}{f_t} \tag{1.4}$$

The mobility of an ion is therefore proportional to its charge and inversely proportional to its friction coefficient. Using Stokes' hydrodynamic friction coefficient (f_h) for a spherical particle with radius r moving through a medium of viscosity η, the expression for mobility can be rewritten in the following form:

$$\mu = \frac{q}{6\pi\eta r} \tag{1.5}$$

Eqn 1.5 is the Hückel equation for ion mobility, and is the simplest and most commonly used mobility expression in CE. It predicts that electrophoretic separations are governed by the charge-to-size ratios of the analytes. However, there exist many instances in which electrophoretic mobility is not accurately described by the Hückel equation. The fundamental limitations of eqn 1.5 and the evolution of more refined mobility models are explored in detail in Chapter 3.

Electrophoretic mobilities can be classified into two main types. The *effective mobility* (μ_e) of an ion is its experimentally-measured mobility. It is influenced by many electrolyte properties such as pH and ionic strength (as will be discussed in Section 1.3). In contrast, the ***absolute ion mobility*** (μ_o) is the mobility of a fully-charged ion at infinite dilution (zero buffer ionic strength). It is independent of experimental conditions and is a characteristic constant for a given ion in a given solvent. The Hückel equation (eqn 1.5) is generally expressed in terms of the absolute mobility of the ion. Absolute mobilities can be determined by extrapolation of effective mobilities to zero ionic strength, as will be discussed in Chapter 3 (Section 3.5).

1.2.3 Electroosmotic Flow (EOF)

Electroosmotic flow (EOF) is the bulk flow of liquid in the capillary resulting from the surface charge on the interior capillary wall. Under most conditions, the inner walls of fused-silica capillaries possess a negative charge owing to the presence of weakly acidic silanol (SiOH) groups ($pK_a \sim 5.3$ [6]). To maintain charge balance, counter-ions (cations) build up near the surface of the wall, forming an electrical double layer (Figure 1.2). This figure depicts the electrical double layer according to the Gouy-Chapman model refined by Stern and Grahame [7, 8].

Immediately adjacent to the capillary wall is a layer of adsorbed unsolvated ions, located at the inner Helmholtz plane (IHP). This is the closest distance that an unsolvated ion can approach the negative capillary wall. At a slightly further distance from the wall lies the outer Helmholtz plane (OHP), which is the distance of closest approach of solvated ions. The area between the capillary wall and the OHP, also referred to as the Stern layer [9], is the compact portion of the electrical double layer. The diffuse double

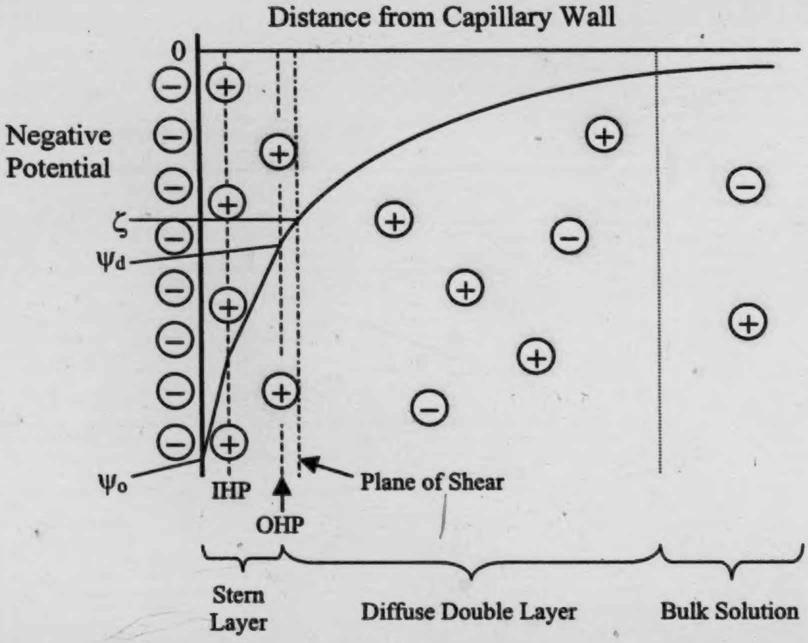
Distance from Capillary Wall
0
Negative Potential
ζ
ψd
ψo
IHP
OHP
Plane of Shear
Stern Layer
Diffuse Double Layer
Bulk Solution

Figure 1.2: Schematic illustration of the electric double layer and the potential variation with the distance from the capillary wall, according to the Gouy-Chapman model refined by Stern and Grahame.

layer extends outward from the OHP to the bulk solution. At or slightly beyond the OHP lies the plane of shear; anything inside the plane of shear remains stationary, while anything beyond this plane moves with the bulk solution. Under an applied voltage, the cations in the diffuse portion of the double layer (beyond the plane of shear) will migrate towards the negative electrode, carrying along with them their solvation shells. This results in a bulk flow (EOF) of the solution towards the negative electrode. Since the driving force for the EOF is uniformly distributed along the length of the capillary, the flow profile is flat (Figure 1.3).

The capillary wall has a negative potential (Ψ_o) owing to the presence of negative silanol groups (Figure 1.2). This potential decreases linearly in both regions of the Stern

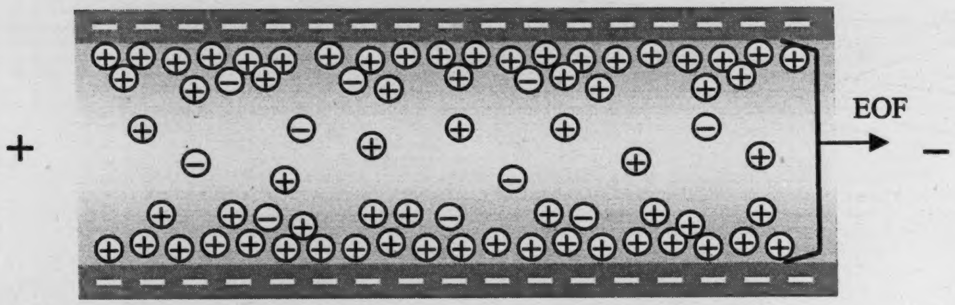

Figure 1.3: Illustration of the flat profile of the electroosmotic flow.

layer due to the adsorbed unsolvated and solvated cations. Beyond the OHP, the potential decreases exponentially from ψ_d until it reaches a value of zero in the bulk solution. The potential at the plane of shear is referred to as the zeta potential (ζ). The relationship between the electroosmotic mobility (μ_{eof}) and the zeta potential is given by the Smoluchowski equation:

$$\mu_{eof} = -\frac{\varepsilon\zeta}{\eta} \tag{1.6}$$

where ε and η are the dielectric constant and viscosity of the solution, respectively.

1.2.4 Modes of Capillary Electrophoresis

Six different modes of capillary electrophoretic separations can be performed with a standard CE instrument. These include capillary zone electrophoresis (CZE), capillary gel electrophoresis (CGE), micellar electrokinetic chromatography (MEKC), capillary electrochromatography (CEC), capillary isoelectric focusing (CIEF) and capillary isotachophoresis (CITP). All modes involve the separation of solutes in a narrow tube in the presence of an electric field, but differ in the composition of the background electrolyte. CZE and MEKC are used in this thesis, and are thus described below.

1.2.4.1 Capillary Zone Electrophoresis (CZE)

The separation mechanism in CZE is based on the differences in the migration velocities of ionic species in the electrophoretic buffer. The net movement of a solute is governed by its own electrophoretic mobility (μ_e), as well as by the EOF (μ_{eof}). This net movement is known as the apparent mobility (μ_a) and is given by:

$$\mu_a = \mu_e + \mu_{eof} \tag{1.7}$$

The apparent mobility is calculated experimentally by:

$$\mu_a = \frac{L_t L_d}{t_m V} \tag{1.8}$$

where L_t is the total capillary length, L_d is its length to the detector, t_m is the migration time of the solute, and V is the applied voltage. Similarly, the EOF mobility can be calculated according to eqn 1.8 by recording the migration time of a neutral analyte such as mesityl oxide, benzyl alcohol or acetone.

Figure 1.4 shows a CZE separation within a capillary and the resulting electropherogram. The Hückel equation (eqn 1.5) predicts that solute migration is governed by the solute's charge-to-size ratio (although exceptions to this rule will be demonstrated in Chapters 3-6). Consequently, analytes of higher charge migrate faster than those of lower charge, and analytes of larger size migrate slower than those of smaller size. Further, the effective mobilities of anions and cations will be towards the anode (positive electrode) and cathode (negative electrode), respectively. Generally, the magnitude of the cathodic EOF mobility is greater than the electrophoretic mobilities of the analytes, such that anions, cations and neutrals are simultaneously separated and detected (Figure 1.4b). Cations migrating with the EOF are detected first, while the

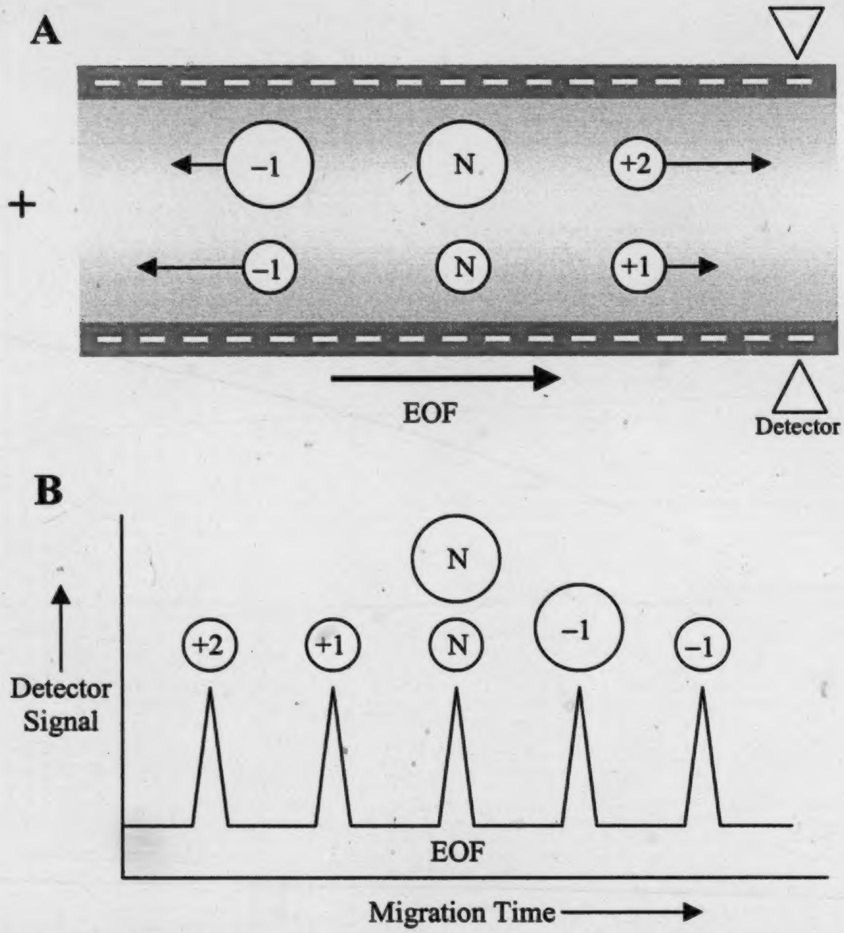
A
+
−
−1
N
+2
−1
N
+1
EOF
Detector
B
Detector Signal
N
+2
+1
N
−1
−1
EOF
Migration Time

Figure 1.4: Illustration of A) a CZE separation inside a capillary and B) the resulting electropherogram.

anions migrating counter to the EOF are detected last. All of the neutral analytes migrate with the EOF and are detected as a single band between the anions and cations.

1.2.4.2 Micellar Electrokinetic Chromatography (MEKC)

While CZE cannot separate neutral species, MEKC is a capillary electrophoretic technique that resolves neutral molecules as well as charged molecules. This technique was first introduced by Terabe and coworkers [10] in 1984. The main separation mechanism in MEKC is based on the partitioning of analytes between the micellar phase and the solution phase. Analytes ‘adopt’ the micelle mobility while they reside within the micelle, and migrate at their intrinsic electrophoretic mobilities while they are in solution. The final analyte separation results from a combination of the effects of charge-to-size ratios, hydrophobicity and charge interactions at the surface of the micelles.

In MEKC, a micellar surfactant solution acts a pseudostationary phase for chromatographic separation. Anionic surfactants such as sodium dodecyl sulfate (SDS) are most commonly used, although cationic, non-ionic, zwitterionic and bile salt surfactants are also employed [11]. The surfactants are introduced into the electrophoretic media at concentrations above their critical micelle concentration (cmc). Under these conditions, the surfactant monomers exceeding the cmc aggregate into micelles, which are dynamic structures that exist in equilibrium with the surfactant monomers [11]. Surfactant monomers are always present in solution at a concentration approximately equal to their concentration at the cmc. In Chapter 2, sodium cholate [12, 13] (a bile salt surfactant) is used for the separation of derivatized polyamines by MEKC. The structure of sodium cholate is given in Figure 1.5. This bile salt forms helical micelles [14] into which analyte molecules may partition based on their hydrophobicity. Sodium cholate

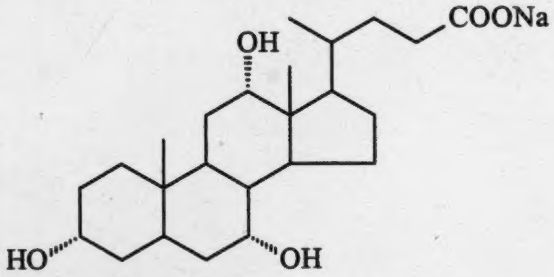

Figure 1.5: Structure of sodium cholate.

has a cmc of 13-15 mM, and the micelles formed above this concentration consist of 2-4 cholate monomers [15].

Figure 1.6a shows an MEKC separation of neutral analytes in a capillary using sodium cholate as surfactant. The resulting electropherogram is illustrated in Figure 1.6b. Although presented for cholate, the following separation concepts also apply for MEKC separations involving other surfactant types. The cholate monomers and micelles

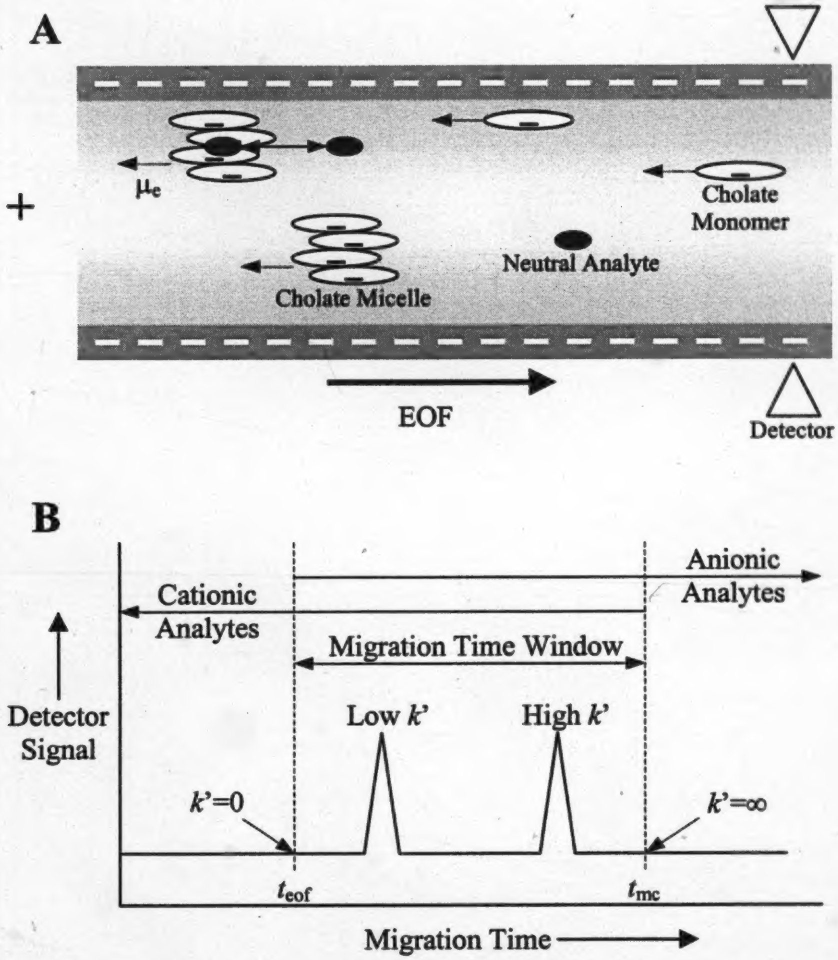
A
+
−
μ_e
Cholate Monomer
Neutral Analyte
Cholate Micelle
EOF
Detector
B
Cationic Analytes
Anionic Analytes
Migration Time Window
Detector Signal
Low k'
High k'
k'=0
k'=∞
t_{eof}
t_{mc}
Migration Time

Figure 1.6: Illustration of A) an MEKC separation of neutral analytes in a capillary using sodium cholate as surfactant, and B) the resulting electropherogram.

are negatively charged, and thus have effective mobilities toward the anode. However, their net migration is toward the cathode since the effective mobilities of the micelles are less than the magnitude of the EOF mobility. Neutral analytes partition into the cholate micelles according to their hydrophobicity. More hydrophobic solutes interact more strongly with the micellar phase than hydrophilic solutes. Terabe et al. [10] have proposed the following equation for the retention factor (k') of neutral analytes in MEKC:

$$k' = \frac{t_m - t_{eof}}{t_{eof}(1 - t_m / t_{mc})} \tag{1.9}$$

where t_m is the migration time of the neutral analyte, t_{eof} is the migration time of the EOF, and t_{mc} is the migration time of the micelle. The retention factor is the ratio of the total moles of solute in the micelles to those in the bulk solution. Strongly-interacting analytes with k' approaching infinity will migrate with the micelles, whereas non-interacting analytes with $k'=0$ will migrate with the EOF. The migration time of a neutral analyte (t_m) must therefore lie between that of the EOF (t_{eof}) and that of the cholate micelles (t_{mc}) (Figure 1.6b). This is often referred to as the migration time window in MEKC.

Anionic and cationic analytes can also be separated by MEKC [11]. For MEKC separations involving anionic micelles, as is the case in Figure 1.6, cationic analytes will be electrostatically attracted to the micelles. Depending on the extent of charge interaction, the cationic species may be detected before or with the micelles (Figure 1.6b). The closer their migration times are to that of the micelles, the greater the degree of electrostatic interaction. In contrast, minimal interaction is expected between anionic solutes and the negative micelles due to electrostatic repulsion. Thus, as in conventional CZE, anionic analytes are detected after the EOF at a time largely dictated by their charge-to-size ratios.

1.2.5 Detection

The sample zones in capillary electrophoresis have small volumes owing to the small capillary dimensions. The development of sensitive detection techniques is therefore of utmost importance. Many detection modes have been explored with varying degrees of success, including absorbance, fluorescence, electrochemical, refractive index, radiometric and mass spectrometric detection [11, 16, 17]. However, the most common methods of detection for CE applications are on-column UV absorbance and fluorescence detection. These were used in my thesis research, and are thus described below.

1.2.5.1 Absorbance Detection

Absorbance (A) is defined by:

$$A = -\log_{10} T_R = \log \frac{P_o}{P} \tag{1.10}$$

where T_R is the transmittance, P_o in the incident radiation power, and P is the radiation power after having passed through the sample. Accordingly, the absorbance increases as the attenuation of the radiation beam by the sample increases. Alternatively, absorbance can be expressed in terms of the optical pathlength (b), the molar absorptivity of the sample (ε'), and the molar concentration of the sample (c) as follows:

$$A = \varepsilon' bc \tag{1.11}$$

Eqn 1.11 is the well-known Beer's law. Since absorbance is directly proportional to path length, the sensitivity of absorbance detection in capillary electrophoresis is limited by the small capillary dimensions. On-column UV absorbance detection in CE typically yields detection limits [11] in the range of 10^{-4}-10^{-6} M.

To overcome the problem of small capillary dimensions, methods have been proposed to increase the path length for optical detection. These include the use of axial illumination [18], the use of a Z-shaped flow cell [19], and the use of a multireflection cell [20]. These modifications allow detection limits of 10^{-8} M to be achieved. Field-amplified sample stacking [21] has also been used to increase the sensitivity of on-column UV absorbance detection in capillary electrophoresis. This technique will be discussed in Section 1.2.5.3.

1.2.5.2 Fluorescence Detection

Fluorescence detection provides higher sensitivity than UV absorbance detection. It can be used to detect analytes that are not natively fluorescent, provided that they are derivatized with a fluorophore prior to detection. A simple energy level diagram illustrating the main processes involved in fluorescence is shown in Figure 1.7. In order for fluorescence to occur, the analyte must first absorb photons from a light source. Upon absorption of a photon, the analyte is converted to any of several excited vibrational levels within an excited electronic state (S_1). In solution, the excess

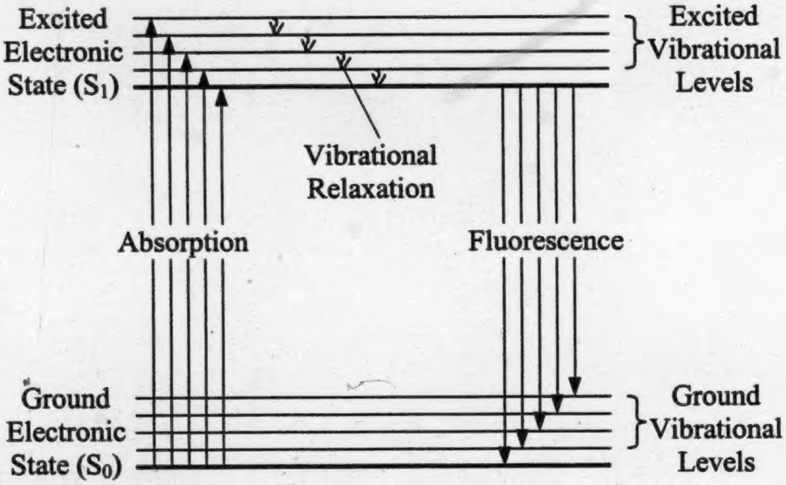
Excited
Electronic
State (S_1)
Excited
Vibrational
Levels
Vibrational
Relaxation
Absorption
Fluorescence
Ground
Electronic
State (S_0)
Ground
Vibrational
Levels

Figure 1.7: Partial energy diagram for a fluorescence system.

vibrational energy is immediately lost as a result of collisions between excited analyte molecules and solvent molecules [22]. The high efficiency of this non-radiative *vibrational relaxation* ensures that fluorescence always involves an energy transition from the lowest vibrational level of an excited electronic state. During fluorescence (a radiative process), the analyte molecule can return to any one of the vibrational levels of the ground electronic state, and then relax to the ground level by vibrational relaxation [22]. Overall, the excitation energy is greater than the emission energy, such that fluorescence emission occurs at longer wavelengths than the excitation. This shift in wavelength is known as Stokes' shift.

At low absorbances ($\varepsilon' bc \leq 0.02$), the power of fluorescent radiation (F) is governed by [22]:

$$F \propto P_o \Phi_F \varepsilon' bc \tag{1.12}$$

where P_o is the power of the incident radiation and Φ_F is the quantum efficiency of the fluorescent process. ε', b and c are as described in eqn 1.11. The fluorescence quantum efficiency is the ratio of the number of molecules that fluoresce to the total number of excited molecules. Not all excited molecules fluoresce, since in addition to fluorescence, excited states can be non-radiatively deactivated through internal and external conversion, intersystem crossing, and dissociation [22]. The quantum efficiency approaches unity for highly fluorescent molecules (e.g., fluorescein) and zero for non-fluorescent species.

Lasers are ideal light sources for use with small-diameter capillaries. They are superior to the conventional arc lamp sources because they have better monochromicity and can be focused into smaller volumes. On-column fluorescence detection using traditional arc lamps typically yields detection limits in the range of 10^{-5}-10^{-8} M, while the use of lasers allows detection limits of 10^{-7}-10^{-9} M to be achieved [11]. Laser-induced fluorescence detection is used in Chapter 2 in both on-column and off-column (sheath flow cuvette) formats. The sheath-flow cuvette (Figure 1.8) was introduced by Dovichi and coworkers in 1988 [23] to minimize stray light during fluorescence detection. Post-column detection is achieved by focusing a laser beam on the sample stream approximately 0.2 mm off the end of the capillary. Off-column laser-induced fluorescence detection with sheath flow cuvette provides superior detection limits of 10^{-9}-10^{-12} M [11].

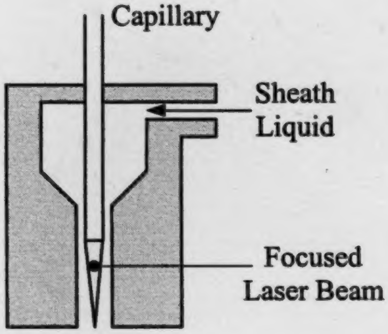

Figure 1.8: Schematic of a sheath flow cuvette.

1.2.5.3 Sample Stacking

A frequently employed method to improve detection limits in CE is sample stacking. This is an on-line sample concentration technique, the procedure for which varies depending on whether CZE or MEKC is performed. In Chapter 2, sample stacking is shown to improve the sensitivity of some derivatized polyamines in an MEKC separation. For the mobility measurements by CZE in Chapters 4-7, care is taken to avoid sample stacking so that unbiased mobility values are obtained. It is thus worthwhile to briefly discuss the concepts of sample stacking.

In the conventional field-amplified sample stacking technique for CZE [21] (Figure 1.9a), a sample plug of lower conductivity than the separation buffer is injected by pressure into the capillary. When a voltage is applied across the capillary, the sample ions in the low-conductivity sample plug experience a higher electric field strength than the buffer ions in the high-conductivity separation buffer. The sample ions thus migrate rapidly to the sample-buffer interface, where they are then slowed down by the lower field strength. This causes the analytes to be concentrated at this interface.

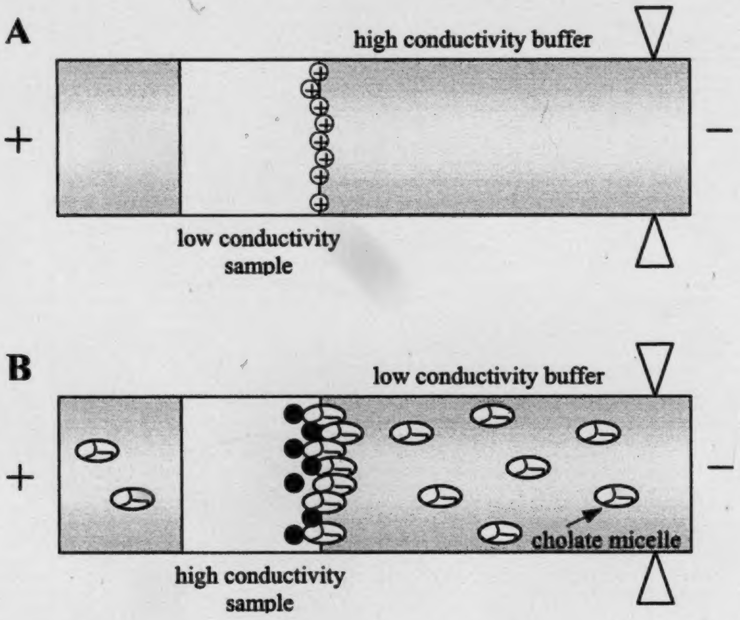
A
high conductivity buffer
+
−
low conductivity sample
B
low conductivity buffer
+
−
cholate micelle
high conductivity sample

Figure 1.9: A) Conventional field-amplified stacking for ionic solutes in CZE. B) High-salt staking for neutral analytes in MEKC.

A high-salt sample stacking technique for neutral analytes in MEKC has been recently introduced by Landers and coworkers [24]. This technique is illustrated in Figure 1.9b for an MEKC separation involving negative cholate micelles. Briefly, micelle stacking is achieved by replacing cholate with sodium chloride in the sample matrix such that the sample has a conductivity 2-3 times higher than the separation buffer. This is the reverse situation to that employed in CZE sample stacking (Figure 1.9a). The cholate micelles in the low-conductivity separation buffer, experiencing a high field strength, will stack at the sample/buffer interface. As a result, neutral analytes that partition into the micelles will concentrate at this micellar front.

Regardless of the mechanism, the result of stacking is to focus sample analytes at the sample/buffer interface. This allows sharpening of the electrophoretic peaks, as well as sample concentration when large volumes of sample are injected.

1.3 Factors Affecting Migration in CE

The main objective of this thesis is to better understand the factors affecting selectivity in CE. The properties of the electrophoretic buffer play a significant role in determining the migration behavior of solutes [25, 26]. Important factors include buffer pH and ionic strength, temperature, organic modifier type and content, and the presence of buffer additives such as surfactants. These are discussed briefly below.

1.3.1 Buffer pH

Manipulation of the buffer pH is a common tool used to modify the separation selectivity in CE [25, 27, 28]. By varying the buffer pH, the degree of ionization of both the analytes and the fused-silica capillary wall ($pK_a \sim 5.3$ [6]) can be altered. Consequently, both the electrophoretic and electroosmotic mobilities are dependent upon pH. The influence of buffer pH on the effective electrophoretic mobility (μ_e) of a weak acid is given by [27]:

$$\mu_e = \mu_{A^-} \frac{K_a}{[H^+] + K_a} \tag{1.13}$$

where μ_{A^-} is the effective mobility of the fully deprotonated solute, K_a is the acid dissociation constant of the solute, and $[H^+]$ is the concentration of hydrogen ions in the buffer solution. Accordingly, changes in buffer pH have the greatest impact on solute electrophoretic mobility when the pH is near the solute's pK_a. Further, varying the buffer pH can alter the selectivity between analytes with different pK_a values.

1.3.2 Buffer Ionic Strength

The ionic strength (I) of an electrolyte solution consisting of n charged species is defined by:

$$I = \frac{1}{2}\sum_{i=1}^{n} c_i z_i^2 \tag{1.14}$$

where c_i and z_i are the molar concentration and charge number of each electrolyte species. In a CE experiment, the electrophoretic mobility of a charged analyte is towards the electrode of opposite charge. According to eqn 1.5, the analyte mobility is a function of its charge-to-size ratio. However, in the presence of an electrolyte solution, the effective charge on the solute will be less than its total charge due to the screening effect of the buffer counterions. As the buffer ionic strength increases, so does the screening of the analyte charge. Consequently, electrophoretic mobility decreases with increasing ionic strength. This behavior has been frequently documented in the CE literature [29-33]. Further, selectivity changes have been achieved in CE by varying the ionic strength [31, 33].

Theoretical models describing the influence of ionic strength on mobility are discussed in greater detail in Chapter 3 (Section 3.5). Of these models, the Pitts' equation will be used in Chapters 4-7 to describe the ionic strength dependence of mobility in aqueous, aqueous-organic and nonaqueous media.

1.3.3 Organic Solvents

The use of organic solvents in capillary electrophoresis as either organic modifiers or as pure nonaqueous media offers many advantages compared to purely aqueous media [34, 35]. Of key importance is the increased solubility of many analytes, which allows the technique to be used for a wider range of applications. Furthermore, dramatic alterations in selectivity can be achieved by varying the type and content of the organic solvent in the buffer [34, 35]. Other potential advantages of aqueous-organic or nonaqueous solvents include lower Joule heating, reduced interaction of hydrophobic analytes with the negative capillary wall, and suitability for detection by mass spectrometry (MS) [35].

The concept of using nonaqueous solvents in electrophoresis is not new. In 1951, Hayek [36] performed electrophoresis on carbon black particles in kerosene and cetane. As early as 1970, organic solvents were used in isotachophoresis [37]. Wahlbroehl and Jorgenson performed the first investigation involving pure nonaqueous media in CZE in 1984 [38]. More recently, aqueous-organic and nonaqueous CE have gained popularity for a variety of applications, such that several reviews have been published on the topic [39-42]. Furthermore, Wright et al. [34] demonstrated that CE could be performed in pure organic solvents without the presence of supporting electrolytes.

Despite the frequent use of organic solvents to alter selectivity in CE [34, 35, 40, 41], the mechanism responsible for these mobility changes is still not well understood. While changes in solvent viscosity have a direct impact on electrophoretic mobility (eqn 1.5), they cannot account for solvent-induced selectivity changes between different analytes. Further, changes in analyte pK_a and solvent pH can only explain some of the observed mobility behavior in aqueous-organic and nonaqueous CE. In Chapter 3, a mobility model incorporating the effects of charge-induced friction will be introduced. Charge-induced friction is a function of both solvent-dependent (dielectric constant (ε), dielectric relaxation time (τ)) and analyte-dependent (q, r) terms. This model will be investigated in Chapters 4-6 as a means to explain solvent-induced selectivity changes in CE.

1.3.4 Temperature

Temperature is an easily-controlled variable that can be used to alter selectivity in CE [43-47]. While temperature-induced shifts in analyte migration are predominantly due to changes in the solvent viscosity (eqn 1.5), temperature can also influence chemical equilibria (eg., acid-base dissociation, complexation) and analyte conformation. As will be discussed in Chapter 3, charge-induced friction is a function of solvent dielectric constant (ε) and dielectric relaxation time (τ), both of which are temperature-dependent. This friction will be investigated in Chapter 7 as a mechanism to explain temperature-induced selectivity changes in CE.

1.3.5 Other Buffer Additives

A variety of buffer additives have been used to modify selectivity in CE [11]. Surfactants are used in MEKC (Section 1.2.4.2) separations to adjust the migration of both neutral and charged molecules [10]. Other additives that have been used in CE include inclusion complexes such as cyclodextrins [48, 49] and crown ethers [50], as well as complexing agents such as 8-hydroxyquinoline-5-sulfonic acid (HQS) [51, 52]. Buffer additives can be combined in order to optimize selectivity [11]. In particular, organic modifiers are often used in conjunction with surfactants in MEKC. In Chapter 2, an MEKC technique employing cholate as surfactant and acetonitrile as organic modifier is developed for the analysis of derivatized polyamines.

1.4 Thesis Overview

Gaining a more fundamental understanding of the factors affecting selectivity in CE is the main objective of my thesis research. Particular attention will be paid to the influence of organic solvents on analyte mobility. While fundamental mobility studies are the main focus of Chapters 3-7, Chapter 2 describes the application of MEKC to the analysis of derivatized polyamines. This project was initiated under the supervision of Dr. Norm Dovichi and completed in Dr. Charles Lucy's research group.

The change in research groups brought about a shift in the overall direction of my research. Selectivity alterations resulting from the use of organic solvents in CE (as observed in Chapter 2) have been frequently documented in the literature. Motivated by the fact that these solvent-induced selectivity changes were not well understood, I undertook fundamental mobility studies to better understand the influence of organic solvents on mobility behavior. Chapter 3 reviews several empirical and theoretical mobility models and evaluates their success at predicting solvent-induced selectivity changes. A theoretical mobility model accounting for charge-induced friction is introduced in this chapter and is used in Chapter 4 to explain the mobility behavior of organic anions and cations in methanol-water media. Prompted by its successful mobility predictions in methanol-water media, this model is further investigated as a mechanism for solvent induced selectivity changes in aqueous-organic media consisting of acetonitrile, ethanol and 2-propanol (Chapter 5), as well as in nonaqueous media consisting of various mixtures of methanol and actonitrile (Chapter 6). Finally, the possibility that charge-induced friction can explain temperature-induced selectivity changes is studied in Chapter 7.

1.5 References

(1) Tiselius, A. *Trans. Faraday Soc.* **1937,** *33*, 524.

(2) Raymond, S.; Weintraub, L. *Science* **1959,** *130*, 711-711.

(3) Hjertén, S. *Chromatogr. Rev.* **1967,** *9*, 122-219.

(4) Jorgenson, J. W.; Lukacs, K. D. *Anal. Chem.* **1981,** *53*, 1298-1302.

(5) Grossman, P. D. In *Capillary Electrophoresis. Theory and Practice*; Grossman, P. D., Colburn, J. C., Eds.; Academic Press: New York, 1992, pp 111-132.

(6) Schwer, C.; Kenndler, E. *Anal. Chem.* **1991,** *63*, 1801-1807.

(7) Shaw, D. J. *Introduction to Colloid and Surface Chemistry*, 3rd ed.; Butterworths: London, 1980.

(8) Hunter, R. J. *Zeta Potential in Colloid Science. Principles and Applications*; Academic Press: New York, 1981.

(9) Hiemenz, P. C. *Principles of Colloid and Surface Chemistry*; Marcel Dekker, Inc.: New York, 1986.

(10) Terabe, S.; Otsuka, K.; Ichikawa, K.; Tsuchiya, A.; Ando, T. *Anal. Chem.* **1984,** *56*, 111-113.

(11) Li, S. F. Y. *Capillary Electrophoresis: Principles, Practice and Applications*; Elsevier: New York, 1993.

(12) Terabe, S.; Shibata, M.; Miyashita, Y. *J. Chromatogr.* **1989,** *480*, 403-411.

(13) Cole, R. O.; Sepaniak, M. J.; Hinze, W. L.; Gorse, J.; Oldiges, K. *J. Chromatogr.* **1991,** *557*, 113-123.

(14) Esposito, G.; Giglio, E.; Pavel, N. V.; Zanobi, A. *J. Phys. Chem.* **1987,** *91*, 356-362.

(15) Terabe, S. *Micellar Electrokinetic Chromatography*; Beckman Instruments, Inc.: Fullerton, 1992.

(16) Swinney, K.; Bornhop, D. J. *Electrophoresis* **2000,** *21*, 1239-1250.

(17) Swinney, K.; Bornhop, D. *Crit. Rev. Anal. Chem.* **2000,** *30*, 1-30.

(18) Xi, X.; Yeung, E. S. *Appl. Spectrosc.* **1991,** *45*, 1199-1203.

(19) Chervet, J. P.; van Soest, R. E. J.; Ursem, M. *J. Chromatogr.* **1991,** *543*, 439-449.

(20) Wang, T.; Aiken, J. H.; Huie, C. W.; Hartwick, R. A. *Anal. Chem.* **1991,** *63*, 1372-1376.

(21) Burgi, D. S.; Chien, R.-L. *Anal. Chem.* **1991,** *63*, 2042-2047.

(22) Skoog, D. A.; Leary, J. J. *Principles of Instrumental Analysis*, 4th ed.; Harcourt Brace College Publishers: New York, 1992.

(23) Cheng, Y.-F.; Dovichi, N. J. *Science* **1988,** *242*, 562-564.

(24) Palmer, J.; Munro, N. J.; Landers, J. P. *Anal. Chem.* **1999,** *71*, 1679-1687.

(25) de Boer, T.; de Zeeuw, R. A.; de Jong, G. J.; Ensing, K. *Electrophoresis* **1999,** *20*, 2989-3010.

(26) Lucy, C. A. *J. Chromatogr. A* **1999,** *850*, 319-337.

(27) Smith, S. C.; Khaledi, M. G. *Anal. Chem.* **1993,** *65*, 193-198.

(28) Jones, W. R.; Jandik, P. *J. Chromatogr.* **1991,** *546*, 445-458.

(29) Friedl, W.; Reijenga, J. C.; Kenndler, E. *J. Chromatogr. A* **1995,** *709*, 163-170.

(30) Cao, C.-X. *J. Chromatogr. A* **1997,** *771*, 374-378.

(31) Mechref, Y.; Ostrander, G. K.; Rassi, Z. E. *J. Chromatogr. A* **1997,** *792*, 75-82.

(32) Survay, M. A.; Goodall, D. M.; Wren, S. A. C.; Rowe, R. C. *J. Chromatogr. A* **1996,** *741*, 99-113.

(33) Li, D.; Fu, S.; Lucy, C. A. *Anal. Chem.* **1999,** *71*, 687-699.

(34) Wright, P. B.; Lister, A. S.; Dorsey, J. G. *Anal. Chem.* **1997,** *69*, 3251-3259.

(35) Karbaum, A.; Jira, T. *Electrophoresis* **1999,** *20*, 3396-3401.

(36) Hayek, M. *J. Phys. Colloid Chem.* **1951,** *55*, 1527-1533.

(37) Beckers, J. L.; Everaerts, F. M. *J. Chromatogr.* **1970,** *51*, 339-342.

(38) Walbroehl, Y.; Jorgenson, J. W. *J. Chromatogr.* **1984,** *315*, 135-143.

(39) Valkó, I. E.; Sirén, H.; Riekkola, M.-L. *LC-GC* **1997,** *15*, 560-567.

(40) Sarmini, K.; Kenndler, E. *J. Chromatogr. A* **1997,** *792*, 3-11.

(41) Riekkola, M.-L.; Jussila, M.; Porras, S. P.; Valkó, I. E. *J. Chromatogr. A* **2000,** *892*, 155-170.

(42) Wang, F.; Khaledi, M. G. *J. Chromatogr. A* **2000,** *875*, 277-293.

(43) Oda, R. P.; Landers, J. P. In *Handbook of Capillary Electrophoresis*; Landers, J. P., Ed.; CRC Press: Boca Raton, 1994, pp 9-42.

(44) Nielen, M. W. F. *J. Chromatogr.* **1991,** *542*, 173-183.

(45) Rush, R. S.; Cohen, A. S.; Karger, B. L. *Anal. Chem.* **1991,** *63*, 1346-1350.

(46) Gil, E. C.; Dehouck, P.; van Schepdael, A.; Roets, E.; Hoogmartens, J. *Electrophoresis* **2001,** *22*, 497-502.

(47) François, C.; Morin, P.; Dreux, M. *J. High Resol. Chromatogr.* **1996,** *19*, 5-16.

(48) Terabe, S.; Ozaki, H.; Otsuka, K.; Ando, T. *J. Chromatogr.* **1985,** *332*, 211-217.

(49) Fanali, S. *J. Chromatogr.* **1989,** *474*, 441-446.

(50) Stover, F. S. *J. Chromatogr.* **1984,** *298*, 203-210.

(51) Swaile, D. F.; Sepaniak, M. J. *Anal. Chem.* **1991,** *63*, 179-184.

(52) Vos, C. J.; Melanson, J. E.; Lucy, C. A. *Anal. Sci.* **2001,** *17*, 225-227.

CHAPTER TWO. Selective Fluorometric Detection of Polyamines Using Micellar Electrokinetic Chromatography with Laser-Induced Fluorescence Detection[‡§]

2.1 Introduction

Putrescine, spermidine, spermine, and to a lesser extent cadaverine, are the major cellular polyamines in the human body [1]. These biogenic amines are involved in cellular growth and differentiation, regulation of nucleic acid and protein synthesis, stabilization of lipids, brain development, and nerve growth and regeneration [1]. They also play a major role in the body's response to brain injury and stress, and in the regulation of neuronal ion channels and brain neurotransmitter receptors [1]. Some studies have also shown that the high concentration of polyamines found in human milk may play a role in the apparent protective effect of human milk against allergies [2].

There has been recent evidence linking elevated polyamine levels and cancer. Nairn et al. [3] have reported high polyamine concentrations in breast cancer and colon cancer cells. McCloskey et al. [4] and Bergeron et al. [5] have demonstrated the arrest of cancer cell growth using polyamine analogues. Pentaazapentacosane pentahydrochloride, an anti-cancer agent, is also analogous in structure to both spermine and spermidine [6]. The antiproliferative nature of these analogues is possibly due to the disruption of polyamine metabolism in cancer cells. The potential link between polyamine levels and cancer has promoted interest in the development of sensitive analytical techniques capable of detection and quantification of biogenic amines in biological fluids.

[‡] A version of this chapter has been published. Paproski, R. E.; Roy, K. I.; Lucy, C. A. *Journal of Chromatography A* **2002**, 946, 265-273.

[§] This chapter describes a research project that was started in Dr. Norman Dovichi's research group and completed in Dr. Charles Lucy's group. The results that I obtained while in Dr. Dovichi's group are presented in the Preliminary Work Section.

Polyamines do not exhibit any structural features that enable their direct detection in a sensitive manner. There are some reports of native, non-derivatized polyamine detection using ion chromatography with integrated pulse amperometric detection [7], enzymatic differential assays [8] and competitive enzyme-linked immunosorbent assays (ELISA) using polyamine-specific monoclonal antibodies [9]. These techniques, however, suffer from poor sensitivity.

Therefore, most analytical techniques reported for the determination of polyamines include both a derivatization step and a separation step. Dorhout et al. [10] used capillary gas chromatography with nitrogen-phosphorous detection for the detection of spermidine, spermine and putrescine in leukemia cells following derivatization by methylation. However, high-performance liquid chromatography (HPLC), preceded by amine derivatization, is by far the most frequently reported technique for polyamine separation and quantification [11-21]. Fu et al. [11] have used HPLC with dansyl chloride derivatization to evaluate putrescine, spermidine and spermine levels in human prostate, and they have reported detection limits of ~10 nm using fluorescence detection. Other common derivatization agents used with HPLC include naphthalene-2,3-dicarboxaldehyde (NDA) [18] and *o*-phthalaldehyde (OPA) [12, 14, 16] with fluorescence detection, benzoyl chloride with UV detection [17], and ferrocene derivatives with electrochemical detection [15].

Since the work of Jorgenson and Lukacs in the early 1980s [22], capillary electrophoresis (CE) has become widely accepted as an analytical tool. CE offers many advantages over its counterpart, HPLC, such as higher column efficiency (10^5-10^6 theoretical plates), lower sample volumes (~10 nL), and very high sensitivity with femtomole to zeptomole limits having been reported [23-26]. As for detection, laser-induced fluorescence (LIF) provides the greatest degree of sensitivity of any detector currently available for CE, with detection limits approaching the molecular level [23]. The use of CE-LIF for separation and quantification of polyamines is becoming increasingly popular, and there are reports in the literature demonstrating the analysis of polyamines using CE-LIF with 6-aminoquinolyl-N-hydroxysuccinimidyl carbamate (AccQ) [27], OPA [28-30] and fluorescein isothiocyanate (FITC) [31] derivatization. Similarly, Rodriguez et al. [32] have reported the microchannel electrophoretic separation of putrescine, cadaverine, spermidine and spermine by micellar electrokinetic chromatography (MEKC) following derivatization by FITC. The limits of detection were ~1 μM.

There are some limitations to the common derivatization reagents used. For instance, FITC and AccQ are natively fluorescent and, depending on the separation, may interfere with the detection of the polyamines of interest. Further, OPA derivatives are unstable and the reaction must be carefully timed to enable quantification [33]. Another limitation is that most of the polyamine derivatization reagents also react with monoamines that are present in the samples. Without further sample pretreatment, this leads to numerous peaks that may interfere with the detection of the polyamines. Finally, polyamines labeled with NDA [34], OPA [35, 36] and 5-furoylquinoline-3-carboxaldehyde (FQ) (see Preliminary Work, Section 2.2) suffer from poorer sensitivity due to intramolecular fluorescence quenching. This concept is discussed in detail below.

When two or more conjugated molecules are in close proximity with one another, their π-electron systems can interact, resulting in a shift in the relative spacings between the ground and excited state energy levels [37]. Depending on the geometry, these molecules can interact either constructively or destructively. If the aromatic rings of the molecules overlap (stack), the fluorescence will generally be quenched [37]. In other words, an excited molecule interacting in this fashion with a second non-excited molecule will relax from its excited state in a non-radiative manner. For the multiply-labeled polyamines described above, the multiple labels can interact intramolecularly and result in fluorescence quenching. In contrast, molecules aggregating in a plane (edge-on) will generally result in intense fluorescence at longer wavelengths than in the single molecule [37]. These emitting aggregates are termed *excimers* if they are composed of identical molecules, and *exciplexes* if they are composed of different molecules.

Recently, Yamaguchi and coworkers [38, 39] have developed sensitive and selective reversed-phase HPLC methods for the determination of polyamines using 1-pyrenebutanoic acid succinimidyl ester (PSE) as the derivatization reagent. PSE labels amines with a fluorescent pyrene group, as shown in Figure 2.1a. In analytes with multiple labeling sites, an excited pyrene group can form an intramolecular *excimer* with a second ground state pyrene group. This excimer emits at longer wavelengths (450-520 nm) than mono-labeled analytes (360-420 nm) [38] (Figure 2.1b). High selectivity for polyamines can thus be achieved by using PSE with detection at 490 nm. It has been shown that PSE-labeled monoamines do not give any significant response at these longer wavelengths [38], making PSE an obvious choice for use with biological samples whose matrices include monoamines such as most amino acids.

In the Preliminary Work Section of this chapter, a MEKC-LIF technique for the analysis of polyamines is described using FQ as the derivatization reagent. The remainder of the chapter focuses on a more sensitive and selective method for the

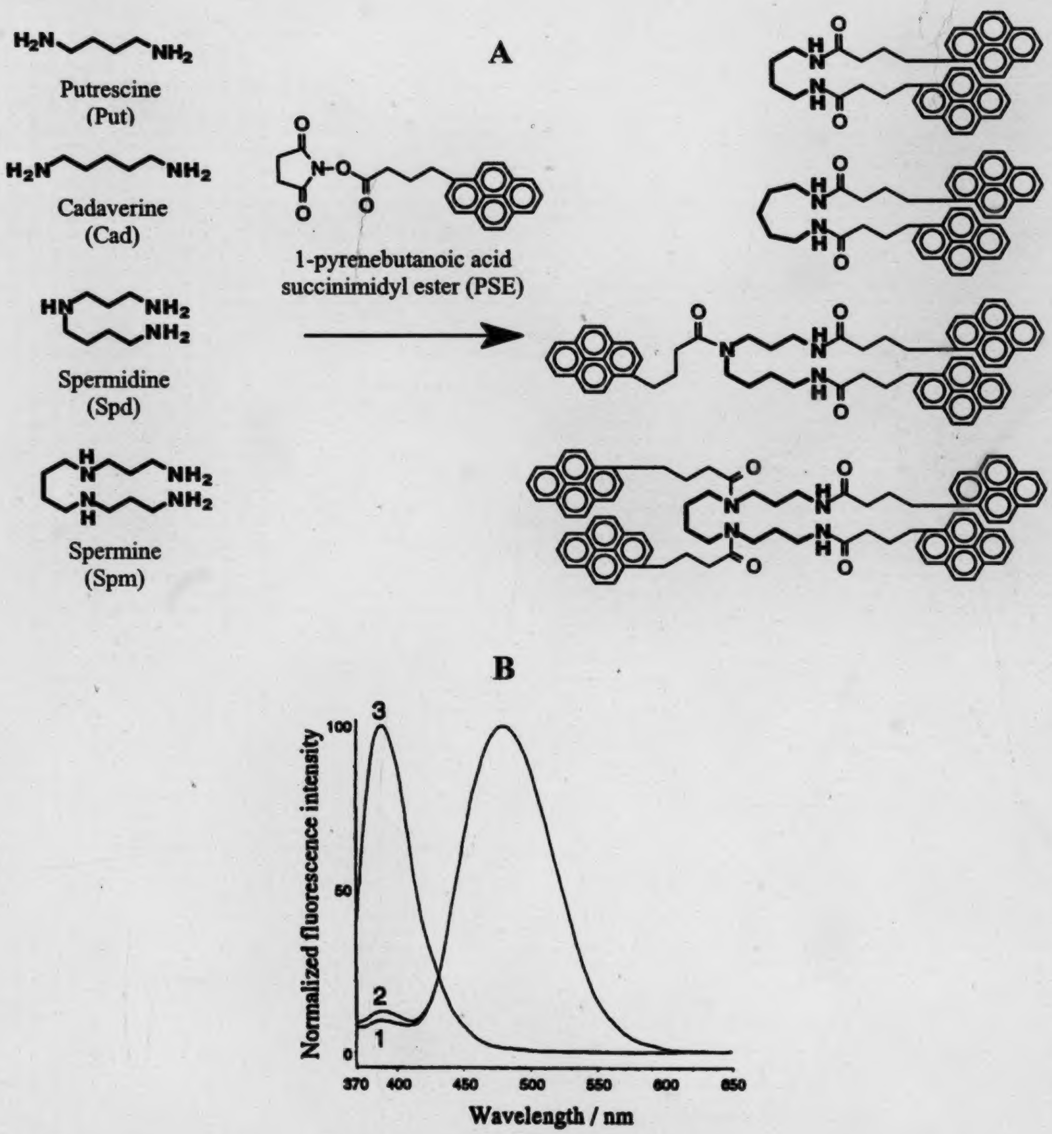
A
Putrescine
(Put)
Cadaverine
(Cad)
Spermidine
(Spd)
Spermine
(Spm)
1-pyrenebutanoic acid
succinimidyl ester (PSE)
B
Normalized fluorescence intensity
Wavelength / nm
3
2
1
0
50
100
370
400
450
500
550
600
650

Figure 2.1: A) Reaction scheme for the derivatization of polyamines with PSE. Adapted from ref 38. B) Fluorescence emission spectrum of PSE-labeled polyamines (Traces 1 and 2) and PSE-labeled monoamines (Trace 3). The peak at ~450-520 nm is the *excimer* fluorescence, while the peaks at ~360-420 nm is the monomer fluorescence. Reprinted with permission from Anal. Sci. 17 (2001) 107-112. Copyright 2001, The Japan Society for Analytical Chemistry.

determination of polyamines. Polyamines of biological importance are first derivatized with PSE, followed by separation and quantification by MEKC-LIF. The multiply-labeled polyamines are selectively detected at 490 nm. To our knowledge, this is the first report of a capillary electrophoretic technique employing PSE as a derivatization reagent.

2.2 Preliminary Work*

The goal of this project was to develop a separation scheme based on micellar electrokinetic chromatography for the sensitive determination of FQ-labeled putrescine (Put), cadaverine (Cad), spermine (Spm) and spermidine (Spd). FQ was selected as a derivatization reagent because previous CE-LIF studies of amino acids, peptides and proteins [40-42] have shown that FQ is an effective fluorogenic reagent for primary amines (Figure 2.2).

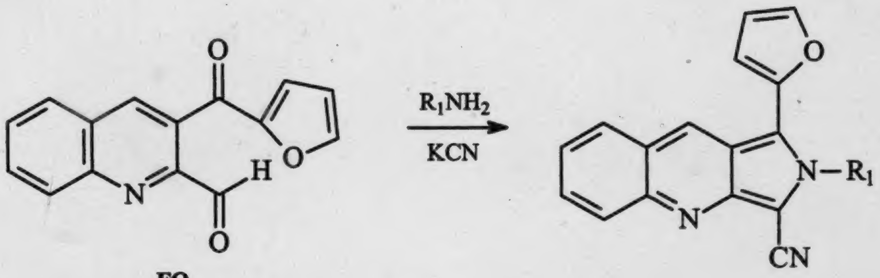

FQ

Figure 2.2: Reaction scheme for the derivatization of primary amines with FQ. Adapted from ref 43.

2.2.1 Capillary Electrophoresis System

Capillary electrophoresis was performed on a laboratory-built single-capillary instrument with sheath flow cuvette, as described elsewhere [23]. Bare fused-silica capillaries (Polymicro Technologies, Phoenix, AZ) had inner diameters of 53 μm, outer diameters of 141 μm, and lengths of 38.5-40.0 cm. A blue argon ion laser (Uniphase, San Jose, CA) operated at 11.0 mW and 488 nm was used for excitation. Fluorescence was filtered through a 630-nm (630df30) bandpass filter (Omega Optical, Brattleboro, VT) and was detected with an R1477 photomultiplier tube (Hamamatsu, Middlesex, NJ).

---

* This work was performed under the supervision of Dr. N. J. Dovichi.

2.2.2 Derivatization Procedure with FQ

A stock solution of 10 mM 5-furoylquinoline-3-carboxaldehyde (FQ; Molecular Probes, Eugene, OR) was prepared in methanol. From this solution, 10-μL aliquots were transferred into 500-μL microcentrifuge tubes, and the solvent was removed under vacuum using a Speed Vac (Savant Instruments Inc., Farmingdale, NY). The dried FQ aliquots, each consisting of 100 nmol FQ, were stored at –20°C. These precautions were necessary because FQ degrades slowly in solution, even if the solutions are stored at –20°C. The dried and frozen FQ aliquots were stable for at least two months.

The hydrochloride salts of putrescine, cadaverine, spermine and spermidine were obtained from Sigma (St. Louis, MO). Biogenic amine stock solutions were prepared in water at concentrations of 10 mg/mL, and were diluted to the desired concentration prior to derivatization with FQ.

Sample and standard solutions were labeled with FQ by adding 4 μL of sample (or standard) and 4 μL of 25 mM KCN (in 10 mM borate pH 9.2) to a microcentrifuge tube containing 100 nmol dry FQ. This mixture was then allowed to react for 30 min at 65°C. The reaction between FQ and primary amines [43] is illustrated in Figure 2.2. In order to stop the reaction after 30 min, the reaction mixture was diluted 20-fold with running buffer.

2.2.3 Separation of FQ-Labeled Polyamines by MEKC

The FQ-labeled polyamines gave fluorescence intensities that were low relative to FQ-labeled monoamines. Moreover, FQ-spermine did not produce an observable fluorescence signal. This lack of fluorescence intensity likely results from intramolecular quenching of the two FQ labels on the polyamines. Similar behavior has been reported with NDA [34] and OPA [35, 36] derivatives. The total absence of a fluorescence signal for FQ-Spm may indicate that intramolecular quenching is sterically favored in this labeled polyamine. Further, a black precipitate formed during the labeling reaction of Spm with FQ, suggesting that the reaction may not be favorable. Since FQ-spermine could not be detected, spermine was excluded from the reaction mixture in all further studies.

Optimal separation of putrescine, cadaverine and spermidine was achieved using a buffer consisting of 50 mM pH 7.17 phosphate, 30 mM sodium cholate and 15% (v/v) acetonitrile. The separation is illustrated in Figure 2.3, where the peaks used for quantification are labeled in bold. Two peaks were observed for Put and Spd, while four peaks were observed for Cad. There are two possibilities for the origin of these multiple peaks. First, they may result from impurities present in the polyamine standards. An alternate possibility is that these multiple peaks result from different degrees of polyamine labeling. As seen in Figure 2.1, Put, Cad and Spd each possess two primary amine labeling sites. Therefore, if the derivatization reaction does not go to completion, singly- and doubly-labeled polyamines will exist and will migrate at different rates. The Spd, Put and Cad peaks at ~11, 12 and 13 min, respectively, are attributed to the singly-labeled polyamines. Being less hydrophobic than their doubly-labeled counterparts, these neutral singly-labeled polyamines will partition less into the cholate micelles and will thus elute first. The Cad peaks at ~17.5 min are assigned to impurities in the cadaverine standard.

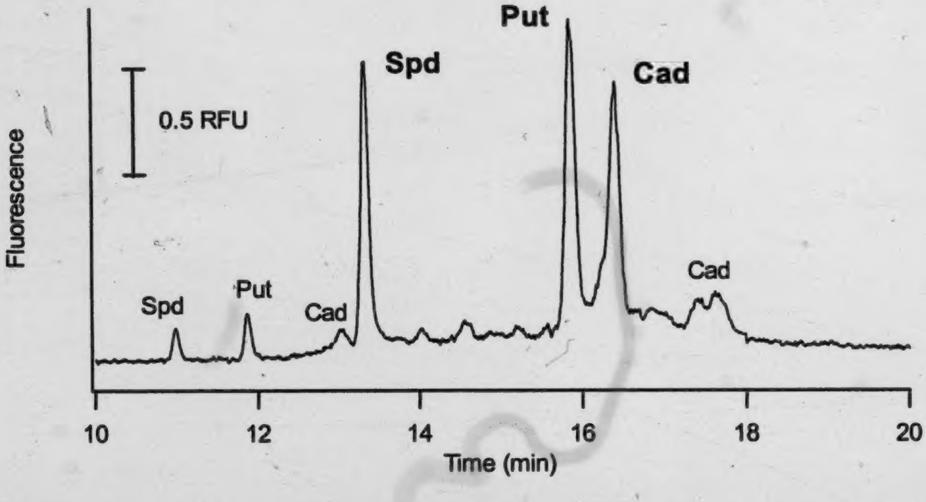

Figure 2.3: Separation of FQ-labeled Put, Cad and Spd. A solution consisting of 2.0×10^{-4} M Spd, 6.2×10^{-5} M Put and 5.7×10^{-5} M Cad was derivatized according to the procedure described in Section 2.2.2, and diluted 20-fold with the separation buffer. The origin of each peak is identified on the figure. The peaks identified in bold were used for quantification. Separation buffer: 50 mM pH 7.17 phosphate, 30 mM cholate, 15% (v/v) ACN. Separation conditions: 38.7-cm capillary, 200 V/cm applied, 5 s injection at 100 V/cm, detection at 630 nm.

Limits of detection (LOD) were calculated according to:

$$LOD = \frac{3 \times S_b}{m} \tag{2.1}$$

where S_b is the standard deviation of the baseline and m is the slope of the linear calibration curve between fluorescence signal and concentration. Using peak heights, the detection limits for Put, Cad and Spd were 10, 7 and 36 nM injected, respectively. In comparison, detection limits for the FQ-labeled monoamines taurine and glycine were 0.1 nM and 1 nM, respectively, under similar experimental conditions [40]. The detection limit for spermidine is higher than for the other two polyamines possibly due to a greater degree of intramolecular quenching. Spd has a structure similar to Spm, for which a fluorescence signal was completely absent (as discussed above).

Inter- and intra-assay reproducibilities were also determined for the FQ-labeled polyamines investigated herein. Inter-assay refers to the repeated derivatization and injection of a sample, while intra-assay refers to the repeated injection of the same derivatized sample. Using the peaks highlighted in Figure 2.3 at concentrations of 30 × the LOD's, the inter-assay peak height RSD (n=9) was 8.0% for Put, 9.5% for Cad and 17.8% for Spd. The intra-assay RSD's (n=3) for Put, Cad and Spd were 6.4%, 8.2% and 12.2%, respectively. These intra-assay RSD values are much greater than 2%, which according to Demarest et al. [44] is the maximum allowable variation in peak response for a successful CE analysis. Using Rhodamine 6G as an internal standard improved the intra-assay reproducibilities of Put, Cad and Spd to 4.8%, 5.5% and 5.8%, respectively, but did not improve the inter-assay RSD's. o-Methyl-L-threonine was also investigated as an internal standard, but it failed to improve either the intra- or inter-assay RSD's. The inability of an internal standard to improve the inter-assay variance reflects the irreproducibility of the derivatization reaction.

2.2.4 Analysis of Real Samples

At concentrations of 20 μmol/g of brain tissue, spermidine is the most concentrated polyamine in the adult brain [1]. This is followed by spermine (3 μmol/g) and putrescine (1 μmol/g), while cadaverine is present at even lower concentrations [1]. To determine whether the above method could be applied to the analysis of real samples, Dr.

Glen Baker from the Department of Psychiatry at the University of Alberta generously provided me with rat brain microdialysate and rat liver homogenate samples.

The microdialysate samples were collected as described elsewhere [40, 45]. Brain microdialysates and liver homogenates were used as received, and were derivatized according to the procedure described in Section 2.2.2. The electropherograms obtained for the brain and liver samples are illustrated in Figures 2.4a and 2.5a, respectively.

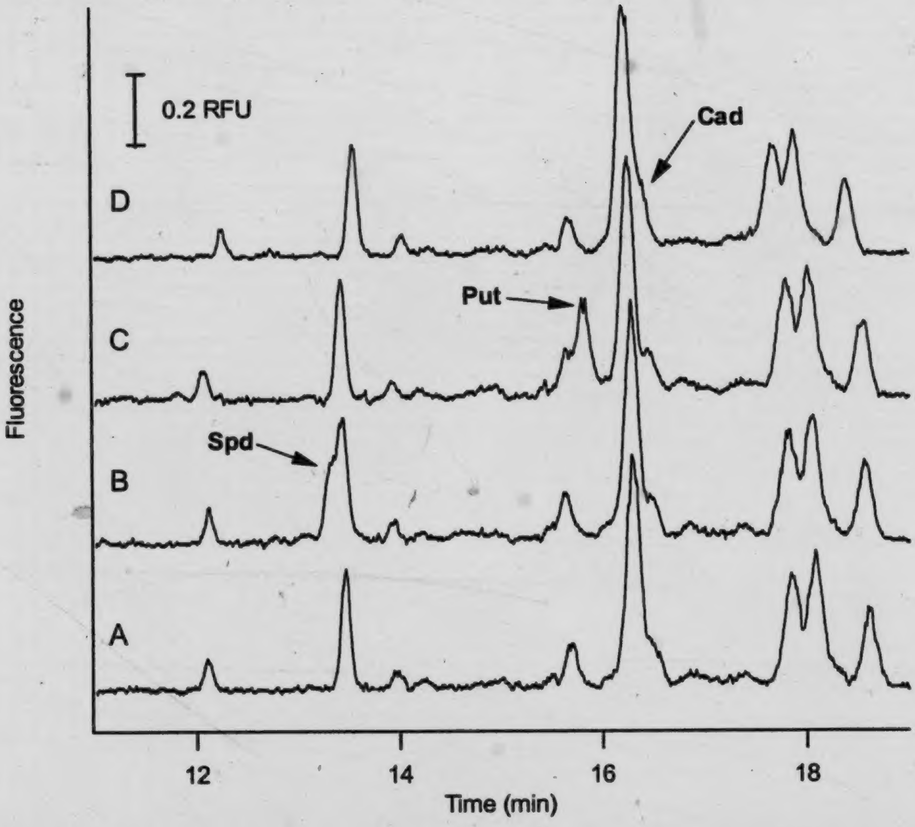

Figure 2.4: Separation by MEKC of a rat brain microdialysate sample derivatized with FQ. (A) shows the pure microdialysate sample, while (B)-(D) show the sample spiked with B) 9.9×10^{-7} M Spd, C) 3.1×10^{-7} M Put and D) 2.9×10^{-7} M Cad. The peaks resulting from the spikes are identified in bold. Capillary length: 39.5 cm. Separation buffer and conditions as in Figure 2.3.

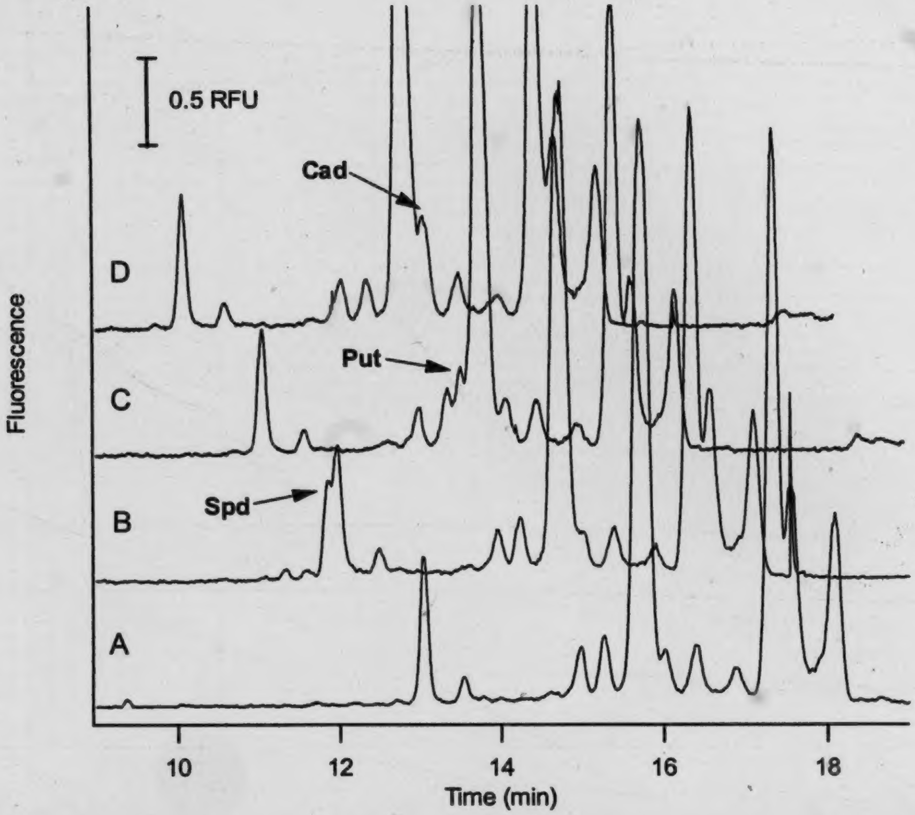

Figure 2.5: Separation by MEKC of a rat liver homogenate sample derivatized with FQ. (A) shows the pure liver homogenate sample, while (B)-(D) show the sample spiked with B) 9.9×10^{-7} M Spd, C) 3.1×10^{-7} M Put and D) 2.9×10^{-7} M Cad. The peaks resulting from the spikes are identified in bold. For clarity, (B) is offset by –1 min, (C) is offset by –2 min, and (D) is offset by –3 min. Capillary length: 39.5 cm. Separation and buffer conditions as in Figure 2.3.

Upon first inspection, the electropherograms for the brain and liver samples look promising as they show numerous distinct peaks. However, as seen from the location of the putrescine and spermidine peaks in the spiked samples (traces B and C in Figures 2.4 and 2.5), these polyamines were not detected in the original brain microdialysate or liver homogenate. Further, it appears from the Cad-spiked samples (D traces) that the cadaverine peak lies beneath the shoulder of the large signal at ~16 min for both the liver and brain samples. However, this shoulder peak in the original (non-spiked) samples is not attributed to Cad, since Put and Spd were not detected in these samples and Cad should be present at an even lower concentration [1]. It thus appears as though the Cad spike co-migrates with another species.

The inability to detect the FQ-labeled polyamines in the brain microdialysates and liver homogenates may result from one of several possibilities. First, the polyamines might be present at concentrations below the detection limits of the present method. However, Morrison et al. [1] have reported that spermidine concentrations in the average adult human brain range between 55-1410 μM, and that polyamine levels are higher in rat brain tissue than in human brain tissue. This concentration is well above the detection limit of the present method. Another possibility is that the amino acids and other biogenic amines present in the real samples are preferentially labeled by FQ. Further, these labeled amino acids and biogenic amines can interfere with the detection of the polyamines of interest. This was observed in Figures 2.4 and 2.5, whereby cadaverine was observed to co-migrate with another species.

Chen et al. [40] observed high levels of alanine (Ala), taurine (Taur) and glutamine (Glu) in rat brain microdialysate samples. The real samples investigated herein were spiked with these biogenic amines to determine whether they may be responsible for some of the fluorescence signals observed in Figures 2.4 and 2.5. Indeed, for the brain microdialysate sample (Figure 2.4a), the peak at ~18.5 min can be attributed to a combination of Ala and Taur, and the large signal slightly after 16 min can be attributed to Glu. For the liver homogenate (Figure 2.5a), the signal at ~18 min can be assigned to

Ala and Taur, while the Glu spike resulted in the formation of a new peak. These results support the fact that the multiple peaks observed in the electropherograms for the real samples likely result from the numerous amino acids and biogenic amines present in these samples. This can render the detection of the desired polyamines difficult.

2.2.5 Motivation for an Improved Method for Polyamine Analysis

The analysis of FQ-labeled polyamines by MEKC described herein suffers from several limitations. First, the sensitivity is poor for spermidine, while spermine can not be detected at all. This is likely due to intramolecular quenching of the fluorescence. Second, the intra-assay reproducibilities are far from optimal, and the inability of an internal standard to improve the inter-assay RSD's suggests that the derivatization reaction is irreproducible. Moreover, this technique is not selective for polyamines, so numerous peaks corresponding to amino acids and other biogenic amines are observed in the electropherograms of real samples (Figures 2.4 and 2.5). These limitations are motivators for developing an improved polyamine analysis method. The remainder of this chapter describes an MEKC method for the analysis of polyamines based on derivatization with 1-pyrenebutanoic acid succinimidyl ester (PSE). This technique is selective for polyamines and offers improved sensitivity (for spermine and spermidine) and reproducibility. The analysis is also performed in under 10 minutes, which is superior to the 16 minute separation developed for the analysis of FQ-polyamines.

2.3 Experimental

2.3.1 Apparatus

A P/ACE 2100 (Beckman, Fullerton, CA) system equipped with an LIF detector module was used for all experiments. Data acquisition and instrument control were performed with P/ACE Station software (Beckman) for Windows 95 on a 486 PC. Laser power measurements were performed with a PocketPower handheld power meter (Melles Griot, Irvine, CA).

The single-wavelength He-Cd laser was operated at 325 nm with a power output of 5 mW, and was equipped with a SMA fiber optic receptacle (Model 3056-8M; Omnichrome, Irvine, CA). The laser beam was coupled to the LIF detector through a 1-m multimode fiber optic patchcord with a 100/140-μm (core/cladding) diameter and SMA 906 connectors (Polymicro Technologies, Phoenix, AZ). The optical power measured out of the fiber was ~2 mW. Fluorescence was collected through a 490-nm (490DF10) band pass filter (Omega Optical, Brattleboro, VT), unless otherwise noted.

2.3.2 Chemicals

All solutions were prepared in Nanopure 18-MΩ water (Barnstead, Chicago, IL). Acetonitrile (ACN) was HPLC-grade and was obtained from Fisher Scientific (Fair Lawn, NJ). Dimethyl sulfoxide (DMSO) and tetrahydrofuran (THF) were reagent-grade and were obtained from ACP (Montreal) and BDH (Toronto), respectively. 1-Pyrenebutanoic acid succinimidyl ester (PSE, Figure 2.1) was obtained from Molecular Probes (Eugene, OR). Sodium dihydrogen orthophosphate and potassium carbonate were reagent-grade and were obtained from BDH. Cholic acid (sodium salt) was of 99% minimum purity and was purchased from Sigma (St. Louis, MO). The hydrochloride salts of putrescine (Put), cadaverine (Cad), spermidine (Spd) and spermine (Spm) were purchased from Sigma. The structures of these analytes are shown in Figure 2.1.

The separation buffer was prepared by dissolving sodium dihydrogen orthophosphate in water, bringing the pH to 7.2 with concentrated aqueous NaOH (BDH), adding the required volume of acetonitrile, and finally by adding cholate. The optimized separation buffer consisted of 10 mM pH 7.2 phosphate, 30 mM cholate and 30% (v/v) acetonitrile. Fresh buffers were prepared weekly.

Polyamine stock solutions (100 mM) were prepared in water and stored frozen at –15°C in plastic vials. These solutions were stable for at least three months. Polyamine standards were prepared from the stock solutions by diluting with a THF-DMSO-water (1:2:1, v/v) solvent mixture before use. PSE (10 mM) was made up in acetonitrile and stored at –15°C under dark conditions. It was stable for at least one week.

An amino acid standard solution was used to evaluate the selectivity of the method. The standard solution was obtained from Sigma, and contained the following 17 amino acids: L-alanine, L-arginine, L-aspartic acid, L-cystine, L-glutamic acid, glycine, L-histidine, L-isoleucine, L-leucine, L-lysine, L-methionine, L-phenylalanine, L-proline, L-serine, L-threonine, L-tyrosine and L-valine. Before use, the standard solution was diluted 2.5-fold with a THF-DMSO-water (1:2:1, v/v) solvent mixture. All amino acids were 25 μM in the original standard solution, except L-cystine which was 12.5 μM.

2.3.3 Derivatization Procedure with PSE

This derivatization procedure is based on that by Nohta et al. [38]. Briefly, 200 μL of a polyamine standard, 10 μL of 1 M potassium carbonate (aqueous) and 200 μL of 10 mM PSE were added to a 1-mL Reacti-vial (Pierce, Rockford, IL). The vial was sealed and heated in boiling water at ~95°C for 40 min. The reaction mixture was cooled in ice water and diluted 10-fold with the separation buffer prior to injection. Sample blanks were made by replacing the polyamine standard with 200 μL of the THF-DMSO-water (1:2:1) solvent mixture. The reaction mixture and diluted samples were stable for at least 6 h when protected from light.

For the sample stacking experiments, the reaction mixtures were diluted with a solution consisting of 10 mM pH 7.2 phosphate, 30% acetonitrile and 100 mM NaCl (BDH). This solution differs from the separation buffer in that the cholate is replaced by a high concentration of salt.

2.3.4 Capillary Electrophoresis

Untreated fused-silica capillaries (Polymicro Technologies) with total lengths of 37 cm and 57 cm (30 cm and 50 cm to the detector, respectively), inner diameters of 50 μm, and outer diameters of 365 μm were used. New capillaries were flushed at 20 psi with 1 M sodium hydroxide for 10 min, water for 10 min, 0.1 M sodium hydroxide for 5 min, and finally with water for 10 min. Before each run, the capillary was rinsed for 3 min with 0.1 M sodium hydroxide, 3 min with water, and 5 min with the separation buffer. Injections were performed hydrodynamically using 0.5 psi for 3 s, and separation voltages ranged from 12-30 kV. Data was collected at 10 Hz with a detector response time of 0.5 s. Capillaries were thermostatted at 25°C in all experiments.

2.4 Results and Discussion

2.4.1 Separation of PSE-Labeled Polyamines by MEKC

Separation between PSE-labeled putrescine, cadaverine, spermidine and spermine was achieved using MEKC with cholate as the surfactant and acetonitrile as an organic modifier. As reported by Nohta et al. [38], the use of organic modifiers is necessary to solvate the pyrene-labeled polyamines, as was evidenced by a decrease in excimer fluorescence in media containing less that ~50% organic solvent. Cholate is a bile salt that forms helical micelles between which analyte molecules may partition based on their hydrophobicity [46-51]. Cholate was chosen over the more commonly used sodium dodecyl sulfate (SDS) because the structure of the bile salt micelle is much more tolerant to the addition of organic solvents [47-49]. Thus cholate has a greater ability to separate highly hydrophobic analytes in the presence of high amounts of organic modifier [47-49].

Since labeled Put and Cad differ by only one methylene group (Figure 2.1), they were the most difficult to separate by MEKC. Therefore, their separation was used to optimize the separation conditions. First, the optimum amount of acetonitrile for both separation and dissolution was determined. Figures 2.6a and 2.6b show the improvement in separation between Put and Cad that was achieved upon decreasing the ACN content from 50% to 27%. The decrease in organic modifier content resulted in a substantial decrease in fluorescence intensity, as evidenced in Figures 2.6a and 2.6b. Little improvement in resolution was achieved by varying the ACN content between 25% and 30%. Generally, highly hydrophobic analytes are best separated when the minimum amount of organic modifier needed for full dissolution is used [52]. This allows for complete solubility of the analytes while minimizing the organic modifier's negative impact on micelle formation. However, as the solubility of the PSE-labeled analytes decreased sharply at 25% ACN, 30% ACN was chosen for the separation of the four PSE-labeled polyamines.

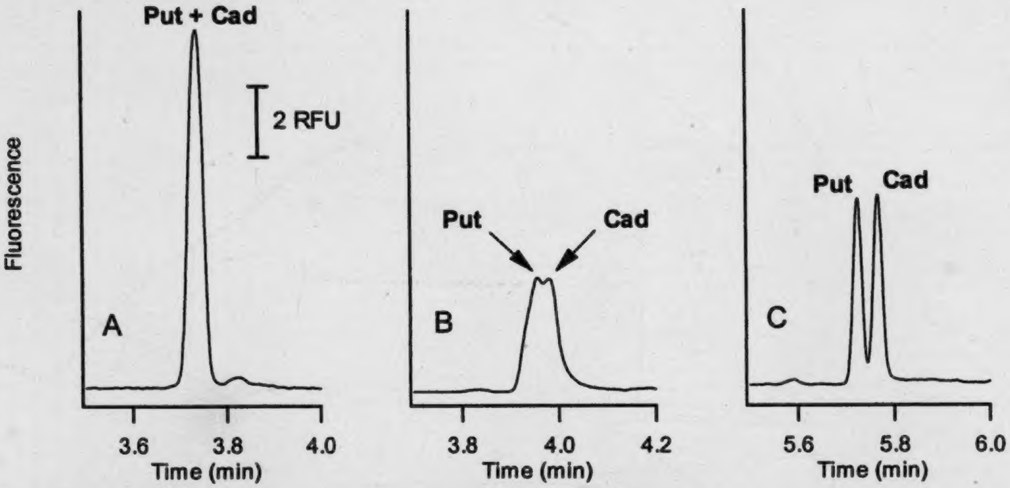

Figure 2.6: Optimization of the separation of PSE-labeled Put and Cad. A mixture of 500 µm Put and 500 µm Cad was derivatized according to the procedure described in Section 2.3.3, and diluted 1000-fold with the separation buffer. (A) 37-cm capillary (30 cm to detector), 20 kV applied voltage, separation buffer: 10 mM pH 7.2 phosphate, 30 mM cholate, 50% ACN. (B) 37-cm capillary (30 cm to detector), 20 kV applied voltage, separation buffer: 10 mM pH 7.2 phosphate, 30 mM cholate, 27% ACN. (C) 57-cm capillary (50 cm to detector), 30 kV applied voltage, separation buffer: 10 mM pH 7.2 phosphate, 30 mM cholate, 27% ACN. Detection was at 490 nm in all cases.

Using 27% ACN and a 37-cm capillary, the resolution between Put and Cad improved from being unresolvable to ~0.6 as the cholate content was increased from 15 to 30 mM, with little improvement observed above 30 mM. Therefore, to minimize Joule heating, 30 mM cholate was used in all further experiments. Also, since adequate resolution for quantification could not be obtained on a 37-cm capillary, the capillary length was increased to 57 cm (50 cm to the detector). The separation voltage was also increased from 20 to 30 kV in order to keep the field strength constant. The increased separation time provided by a longer capillary resulted in a near baseline resolution of 1.1 between Put and Cad (Figure 2.6c). Therefore, a 57-cm capillary was used in all further experiments involving the separation of the four PSE-labeled polyamines. The increase in resolution observed upon increasing the column length is slightly larger than that predicted by the increase in capillary length, indicating that other extra-capillary factors may be significant (eg., injector, detector, etc…).

Using the optimized conditions, Put, Cad, Spd and Spm were separated in under 10 min. The separation is shown in Figure 2.7, where the peaks used for quantification are labeled in bold. Several peaks resulted from PSE and/or its byproducts (evidence for PSE byproducts is presented later), since this derivatization reagent is present at sufficiently high concentration for *inter*molecular excimer complexes to be formed. Also, several distinct peaks were observed for PSE-labeled Spd and Spm. The origin of these peaks is discussed in the next section.

2.4.2 Characterization of Labeled Polyamines

As seen in Figure 2.7, Spd and Spm have multiple peaks resulting from different degrees of labeling. Spermine, having four available amines for labeling (Figure 2.1), was used to study the effects of reaction time and PSE concentration on the extent of the reaction. Figure 2.8 shows the change in Spm peak intensities while varying the PSE concentration between 5 and 20 mM. These experiments were performed using 50% acetonitrile in the buffer, which Nohta et al. [38] had determined to be the optimal organic content for maximum excimer fluorescence. Peak 4 (which corresponds to the Spm peak identified in bold in Figure 2.7) increased in intensity with increasing PSE, while the peak with the shortest migration time (peak 1) decreased in intensity. This implies that

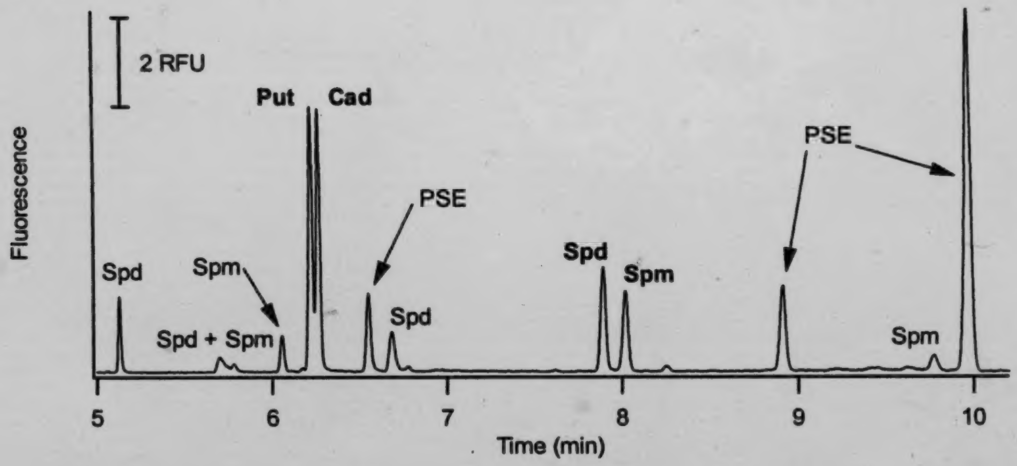

Figure 2.7: Separation of PSE-labeled Put, Cad, Spd and Spm in under 10 min. A solution consisting of 50 μm Put, 50 μm Cad, 50 μm Spm and 50 μm Spd was derivatized according to the procedure described in Section 2.3.3, and diluted 100-fold with the separation buffer. The origin of each peak is identified on the figure. The peaks identified in bold are used for quantification. Separation buffer: 10 mM pH 7.2 phosphate, 30 mM cholate, and 30% ACN. Separation conditions: 57-cm capillary (50 cm to detector), 30 kV applied, detection at 490 nm.

the later-eluting peaks correspond to the more fully labeled analytes. This seems reasonable since more fully substituted polyamines will possess more pyrene groups, increasing their hydrophobicity and thus their partitioning into the cholate micelles. Peak 5 likely results from an impurity in the Spm sample. The product distribution was less dependent on reaction time. Upon increasing the reaction time from 20 to 80 min, the heights of each of the peaks varied by less than 10%. Despite numerous attempts, the reaction could not be driven to completion so as to yield only the fully-labeled polyamines.

As described in Section 2.3.3, the derivatization procedure used for all analyses (except Figure 2.8) involves 10 mM PSE and a 40-min reaction time. This PSE concentration was selected as a compromise between polyamine sensitivity and interferences arising from PSE. Figure 2.8 shows that the fluorescence signal of the fully-labeled Spm increases with increasing PSE concentration. However, interfering peaks arising from the *inter*molecular excimer fluorescence of PSE and its byproducts also increase in intensity as the PSE concentration is increased (evidence for PSE byproducts is presented later). These PSE peaks in Figure 2.8 are not overly problematic since the reaction mixture was diluted 1000-fold prior to analysis. However, 10- and 100-fold dilutions are desirable in order to take full advantage of the sensitivity of the

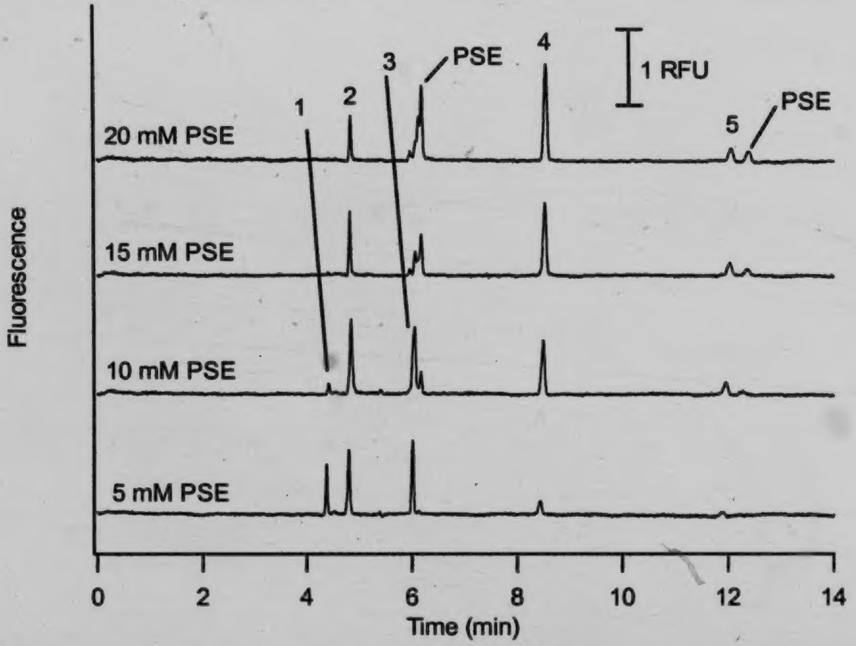

Figure 2.8: Variation in the intensities of the PSE-labeled Spm peaks (peaks 1-5) as a function of PSE concentration. A 500 µm Spm solution was derivatized according to the procedure described in Section 2.3.3, and diluted 1000-fold with the separation buffer. Separation buffer: 10 mM pH 7.2 phosphate, 30 mM cholate, 50% ACN. Separation conditions: 37-cm capillary (30 cm to detector), 12 kV applied voltage, detection at 490 nm.

method. At these lower dilutions, the PSE peaks begin to interfere with the polyamines of interest, especially when 15 or 20 mM PSE is used in the derivatization reaction.

Figure 2.9 illustrates the difference between *inter*molecular and *intra*molecular excimer formation. To confirm that the peaks of interest corresponded to multiply-labeled polyamines exhibiting *intra*molecular excimer fluorescence, and not mono-labeled polyamines or PSE byproducts exhibiting *inter*molecular excimer fluorescence, each polyamine was run using a 400 nm filter as well as the 490 nm filter. If the peaks observed at 490 nm result from intermolecular excimer formation, then the corresponding peaks at 400 nm (monomer fluorescence region) should have even greater intensities. The electropherograms obtained for Spm at each detection wavelength are shown in Figure 2.10. As in Figure 2.8, these studies were performed with 50% acetonitrile in the buffer. The spermine peaks observed at 490 nm clearly result from intramolecular excimer fluorescence, since these peaks have a higher response in the 490 nm (excimer) region than in the 400 nm (monomer) region. Further, most of the PSE byproducts give

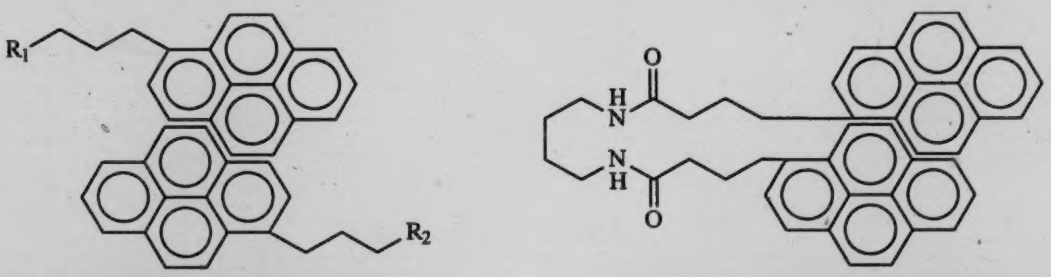

***INTER*MOLECULAR EXCIMER (between 2 pyrene groups on 2 separate molecules)**

***INTRA*MOLECULAR EXCIMER (between 2 pyrene groups on 1 molecule – Put is shown here)**

Figure 2.9: Pictorial representation of the difference between *inter*molecular and *intra*molecular excimer formation.

signals that are orders of magnitude higher in the 400 nm region than in the 490 nm region. Thus the PSE byproducts observed at 490 nm likely result from *inter*molecular excimer fluorescence.

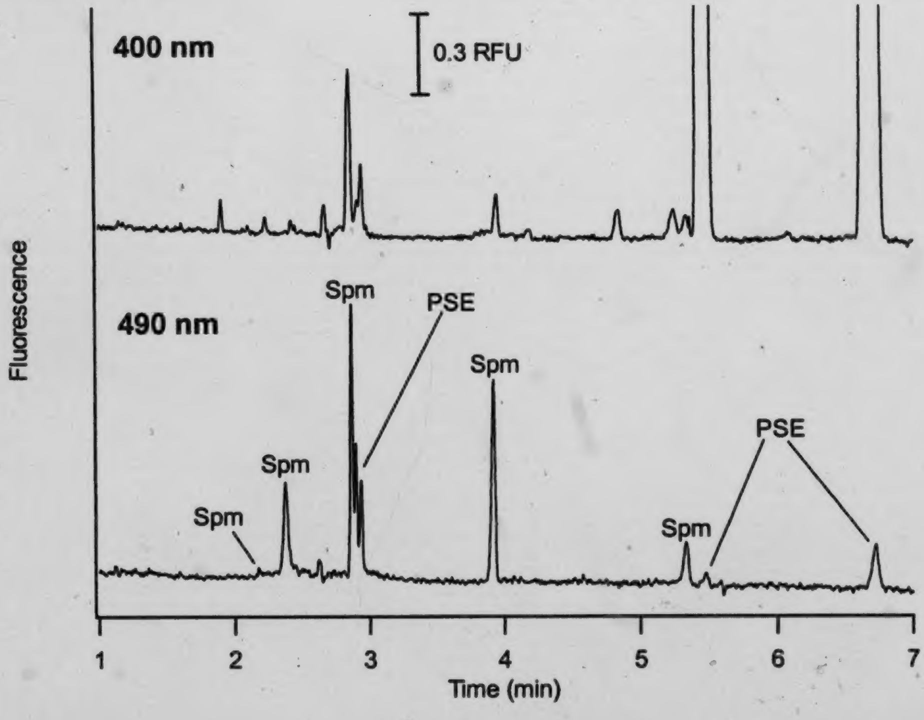

Figure 2.10: Comparison of the fluorescence profiles of PSE-labeled Spm at 400 nm and 490 nm. A 500 μm Spm solution was derivatized according to the procedure in Section 2.3.3, and diluted 1000-fold with the separation buffer. Separation buffer: 10 mM pH 7.2 phosphate, 30 mM cholate, 50% ACN. Separation conditions: 37-cm capillary (30 cm to detector), 20 kV applied voltage.

The origin of the PSE peaks in Figure 2.7 was determined by analyzing a fresh PSE standard solution. The resulting single peak eluted at ~5.5 min using the conditions employed in Figure 2.7, and thus did not correspond to any of the PSE peaks observed. This indicates that following reaction and dilution with the separation buffer, the majority of the remaining PSE has been transformed into unidentified byproducts. Therefore it is these byproducts, not native PSE, that are detected.

2.4.3 Precision and Limits of Detection

The minimum possible dilution of the reaction mixture with separation buffer was determined to be 10-fold. Using this dilution factor, the PSE byproducts became quite large. Nevertheless, the polyamine peaks of interest remained free from interferences. However, below this dilution factor, small impurity peaks began to interfere with the polyamine peaks. Therefore, a 10-fold dilution of the reaction mixture was used in all calibration studies.

The polyamine peaks used for quantification are identified in bold in Figure 2.7. These peaks were chosen because they gave the highest response and were free from interferences with PSE peaks. Although the described method produces multiple peaks for spermidine and spermine, a single peak for each polyamine can be used for quantification owing to the good reproducibility of the technique. Using the peaks highlighted in Figure 2.7, the inter-assay (repeated derivatization and injection of sample) peak height RSD was 7.9% for Put (n=4), 4.1% for Cad (n=4), 6.0% for Spd (n=4), and 3.1% for Spm (n=5). These are superior to those obtained for FQ-labeled polyamines, and should improve with the use of an appropriate internal standard. Further, the intra-assay (repeated injections of same derivatized sample) RSD's (n=3) for Put, Cad, Spd and Spm were 0.2, 0.8, 0.8 and 1.1%, respectively. These are below 2%, which according to Demarest et al. [44] is the maximum allowable variation in peak response for a successful CE analysis. The use of a commercial CE instrument for the PSE studies instead of a home-built instrument (as used in the FQ studies) may partly explain this improvement in inter- and intra-assay reproducibilities.

Using peak height, linear calibration curves were obtained for all four polyamines (Put R=0.998 (n=6), Cad R=0.996 (n=6), Spd R=0.996 (n=5), Spm R=0.994 (n=5)), with y-intercepts that were not statistically different from zero at the 95% confidence level. The detection limits for Put, Cad, Spd and Spm were 2, 2, 4 and 5 nM injected, respectively, as calculated according to eqn 2.1. These correspond to concentrations of 35, 30, 80 and 90 nM in the original sample. These limits of detection are superior to those for FQ-polyamines, and are comparable or superior to those previously reported in the literature for fluorescence detection [27-31].

Sample stacking based on a method described by Palmer et al. [53] (Section 1.2.5.3) was achieved by diluting the reaction mixture 10-fold with a solution containing 10 mM pH 7.2 phosphate, 30% acetonitrile, and 100 mM NaCl. This enabled the injection time to be increased to 30 s without significant deterioration in peak shape for both Spd and Spm (Figure 2.11). The resolution between Spd and Spm in Figure 2.11 is 2.2, which is not significantly different from the resolution of 2.1 observed in Figure 2.7. Comparing the peak heights in Figure 2.11 to those predicted from the calibration curves constructed for the non-stacking experiment, sample stacking yielded a ~17-fold increase in signal for Spd and a ~10-fold increase in signal for Spm. Sample stacking can therefore be employed with this MEKC-LIF technique to improve the detection limits for Spd and Spm. The Put and Cad signals could not be improved through stacking, since the longer injection times resulted in peak overlap. It should be noted that shorter migration times

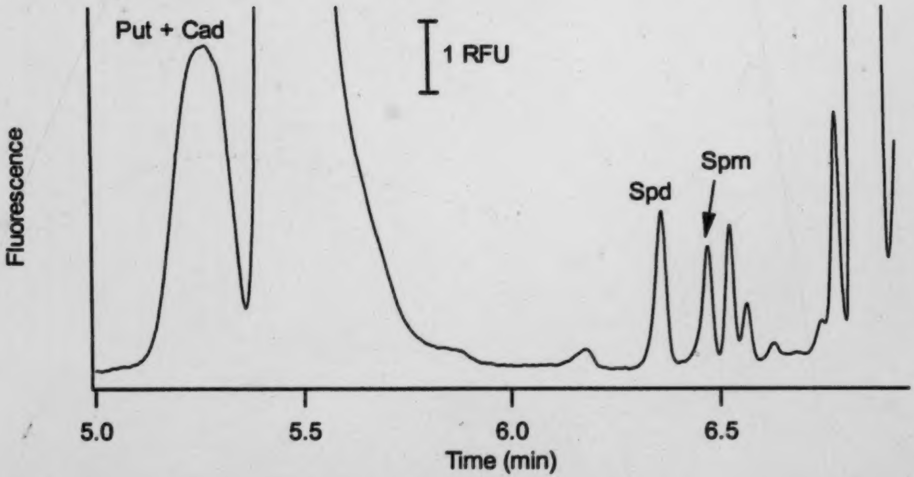

Figure 2.11: Improvement of the method's sensitivity for Spd and Spm by sample stacking. A solution consisting of 1 μm Put, 1 μm Cad, 1 μm Spd and 1 μm Spm was derivatized according to the procedure described in Section 2.3.3, and diluted 10-fold with the dilution buffer. Dilution buffer: 10 mM pH 7.2 phosphate, 100 mM NaCl, 30% ACN. Separation buffer: 10 mM pH 7.2 buffer, 30 mM cholate, 30% ACN. Separation conditions: 57-cm capillary (50 cm to detector), 30 kV applied, 30-s injection, detection at 490 nm.

are observed in the sample stacking studies (Figure 2.11) than in the non-stacking experiments (Figure 2.7). Palmer et al. [53] did not observe such behavior.

2.4.4 Selectivity of the Method

A 10-μM mixture of 17 amino acids was analyzed to demonstrate the selectivity of the method towards polyamines. The corresponding electropherogram is shown in Figure 2.12. As expected, only those amino acids possessing more that one labeling site were detected at 490 nm. L-lysine gave a strong response, while L-arginine and L-histidine gave rather low responses within the time window of interest. Further, none of these amino acid peaks overlapped with the polyamine peaks of interest (Figure 2.7). This demonstrates the selectivity of the method for polyamines, and its suitability for use with biological samples.

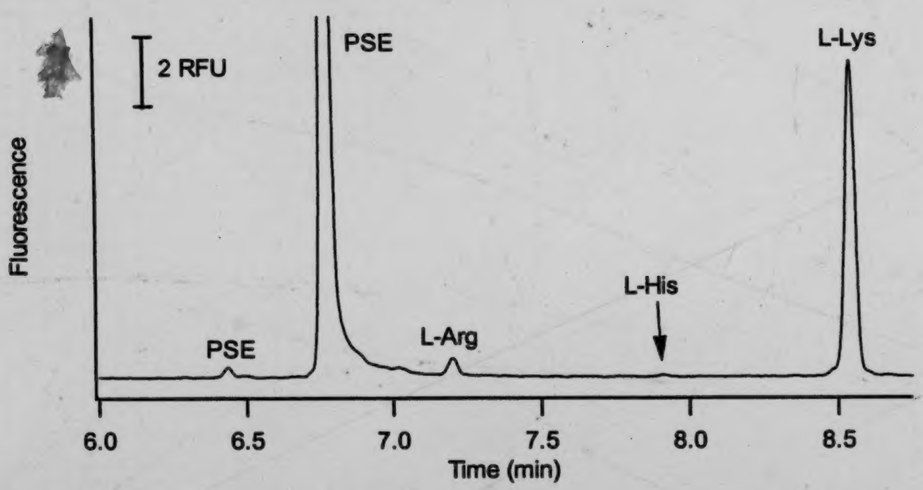

Figure 2.12: Illustration of the selectivity of the method towards polyamines. A solution consisting of 17 amino acids (see Section 2.3.2) was derivatized according to the procedure described in Section 2.3.3, and diluted 10-fold with the separation buffer. Before dilution, each amino acid was at 10 μM except for L-cystine which was at 5 μM. Only three PSE-labeled amino acids gave detectable responses at 490 nm, and are identified in the figure. Separation buffer and conditions as in Figure 2.7.

Until recently, it was believed that agmatine, a polyamine precursor for putrescine, was present only in bacteria. This "bacterial polyamine" is formed from the amino acid L-arginine in the metabolism of many bacteria [54]. However, the presence of agmatine in mammalian tissue has been recently reported [55-57]. Preliminary studies involving the present method showed that agmatine gave two peaks, the second of which overlapped with putrescine.

2.5 Concluding Remarks

PSE-labeled putrescine, cadaverine, spermine and spermidine were separated and quantified in under 10 min using MEKC with LIF detection. Sensitivity, reproducibility and selectivity were superior to those observed for FQ-labeled polyamines. Since polyamines possess several amine labeling sites, the multiple pyrene labels can form intramolecular excimers that emit at longer wavelengths (450-520 nm) than mono-labeled analytes (360-420 nm). Selective determination of the PSE-labeled polyamines was achieved using detection at 490 nm. The insensitivity of the technique towards amino acids containing a single amine group was demonstrated, thus showing that this method would be suitable for complex biological samples. PSE-labeled lysine, arginine and histidine, which emitted excimer fluorescence detectable at 490 nm, did not interfere with the polyamine peaks of interest. The described technique provides polyamine detection limits that are superior or comparable to those previously reported in the literature using fluorescence detection. To our knowledge, this is the first use of PSE with a capillary electrophoretic technique.

2.6 References

(1) Morrison, L. D.; Becker, L.; Ang, L. C.; Kish, S. J. *J. Neurochem.* **1995,** *65*, 636-642.

(2) Romain, N.; Dandrifosse, G.; Jeusette, F.; Forget, P. *Pediatr. Res.* **1992,** *32*, 58-63.

(3) Nairn, L. M.; Lindsay, G. S.; Woster, P. M.; Wallace, H. M. *J. Cell. Physiol.* **2000,** *182*, 209-213.

(4) McCloskey, D. E.; Woster, P. M.; Casero, R. A. J.; Davidson, N. E. *Clin. Cancer Res.* **2000,** *6*, 17-23.

(5) Bergeron, R. J.; Müller, R.; Bussenius, J.; McManis, J. S.; Merriman, R. L.; Smith, R. E.; Yao, H.; Weimar, W. R. *J. Med. Chem.* **2000,** *43*, 224-235.

(6) Heimbecher, S.; Lee, Y.-C.; Tabibi, S. E.; Yalkowsky, S. H. *J. Chromatogr. B* **1997,** *691*, 173-178.

(7) Draisci, R.; Giannetti, L.; Boria, P.; Lucentini, L.; Palleschi, L.; Cavalli, S. *J. Chromatogr. A* **1998,** *798*, 109-116.

(8) Isobe, K.; Yamada, H.; Soejima, Y.; Otsuji, S. *Biochem. Med. Metab. Biol.* **1987,** *37*, 110-120.

(9) Garthwaite, I.; Stead, A. D.; Rider, C. C. *J. Immunol. Methods* **1993,** *162*, 175-178.

(10) Dorhout, B.; Kingma, A. W.; de Hoog, E.; Muskiet, F. A. J. *J. Chromatogr. B* **1997,** *700*, 23-30.

(11) Fu, S.; Zou, X.; Wang, X.; Liu, X. *J. Chromatogr. B* **1998,** *709*, 297-300.

(12) van Eijk, H. M. H.; Rooyakkers, D. R.; Deutz, N. E. P. *J. Chromatogr. A* **1996,** *730*, 115-120.

(13) Rosier, J.; Van Peteghem, C. *Z. Lebensm.-Unters. Forsch.* **1988,** *186*, 25-28.

(14) Whitmore, W. L.; Slotkin, T. A. *Experientia* **1985,** *41*, 1209-1211.

(15) Shimada, K.; Oe, T.; Tanaka, M.; Nambara, T. *J. Chromatogr.* **1989,** *487*, 247-255.

(16) Seiler, N.; Knodgen, B. *J. Chromatogr.* **1980,** *221*, 227-235.

(17) Oefner, P. J.; Wongyai, S.; Bonn, G. *Clin. Chim. Acta* **1992,** *205*, 11-18.

(18) Koning, H.; Wolf, H.; Venema, K.; Korf, J. *J. Chromatogr.* **1990,** *533*, 171-178.

(19) Bontemps, J.; Laschet, J.; Dandrifosse, G.; van Cutsem, J.-L.; Forget, P.-P. *J. Chromatogr.* **1984,** *311*, 59-67.

(20) Koski, P.; Helander, I. M.; Sarvas, M.; Vaara, M. *Anal. Biochem.* **1987,** *164*, 261-266.

(21) Lange, J.; Thomas, K.; Wittman, C. *J. Chromatogr. B* **2002,** *779*, 229-239.

(22) Jorgenson, J. W.; Lukacs, K. D. *Anal. Chem.* **1981,** *53*, 1298-1302.

(23) Wu, S.; Dovichi, N. J. *J. Chromatogr.* **1989,** *480*, 141-155.

(24) Chen, D.; Dovichi, N. J. *Anal. Chem.* **1996,** *68*, 690-696.

(25) Swerdlow, H.; Zhang, J. Z.; Chen, D. Y.; Harke, H. R.; Grey, R.; Wu, S.; Dovichi, N. J.; Fuller, C. *Anal. Chem.* **1991,** *63*, 2835-2841.

(26) Zhao, J. Y.; Dovichi, N. J.; Hindsgaul, O.; Gosselin, S.; Palcic, M. M. *Glycobiology* **1994,** *4*, 239-242.

(27) Kovács, Á.; Simon-Sarkadi, L.; Ganzler, K. *J. Chromatogr. A* **1999,** *836*, 305-313.

(28) Oguri, S.; Watanabe, S.; Abe, S. *J. Chromatogr. A* **1997,** *790*, 177-183.

(29) Oguri, S.; Tsukamoto, A.; Yura, A.; Miho, Y. *Electrophoresis* **1998,** *19*, 2986-2990.

(30) Male, K. B.; Luong, J. H. T. *J. Chromatogr. A* **2001,** *926*, 309-317.

(31) Nouadje, G.; Nertz, M.; Verdeguer, P.; Couderc, F. *J. Chromatogr. A* **1995,** *717*, 335-343.

(32) Rodriguez, I.; Lee, H. K.; Li, S. F. Y. *Electrophoresis* **1999,** *20*, 118-126.

(33) de Montigny, P.; Stobaugh, J. F.; Givens, R. S.; Carlson, R. G.; Srinivasachar, K.; Sternson, L. A.; Higuchi, T. *Anal. Chem.* **1987,** *59*, 1096-1101.

(34) Matuszewski, B. K.; Givens, R. S.; Srinivasachar, K.; Carlson, R. G.; Higuchi, T. *Anal. Chem.* **1987,** *59*, 1102-1105.

(35) Jones, B. N.; Pääbo, S.; Stein, S. *J. Liq. Chromatogr.* **1981,** *4*, 565-586.

(36) Singh, H. N.; Hinze, W. L. *Analyst* **1982,** *107*, 1073-1080.

(37) Schulman, S. G. In *Molecular Luminescence Spectroscopy: Methods and Applications - Part 1*; Schulman, S. G., Ed.; John Wiley & Sons: New York, 1985, pp 1-28.

(38) Nohta, H.; Satozono, H.; Koiso, K.; Yoshida, H.; Ishida, J.; Yamaguchi, M. *Anal. Chem.* **2000,** *72*, 4199-4204.

(39) Yoshida, H.; Nakano, Y.; Koiso, K.; Nohta, H.; Ishida, J.; Yamaguchi, M. *Anal. Sci.* **2001,** *17*, 107-112.

(40) Chen, Z.; Wu, J.; Baker, G. B.; Parent, M.; Dovichi, N. J. *J. Chromatogr. A* **2001,** *914*, 293-298.

(41) Pinto, D. M.; Arriaga, E. A.; Craig, D.; Angelova, J.; Sharma, N.; Ahmadzadeh, H.; Dovichi, N. J. *Anal. Chem.* **1997,** *69*, 3015-3021.

(42) Pinto, D. M.; Arriaga, E. A.; Sia, S.; Li, Z.; Dovichi, N. J. *Electrophoresis* **1995,** *16*, 534-540.

(43) Beale, S. S.; Hsieh, Y.-Z.; Wiesler, D.; Novotny, M. *J. Chromatogr.* **1990,** *499*, 579-587.

(44) Demarest, C. W.; Monnot-Chase, E. A.; Jiu, J.; Weinberger, R. In *Capillary Electrophoresis: Theory and Practice*; Grossman, P. D., Colburn, J. C., Eds.; Academic Press, Inc.: New York, 1992, pp 301-341.

(45) Parent, M.; Bush, D.; Rauw, G.; Master, S.; Vaccarino, F.; Baker, G. *Methods* **2001,** *23*, 11-20.

(46) Cole, R. O.; Sepaniak, M. J.; Hinze, W. L. *J. High Resolut. Chromatogr.* **1990,** *13*, 579-582.

(47) Cole, R. O.; Sepaniak, M. J.; Hinze, W. L.; Gorse, J.; Oldiges, K. *J. Chromatogr.* **1991,** *557*, 113-123.

(48) Nishi, H.; Fukuyama, T.; Matsuo, M.; Terabe, S. *J. Chromatogr.* **1990,** *498*, 313-323.

(49) Aguilar, M.; Farran, A.; Serra, C.; Sepaniak, M. J.; Whitaker, K. W. *J. Chromatogr. A* **1997,** *778*, 201-205.

(50) Yang, S.; Khaledi, M. G. *Anal. Chem.* **1995,** *67*, 499-510.

(51) Muijselaar, P. G.; Otsuka, K.; Terabe, S. *J. Chromatogr. A* **1997,** *780*, 41-61.

(52) Altria, K. D.; Clark, B. J.; Kelly, M. A. *J. High Resolut. Chromatogr.* **1999,** *22*, 55-58.

(53) Palmer, J.; Munro, N. J.; Landers, J. P. *Anal. Chem.* **1999,** *71*, 1679-1687.

(54) Molderings, G. J., MD; Burian, M., MD; Homann, J., MD; Nilius, M., PhD; Göthert, M., MD *Dig. Dis. Sci.* **1999,** *44*, 2397-2404.

(55) Li, G.; Regunathan, S.; Barrow, C. J.; Eshraghi, J.; Cooper, R.; Reis, D. J. *Science* **1994,** *263*, 966-969.

(56) Raasch, W.; Regunathan, S.; Li, G.; Reis, D. J. *Life Sci.* **1995,** *56*, 2319-2330.

(57) Zhao, S.; Feng, Y.; LeBlanc, M. H.; Piletz, J. E.; Liu, Y.-M. *Anal. Chim. Acta* **2002,** *470*, 155-161.

CHAPTER THREE. Theory of Ion Mobility

3.1 Introduction

The success of the polyamine analysis in Chapter 2 was dependent on the proper selection of surfactant and organic modifier for selectivity adjustment. As described in Chapter 1, organic solvents are frequently used to alter selectivity in CE. It is therefore imperative to understand the exact mechanism by which organic solvents alter mobility. Several models have been developed to predict ion mobility. These can be classified into three main categories: 1) models considering only hydrodynamic friction, 2) empirical and semi-empirical models, and 3) models accounting for charge-induced friction. This chapter reviews the success of these models at predicting mobility and solvent-induced selectivity changes, and introduces the model that I will be investigating in the remainder of this thesis. Further, the history of ionic strength theories will be summarized, concluding with the theory that will be employed in the remaining chapters.

3.2 Models Accounting for Hydrodynamic Friction

3.2.1 Hückel Model

As described in Chapter 1, the Hückel equation (eqn 1.5) is the simplest and most commonly used mobility model in CE [1, 2]:

$$\mu_o = \frac{q}{6\pi\eta r} \tag{1.5}$$

Here, μ_o is the absolute ion mobility, q is the ion charge, η is the solvent viscosity, and r is the radius of the ion. The denominator in eqn 1.5 is the hydrodynamic friction coefficient obtained from Stokes' law [3] for spherical particles. The constant *6* was derived assuming that the ion experiences 'perfect stick' conditions. It includes a pressure contribution of $2\pi\eta r$ to the total friction coefficient, and a shear stress contribution of $4\pi\eta r$ [4]. Under 'perfect slip' conditions, the denominator in eqn 1.5 reduces to $4\pi\eta r$. While Stokes' law suggests a constant of *6*, others [4-6] have found that lower values of 2-5 should be used for small ions (r<5 Å).

Since the Hückel equation is related to Stokes' law, it assumes that the ion is spherical and is moving in a continuum fluid [4, 7]. As such, the bulk fluid viscosity (η) is considered instead of the local viscosity in the vicinity of the ion. This continuum approximation is valid provided that the solute is large compared to the solvent [6, 8]. It is therefore not surprising that the Hückel model fails for small ions [7, 8]. To demonstrate this failure, eqn 1.5 can be rearranged into the following form:

$$\mu_o \eta = \frac{q}{6\pi r} \tag{3.1}$$

Given that mobility and conductivity (λ) are related by

$$\mu_o = \frac{\lambda_o}{F} \tag{3.2}$$

where F is the Faraday constant, eqn 3.1 can be expressed in terms of conductivity:

$$\lambda_o \eta = \frac{Fq}{6\pi r} \tag{3.3}$$

Accordingly, for ions of a given charge, the Walden product ($\mu_o\eta$ or $\lambda_o\eta$) should decrease linearly with increasing ion radius.

Figure 3.1 shows the Walden plots constructed for alkali metal (●), halide (▲) and tetraalkylammonium (■) ions using literature data [9] for crystallographic radii and conductivity. A maximum is observed in the Walden plots for alkali metal ions and halide ions. In contrast, the larger tetraalkylammonium ions appear to obey eqn 3.3. Similar behavior has been previously reported [7, 8]. The Hückel model fails at predicting the mobilities of small ions because it was derived for the case of large spherical ions.

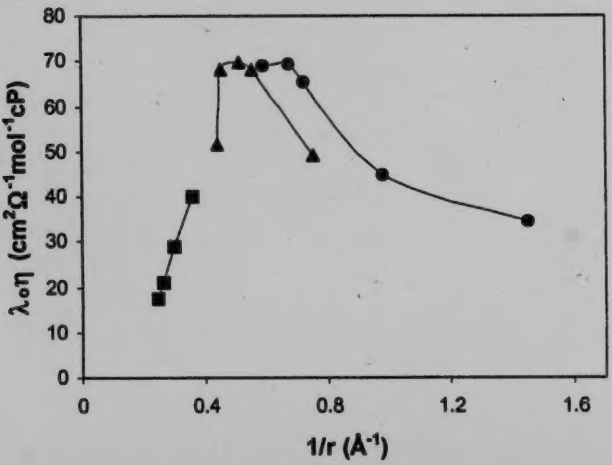

Figure 3.1: Plot of Walden product ($\lambda_o\eta$) versus reciprocal crystallographic radius ($1/r$) for alkali metal (●), halide (▲) and tetraalkylammonium (■) ions in water at 25°C.

Another apparent failure of the Hückel equation is that it does not predict solvent-induced or temperature induced selectivity changes. As described in Chapter 1, organic solvent content and temperature are variables that can be fine-tuned to adjust the selectivity of a separation in CE. However, eqn 3.1 predicts that plots of $\mu_o\eta$ versus temperature or organic solvent content should be horizontal. This is illustrated in Figure 3.2. Contrary to this expected behavior, Kay [7] has shown both positive and negative deviations from the horizontal in plots of $\lambda_o\eta$ versus temperature. A possible reason why the Hückel model fails at predicting solvent- and temperature-induced selectivity changes is that it only considers hydrodynamic friction. This may also explain the failure of the model for small ions, as discussed above. The importance of an additional frictional force is discussed in Section 3.4.

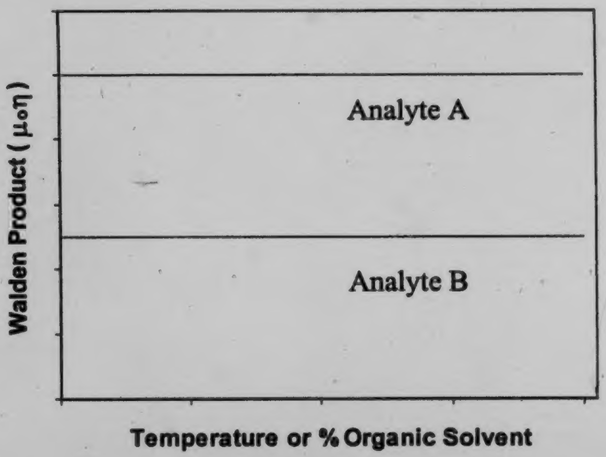

Figure 3.2: Inability of the Hückel equation to predict solvent- and temperature-induced selectivity changes. The Walden products are invariant with solvent content and temperature, such that no selectivity changes are expected.

The discussion above regarding the inability of the Hückel model at predicting solvent-induced selectivity changes has assumed that the radius of the ion (*r*) remains the same as the solvent system is changed. However, if *r* is taken to be the hydrated (solvated) radius of the ion, then it will likely be solvent-dependent. Herein lies another limitation of the Hückel model. The radius of the solvated ion is generally used in eqn 1.5 [1, 10]. However, in reality, *r* is the Stokes' radius [11] and is an adjustable parameter used to fit the Hückel equation to experiment [12]. While the Stokes' radius and the solvated radius are related, they are not the same [9]. This leads to a circular argument: the Stokes' radius must be determined from the ion mobility using eqn 1.5, yet this radius is required in eqn 1.5 in order to predict the mobility! The uncertainty in *r* is a clear limitation of the Hückel model. The use of solvated radii in predicting solvent-induced selectivity changes will be discussed in greater detail in Section 3.4.2.

3.2.2 Perrin's and Elworthy's Shape Models

While the Hückel equation applies to spherical molecules, most ions of interest are not spherical. To compensate for this, a friction ratio ($f_h/f_{h,o}$) can be introduced into eqn 1.5 to correct the friction coefficient for the non-spherical shape of the ion. Eqn 1.5 thus becomes:

$$\mu_o = \frac{q}{6\pi\eta r(f_h / f_{h,o})} \tag{3.4}$$

where f_h is the hydrodynamic friction coefficient of the non-spherical ion and $f_{h,o}$ is the hydrodynamic friction coefficient of a spherical ion of the same volume.

For many molecules, ellipsoids provide a good approximation of the friction ratios [13, 14]. In the 1930's, Perrin [15, 16] developed expressions for $f_h/f_{h,o}$ for ellipsoids in terms of the axial ratios. Figure 3.3 illustrates an ellipsoid with the semi-axes labeled as *a*, *b* and *c*. Perrin derived his expressions for two types of ellipsoids, oblate (disk-shaped) and prolate (cigar-shaped):

oblate ($a<b=c$)

$$\frac{f_h}{f_{h,o}} = \frac{\left[(b/a)^2 - 1\right]^{1/2}}{(b/a)^{2/3}\tan^{-1}\left[(b/a)^2 - 1\right]^{1/2}} \tag{3.5}$$

prolate ($a>b=c$)

$$\frac{f_h}{f_{h,o}} = \frac{\left[1-(b/a)^2\right]^{1/2}}{(b/a)^{2/3}\ln\left\{\dfrac{1+\left[1-(b/a)^2\right]^{1/2}}{(b/a)}\right\}} \tag{3.6}$$

Some values of $f_h/f_{h,o}$ and b/a are available in the literature [14], but they can also be easily calculated. The accuracy of this model is limited by the user's subjective judgement as to how close two of the semi-axes need to be for the equations to be valid.

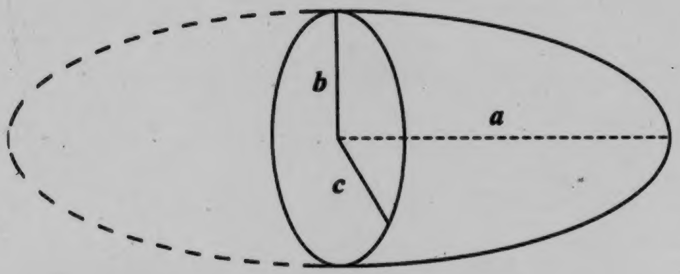

Figure 3.3: Illustration of an ellipsoid showing the different semi-axes.

Elworthy [17] refined Perrin's model to apply to ellipsoids with three different semi-axes. This has the advantage that the classification of an ellipsoidal molecule as either oblate or prolate is avoided. The friction ratio ($a>b>c$) obtained by Elworthy is:

$$\frac{f_h}{f_{h,o}} = \frac{a\left[1-(c^2/a^2)\right]^{1/2}}{rF(\theta,\phi)} \tag{3.7}$$

where F(θ,ϕ) is the elliptic integral of the first kind and θ and ϕ are functions of *a*, *b* and *c*. Some values for F(θ,ϕ) are provided in the literature [18], but the list is far from complete. Elworthy's procedure for determining $f_h/f_{h,o}$ is much more laborious than Perrin's, and has not yet been demonstrated to significantly improve the prediction of electrophoretic mobility [14]. Indeed, Li [19] has reported a relative error of only 0.71% between the friction ratios calculated by the two methods for a series of aromatic carboxylates and sulfonates.

Although these ellipsoidal models improve our understanding of electrophoretic mobility, their success is still limited. Indeed, not all molecules can be approximated as ellipsoids. Previous studies in our research group [19-21] have shown that Perrin's model cannot accurately predict the mobilities of small ions in CE. Further, these ellipsoidal models fail to explain solvent- and temperature-induced selectivity changes.

3.2.3 Gurney-Frank-Wen Model

As described in Section 3.2.1, plots of Walden product versus either temperature or $1/r$ deviate from the behavior predicted by the Hückel equation. Gurney [22] was the first to provide a reasonable explanation for these deviations. He introduced the concept of an *ionic cosphere*, which is the part of the solvent surrounding an ion whose physical properties are different from those of the bulk solvent due to the presence of the ion [7].

In 1957, Frank and Wen [23] proposed a model that demonstrated Gurney's ideas. In this model, which was developed for aqueous systems, three distinct solvent regions (Figure 3.4) exist around an ion. These regions result from the competing orienting influences of neighboring solvent dipoles and ionic charge that act on any given water molecule. In region A, water molecules are immobilized around the ion by electrostriction, resulting in a solvation shell. In region C, where the effects of the ionic

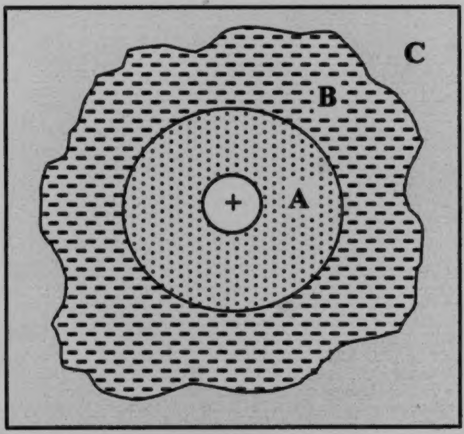

Figure 3.4: The different solvent regions surrounding an ion, according to the Gurney-Frank-Wen model. (A) Region of immobilized water molecules due to electrostriction (*structure-making*). (B) Region of *structure-breaking*. (C) Bulk water.

charge are insignificant, the water molecules will be oriented by their neighboring solvent molecules and will have the properties of pure water. In the intermediate region B, the ionic charge will not be strong enough to orient the solvent molecules completely as in A, but will interfere with the normal water structure present in C. This region will be one with less solvent structure than in pure water, and is referred to as the *structure-breaking* region.

According to the Frank-Wen model, ions can be separated into three main categories [7]. The first class contains those ions which are small and have large charge densities. For these ions, the cosphere contains a strongly-bound layer of oriented water molecules (electrostriction, region A), resulting in an increase in the effective ion radius. The Walden products for these ions are therefore less than predicted by the Hückel equation, and are generally invariant with temperature since the solvent binding is strong. Ions generally exhibiting this *structure-making* or *structure-forming* behavior include F^-, OH^-, and cations with higher charge densities than K^+ [23].

Larger ions with lower charge densities are in a second category of ions. The charge density of these ions is insufficient to completely orient most of the water molecules, but is sufficient to interfere with the normal three-dimensional structure of water [7]. Region B (Figure 3.4) is therefore significant, and the ions are surrounded by less-structured water whose viscosity is less than that of bulk water. Such ions have been described as *structure-breakers*, and have mobilities greater than predicted by the Hückel equation. Since water structure increases with decreasing temperature, these ions have Walden products that increase with decreasing temperature. Such behavior will be observed in Chapter 7. Ions exhibiting *structure-breaking* behavior include cations with equivalent or lower charge densities than K^+, as well as anions with lower charge densities than F^- [23].

The third class includes large ions with hydrophobic surfaces, such as quaternary ammonium ions possessing large hydrophobic side chains. These ions are postulated to be surrounded by water molecules which are more highly hydrogen-bonded than in bulk water [7, 24]. This *structure-making* behavior results in lower-than-expected Walden products. However, in contrast to the first class of ions, the Walden products should increase with temperature since hydrogen-bonding decreases with increasing temperature.

The Gurney-Frank-Wen model can explain some of the anomalous mobility behavior observed in aqueous media, such as the temperature dependence of Walden products and the lower-than-expected mobilities observed for small ions of high charge density (Figure 3.1). While the concepts can be extended to other solvent systems, the theory is limited by its qualitative nature. Without a mathematical representation, it is difficult to apply this model for mobility prediction.

3.3 Empirical and Semi-Empirical Models

The lack of success of the fundamental models at predicting mobility has prompted the development of numerous empirical and semi-empirical mobility models for specific classes of compounds. These models correlate the experimental mobility of an ion to some of its physicochemical parameters, such as charge, molecular weight, etc. Although empirical and semi-empirical models lack sound theoretical rationale for all of the terms that appear in their equations, they are generally practical and easy to use. This section describes several of these models. They will be divided into two main categories: 1) models designed for mobility prediction in aqueous media, and 2) models designed for mobility predicting in aqueous-organic media.

3.3.1 Mobility Prediction in Aqueous Media

Empirical correction factors have been commonly introduced into Stokes equation (denominator in eqn 1.5) in order to validate its use. As mentioned briefly in Section 3.2.1, a constant of less than 6 should be used in the denominator of eqn 1.5 for molecules in water having radii < 5 Å [4]. The determination of these empirical constants is discussed in greater detail here. Just as mobility can be expressed by the Hückel equation (eqn 1.5), diffusion coefficients (D^o) can be expressed by:

$$D^o = \frac{k_B T}{n\pi\eta r(f_h / f_{h,o})} \tag{3.8}$$

where k_B is Boltzmann's constant and T is the absolute temperature. When the friction ratio ($f_h/f_{h,o}$, Section 3.2.2) is 1 and n is 6, eqn 3.8 is known as the Stokes-Einstein equation. For 44 widely different molecules in water, Edward [4] compared literature diffusion coefficients to those predicted by eqn 3.8, and determined the optimal value of n for each molecule. His results are illustrated in Figure 3.5 as a function of the van der Waals radii of the molecules (r_W). Using the solid curve in Figure 3.5, Edward proceeded to tabulate optimal values of n for different values of r_W. These values are presented in Table 3.1. Clearly, for molecules in water having radii < 5 Å, the Stokes' friction coefficient (denominator in eqn 3.8 with f/f_o=1) must be modified by using a constant n less than 6. The empirical constants in Table 3.1 can also be applied to the Hückel equation (eqn 1.5), since this model is related to the Stokes' friction coefficient as well. Other researchers [25-27] have proposed empirical corrections to the Stokes equation, but they are based on a limited amount of data and are less successful than Edward's tabulated values [4]. Although these empirical correction factors improve the success of the Hückel equation, they do not provide any understanding as to why the model fails in the first place. In other words, it remains unclear what the adjustment in *n* is precisely correcting for.

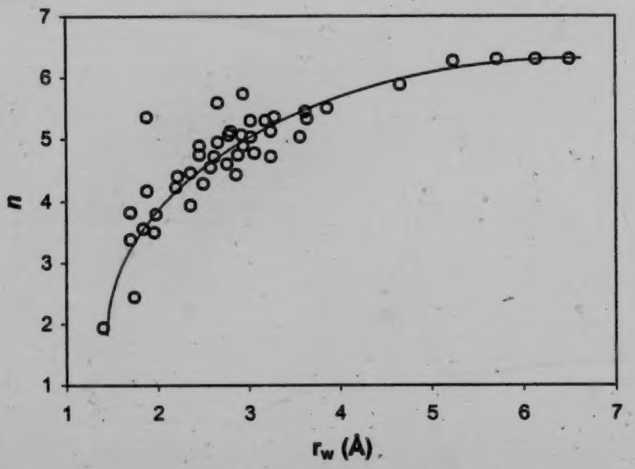

Figure 3.5: Empirical constants of *n* in the Stokes-Einstein equation (eqn 3.8), as determined by Edwards [4]. Constructed using the data in ref 4.

Table 3.1: Dependence of the Empirical Correction Factor *n* on the van der Waals Radii (r_w), as Determined by Edward [4] from the Solid curve in Figure 3.5

r_w (Å)	*n*	r_w (Å)	*n*
1.5	2.2	3.5	5.4
2.0	3.9	4.0	5.6
2.5	4.8	4.5	5.8
3.0	5.1	5.0	6.0

In 1966, Offord [28] developed an empirical model to describe the mobility of peptides in paper electrophoresis. He assumed that the frictional drag experienced by the peptide was related to its surface area, which in turn is proportional to (molecular mass)$^{2/3}$. His expression for ion mobility is:

$$\mu_o = \frac{kq}{M^{2/3}} \tag{3.9}$$

where μ_o is the absolute mobility of the peptide, k is an empirical constant, q is the net peptide charge, and M is the molecular mass of the peptide. The mobility of a peptide is therefore predicted to vary linearly with $M^{2/3}$. In addition to applying to paper electrophoresis, several researchers have shown that this model is also successful at predicting peptide mobility in capillary electrophoresis [29-31]. However, since the Offord model was developed assuming a spherical shape for the peptides, it cannot account for differences in peptide conformation and charge distribution. Indeed, Bayer and coworkers [32] have reported that although Offord's model works quite well for peptides with different values of $q/M^{2/3}$, it cannot differentiate between peptides with similar charge-to-mass ratios.

Grossman et al. [33] have also proposed a semi-empirical model for peptide mobility in free-solution capillary electrophoresis:

$$\mu = \frac{k\ln(q+1)}{n_a^{0.43}} \tag{3.10}$$

In eqn 3.10, μ is the peptide mobility, q is the peptide charge, k is an empirical constant related to the solvent system, and n_a is the number of amino acids in the peptide chain. This equation was derived by treating the peptide as a classical polymer in solution, and using the simplest model of a 'freely joined chain' to describe its molecular size. For 40 peptides consisting of 3-39 amino acids, a plot of μ versus $1/n_a^{0.43}$ showed good correlation (r=0.989). However, as with the Offord model, the Grossman model does not account for differences in peptide conformation or charge distribution. As a result, it cannot differentiate between peptides with similar charge-to-size ratios [32]. Further, Grossman et al. themselves reported that eqn 3.10 was not successful at predicting protein mobilities, possibly due to the tighter folding conformation observed in proteins than in peptides [33].

Jokl [34] has empirically modeled the mobility of organic anions, cations, and metal complexes in paper electrophoresis using the expression:

$$\frac{\mu}{z} = \frac{14.7}{\sqrt{M}} - 0.29 \tag{3.11}$$

where z is the ion charge and M is the molecular mass of the ion. Although no theoretical rationale is given for the square-root dependence of molecular mass, this relationship yielded an average relative error of only 8.6% for a set of 27 organic anions, 13 organic cations and 20 metal complexes [34].

Fu and Lucy [20] have recently proposed an empirical model to predict the mobilities of aliphatic monoamines in aqueous media. Their model is based on the molecular weight (M) of the monoamine, and incorporates the effects of hydration using the McGowan waters of hydration increments (H):

$$\mu_o = \frac{(5.55 \pm 0.73) \times 10^{-3}}{M^{0.579 \pm 0.026} + (0.171 \pm 0.054)H} \tag{3.12}$$

This expression was derived using a data set comprised of 34 monoamines possessing no other functional groups. With this data set, eqn 3.12 yielded an average prediction error of 4.1%. When tested against other literature and experimental data sets, the average prediction errors were 7.2% and 3.3%, respectively [20]. While this model is successful at predicting aliphatic monoamine mobilities, it is doubtful that it can be extended to other classes of solutes.

An empirical mobility model accounting for both size and shape effects has been proposed by McKillop et al. [35] to predict the electrophoretic mobilities (μ) of alkylpyridines. In this model, the van der Waals radii (r_w) are used as size parameters and the rotational radii (r_{rot}) and inertial radii (r_i) are used as shape parameters:

$$\mu = \left(3.22\frac{1}{r_w} + 0.570\frac{1}{r_{rot}} - 0.0114\frac{1}{r_i} - 0.604 \right) \times 10^3 \tag{3.13}$$

The various radii are determined by molecular modeling. Eqn 3.13 shows that the size factor (r_w) is by far the most dominant term, confirming that shape effects do not significantly affect mobility. Similar conclusions have been previously documented [20, 21]. While the McKillop model accurately predicts n-alkylpyridine mobilities to within 4%, it was developed for a very specific data set and will likely not extend to other solute classes. Indeed, McKillop et al. have themselves noted that their model has only limited success at predicting the mobilities of alkenylpyridines and alkylpyridines with branched alkyl chains [35].

In recent years, artificial neural networks [36, 37] have been used to predict the mobilities of sulfonamides, alkylpyridines and alkenylpyridines in capillary electrophoresis. An artificial neural network is a mathematical system that simulates a biological neural network. It consists of a number of 'neurons' (regression equations) that receive data from the outside, process the data, and output a signal. Although the predictive ability of these neural networks is impressive (yielding standard errors of prediction of less than 2% for the above-mentioned analytes), they are developed for limited data sets. The network must be 're-trained' before it can be applied to a different class of solutes, which is rather time consuming. Further, when neural networks are used to predict mobility, the user is not rewarded with a better understanding of the factors influencing ion migration.

The above empirical and semi-empirical models have been developed to describe mobility in aqueous media. Consequently, they cannot explain solvent-induced selectivity changes. The next section deals with empirical and semi-empirical mobility models that have been specifically developed to account for such effects.

3.3.2 Mobility Prediction in Aqueous-Organic Media

Jouyban and coworkers [38-41] have presented mathematical models and mixture response surface methods to correlate/predict the electrophoretic mobilities of acidic and basic analytes in capillary electrophoresis at different concentrations of organic modifier. Their first investigation [38] involved equations of the form:

$$\ln \mu = f_w \ln \mu_w + f_c \ln \mu_c + L_o f_c f_w + L_1 f_c f_w (f_c - f_w) \tag{3.14}$$

and

$$\ln \mu = 1 - \frac{J_1 f_c}{f_c + \Lambda_1 f_w} - \frac{J_2 f_w}{\Lambda_2 f_c + f_w} \tag{3.15}$$

where μ_c and μ_w denote the electrophoretic mobilities in organic modifier and water, respectively, f_c and f_w denote the volume fractions of organic modifier and water, respectively, and L_o, L_1, J_1, J_2, Λ_1 and Λ_2 are the model constants. Eqn 3.14 is reorganized from a model originally presented for calculating the viscosity of aqueous and nonaqueous binary solvent mixtures [38]. Eqn 3.15 is a modified form of the Wilson model, which is used for calculating solute solubilities in mixed solvent systems [38]. When these models were tested against the data set used to generate the model constants (a set of 5 benzoic and naphthoxyacetic acids in methanol-water media), eqns 3.14 and

3.15 gave average prediction errors of 0.6% and 1.0%, respectively. Further studies were performed whereby model constants were generated using a limited data set (4 methanol contents), and then used to predict mobilities at other methanol concentrations. The resulting average prediction errors were 1.2% for eqn 3.14 and 0.8% for eqn 3.15. It was thus reasoned that eqn 3.14 is more successful when a large amount of experimental data is available for computing the model constants, whereas eqn 3.15 is preferred when a limited number of experiments are used for building the model.

In a more recent investigation [39], the authors investigated the ability of a modified form of eqn 3.14 at correlating/predicting electrophoretic mobility in methanol-water media. The modified expression is:

$$\ln \mu = f_c^3 \ln \mu_c + f_w^3 \ln \mu_w + A_o f_c f_w + A_1 \left[\frac{f_c f_w}{f_c (M_c / M_w)^2 + f_w} \right] \qquad (3.16)$$

where M_c and M_w are the molecular weight of organic modifier and water, and A_o and A_1 are the curve-fit parameters. These parameters represent solvent-solvent and solvent-solute interactions in the electrophoretic media. When this model was tested against the data set used to generate the curve-fit parameters (a set of 5 basic drugs in methanol-water media), an average prediction error of 0.6% was achieved. As in their initial investigation [38], further studies were performed whereby curve-fit parameters were generated using a limited data set (4 methanol contents), and then used to predict mobilities at other methanol concentrations. The resulting average prediction error was 1.4%. The small prediction errors of eqns 3.14-3.16 suggest that these models can be used to predict mobility at any methanol content. However, these models were developed using very limited data sets for which the curve-fit parameters were determined. They cannot be used to predict the mobilities of other solutes without first determining new curve-fit parameters for the specific solutes of interest. Further, these empirical models do not fundamentally explain the mobility behavior in aqueous-organic media.

Another mathematical model has been developed by Guillaume et al. [42] to describe the mobility of benzoate derivatives in acetonitrile-water media. While this model accounts for the influence of pH and pK_a on mobility, the authors are unique in their consideration of effects pertaining to solvent cluster formation. The final expression, which contains terms relating to the kinetics of acetonitrile cluster formation and solute solvation, is rather lengthy and complex, and is therefore not shown here. Suffice it to say that the correlation between the experimental and predicted mobilities for 12 benzoate derivatives was excellent, with a slope of 1.000 and a correlation coefficient of 0.994. Moreover, the authors were successful in using their expression to optimize the selectivity between these 12 solutes. However, as was the case with the previous models, the unknown constants were determined for a specific class of solutes and must therefore be recalculated if the model is to be used for other analytes and solvent systems. Further, by using this empirical model, little knowledge is gained concerning the mechanism of solvent-induced selectivity changes.

It is generally accepted that the electrophoretic mobility of a solute is a function of the mobility of each charged species and its corresponding molar fraction. Based on this principle, Barrón et al. [43, 44] developed a semi-empirical mobility model for quinolones in acetonitrile-water media that accounts for the effect of activity coefficients, pK_a values and solvent pH. Their resultant expression is:

$$\mu_e = \frac{a_{H^+}^2 \mu_a + K_{a1}K_{a2}\mu_b}{a_{H^+}^2 + K_{a1}a_{H^+}y + K_{a1}K_{a2}} \qquad (3.17)$$

where μ_a is the mobility of the fully protonated quinolone (H_2Q^+), μ_b is the mobility of the fully deprotonated species (Q^-), a_{H+} is the hydrogen ion activity in the acetonitrile-water media, K_{a1} and K_{a2} are the acid dissociation constants of the quinolone in the acetonitrile-water media, and y is the activity coefficient of the species H_2Q^+ or Q^-. No rationale was given for the inclusion of the activity coefficient in the denominator of eqn 3.17. This equation allows the calculation of electrophoretic mobility for any substance at any pH, provided that the values of μ_a, μ_b, y, pK_{a1} and pK_{a2} are known. Although this model can explain the mobilities of quinolones in acetonitrile-water media based on changes in solvent pH and analyte pK_a, it cannot account for all of the solvent-induced selectivity changes that have been observed in the literature. For example, the migration order reversal observed [45] between NO_3^- and SO_4^{2-} (conjugate bases of strong acids) at pH 9.5 and 10% (v/v) methanol cannot be explained by changes in solvent pH and solute pK_a.

The development of the above empirical and semi-empirical mobility models was prompted by the failure of the Hückel model at predicting solvent-induced selectivity changes. While these models are successful within the class of solutes and solvent systems for which they were developed, they cannot be universally extended to explain all mobility behavior. In the next section, the discussion returns to fundamental mobility models that incorporate an additional friction term not considered by Hückel, Perrin or Elworthy: charge-induced friction.

3.4 Models Accounting for Charge-Induced Friction

3.4.1 What is Charge-Induced Friction?

One of the main limitations of the Hückel equation (eqn 1.5) is that it only considers hydrodynamic friction (viscous drag). Indeed, it seems likely that an ion will also experience an additional frictional force due to its charge. The friction resulting from the interaction between the ion and the solvent dipoles is what is referred to as *charge-induced friction*.

The effects of charge-induced friction have been included in some semi-empirical mobility models. Lucy and coworkers [21, 46] have used analyte pK_a, pK_b and z^2/volume as estimates of charge-induced friction for carboxylates, sulfonates and amines. These terms were incorporated into equations of the general type:

$$\mu_o = \frac{Az}{BV_o^x + CF_{CI}} \tag{3.18}$$

where A, B, C and x are constants, z is the solute charge, V_o is the solute volume, and F_{CI} is the charge-induced friction term represented by either pK_a, pK_b or z^2/volume. The incorporation of z^2/volume in eqn 3.18 resulted in the successful prediction of aqueous aromatic carboxylate mobilities to within 4.4% [21]. The use of pK_a and pK_b values yielded average mobility prediction errors of 3.7% and 4.5% for aliphatic carboxylates and monoamines, respectively. Further, a semi-empirical mobility model based on the additivity of friction coefficients relative to the charged and uncharged parts of a molecule has been proposed by Cottet et al. [47, 48]:

$$\mu_o = \frac{ze}{f_b + n_o \delta\mathcal{F}_o + z\delta\mathcal{F}^{\pm}} \tag{3.19}$$

In eqn 3.19, z is the overall solute charge number, e is the elemental charge, f_b is the hydrodynamic friction coefficient associated with the solute backbone, n_o is the number of identical ionizable acido-basic moieties attached to the backbone, $\mathscr{F}_o$ is the hydrodynamic friction coefficient for an uncharged moiety, and $\mathscr{F}^{\pm}$ is the friction due to the charge of each moiety. This equation was used to predict the aqueous mobilities of polystyrenesulfonates, polycarboxylates, dichondroitin sulfates, fatty acids, polyanalines, polyglycines, and polycytidines.

The above models described semi-empirical representations of charge-induced friction. There exist two fundamental pictures of this friction: the solvent-berg model and the dielectric friction model. These two models are discussed in detail in the proceeding sections.

3.4.2 Solvent-Berg Model

The first and oldest picture of charge-induced friction is the *solvent-berg* model [10, 25, 49]. In this model, the solvent molecules are immediately adjacent to the ion and are rigidly bound to it. This is what is referred to when one talks of the hydration or solvation shell, and is equivalent to the structure-making region in the Gurney-Frank-Wen model (Section 3.2.3). The ion moves through solution together with its solvation shell, forming an entity that is termed a 'solvent-berg'. This is illustrated pictorially in Figure 3.6. Since the solvent-berg has an effective radius that is larger than the radius of the bare ion, the ion mobility will be less than predicted by the Hückel equation. The relative size of the solvent-berg increases as the crystallographic radius of the ion decreases, such that solvation affects the mobilities of small ions to a greater extent than

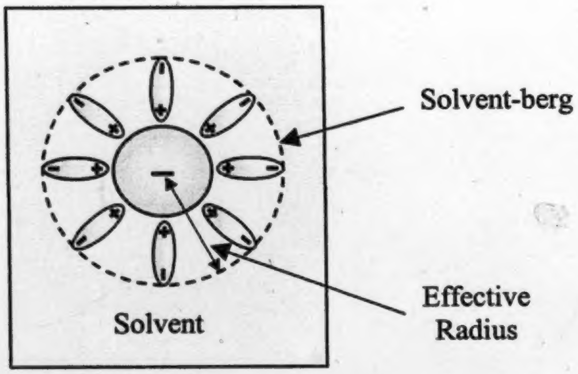

Figure 3.6: Pictorial representation of a solvent-berg.

for large ions. Therefore, the solvent-berg model can qualitatively explain the failure of the Hückel equation for small ions seen in Figure 3.1.

The solvent-berg model can be expressed quantitatively by considering an ion's 'solvation number', which is the number of solvent molecules which remain with the ion while it moves through solution. The radius of the bare ion together with its solvation shell is referred to as the 'solvated' radius of the ion, and is often used in place of Stokes' radius in eqn 1.5 [1, 10] (as mentioned in Section 3.2.1). Obviously, as the solvent composition is varied, the number and type of solvent molecules that are bound to the ion will change. The consequent variation in the 'solvated' radius may enable the Hückel equation (eqn 1.5) to account for some solvent-induced selectivity changes. However, the solvent-berg model is difficult to quantify, as is reflected by the discrepancies in hydration numbers reported for even simple ions in pure water [10, 50]. Table 3.2 lists some hydration numbers determined using different methods of measurement [50]. Indeed, Bockris and Reddy [10] have reported hydration numbers ranging between 1-71 for Na^+.

The uncertainty in hydration/solvation numbers makes it difficult to use the Hückel equation as a predictive tool for solvent-induced selectivity changes.

Table 3.2: Hydration Numbers in Pure Water for Simple Ions Obtained by Different Methods [50]

Ion	Method 1	Method 2	Method 3
Li^+	2.3	5.2	7.4
Ba^{2+}	10.3	5.3	9.6
Me_4N^+	0.4	1.3	1.8
F^-	6.7	2.7	5.5
I^-	0.6	1.6	2.8
CH_3COO^-	4.0	2.2	1.1

3.4.3 Dielectric Friction Model

3.4.3.1 Theory of Dielectric Friction

An alternate model of charge-induced friction is that of *dielectric friction*. The concept of dielectric friction was first introduced by Max Born in 1920 [51], whereby he modified the hydrodynamic model by considering the dynamic perturbation of the solvent orientation caused by the ion's charge. Dielectric friction results from the non-instantaneous relaxation (back to equilibrium positions) of the solvent dipoles behind the migrating ion. Consequently, an excess of oriented solvent dipoles exists behind the moving ion, which creates a small electric field that opposes the ion's motion. This is pictured in Figure 3.7. The retarding force experienced by the ion as a result of the unsymmetrical solvent polarization cloud is termed dielectric friction. By assuming that the hydrodynamic and dielectric contributions to friction were additive, Born developed an expression for the overall friction experienced by an ion moving through a viscous continuum:

$$f_t = f_h + f_d \tag{3.20}$$

Here, f_t is the total friction coefficient of the ion, and f_h and f_d are the hydrodynamic (viscous drag) and dielectric (charge-induced) friction coefficients, respectively.

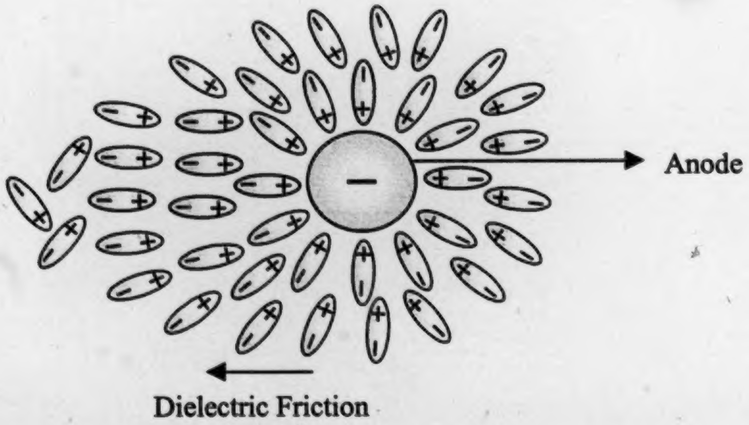

Figure 3.7: Pictorial representation of the retarding force (dielectric friction) experienced by an ion due to the non-instantaneous relaxation of solvent dipoles.

Although Born introduced the concept of dielectric friction in 1920, his ideas were not fully appreciated until the late 1950's when a resurgence in interest in mobility and conductivity was observed throughout the scientific community. The mobility models that emerged from Born's initial ideas can be divided into two categories: 1) continuum dielectric friction models, and 2) molecular dielectric friction models. These are discussed below.

3.4.3.2 Continuum Dielectric Friction Models

Before discussing the evolution of these models, the meaning of the term *continuum* should be clarified. Continuum models represent the solvent as a viscous dielectric continuum. In other words, they assume that there is a continuous medium up to the surface of the ion, and therefore ignore the molecularity of the solvent. Continuum models do not address the microscopic mechanism of ion motion in terms of the solvent structure or the ion-solvent interactions [8, 52].

3.4.3.2.1 The Evolution of Continuum Dielectric Friction Models

Following its introduction in 1920, the concept of dielectric friction remained undeveloped until 1959. At this time, Fuoss [53] noticed the effect of dielectric constant on ionic conductivity in mixed solvents and invoked a dielectric relaxation effect like Born's to explain this behavior. He suggested that the variation in the Walden product with solvent content was due to the electrostatic interaction between the fields of the moving ions and those of the solvent dipoles in the surrounding solvent. This electrostatic coupling between the ion and the solvent could be regarded as an effective increase in the local viscosity surrounding the ion. The equation proposed to account for such effects was:

$$\lambda_o = \frac{Fq}{1800\pi\eta(r_\infty + B/\varepsilon)} \tag{3.21}$$

where λ_o is the limiting ion conductivity, q is the ion charge, F is the Faraday constant, η is the solvent viscosity, r_∞ is the hydrodynamic radius of the ion in a hypothetical solvent of infinite dielectric constant, B is an empirical constant, and ε is the static (low frequency) solvent dielectric constant (refer to Section 3.4.3.2.2 for a definition of ε). B and r_∞ are determined from the intercept and slope of a plot of $r_s\varepsilon$ versus ε, respectively, where r_s is the ion radius calculated from Stokes' law.

In 1961, Boyd [54] refined Fuoss' semi-empirical model by treating Fuoss' concepts theoretically on a macroscopic basis. His resultant theoretical expression for the dielectric friction coefficient was:

$$f_d = \frac{4}{9}\left(\frac{q^2\tau}{r^3\varepsilon}\right) \tag{3.22}$$

where q and r are the ion charge and radius, respectively, and τ is the single Debye relaxation time of the solvent system. Using this model, Boyd showed that the dielectric relaxation times of polar solvents are of such a magnitude that dielectric relaxation does contribute significantly to the frictional force experienced by an ion. This was the first indication that conductivity/mobility is governed in part by the solvent relaxation time (τ).

Although Boyd's derivation is based on essentially correct ideas, it contains some approximations that lead to slightly incorrect numerical results [55]. In 1963, Zwanzig [55] used a different derivation method to obtain a corrected version of eqn 3.22. Under 'perfect stick' conditions (refer to Section 3.2.1), his expression for conductivity was:

$$\lambda_o = \frac{Fq}{6\pi\eta r + \frac{2}{3}\frac{\tau q^2}{r^3}\left(\frac{\varepsilon - \varepsilon_\infty}{\varepsilon^2}\right)} \tag{3.23}$$

where ε and ε_∞ are the low and high frequency dielectric constants, respectively. These parameters will be explained in detail in Section 3.4.3.2.2. The left-hand term in the denominator is the hydrodynamic (viscous drag) friction predicted by Stokes, and the right-hand term in the denominator is the dielectric friction. Under 'perfect slip' conditions, the constant *6* in eqn 3.23 becomes *4*.

While Boyd's (eqn 3.22) and Zwanzig's (eqn 3.23) theories qualitatively explain ionic conductivity/mobility data, they are in serious quantitative disagreement with experiment [56]. One of the main reasons for this is that they treat the dielectric friction independently of the hydrodynamic friction. In other words, they assume that the hydrodynamic disturbance of the solvent due to the ionic motion has no influence on the dielectric relaxation, and vice versa [54]. In 1970, Zwanzig [57] proposed a revised theory to account for such effects. According to this revised model, ion conductivity under 'perfect stick' conditions is described by:

$$\lambda_o = \frac{Fq}{6\pi\eta r + \frac{3}{8}\frac{\tau q^2}{r^3}\frac{(\varepsilon - \varepsilon_\infty)}{\varepsilon(2\varepsilon + 1)}} \tag{3.24}$$

For 'perfect slip' conditions, the constants *6* and *3/8* become *4* and *3/4*, respectively. This theory partially considers the influence of solvent flow on solvent polarization, but does not consider the reciprocal effect [56]. Nonetheless, the agreement between experiment and theory did improve [58]. The success of the revised Zwanzig model (eqn 3.24) at predicting conductivity in methanolic media is illustrated in Figure 3.8 (reprinted with permission from Biswas et al. [8]). For the small ions, this model clearly over-estimates the dielectric friction and predicts conductivities that are much lower than the observed experimental values.

Hubbard and Onsager [59, 60] were the first to fully consider the coupling between hydrodynamic (viscous) momentum transfer and dielectric relaxation. In the words of Wolynes [56], the Hubbard-Onsager model is "*the ultimate achievement in a purely continuum theory of ionic mobility*". Being the most advanced continuum formulation of the dielectric friction theory, this model will be used throughout the remainder of this thesis in attempting to explain solvent-induced selectivity changes in CE. The next section is devoted entirely to a discussion of the theory, assumptions and limitations of the Hubbard-Onsager dielectric friction model.

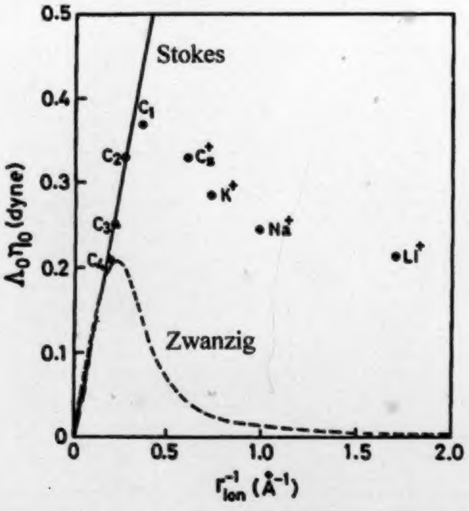

Figure 3.8: Agreement between the revised Zwanzig model (eqn 3.24) and experimental Walden products, in methanol at 298 K. The experimental results are denoted by the solid circles. Solutes C_1-C_4 represent tetraalkylammonium ions of the type $(C_nH_{2n+1})_4N^+$, *n* being 1, 2, 3 or 4. Here, $\Lambda_o = \lambda_{o,+} + \lambda_{o,-}$. This figure is reprinted with permission from J. Chem. Phys. 106 (1997) 5587-5598. Copyright 1997, American Institute of Physics.

3.4.3.2.2 Hubbard-Onsager Dielectric Friction Model

The Hubbard-Onsager model [59, 60] is a continuum model in which the ion is treated as an impenetrable sphere with a symmetric charge distribution. The solvent is regarded as an incompressible fluid with a uniform viscosity and dielectric constant and a single dielectric relaxation time, τ [59, 61]. By generalizing the Navier-Stokes hydrodynamic flow equations to include solvent relaxation, and by solving these equations with a distance-dependent viscosity, Hubbard and Onsager obtained the following expression for the total friction experienced by an ion [8, 56, 59]:

$$f_t = 6\pi\eta r + \left(\frac{17}{280}\right)\frac{\tau q^2}{r^3}\left(\frac{\varepsilon - \varepsilon_\infty}{\varepsilon^2}\right) \tag{3.25}$$

Here, η is the solvent viscosity, r is the radius of the ion, q is the charge of the ion, and τ, ε and ε_∞ are the Debye dielectric relaxation time and the low- and high-frequency dielectric constants, respectively. The first term in eqn 3.25 is the Stokes' friction coefficient as seen in the Hückel equation (eqn 1.5), and denotes the hydrodynamic contribution to the overall friction under 'perfect stick' conditions. The second term is the dielectric friction. Interestingly, this model essentially describes an enhanced fluid viscosity in the vicinity of the ion, which is precisely how Fuoss originally interpreted the dielectric friction effect [56, 61].

Several assumptions were involved in obtaining eqn 3.25. Hubbard and Onsager ignored electrostriction and dielectric saturation effects [61]. Electrostriction is the formation of a rigidly-bound solvation shell around the ion, and can be pictured in terms of the solvent-berg model (Section 3.4.2) or the structure-making region in the Gurney-Frank-Wen model (Section 3.2.3). Dielectric saturation involves a local depression in the dielectric constant due to the electric field surrounding the ion. A model considering such effects will be presented in the next section. Further, the simplified Hubbard-Onsager equation (eqn 3.25) was derived for the case in which hydrodynamic friction is dominant (>> 50% of the total friction, $f_h >> f_d$). Without this simplifying condition, the total friction coefficient in eqn 3.25 would be expressed as an infinite series in positive ($f_h < f_d$) and inverse ($f_h > f_d$) powers of r [60, 61]. It is important to clarify that the above simplifying condition is not obeyed by all of the analytes and solvent systems investigated in the following chapters. Indeed, with the exception of the monocharged analytes in water and acetonitrile-water (30/70 (v/v)) media, dielectric friction is always greater than hydrodynamic friction. However, this will not affect the interpretation of the results. The goal of the remaining chapters is not to quantitatively predict the dielectric friction, but rather to use the Hubbard-Onsager model as guidance in explaining solvent-induced mobility trends.

Figure 3.9 illustrates the agreement between experimental conductivities and those predicted by the Hubbard-Onsager equation (eqn 3.25). The predictive curve from the refined Zwanzig equation (eqn 3.24) is shown for comparison. Although the Hubbard-Onsager equation predicts the conductivity of large ions correctly, it cannot quantitatively explain the experimental results for small ions. However, it can predict the saturation effect on the friction experienced by the smaller ions like Na^+ and Li^+, which

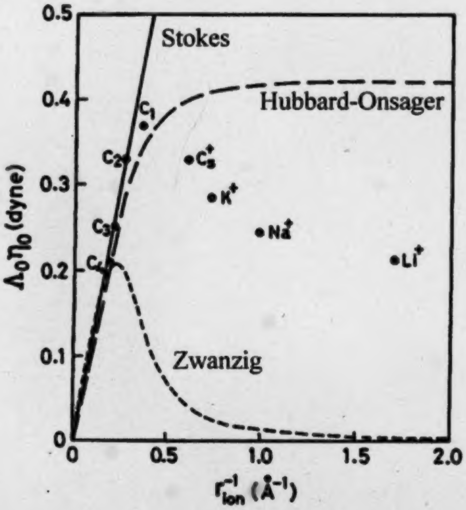

Figure 3.9: Agreement between the Hubbard-Onsager model (eqn 3.25) and experimental Walden products, in methanol at 298 K. The experimental results are denoted by the solid circles. Solutes C_1-C_4 represent tetraalkylammonium ions of the type $(C_nH_{2n+1})_4N^+$, *n* being 1, 2, 3 or 4. Reprinted with permission from J. Chem. Phys. 106 (1997) 5587-5598. Copyright 1997, American Institute of Physics.

was absent in the earlier theories [8]. The analytes investigated in the following chapters are aromatic acids and bases, and are thus larger in size than the tetraalkylammonium ions in Figure 3.9. Their mobility behavior should therefore be successfully modeled by the Hubbard-Onsager equation. Consequently, the deviation between experiment and the Hubbard-Onsager theory at small ion sizes is not a concern. Since the Hubbard-Onsager theory is valid over a wider range of large ions than the Zwanzig theory (Figure 3.9), it was selected for the mobility investigations in the following chapters.

Some of the variables in eqn 3.25 require further clarification. When a constant electric field is applied to a conducting solution, a small excess current (reorientation current) is generated before the current levels off at a steady value. This reorientation current decays exponentially with time, and the characteristic time of this decay is the Debye relaxation time, τ [59]. By considering a single relaxation time τ, the Hubbard-Onsager model treats the solvent as a simple Debye liquid whose dielectric behavior is described by the Debye equation [8, 62]:

$$\varepsilon(\omega) = \varepsilon_{\infty} + [(\varepsilon - \varepsilon_{\infty})/(1 + i\omega\tau)] \tag{3.26}$$

where ω is the circular frequency of the field. The solvent relaxation time is short for water (10 ps), and much greater for nonaqueous solvents like methanol (53 ps) and ethanol (143 ps) [63]. It should be noted that the assignment of a single relaxation time to a solvent is a simplified approximation. Indeed, there exists evidence for two relaxation processes for water and three relaxation processes for alcohols such as methanol, ethanol and 2-propanol [64, 65]. The value of τ in eqn 3.25 is taken to be that of the slowest (longest) relaxation process.

In eqn 3.25, ε and ε_∞ are the dielectric constants measured in the presence of low- and high-frequency electric fields, respectively. The dielectric constant typically reported for solvents is the low-frequency (static) dielectric constant, ε. ε includes polarization contributions arising from the permanent dipole moments (orientation polarization), the distortion of the position of the nuclei (distortion polarization), and the distortion of the electron distribution (electronic polarization). When the electric field has a high frequency, the solvent molecules cannot orient themselves fast enough to follow the change in direction of the applied field. Therefore, orientation polarization does not contribute to the overall polarization of the solution, and ε_∞ is small [66]. Typical values of ε are 78.5 for water and 32.7 for methanol [67], whereas the corresponding values for ε_∞ are only 1.9-5.7 for many polar liquids [68]. Thus, by assuming that $\varepsilon_\infty << \varepsilon$, and then substituting eqn 3.25 into the general expression for absolute mobility ($\mu_o = q/f_t$), the Hubbard-Onsager model of ion mobility becomes:

$$\mu_o = \frac{q}{6\pi\eta r + \left(\frac{17}{280}\right)\frac{\tau q^2}{r^3 \varepsilon}} \tag{3.27}$$

The use of ε in place of $\varepsilon^2/(\varepsilon-\varepsilon_\infty)$ is justified for aqueous-organic media, since the variation in ε with changing organic content is greater than the <10% variation between ε and $\varepsilon^2/(\varepsilon-\varepsilon_\infty)$. However, the importance of ε_∞ should not be overlooked for nonaqueous methanol-acetonitrile solvent systems, since methanol and acetonitrile have similar dielectric constants. This issue will be addressed in Section 6.3.2.

Eqn 3.27 is the form of the Hubbard-Onsager dielectric friction model that will be used throughout the remainder of this thesis. Since dielectric friction is proportional to both analyte-dependent (r, q) and solvent-dependent (τ, ε) terms, its incorporation into mobility equations can conceivably explain solvent-induced selectivity changes in CE. The aromatic ions investigated in the following chapters are actually ellipsoidal rather than spherical, and do not possess a symmetrical charge distribution. This apparently contradicts some of the basic assumptions of the Hubbard-Onsager model. However, Li and Lucy [21] found that no significant improvement in mobility prediction was achieved when the ellipsoid shape of aromatic acids was taken into account. Further, results presented in Chapter 4 will show that the different charge distributions of the *ortho*, *meta* and *para* phthalate isomers do not significantly influence the absolute mobilities of these ions in aqueous and methanol-water media. Therefore, all analytes will be treated as spheres with symmetrical charge distributions.

3.4.3.2.3 Other Advances in Continuum Dielectric Friction Models

The Hubbard-Onsager theory was further extended and modified by Hubbard and Kayser [69], who considered the additional effect of rotational viscosity (η_R) on solvent polarization. In the limit of η_R going to infinity, the Hubbard-Onsager model (eqn 3.25) is recovered. Regardless, inclusion of rotational viscosity effects has remarkably little effect on ionic mobility. Indeed, the mobilities predicted by the Hubbard-Onsager and Hubbard-Kayser theories differ by less than 10% [8, 69].

In additional work, Hubbard and Kayser [70, 71] incorporated dielectric saturation into a continuum treatment of mobility. Dielectric saturation refers to the variation in dielectric constant with electric field strength. As the electric field strength increases, solvent molecules with permanent dipoles will increasingly align themselves along the field direction. At the same time, the static dielectric constant decreases from its low-field bulk value (ε). When no further dipole orientation is possible, the dielectric is said to be fully saturated, and the static dielectric constant can be approximated by ε_∞ [71]. However, while the incorporation of dielectric saturation effects makes the continuum theory more physically sound, the quantitative mobility predictions thus obtained are very similar to those of the Hubbard-Onsager model. The mobilities predicted by each model differ by less than 20% [71]. Indeed, it has been reported [72] that conductivity becomes dependent upon voltage only at field strengths greater than 10^4 V/cm, suggesting that dielectric saturation effects are not significant at lower field strengths.

Chen and Adelman [73] have extended the continuum model of Hubbard and Onsager to include the effects of local solvent structure and dynamics. The resulting hybrid molecular-continuum theory [56] incorporates a desolvation function, Δ, that is a measure of the extent to which an ion is solvated. This desolvation function is equal to 0 for rigidly solvated ions and 1 for completely unsolvated ions. The end result of the Chen-Adelman theory is that the solute radii are renormalized to include solvation dynamics and structure through the desolvation function Δ and the ratio of the radii of the solvated ion to the bare ion [74]. In essence, this theory is attempting to bridge the gap between the totally dynamic solvation picture of the Hubbard-Onsager model and the totally static solvation sphere of the solvent-berg model. However, rather than evaluating the desolvation function from microscopic information, Chen and Adelman introduced an empirical form for Δ [56, 73]:

$$\Delta = \frac{\eta \rho_{loc}}{\eta_{eff}\, \rho} \tag{3.28}$$

where ρ_{loc} and η_{eff} are the local density and viscosity in the first solvation shell of the ion, and ρ and η are the bulk solvent density and viscosity. The local solvent parameters are determined through fitting to experimental conductance data [56]. Owing to this empirical approximation, the Chen-Adelman theory is essentially phenomenological. Further, the separation between hydrodynamic friction and dielectric friction is not as clearly defined as in the Hubbard-Onsager continuum dielectric friction model [74].

These advances in the continuum dielectric friction theory do not provide a significant improvement over the Hubbard-Onsager model. Therefore, due to its simplicity and relatively advanced formulation, the Hubbard-Onsager equation (eqn 3.27) is the continuum model of choice for the mobility investigations in the remaining chapters.

3.4.3.2.4 Limitations of the Continuum Models

Continuum models represent the solvent as a viscous dielectric continuum. As such, the solvent is treated as having a single uniform viscosity, dielectric constant and dielectric relaxation time. No molecularity of the solvent is considered. These models do not address the microscopic mechanism of ion motion in terms of the solvent structure, the ion-solvent interactions, or the nature of the motion of the solvent molecules [8, 52]. Since ion-solvent interactions are ignored, the continuum models cannot explain the different behaviors that have been observed for anions and cations [61]. Likewise, these models will fail if they are used to predict changes in mobility between two different solvent classes (eg., protic and dipolar aprotic) that are characterized by different ion-solvent interactions. These issues will be investigated in later chapters. Molecular models are expected to be more effective at predicting mobilities than continuum models, and as such, they are the topic of discussion in the next section.

3.4.3.3 Molecular Dielectric Friction Models

According to Evans et al. [61], "*the ideal theory of ionic motions in dilute electrolyte solutions would explain the mechanism of ionic mobility in terms of the ion-solvent interaction and the molecular motion of the solvent molecules*". Such theories are known as molecular theories. The usual starting point of molecular models is the following microscopic expression for the friction coefficient [61, 74]:

$$f_t = \frac{1}{k_B T} \int_0^\infty dt \langle F_R(0) \cdot F_R(t) \rangle \tag{3.29}$$

where k_B is Boltzmann's constant, T is the temperature, and F_R is the random force exerted on an ion by the solvent molecules. As such, the friction coefficient is expressed in terms of the correlation function of the random forces acting on the ion [52].

Wolynes and coworkers [49, 52] were the first to initiate a molecular approach to ion mobility. The first major assumption involved in their molecular theory is to replace the random force exerted on a moving ion by the total force on a fixed ion [49, 52, 74, 75]. The second assumption is to split the force into soft and hard terms, allowing the friction coefficient to be separated into four contributions:

$$f_t = f_{HH} + f_{HS} + f_{SH} + f_{SS} \tag{3.30}$$

f_{HH} results from the strong short-range (hard-hard) repulsive force due to the hard collisions of solvent molecules with the reference ion, while f_{SS} results from the weaker long-range (soft-soft) attractive force between the reference ion and the solvent molecules. The hard term f_{HH} is associated with Stokes' hydrodynamic friction, and the soft term f_{SS} is loosely associated with dielectric friction. The two middle terms, f_{HS} and f_{SH}, are the cross-terms resulting from the reciprocal effect of the soft force on the hard force, and vice versa [52]. Wolynes justified neglecting these cross-terms on the basis of the widely different time-scales expected for the hard and soft forces. The resulting simplified expression for the friction coefficient is [49, 52, 61]:

$$f_t = f_h + \frac{1}{k_B T}\left\langle (F^S)^2 \right\rangle \tau_F \tag{3.31}$$

where f_h is the hydrodynamic friction coefficient given by Stokes ($6\pi\eta r$ for 'perfect stick' conditions, as in the denominator of eqn 1.5), $\langle (F^S)^2 \rangle$ is the mean squared fluctuation in the soft long-range attractive force acting on the ion, and τ_F is the characteristic relaxation time of the attractive force. As such, the solvent is treated as a simple Debye liquid with a single relaxation time, τ_F. Wolynes' theory reduces to the continuum dielectric friction model in the limit of weak long-range interactions, and to the solvent-berg picture in the limit of strong short-range interactions [52].

According to eqn 3.31, a large fluctuation ($\langle (F^S)^2 \rangle$) or a long relaxation time (τ_F) in the attractive forces will result in a greater friction on the ion. Figure 3.10 illustrates the predictive success of Wolynes' molecular model. Although Wolynes' approach is much more complicated than the simple continuum theories, the numerical results obtained using this molecular model are quite similar to those obtained by Hubbard and Onsager (Figure 3.9).

Recently, Bagchi and coworkers [8, 76] have extended the molecular theory to include the ultrafast dynamics of the solvent and the self-motion of the ion. As such, the solvent is no longer treated as a simple Debye liquid characterized by a single relaxation time. They maintained Wolynes' initial assumptions, and also neglected the cross-terms. However, their treatment of the hard and soft terms differed from that of Wolynes.

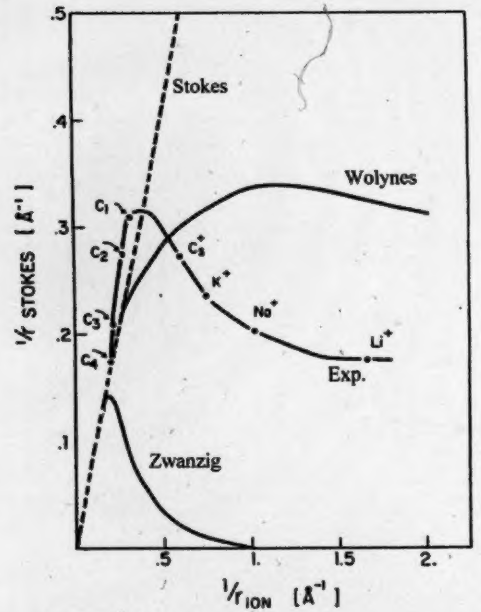

Figure 3.10: Agreement between the Wolynes model (eqn 3.31) and experimental data, in methanol at 298 K. The experimental results are denoted by the solid circles. Solutes C_1-C_4 represent tetraalkylammonium ions of the type $(C_nH_{2n+1})_4N^+$, *n* being 1, 2, 3 or 4. The y-axis scale is slightly different from those in Figures 3.8 and 3.9 because 'perfect slip' conditions were assumed here, whereas 'perfect stick' conditions were assumed in the previous figures. Reprinted with permission from J. Chem. Phys. 71 (1979) 2644-2651. Copyright 1979, American Institute of Physics.

Bagchi's microscopic theory predicts alkali metal ion and tetraalkylammonium ion mobilities that are in excellent agreement with experimental results, as illustrated in Figure 3.11. Further, a dynamical solvent-berg model is recovered in the limit of very slow liquids. However, as with Wolynes' theory, the microscopic model developed by Bagchi does not predict differences in mobilities between positive and negative ions of the same size [74]. Such differences have been frequently reported in the literature [61, 74], and will be observed in Chapter 4.

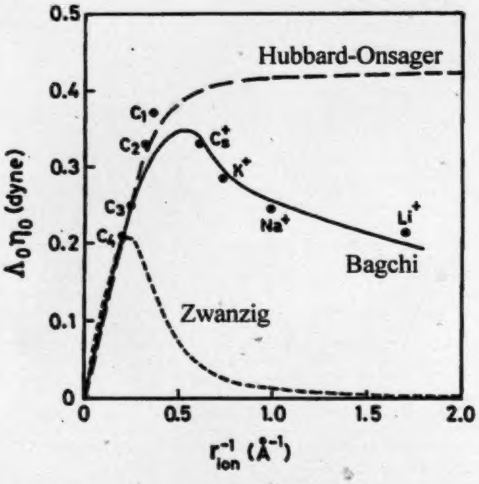

Figure 3.11: Illustration of the excellent agreement between experimental data and the molecular model developed by Bagchi and coworkers, in methanol at 298 K. The experimental results are denoted by the solid circles. Solute C_1-C_4 represent tetraalkylammonium ions of the type $(C_nH_{2n+1})_4N^+$, *n* being 1, 2, 3 or 4. Reprinted with permission from J. Chem. Phys. 106 (1997) 5587-5598. Copyright 1997, American Institute of Physics.

The first molecular theory able to predict the mobility differences between anions and cations has been recently developed by Chong and Hirata [77]. The major improvement in this model compared to the earlier molecular models is the consideration of the cross-terms f_{HS} and f_{SH}. Indeed, Chong and Hirata observed that the magnitude of these cross-terms is quite large for small ions, and therefore cannot be neglected. Molecular dynamics simulations have also been successful at differentiating between positively- and negatively-charged ions. Specifically, in a series of papers, Rasaiah and coworkers [74, 75, 78, 79] have used a computer simulation with the simple point charge model (SPC/E) to predict the mobilities of small ions in aqueous media. Differentiation between anion and cation behavior is achieved by accounting for the asymmetry in the free energy and entropy of solvation as a function of charge sign [75].

3.4.3.4 Why Choose Continuum Models Over Molecular Models?

Since the molecular models start from a molecular viewpoint, they provide a more realistic picture of ion motion. However, their mathematical complexity is significantly greater than that of the continuum models, which makes their application to CE analyses quite tedious. Indeed, Hubbard and Kayser [70] have stated that "*a truly microscopic model will undoubtedly require, for purposes of numerical computation, a large number of simplifying assumptions and approximations, the validity of which may be quite difficult to assess*". This statement was made 20 years ago, and modern advances in computer technology now make these calculations possible, as evidenced by the success of the model developed by Biswas and Bagchi [8] (Figure 3.11). However, the use of microscopic models has thus far been limited to simple spherical ions, and has not been extended to the study of more complex ions as investigated herein. Continuum theories, which make reasonably accurate mobility predictions and are based on relatively simple physical models, are thus more suited for use as predictive tools in routine CE applications. For this reason, the continuum dielectric friction model of Hubbard and Onsager will be employed in the remaining chapters to understand the influence of organic solvents on mobility.

3.5 Effects of Ionic Strength on Mobility

Thus far, this chapter has reviewed various models developed to predict mobility. The majority of these models, including the Hubbard-Onsager dielectric friction theory (eqn 3.27), are concerned with the *absolute* mobility of an ion, μ_o. This is the mobility at zero electrolyte concentration. However, it is the *effective* ion mobility that is measured in CE, since background electrolytes with finite ionic strengths are used. A method of calculating absolute ion mobilities from the measured effective ion mobilities is therefore required. The theory of ion-ion interactions is briefly reviewed in this section, concluding with a discussion of the Pitts' equation, which has been recently shown to successfully predict absolute mobility in CE. This is the equation that will be used in the remaining chapters.

The theoretical ionic strength models discussed below were developed to explain the influence of the ionic atmosphere on the conductivity of the solution. In terms of a CE experiment, this is equivalent to the conductivity of the electrolyte *buffer*, not of the analyte ion. Therefore, it is uncertain whether these models can be applied to describe the mobility of an analyte ion within the electrolyte buffer [80]. To emphasize this uncertainty, the expressions for the theoretical ionic strength models will be presented in terms of ion conductivity rather than ion mobility, keeping in mind that these two variables are related through the Faraday constant (eqn 3.2).

3.5.1 The Debye-Hückel Ionic Cloud Model of Ion-Ion Interactions

In 1923, Debye and Hückel developed the ion-cloud model to describe the spatial distribution of charges around a stationary ion in dilute electrolyte solutions [81]. Their model, which is based on several assumptions, is illustrated in Figure 3.12. The first

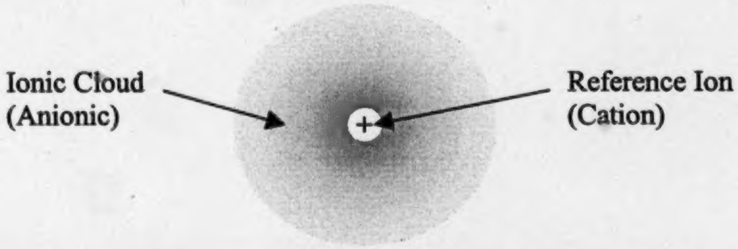

Figure 3.12: Debye-Hückel ionic cloud model of ion-ion interactions.

assumption of the ion-cloud model is that only one ion is arbitrarily selected as having a discrete charge. This *reference ion* is considered separately from all other ionic charges in the electrolyte solution, and is shown as the cation in Figure 3.12. The second assumption is that the solvent is regarded as a continuous dielectric medium characterized by a single dielectric constant (ε). Third, the remaining ions in solution (excluding the reference ion) are smeared into a continuous spatial distribution of charge by their thermal motion. This charge continuum is referred to as the *ionic cloud* (Figure 3.12), and has a total charge that is equal in magnitude but opposite in sign to the charge on the reference ion. For a stationary reference ion in the absence of an applied electric field, the ionic cloud is symmetrically distributed around the reference ion. The thickness of the ionic cloud is given by the Debye-Hückel length, κ^{-1}:

$$\kappa^{-1} = \left(\frac{8\pi N_A e^2}{1000\varepsilon k_B T}\right)^{-1/2} I^{-1/2} \tag{3.32}$$

where N_A is Avogadro's number, e is the charge on an electron, ε is the dielectric constant of the solvent, k_B is Boltzmann's constant, T is the temperature, and I is the ionic strength of the electrolyte solution (eqn 1.14).

Debye and Hückel developed their ion-cloud model to describe the *activity*, or 'effective concentration', of ions in an electrolyte solution. The ionic cloud shields the reference ion from feeling the full potential from other ions in solution, and vice versa. It can thus be regarded as reducing the effective charge on the reference ion. This shielding effect will reduce the attractive force between ions of opposite charge, thereby decreasing the ion activity and shifting the dissociation and solubility equilibria. As is discussed in the following section, Onsager applied Debye and Huckel's ion-cloud model to describe the influence of electrolyte concentration on conductivity/mobility. Just as the shielding effect reduces the activity of an ion, it will also reduce the mobility of an ion in the presence of an electric field. Since the size of the ion cloud decreases with increasing ionic strength (eqn 3.32), the effective shielding will increase. Therefore, an increase in ionic strength should result in a decrease in mobility.

3.5.2 The Debye-Hückel-Onsager Equation

The Debye-Hückel ionic cloud model of ion-ion interactions was developed for the case of a stationary reference ion. However, in the case of mobility or conductivity measurements, the central reference ion is moving in the presence of an applied electric field. A treatment of the ionic cloud around a moving ion is therefore required in order to describe the influence of ion-ion interactions on ion motion.

Let us begin by considering the influence that an applied electric field will have on the shape of the ionic cloud [10]. As the reference ion moves in the presence of an electric field, the ionic cloud will only remain spherically symmetrical (as in Figure 3.12) if its contents immediately readjust to the new position of the central ion. However, the re-establishment of the symmetrical ion cloud requires a finite amount of time. Since the reference ion continues to move during this time, the end result is an egg-shaped ionic cloud surrounding the central ion. This is illustrated in Figure 3.13. Alternatively stated, as the central ion moves, it loses part of its ionic cloud behind it and builds up the ionic cloud in front of it.

The ionic cloud will affect the motion of the reference ion in two ways. First, due to its asymmetrical shape, the center of charge of the ionic cloud is displaced from the center of charge of the reference ion (Figure 3.13). An attractive force thus exists

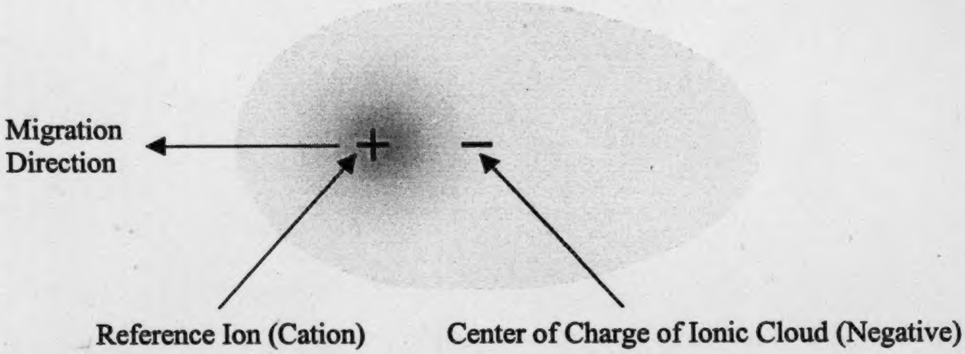

Figure 3.13: The asymmetrical egg-shaped ionic cloud around a moving ion

between the central ion and the lagging ionic atmosphere, which slows the motion of the reference ion. This is known as the *relaxation effect.* Additionally, the ionic cloud possesses a charge equal in magnitude but opposite in sign to the central ion. Thus, under an applied electric field, the ionic atmosphere will migrate in a direction opposite to the reference ion. In doing so, the ionic atmosphere will try to drag along all of its constituent ions, including the reference ion. This *electrophoretic effect* also retards the motion of the central ion.

Taking the asymmetrical ion cloud shape into account, Onsager developed the following expression for the influence of electrolyte concentration on the equivalent conductivity of an anion (in cgs units) [10, 25]:

$$\lambda_- = \lambda_{-,o} - \left(\frac{41.25}{\eta(\varepsilon T)^{1/2}} z_- + \frac{1.40 \times 10^6}{(\varepsilon T)^{3/2}} z_+ z_- \frac{2g}{1+\sqrt{g}} \lambda_{-,o} \right) \sqrt{I} \qquad (3.33)$$

This is the Debye-Hückel-Onsager equation for anion conductivity, and it assumes that the analyte is a point charge. A similar expression can be written for the conductivity of a cation. In eqn 3.33, λ_- is the effective conductivity ($cm^2\Omega^{-1}eq^{-1}$), $\lambda_{-,o}$ is the equivalent conductivity at infinite dilution, z_- is the magnitude of the anion charge, z_+ is the charge of the positive counterion, η is the solvent viscosity, ε is the solvent dielectric constant, and T is the temperature. The numerical constants in eqn 3.33 are the product of a number of fundamental constants including Boltzmann's constant, the Faraday constant, Avogadro's number, and the elemental charge [72]. g is an electrolyte parameter, as supported qualitatively by the data in ref [19, 82], and is defined by [72]:

$$g = \left(\frac{z_+ z_-}{z_+ + z_-}\right)\left(\frac{\lambda_{+,o} + \lambda_{-,o}}{z_+\lambda_{+,o} + z_-\lambda_{-,o}}\right) \tag{3.34}$$

This parameter reflects the deformation of the ionic atmosphere under the effect of an external electric field [72], and is thus a property of the electrolyte rather than the analyte. For symmetrical electrolytes, g is equal to ½.

The bracketed term in eqn 3.33 is often referred to as the *Onsager slope*. The first term in the brackets is the electrophoretic effect, while the second term reflects the relaxation effect [10]. For a given analyte, solvent and electrolyte, the Debye-Hückel-Onsager equation can be expressed by the following generalized form:

$$\lambda = \lambda_o - const \times \sqrt{I} \tag{3.35}$$

This equation has the same form as the empirical relationship initially proposed by Kohlrausch to describe the influence of concentration on equivalent conductivity [10]. It predicts that plots of conductivity versus the square root of ionic strength should be linear, with an intercept equaling the conductivity at zero ionic strength. Mobilities in CE have been commonly plotted in this manner, although non-linearities have been observed in instances where the analyte is highly charged or the electrolyte is of high ionic strength [80, 83, 84].

The failure of the Debye-Hückel-Onsager equation at predicting mobility behavior in CE can be related to the main assumptions of the theory. The most limiting approximation of this model is that the reference ions are treated as point charges. This is valid provided that the ionic cloud is large in comparison to the size of the central ion. However, as the ionic strength increases, the ionic atmosphere decreases in size (eqn 3.32). Therefore, the Debye-Huckel-Onsager equation is valid only for very dilute electrolytes up to 0.001 M [83, 84], whereas typical CE buffers have ionic strengths ranging from 0.001-0.1 M. Further, this model was developed to describe the influence of ion-ion interactions on electrolyte conductivity, not to describe such influences on a dilute solute migrating in a background electrolyte [80]. Indeed, Survay et al. [83] have stated that the extension of the treatment of a 1:1 electrolyte to that of an ion migrating in a 1:1 electrolyte is only justified when the ion and co-ion have identical mobilities.

3.5.3 Empirical and Semi-Empirical Expressions

The limited ionic strength range of the Debye-Huckel-Onsager model has prompted the development of empirical and semi-empirical mobility expressions that apply over a wider range of ionic strengths. Reijenga and coworkers [80, 84, 85] have shown a $\exp(-I^{1/2})$ dependence on mobility for 21 aromatic sulfonates at ionic strengths up to 0.1 M. However, these models lack theoretical justification and will likely not apply to other solutes or buffer systems. Isaac et al. [86] took a more theoretical approach. Starting from the Helmholtz-Smoluchowski equation for mobility (eqn 1.6), they formulated an expression showing the linear dependence of mobility on $I^{1/2}$. Although this model was demonstrated to be effective at ionic strengths up to 0.1 M, it predicts that mobility goes to infinity as the ionic strength goes to zero. It therefore cannot be used to determine absolute mobilities from extrapolation of effective mobilities.

A model that accounts for the finite size of the reference ion should be able to successfully reflect the influence of ion-ion interactions at higher ionic strengths. By using Robinson and Stokes' approximation [25], Survay et al. [83] modified the Debye-Hückel-Onsager equation (eqn 3.33) to account for the ion size. They merely divided the $I^{1/2}$ term in eqn 3.33 by $(1+\kappa a)$, where κ is given by eqn 3.32 and a is the sum of the radii of the analyte ion and the buffer counterion. For a univalent ion migrating in a 1:1 aqueous electrolyte solution, the resultant expression is:

$$\mu_e = \mu_o - \frac{(0.229\mu_o + 3.12)\sqrt{I}}{1 + 3.28a\sqrt{I}} \tag{3.36}$$

where μ_e and μ_o are the effective and absolute ion mobilities in $10^{-4}\mathrm{cm}^2\mathrm{V}^{-1}\mathrm{s}^{-1}$. This model allowed the successful determination of μ_o for oligoalanines and oligoglycines in a wide variety of 1:1 electrolytes ranging in ionic strength from 0.006 M to 0.075 M [83]. However, it is limited to monocharged analytes in uni-univalent electrolytes.

Ionic strength models are required that apply to both wide ionic strength ranges and to analytes and buffers of higher charge. Such a theoretical model has been developed by Pitts and is presented in the next section. Recently, the Pitts' equation has been successfully applied to describe the ionic strength behavior in capillary electrophoresis.

3.5.4 Pitts' Equation

Pitts [87, 88] developed a theoretical model for equivalent conductivity that accounts for the finite size of the reference ion. The asymmetrical ionic cloud surrounding the central ion is as pictured in Figure 3.13, with the exception that the point-charge reference ion is replaced with one of finite size. Pitts' original treatment is extremely complex [87], but a recent study from our research group [82] has demonstrated that a simplified expression can be obtained following rigorous mathematical manipulation of the original equation. Only the simplified expression is presented here; the interested reader is referred to ref 82 for a detailed explanation of the generalizations. The simplified Pitts' equation (in cgs) for the equivalent conductivity of an anion is:

$$\lambda_- = \lambda_{-,o} - \left(\frac{41.25}{\eta(\varepsilon T)^{1/2}} \{z\} z_- + \frac{1.40 \times 10^6}{(\varepsilon T)^{3/2}} \left| z_+ z_- \right| \frac{2g}{1+\sqrt{g}} \lambda_{-,o} \right) \frac{\sqrt{I}}{1 + Ba\sqrt{I}} \qquad (3.37)$$

where a is an ion size parameter (mean distance of closest approach for the ions) and B is a solvent-dependent constant described by:

$$B = \left(\frac{8\pi N_A e^2}{1000 \varepsilon k_B T} \right)^{1/2} \qquad (3.38)$$

All other variables in eqn 3.37 are the same as in eqn 3.33. As in the Debye-Hückel-Onsager equation, the left-hand term in the brackets of eqn 3.37 is the electrophoretic effect, and the right-hand term is the relaxation effect. In the electrophoretic term of eqn 3.37, z is bracketed in order to reflect the discrepancy in charge dependence between the Debye-Huckel-Onsager theory and the Pitts equation [82]. The results presented herein in Chapter 4 support a charge dependence of z_-, not z_-^2, in the electrophoretic effect. Values of the ion size parameter (a) ranging between 3-6 Å have been used in activity coefficient calculations [89]. The constant Ba in eqn 3.37 is therefore expected to be approximately 1-2 for aqueous media.

With the exception of the anomalous charge dependence in the electrophoretic effect, the Pitts equation reduces to the Debye-Hückel-Onsager expression at low ionic strengths. The Pitts expression is successful for 1:1 electrolyte solutions with ionic srengths up to 0.1 M [72, 87, 88]. For 2:2 electrolytes, the validity of the Pitts equation will likely be limited to concentrations below 0.001 M [87].

3.5.4.1 Extension of the Pitts Treatment to Mobility Prediction in CE

Recently, Li et al. [82] have demonstrated that the mobility-equivalent form of the simplified Pitts expression (eqn 3.37) successfully describes the ionic strength dependence of multiply-charged anions in aqueous capillary electrophoresis. The resulting Pitts equations rewritten for mobility are

$$\mu_{-} \approx \mu_{-,o} - \left(\frac{41.25}{\eta(\varepsilon T)^{1/2} F} \{z\} z_{-} + \frac{1.40 \times 10^{6}}{(\varepsilon T)^{3/2}} \left| z_{+} z_{-} \right| \frac{2g}{1+\sqrt{g}} \mu_{-,o} \right) \frac{\sqrt{I}}{1 + Ba\sqrt{I}} \qquad (3.39)$$

for the anions and

$$\mu_{+} \approx \mu_{+,o} - \left(\frac{41.25}{\eta(\varepsilon T)^{1/2} F} \{z\} z_{+} + \frac{1.40 \times 10^{6}}{(\varepsilon T)^{3/2}} \left| z_{+} z_{-} \right| \frac{2g}{1+\sqrt{g}} \mu_{+,o} \right) \frac{\sqrt{I}}{1 + Ba\sqrt{I}} \qquad (3.40)$$

for the cations. The absolute ion mobilities are given as $\mu_{-,o}$ and $\mu_{+,o}$, while the effective ion mobilities are μ_{-} and μ_{+}. The Faraday constant (F) is introduced into these expressions as the proportionality constant relating mobility and conductivity (eqn 3.2).

Li et al. determined that 2.4 was the optimal value for *Ba* based on 42 test analytes (carboxylates, phenols and sulfonates) in aqueous buffers [82]. This value is consistent with literature values for the ionic size parameter *a* (600-700 pm) [89].

Equations 3.39 and 3.40 are the ionic strength expressions that will be used in the remaining chapters to determine the absolute ion mobilities. For aqueous media, a value of 2.4 is assigned to *Ba*, consistent with Li's results. For the investigations involving aqueous-organic and nonaqueous media, the constant *Ba* is adjusted from it value of 2.4 to reflect the change in solvent dielectric constant as per eqn 3.38.

3.6 Summary

This chapter has provided a detailed review of mobility theories, beginning with the basic hydrodynamic model proposed by Hückel and concluding with advanced molecular theories. The failure of the Hückel equation at predicting solvent-induced selectivity changes results, at least in part, from its neglect of charge-induced friction. The Hubbard-Onsager model is one of the most advanced continuum formulations of the dielectric friction theory. Although it is not as physically realistic as molecular theories, the Hubbard-Onsager model is simple in form and provides reasonably good mobility predictions. Likewise, Pitts' treatment of electrolyte conductance has proven useful in accounting for ionic strength effects in capillary electrophoresis. These two models (Hubbard and Onsager's dielectric friction model and Pitts' ionic strength model) will be employed in the following chapters in an attempt to better understand solvent-induced selectivity changes in capillary electrophoresis.

3.7 References

(1) Grossman, P. D. In *Capillary Electrophoresis. Theory and Practice*; Grossman, P. D., Colburn, J. C., Eds.; Academic Press: New York, 1992, pp 111-132.

(2) Oda, R. P.; Landers, J. P. In *Handbook of Capillary Electrophoresis*; Landers, J. P., Ed.; CRC Press: Boca Raton, 1994, pp 9-42.

(3) Hiemenz, P. C. *Principles of Colloid and Surface Chemistry*; Marcel Dekker, Inc.: New York, 1986.

(4) Edward, J. T. *J. Chem. Educ.* **1970,** *47*, 261-270.

(5) Frank, H. S. In *Chemical Physics of Ionic Solutions*; Conway, B. E., Barradas, R. G., Eds.; John Wiley & Sons, Inc.: New York, 1966, pp 53-66.

(6) Cussler, E. L. *Diffusion: Mass Transfer in Fluid Systems*; Cambridge University Press: London, 1984, Chapter 5.

(7) Kay, R. L. *Pure & Appl. Chem.* **1991,** *63*, 1393-1399.

(8) Biswas, R.; Bagchi, B. *J. Chem. Phys.* **1997,** *106*, 5587-5598.

(9) Marcus, Y. *Ion Properties*; Marcel Dekker, Inc.: New York, 1997.

(10) Bockris, J. O. M.; Reddy, A. K. N. *Modern Electrochemistry*; Plenum Press: New York, 1970, Vol. 1, pp 45-171, 420-440.

(11) Sadek, H. *J. Electroanal. Chem.* **1983,** *144*, 11-32.

(12) Ibuki, K.; Nakahara, M. *J. Phys. Chem.* **1986,** *90*, 6362-6365.

(13) Edward, J. T.; Waldron-Edward, D. *J. Chromatogr.* **1965,** *20*, 563-571.

(14) Edward, J. T. In *Advances in Chromatography*; Giddings, J. C., Keller, R. A., Eds.; Marcel Dekker, Inc.: New York, 1966; Vol. 2, pp 63-98.

(15) Perrin, F. *J. Phys. Radium* **1934,** *5*, 497-511.

(16) Perrin, F. *J. Phys. Radium* **1936,** *7*, 1-11.

(17) Elworthy, P. H. *J. Chem. Soc.* **1962**, 3718.

(18) Byrd, P. F.; Friedman, M. D., Eds. *Handbook of Elliptic Integrals for Engineers and Scientists*, 2nd ed.; Springer-Verlag: New York, 1971.

(19) Li, D. M.Sc. Thesis, University of Calgary, Calgary, 2000.

(20) Fu, S.; Lucy, C. A. *Anal. Chem.* **1998,** *70*, 173-181.

(21) Li, D.; Lucy, C. A. *Anal. Chem.* **2001,** *73*, 1324-1329.

(22) Gurney, R. W. *Ionic Processes in Solution*; McGraw-Hill Book Company, Inc.: New York, 1953, Chapter 16.

(23) Frank, H. S.; Wen, W.-Y. *Disc. Faraday Soc.* **1957,** *24*, 133-140.

(24) Kay, R. L.; Evans, D. F. *J. Phys. Chem.* **1966,** *70*, 2325-2335.

(25) Robinson, R. A.; Stokes, R. H. *Electrolyte Solutions*, 2nd ed.; Butterworths: London, 1959.

(26) Schultz, S. G.; Solomon, A. K. *J. Gen. Physiol.* **1961,** *44*, 1189.

(27) Spernol, A. *J. Phys. Chem.* **1956,** *60*, 703.

(28) Offord, R. E. *Nature* **1966,** *211*, 591-593.

(29) Adamson, N.; Riley, P. F.; Reynolds, E. C. *J. Chromatogr.* **1993,** *646*, 391-396.

(30) Rickard, E. C.; Strohl, M. M.; Nielsen, R. G. *Anal. Biochem.* **1991,** *197*, 197-207.

(31) Kasicka, V.; Prusík, Z.; Mudra, P.; Stepánek, J. *J. Chromatogr. A* **1995,** *709*, 31-38.

(32) Gaus, H.-J.; Beck-Sickinger, A. G.; Bayer, E. *Anal. Chem.* **1993,** *65*, 1399-1405.

(33) Grossman, P. D.; Colburn, J. C.; Lauer, H. H. *Anal. Biochem.* **1989,** *179*, 28-33.

(34) Jokl, V. *J. Chromatogr.* **1964,** *13*, 451-458.

(35) McKillop, A. G.; Smith, R. M.; Rowe, R. C.; Wren, S. A. C. *Anal. Chem.* **1999,** *71*, 497-503.

(36) Jalali-Heravi, M.; Garkani-Nejad, Z. *J. Chromatogr. A* **2001,** *927*, 211-218.

(37) Jalali-Heravi, M.; Garkani-Nejad, Z. *J. Chromatogr. A* **2002,** *971*, 207-215.

(38) Jouyban-Gharamaleki, A.; Khaledi, M. G.; Clark, B. J. *J. Chromatogr. A* **2000,** *868*, 277-284.

(39) Jouybana, A.; Chan, H. K.; Clark, B. J.; Kenndler, E. *J. Microcolumn Sep.* **2001,** *13*, 346-350.

(40) Jouyban, A.; Batish, A.; Rumbelow, S. J.; Clark, B. J. *Analyst* **2001,** *126*, 1958-1962.

(41) Jouyban, A.; Grosse, S. C.; Coleman, M. W.; Chan, H. K.; Kenndler, E.; Clark, B. J. *Analyst* **2002,** *127*, 1188-1192.

(42) Guillaume, Y. C.; Peyrin, E.; Ravel, A.; Guinchard, C. *J. Liq. Chromatogr. Rel. Technol.* **2000,** *23*, 2789-2806.

(43) Barrón, D.; Irles, A.; Barbosa, J. *J. Chromatogr. A* **2000,** *871*, 367-380.

(44) Barrón, D.; Jiménez-Lozano, E.; Irles, A.; Barbosa, J. *J. Chromatogr. A* **2000,** *871*, 381-389.

(45) Yang, Y.; Liu, F.; Kang, J.; Ou, Q. *J. Chromatogr. A* **1999,** *834*, 393-399.

(46) Fu, S.; Li, D.; Lucy, C. A. *Analyst* **1998,** *123*, 1487-1492.

(47) Cottet, H.; Gareil, P. *Electrophoresis* **2000,** *21*, 1493-1504.

(48) Cottet, H.; Gareil, P.; Theodoly, O.; Williams, C. E. *Electrophoresis* **2000,** *21*, 3529-3540.

(49) Colonomos, P.; Wolynes, P. G. *J. Chem. Phys.* **1979,** *71*, 2644-2651.

(50) Marcus, Y. *Ion Properties*; Marcel Dekker: New York, 1997, pp 177-185.

(51) Born, M. *Z. Phys.* **1920,** *221*, 1.

(52) Wolynes, P. G. *J. Chem. Phys.* **1978,** *68*, 473-483.

(53) Fuoss, R. M. *Proc. Natl. Acad. Sci.* **1959,** *45*, 807-813.

(54) Boyd, R. H. *J. Chem. Phys.* **1961,** *35*, 1281-1283.

(55) Zwanzig, R. *J. Chem. Phys.* **1963,** *38*, 1603-1605.

(56) Wolynes, P. G. *Ann. Rev. Phys. Chem.* **1980,** *31*, 345-376.

(57) Zwanzig, R. *J. Chem. Phys.* **1970,** *52*, 3625-3628.

(58) Kay, R. L. In *Water: A Comprehensive Treatise*; Franks, F., Ed.; Plenum Press: New York, 1973; Vol. 3, pp 173-210.

(59) Hubbard, J.; Onsager, L. *J. Chem. Phys.* **1977,** *67*, 4850-4857.

(60) Hubbard, J. B. *J. Chem. Phys.* **1978,** *68*, 1649-1664.

(61) Evans, D. F.; Tominaga, T.; Hubbard, J. B.; Wolynes, P. G. *J. Phys. Chem.* **1979,** *83*, 2669-2677.

(62) Daniel, V. V. *Dielectric Relaxation*; Academic Press: New York, 1967.

(63) Jenkins, H. D. B.; Marcus, Y. *Chem. Rev.* **1995,** *95*, 2695-2724.

(64) Barthel, J.; Bachhuber, K.; Buchner, R.; Hetzenauer, H. *Chem. Phys. Lett.* **1990,** *165*, 369-373.

(65) Barthel, J.; Buchner, R. *Pure & Appl. Chem.* **1991,** *63*, 1473-1482.

(66) Atkins, P. W. In *Physical Chemistry*; Oxford University Press: Oxford, 1990, pp 995.

(67) Akhadov, Y. Y. *Dielectric Properties of Binary Solutions. A Data Handbook*; Pergamon Press: New York, 1980.

(68) Buckley, F.; Maryott, A. A. *Tables of Dielectric Dispersion Data for Pure Liquids and Dilute Solutions, NBS Circ. 589*: Washington, 1958, Vol. NBS Circ. 589.

(69) Hubbard, J. B.; Kayser, R. F. *J. Chem. Phys.* **1981,** *74*, 3535-3545.

(70) Hubbard, J. B.; Kayser, R. F. *Chem. Phys.* **1982,** *66*, 377-382.

(71) Stiles, P. J.; Hubbard, J. B.; Kayser, R. F. *J. Chem. Phys.* **1982,** *77*, 6189-6196.

(72) Erdey-Grúz, T. *Transport Phenomena in Aqueous Solutions*; John Wiley & Sons: New York, 1974, Chapter 4.

(73) Chen, J.-H.; Adelman, S. A. *J. Chem. Phys.* **1980,** *72*, 2819-2831.

(74) Koneshan, S.; Lynden-Bell, R. M.; Rasaiah, J. C. *J. Am. Chem. Soc.* **1998,** *120*, 12041-12050.

(75) Rasaiah, J. C.; Lynden-Bell, R. M. *Phil. Trans. R. Soc. Lond. A* **2001,** *359*, 1545-1574.

(76) Biswas, R.; Roy, S.; Bagchi, B. *Phys. Rev. Lett.* **1995,** *75*, 1098-1101.

(77) Chong, S.-H.; Hirata, F. *J. Chem. Phys.* **1999,** *111*, 3654-3667.

(78) Lee, S. H.; Rasaiah, J. C. *J. Phys. Chem.* **1996,** *100*, 1420-1425.

(79) Koneshan, S.; Rasaiah, J. C.; Lynden-Bell, R. M.; Lee, S. H. *J. Phys. Chem. B* **1998,** *102*, 4193-4204.

(80) Friedl, W.; Reijenga, J. C.; Kenndler, E. *J. Chromatogr. A* **1995,** *709*, 163-170.

(81) Bockris, J. O. M.; Reddy, A. K. N. *Modern Electrochemistry*; Plenum Press: New York, 1970, Vol. 1.

(82) Li, D.; Fu, S.; Lucy, C. A. *Anal. Chem.* **1999,** *71*, 687-699.

(83) Survay, M. A.; Goodall, D. M.; Wren, S. A. C.; Rowe, R. C. *J. Chromatogr. A* **1996,** *741*, 99-113.

(84) Reijenga, J. C.; Kenndler, E. *J. Chromatogr. A* **1994,** *659*, 403-415.

(85) Cao, C.-X. *J. Chromatogr. A* **1997,** *771*, 374-378.

(86) Isaaq, H. J.; Atamna, I. Z.; Muschik, G. M.; Janini, G. M. *Chromatographia* **1991,** *32*, 155-161.

(87) Pitts, E. *Proc. R. Soc. A*. **1953,** *217*, 43-70.

(88) Pitts, E.; Tabor, B. E.; Daly, J. *J. Trans. Faraday Soc.* **1970,** *66*, 693.

(89) Harris, D. C. *Quantitative Chemical Analysis*, 4th ed.; W. H. Freeman and Company: New York, 1995, Table 8.1.

CHAPTER FOUR. Dielectric Friction in Capillary Electrophoresis: Mobility of Organic Anions and Cations in Mixed Methanol-Water Media‡

4.1 Introduction

As discussed in Chapter 1, the use of organic solvents as either organic modifiers or as pure nonaqueous media has several advantages compared to aqueous CE. Of key importance are the increased solubility of many analytes, and the possibility of achieving dramatic selectivity alterations by varying the type and content of the organic solvent in the buffer. It is therefore not surprising that the use of organic solvents in CE has become widespread. More specifically, methanol-water mixtures and pure methanol have been frequently employed in CE for the analysis of both anionic and cationic species. Included are the analyses of anionic surfactants [1], porphyrins [2, 3], inorganic anions [4-6], substituted benzoic acids [7, 8], fatty acids [9, 10], heterocyclic aromatic amines [11, 12], quaternary ammonium herbicides [13], alkali and alkaline earth metal ions [14, 15], and cationic drugs [8, 16, 17]. Many of the selectivity changes observed in these studies can be explained by solvent-induced shifts in the pH or pK_a. However, there are several instances in which the resulting selectivity changes cannot be explained in this manner. For example, Yang et al. [5] observed a migration order reversal between NO_3^- and SO_4^{2-} (conjugate bases of strong acids) at pH 9.5 and 10% (v/v) methanol. Therefore, a better understanding of the mechanisms responsible for solvent-induced selectivity changes is required.

---

‡ A version of this chapter has been published. Anions: Roy, K. I.; Lucy, C. A. *Analytical Chemistry* **2001**, 73, 3854-3861. Cations: Roy, K. I.; Lucy, C. A. *Electrophoresis* **2003**, in press.

Solvent viscosity (η), dielectric constant (ε) and dielectric relaxation time (τ) all vary as a function of solvent composition. Table 4.1 shows how these solvent parameters change as the methanol content is varied from 0-75% (v/v). The importance of the ratio ε/η to the electroosmotic and electrophoretic mobilities has been frequently cited in the CE literature [1, 4, 18-22], whereas the importance of τ has been largely overlooked. According to the model of Hubbard and Onsager (eqn 3.27), dielectric friction is proportional to τ/ε and should thus increase with increasing methanol content and with increasing analyte charge. Therefore, dielectric friction may be responsible for methanol-induced selectivity changes.

Table 4.1: Effect of Buffer Methanol Content on Solvent Parameters

% MeOH (v/v)	η^a (cP)	ε^b	τ^c (ps)	τ/ε
0	0.89[d]	78.48[e]	8.25[e]	0.105
30	1.46	67.61	16.57	0.245
60	1.50	55.00	29.23	0.531
75	1.25	47.78	37.38	0.782

[a] Values calculated by multiplying the relative viscosities of the MeOH-H_2O mixtures (see Experimental section) and the viscosity of water. [b] Values obtained from interpolation of literature data [23]. ε was determined at 30, 60 and 75% (v/v) MeOH from a linear plot of ε versus weight % MeOH. [c] Values calculated using the data presented in the literature [24]. For each % MeOH, values for τ were determined at 25°C using the relationship [25] $\tau = A \exp(w/kT)$. A 2nd-order polynomial was then fit to a plot of τ versus % MeOH, at 25°C, to determine τ at 30, 60 and 75% MeOH. [d] Literature value [26]. [e] Literature values [23].

In this chapter, I investigate the effect of methanol on the mobilities of organic aromatic carboxylates, sulfonates and ammonium ions that are similar in size and range in charge from –1 to –4 and +1 to +3. The Hubbard-Onsager dielectric friction model (eqn 3.27) is used to describe the changes in ion mobility and selectivity that occur upon varying the concentration of methanol in the electrophoretic media. Changes in ion mobility correlate to the corresponding changes in solvent τ, ε and η. To my knowledge, this is the first report demonstrating the importance of solvent τ to mobility in CE. Further, the effects of ion charge and solvent composition on the ionic strength effects are also studied.

4.2 Experimental

4.2.1 Apparatus

All of the mobility measurements were made using a P/ACE MDQ capillary electrophoresis system (Beckman Instruments, Fullerton, CA), with a UV absorbance detector set at 214 nm. The data acquisition and control were performed on a Pentium 300 MHz IBM computer using P/ACE Station Software for Windows 95 (Beckman). The data acquisition rate was set at 4.0 Hz. Beakers containing methanol-water mixtures were placed in the instrument compartment to saturate the atmosphere within the instrument with solvent, thereby eliminating evaporative losses from the solution vials during the runs.

Untreated fused-silica capillaries (Polymicro Technologies, Phoenix, AZ) with inner diameters of 50 μm, outer diameters of 365 μm, and total lengths of 60 cm (50 cm to detector) were used for both the cation and anion analyses, unless otherwise noted. Same-dimension PEO-coated μSIL-WAX capillaries (Agilent Technologies, Wilmington, DE) were used to verify that the cations were not adsorbing to the bare fused-silica wall. New capillaries were used for each methanol content, and their precise lengths were determined before discarding. New uncoated capillaries were conditioned by rinsing at high pressure (20 psi) for 10 min with 1 M NaOH, 15 min with H_2O, 5 min with 0.1 M NaOH, and finally with H_2O for 10 min. Between runs, the capillaries were rinsed at high pressure for 3 min each with 0.1 M NaOH and H_2O, followed by a 5-min rinse with the running buffer. New PEO-coated capillaries required no preconditioning prior to use, and were rinsed between runs at 20 psi with 1 mM HCl for 2 min, H_2O for 2 min, and running buffer for 5 min.

4.2.2 Chemicals

All of the solutions were prepared with Nanopure 18 MΩ water (Barnstead, Chicago, IL) and were filtered through 0.45-μm Millex syringe-driven filters (Millipore, Bedford, MA). Buffers were prepared from reagent-grade sodium hydroxide (BDH, Darmstadt, Germany), reagent-grade hydrochloric acid (Fisher, Fair Lawn, NJ), reagent-grade sodium chloride (BDH), and HPLC-grade methanol (MeOH; Fisher). For the anion studies, all of the buffers consisted of 0.005 M NaOH, prepared by dilution of a 0.1 M stock solution, and the ionic strength was adjusted from 0.005 to 0.08 M by the addition of NaCl. Buffers for the cation studies were prepared in the same way using HCl in place of NaOH, and the ionic strengths ranged from 0.005-0.09 M. For the buffers containing 30%, 60% and 75% (v/v) methanol, the required volume of methanol was added before final dilutions with Nanopure water. The lower limit of ionic strength (0.005 M) was dictated by the concentration of sodium hydroxide or hydrochloric acid required for sufficient buffering capacity. Both sodium hydroxide and hydrochloric acid can be used as buffers because strongly basic or acidic solutions show little change in pH when acid or base is added, respectively [27]. They were used in this study to ensure that all analytes were completely ionized while avoiding the complicated task of measuring pH in mixed aqueous-organic solutions. It has been reported that in mixed methanol-water media, the pK_a of aromatic acids can increase by up to 2 units [28], and the pK_a of acidic amines can decrease by ~1 unit [29]. Therefore, the carboxylates and sulfonates used in this study will be completely ionized in the high pH NaOH solutions, and the aromatic amines will be completely protonated in the low pH HCl solutions. Table 4.2 lists the aqueous pK_a values for the analytes of interest.

Table 4.2: pK_a Values for the Analyte Anions and Cations

Analyte Ion	pK_a[a]
ANIONS	
p-Nitrobenzoate	3.44
Benzenesulfonate	0.70[b]
2,6-Naphthalenedicarboxylate	4.52±0.30[c]
2,6-Naphthalenedisulfonate	N/A[e]
Phthalate (*ortho*)	5.41
Isophthalate (*meta*)	4.50
Terephthalate (*para*)	4.46[d]
1,3,5-Benzenetricarboxylate	5.18
1,3,(6 or 7)-Naphthalenetrisulfonate	N/A[e]
1,2,4,5-Benzenetetracarboxylate	6.23
1,4,5,8-Naphthalenetetracarboxylate	4.46±0.33[c]
CATIONS	
Benzylammonium	9.33[b]
p-Xylylenediammonium	8.48±0.10[c]
m-Xylylenediammonium	8.79±0.29[c]
1,3,5-Triammoniummethylbenzene	8.30±0.50[c]
N-Benzylmethylammonium	9.75±0.10[c]
N,N-Dimethylbenzylammonium	8.80±0.28[c]
Benzyltrimethylammonium	Ø[f]

[a] pK_a values at 25°C and zero ionic strength obtained from *Critical Stability Constants* by A. E. Martell and R. M. Smith [30, 31], unless otherwise noted. The pK_a values listed for the anions are for the last acid dissociation step (i.e., $HL^{-3} \leftrightarrow H^{+} + L^{-4}$ for the –4 ions). The values listed for the cations are for the first acid dissociation step (i.e., $H_3L^{+3} \leftrightarrow H^{+} + H_2L^{+2}$ for the +3 ion). [b] Values from the *CRC Handbook of Chemistry and Physics* [26]. [c] Values calculated at 25°C and zero ionic strength using the ACD/Ilab pKa Calculator. [d] Value obtained from *Dissociation Constants of Organic Acids in Aqueous Solution* by Kortum et al. [32] [e] Literature value not available. [f] Benzyltrimethylammonium is a quaternary amine and thus has a charge of +1 regardless of pH.

Phthalic acid, isophthalic acid, terephthalic acid, 2,6-naphthalenedicarboxylic acid, 2,6-naphthalenedisulfonic acid, 1,3,5-benzenetricarboxylic acid, 1,3,(6 or 7)-napthalenetrisulfonic acid, 1,2,4,5-benzenetetracarboxylic acid, 1,4,5,8-naphthalenetetracarboxylic acid, benzylamine, m-xylylenediamine, p-xylylenediamine, N-benzylmethylamine and N,N-dimethylbenzylamine were obtained from Aldrich (Milwaukee, WI). Benzenesulfonic acid and p-nitrobenzoic acid were purchased from Eastman (Rochester, NY), and benzyltrimethylammonium chloride was from TCI America (Portland, OR). The carboxylic acids and amines were obtained as free acids and bases, respectively, while the sulfonic acids were obtained as sodium salts. They were of reagent grade or better, and used without any further purification. 1,3,5-triaminomethylbenzene was synthesized according to the procedure described by Weitl and Raymond [33], and was characterized by ^{1}H NMR. Sample solutions were prepared at concentrations of 1×10^{-3} M in water, and were diluted to 1×10^{-4} M in the corresponding buffer solution to eliminate sample stacking during electrophoresis. Mesityl oxide (Aldrich) was used as the neutral electroosmotic flow (EOF) marker at a concentration of 4 mM.

4.2.3 Determination of Absolute Mobilities

Two different methods were used for the determination of the effective mobilities. For the anions in 100% aqueous media, standard electrophoretic runs were performed in which the anions and the neutral marker were simultaneously injected for 1 s at 0.1 psi. Electrophoretic separation was then carried out at 25°C with a constant voltage of 4.0 kV. This voltage was within the linear region of an Ohm's plot, and produced a current of 21.0 μA for a 0.08 M ionic strength solution. The effective mobilities, μ_e, of the anions were calculated from the migration time of the anions (t_m) and the migration time of the electroosmotic flow (t_{eof}) using the following equation:

$$\mu_e = \frac{L_t L_d}{V}\left(\frac{1}{t_m} - \frac{1}{t_{eof}}\right) \tag{4.1}$$

where L_t is the total length of the capillary (~30 cm), L_d is the length to the detector (~20 cm), and V is the total voltage applied across the capillary. Migration times were determined at the center of gravity of the corresponding peaks

When methanol was added to the buffers, the mobilities of the anions became closely matched to that of the EOF but opposite in direction, resulting in very long run times. In a series of papers on capillary electrophoresis in mixed aqueous-organic media, Sarmini et al. [28, 34, 35] overcame this problem by using Williams and Vigh's method for mobility determination [36]. This method, which consists of two pressure steps combined with an electrophoretic separation step, was used in the present studies in conjunction with the buffers containing 30, 60 and 75% (v/v) methanol, as well as for the amines in aqueous media. Briefly, for the anions, a mixture of mesityl oxide and the anion of interest was injected into the capillary (length ~60 cm, ~50 cm to detector) for 4 s (0.5 psi) and was then transferred a certain distance into the capillary by pressure for 3.5 min (1.0 psi). The anion was then separated from mesityl oxide by applying a voltage of 10.0 kV for 2.5-5.5 min, depending on the mobility of the anion. For 0.07 M ionic strength solutions containing 30, 60 and 75% MeOH, this voltage was within the linear region of an Ohm's plot and corresponded to currents of 17.5 μA, 13.6 μA and 13.3 μA, respectively. Following this separation, mesityl oxide was injected into the capillary for 4 s (0.5 psi), and 1.0 psi pressure was applied to push the three bands past the detector.

The effective anion mobilities were then determined from the relative spacing between the peaks according to [36]

$$\mu_e = \frac{(t_A - t_{N1})L_t L_d}{V(t_{N3} + t_{inj}/2 - t_d)(t_{migr} - t_{ramp-up}/2 - t_{ramp-down}/2)} \tag{4.2}$$

where t_{N1}, t_{N3} and t_A are the migration times of the first EOF marker, the second EOF marker, and the analyte, respectively (measured at the center of gravity of the peaks); L_t is the total length of the capillary (~60 cm); L_d is the length of the capillary to the detector (~50 cm); t_{migr} is the time for which the run potential, V, is applied; t_{inj} is the injection time; t_d is the experimentally determined delay time (9 s); and $t_{ramp-up}$ and $t_{ramp-down}$ are the times it takes for the voltage to change between 0 and V. It has been demonstrated in our laboratory that this method yields mobilities that are statistically equivalent at the 95% confidence level to those obtained by the traditional method. For example, in aqueous media, the mobilities of 1,4,5,8-naphtalenetetracarboxylate determined by Williams and Vigh's method (eqn 4.2) and the conventional method (eqn 4.1) were $(7.94 \pm 0.10) \times 10^{-4}$ cm^2/Vs and $(7.80 \pm 0.06) \times 10^{-4}$ cm^2/Vs, respectively. These are not significantly different at the 95% confidence level. Since Williams and Vigh's method (eqn 4.2) measures analyte migration relative to that of an EOF marker, it is self-correcting for variations in EOF.

Similarly, effective cation mobilities in all solvent systems (including 0% MeOH) were determined using eqn 4.2. Although the EOF co-migrated with the cations, the high viscosities of the methanol-water solvent systems nonetheless resulted in long run times. For this reason, Williams and Vigh's method of mobility determination was preferred. The procedure was the same as for the anions, with the exception that the times, pressures and voltages were varied to adjust for changes in solution viscosity and cation mobility.

For the cations, injections were performed for 3-5 s at 0.5 psi, sample plugs were transferred into the capillary using 0.5-1.0 psi for 3-3.5 min, separation voltages of 7.0 kV (aqueous) or 10.0 kV (MeOH/H_2O) were applied for 3.5-6.0 min, and bands were mobilized past the detector window using pressures of 0.5-1.0 psi. At 0.09 M ionic strength, these voltages corresponded to currents of 27.0, 24.2, 18.3 and 17.0 μA for the solutions containing 0, 30, 60 and 75% MeOH, respectively. It has been reported that mobilities become dependent upon voltage only at field strengths greater than 10^4 V/cm (Wien Effect) [37]. Therefore, at the voltages used in this study (4.0-10.0 kV), the measured mobilities are independent of the applied voltage.

From the effective mobilities of the anions and cations, the absolute ion mobilities (μ_o) at zero buffer ionic strength were determined by plotting μ_e versus $I^{1/2}/(1 + Ba \times I^{1/2})$ according to the Pitts equation (eqn 3.39 and 3.40).

4.2.4 Measurement of Relative Viscosity

To correct the mobilities for viscosity effects, the viscosities of the buffers containing MeOH were measured relative to that of the pure aqueous buffer. For each of the buffers studied, mesityl oxide was injected into the capillary (4 s at 0.5 psi) and was then pushed past the detector using 1.0 psi pressure. The relative viscosities were determined from the ratios of the mesityl oxide elution times in the MeOH-containing and aqueous buffers.

4.3 Results and Discussion

4.3.1 Ionic Strength Effects

The absolute mobilities of the anions and cations in the aqueous electrolyte solutions were determined using the Pitts equation (eqn 3.39 and 3.40 for anions and cations) with a constant of 2.4. For the methanol-water mixtures, the constant *Ba* was adjusted to reflect the change in *B* as a function of dielectric constant, as per eqn 3.38. The ion size parameter (*a* in the constant *Ba*) was assumed to remain unchanged as methanol was added to the buffer, in keeping with the extended Bates-Guggenheim convention for solvent mixtures with water [38-40]. Using the values of ε in Table 4.1, the adjusted *Ba* for 30, 60 and 75% MeOH were calculated to be 2.6, 2.9 and 3.1, respectively. The corresponding Pitts' plots for the anions and cations are in Figures 4.1 and 4.2. For clarity, only the plots for 0% MeOH are shown with full extrapolation to zero ionic strength. The correlation coefficients, Onsager slopes and intercepts (absolute mobilities, μ_o) are presented in Tables 4.3 and 4.4. Ion pairing effects were not of concern, because extrapolation to zero buffer ionic strength should diminish such effects [41].

Good linearity is observed in the Pitts' plots, suggesting that the Pitts equation with *Ba* values adjusted according to eqn 3.38 is appropriate for use with the present solvent systems. The p-values for all of the analytes in MeOH/H_2O media are less than 0.01, indicating that the data obey linear relationships at the 99% confidence level. The intercept and slope errors listed in Tables 4.3 and 4.4 are the standard deviations obtained from the regression analysis. Therefore, the error in the intercept should reflect the long range over which extrapolation is performed (as illustrated in Figure 4.1a).

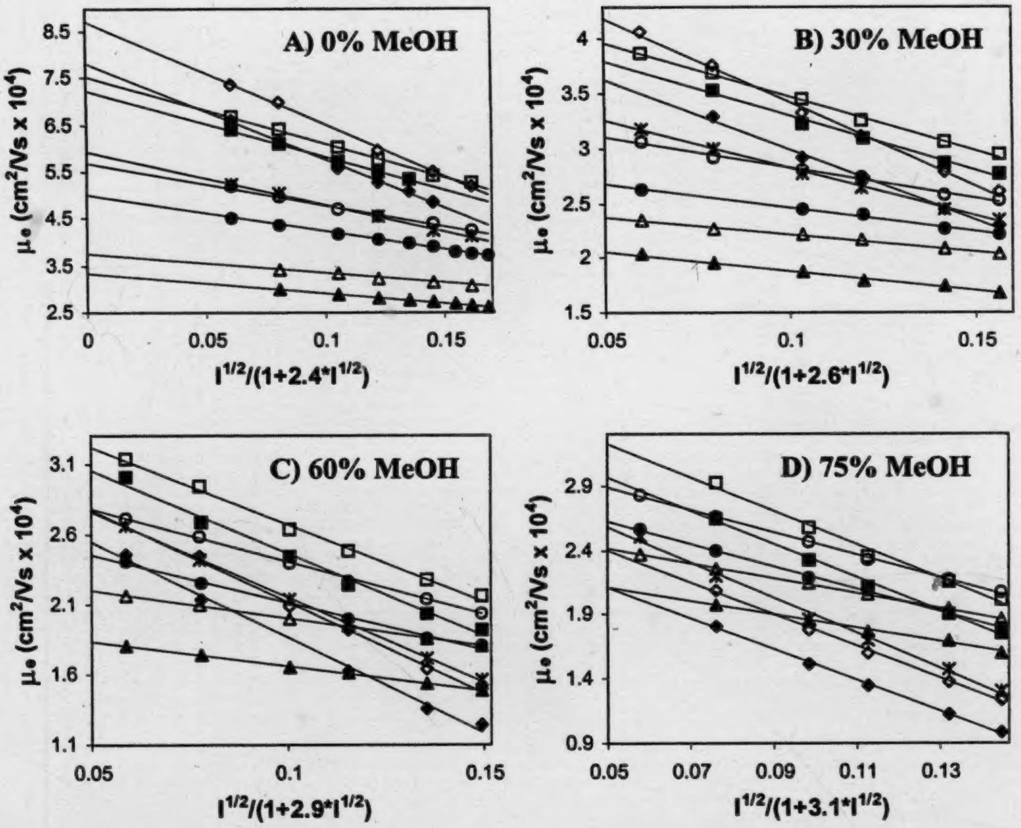

Figure 4.1: Ionic strength effects on the mobilities of organic anions for buffers containing (A) 0% MeOH, (B) 30% MeOH, (C) 60% MeOH and (D) 75% v/v MeOH. Solutes: ▲, p-nitrobenzoate; Δ, benzenesulfonate; ●, 2,6-naphthalenedicarboxylate; O, 2,6-naphthalenedisulfonate; ∗, phthalate; ■, 1,3,5-benzenetricarboxylate; □, 1,3,(6 or 7)-naphthalenetrisulfonate; ♦, 1,4,5,8-naphthalenetetracarboxylate; ◊, 1,2,4,5-benzenetetracarboxylate. Experimental conditions: UV detection at 214 nm; 30-cm capillary (20 cm to detector) for (A), 60-cm capillary (50 cm to detector) for (B)-(D); 4.0 kV applied for (A), 10.0 kV applied for (B)-(D); 1 × 10^{-4} M sample concentration; 5 mM NaOH buffer, ionic strength adjusted using NaCl.

Table 4.3: Ionic Strength Effects on the Mobility of Anions in MeOH/H_2O Media[a]

Anion	Charge	Pitts Equation			
		N[b]	R^2	Onsager Slope[c]	Intercept[d], μ_o
0% MeOH					
p-Nitrobenzoate	-1	8	0.9980	-4.12±0.07	3.320±0.009
Benzenesulfonate	-1	5	0.9847	-4.2±0.3	3.76±0.04
2,6-Naphthalenedicarboxylate	-2	9	0.9995	-7.64±0.07	4.994±0.009
2,6-Naphthalenedisulfonate	-2	6	0.9905	-8.9±0.4	5.69±0.05
Phthalate (*ortho*)	-2	5	0.9973	-11.4±0.3	5.94±0.04
1,3,5-Benzenetricarboxylate	-3	5	0.9989	-14.1±0.3	7.24±0.03
1,3,(6 or 7)-Naphthalenetrisulfonate	-3	6	0.9970	-14.4±0.4	7.55±0.05
1,4,5,8-Naphthalenetetracarboxylate	-4	6	0.9974	-20.5±0.5	7.80±0.06
1,2,4,5-Benzenetetracarboxylate	-4	5	0.9978	-21.9±0.6	8.70±0.07
30% MeOH					
p-Nitrobenzoate	-1	6	0.9957	-3.5±0.1	2.23±0.01
Benzenesulfonate	-1	6	0.9972	-3.07±0.08	2.519±0.009
2,6-Naphthalenedicarboxylate	-2	5	0.9926	-4.2±0.2	2.88±0.03
2,6-Naphthalenedisulfonate	-2	6	0.9958	-5.5±0.2	3.38±0.02
Phthalate (*ortho*)	-2	6	0.9984	-8.8±0.2	3.69±0.02
1,3,5-Benzenetricarboxylate	-3	5	0.9892	-9.9±0.6	4.29±0.07
1,3,(6 or 7)-Naphthalenetrisulfonate	-3	6	0.9973	-9.8±0.3	4.47±0.03
1,4,5,8-Naphthalenetetracarboxylate	-4	5	0.9945	-12.8±0.6	4.27±0.07
1,2,4,5-Benzenetetracarboxylate	-4	6	0.9949	-15.2±0.5	4.95±0.06
60% MeOH					
p-Nitrobenzoate	-1	6	0.9969	-3.5±0.1	2.01±0.01
Benzenesulfonate	-1	6	0.9973	-4.0±0.1	2.40±0.01
2,6-Naphthalenedicarboxylate	-2	5	0.9957	-6.8±0.3	2.79±0.03
2,6-Naphthalenedisulfonate	-2	6	0.9965	-7.5±0.2	3.15±0.03
Phthalate (*ortho*)	-2	6	0.9989	-12.2±0.2	3.37±0.02
1,3,5-Benzenetricarboxylate	-3	6	0.9901	-11.8±0.6	3.64±0.07
1,3,(6 or 7)-Naphthalenetrisulfonate	-3	6	0.9941	-11.0±0.4	3.77±0.05
1,4,5,8-Naphthalenetetracarboxylate	-4	5	0.9944	-13.5±0.6	3.22±0.07
1,2,4,5-Benzenetetracarboxylate	-4	5	0.9953	-13.0±0.5	3.42±0.06
75% MeOH					
p-Nitrobenzoate	-1	5	0.9968	-5.2±0.2	2.36±0.02
Benzenesulfonate	-1	6	0.9990	-5.77±0.09	2.71±0.01
2,6-Naphthalenedicarboxylate	-2	6	0.9985	-8.8±0.2	3.06±0.02
2,6-Naphthalenedisulfonate	-2	6	0.9992	-8.7±0.1	3.32±0.01
Phthalate (*ortho*)	-2	6	0.9935	-13.6±0.6	3.25±0.06
1,3,5-Benzenetricarboxylate	-3	5	0.9916	-12.9±0.7	3.61±0.08
1,3,(6 or 7)-Naphthalenetrisulfonate	-3	5	0.9866	-13.0±0.9	3.9±0.1
1,4,5,8-Naphthalenetetracarboxylate	-4	5	0.9987	-12.0±0.3	2.71±0.03
1,2,4,5-Benzenetetracarboxylate	-4	5	0.9971	-12.3±0.4	3.01±0.05

[a] Uncertainties are one standard deviation. [b] Number of data points used in the regression analysis. [c] Units = $10^{-4} cm^2 V^{-1} s^{-1} mol^{-0.5} L^{-0.5}$. [d] Units = $10^{-4} cm^2 V^{-1} s^{-1}$.

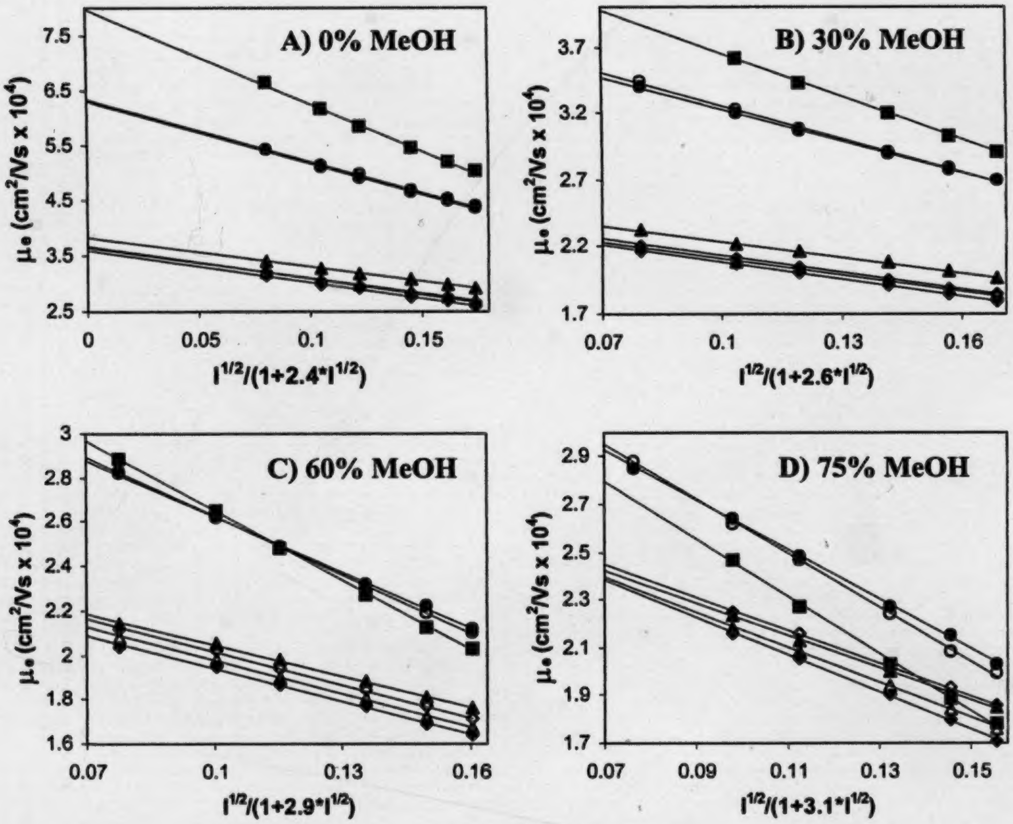

Figure 4.2: Ionic strength effects on the mobilities of organic cations for buffers containing (A) 0% MeOH, (B) 30% MeOH, (C) 60% MeOH and (D) 75% v/v MeOH. Solutes: ▲, benzylammonium; Δ, N-benzylmethylammonium; ♦, N,N-dimethylbenzylammonium; ◊, benzyltrimethylammonium; ●, p-xylylenediammonium; ○, m-xylylenediammonium; ■, 1,3,5-triammoniummethylbenzene. Experimental conditions: UV detection at 214 nm; bare fused-silica 60-cm capillary (50 cm to detector); 7.0 kV applied for (A), 10.0 kV applied for (B)-(D); 1 × 10^{-4} M sample concentration; 5 mM HCl buffer, ionic strength adjusted using NaCl.

Table 4.4: Ionic Strength Effects on the Mobility of Cations in MeOH/H_2O Media[a]

		Pitts Equation			
Cation	Charge	N[b]	R^2	Onsager Slope[c]	Intercept[d], μ_o
0% MeOH					
Benzylammonium	+1	6	0.9998	-5.20±0.04	3.823±0.005
N-Benzylmethylammonium	+1	6	0.9994	-5.46±0.06	3.642±0.009
N,N-Dimethylbenzylammonium	+1	6	0.9995	-5.69±0.06	3.602±0.008
Benzyltrimethylammonium	+1	6	0.9996	-5.74±0.06	3.672±0.008
p-Xylylenediammonium	+2	6	0.9966	-11.2±0.3	6.30±0.04
m-Xylylenediammonium	+2	6	0.9997	-11.24±0.09	6.34±0.01
1,3,5-Triammoniummethylbenzene	+3	6	0.9961	-17.2±0.5	7.98±0.07
30% MeOH					
Benzylammonium	+1	6	0.9985	-3.83±0.07	2.62±0.01
N-Benzylmethylammonium	+1	6	0.9970	-4.0±0.1	2.51±0.01
N,N-Dimethylbenzylammonium	+1	6	0.9997	-4.28±0.04	2.515±0.005
Benzyltrimethylammonium	+1	6	0.9998	-4.17±0.03	2.546±0.004
p-Xylylenediammonium	+2	6	0.9982	-7.9±0.2	4.03±0.02
m-Xylylenediammonium	+2	6	0.9982	-8.4±0.2	4.10±0.02
1,3,5-Triammoniummethylbenzene	+3	5	0.9998	-10.81±0.09	4.73±0.01
60% MeOH					
Benzylammonium	+1	6	0.9981	-4.6±0.1	2.50±0.01
N-Benzylmethylammonium	+1	6	0.9992	-5.00±0.07	2.475±0.009
N,N-Dimethylbenzylammonium	+1	6	0.9981	-5.0±0.1	2.44±0.01
Benzyltrimethylammonium	+1	6	0.9991	-4.96±0.07	2.512±0.009
p-Xylylenediammonium	+2	6	0.9993	-8.44±0.01	3.47±0.01
m-Xylylenediammonium	+2	6	0.9997	-8.83±0.07	3.511±0.009
1,3,5-Triammoniummethylbenzene	+3	6	0.9993	-10.5±0.1	3.70±0.02
75% MeOH					
Benzylammonium	+1	5	0.9992	-6.8±0.1	2.90±0.01
N-Benzylmethylammonium	+1	5	0.9995	-7.37±0.09	2.91±0.01
N,N-Dimethylbenzylammonium	+1	5	0.9998	-7.77±0.07	2.926±0.009
Benzyltrimethylammonium	+1	5	0.9988	-6.8±0.1	2.92±0.02
p-Xylylenediammonium	+2	6	0.9991	-10.5±0.2	3.66±0.02
m-Xylylenediammonium	+2	6	0.9995	-11.3±0.1	3.74±0.02
1,3,5-Triammoniummethylbenzene	+3	5	0.9986	-12.0±0.3	3.64±0.03

[a] Uncertainties are one standard deviation. [b] Number of data points used in the regression analysis. [c] Units = $10^{-4}cm^2V^{-1}s^{-1}mol^{-0.5}L^{-0.5}$. [d] Units = $10^{-4}cm^2V^{-1}s^{-1}$.

The Pitts' plots for the cations (Figure 4.2) are constructed using mobilities measured on bare fused-silica capillaries. Low-pH buffers are commonly used to minimize protein adsorption on bare capillaries [42]. It is therefore reasonable to expect that in the 5 mM HCl electrolytes investigated herein, minimal adsorption of the aromatic amines to the capillary wall is occurring. However, to verify that this is indeed the case, the mobilities of the +3 ammonium ion were also measured on PEO-coated μSIL-WAX capillaries. According to product specifications and literature [43-46] reports, this neutral hydrophilic coating prevents protein and peptide adsorption and should thus minimize adsorption of the aromatic ammonium ions. As suggested by Miller and Miller [47], the results were compared at each % methanol by plotting the mobilities from the uncoated capillary versus the mobilities from the coated capillary. The results from the corresponding regression analyses are in Table 4.5. For all methanol contents, the slopes and intercepts are not significantly different from the ideal values of 1 and 0, respectively, at the 95% confidence level. There is therefore no evidence for systematic differences between the mobilities measured on coated and uncoated capillaries. This confirms that analyte adsorption to the bare fused-silica capillary wall is not occurring. All further discussions will refer to the data obtained on uncoated capillaries.

Table 4.5: Correlation Between the Cation Mobilities Measured on Coated and Uncoated Capillaries

% MeOH	R^2	Slope (95% CI)	Intercept[a] (95% CI)
0	0.9968	1.01±0.08	$0.2_7 \pm 0.4_7$
30	0.9988	1.03±0.06	$0.1_9 \pm 0.2_2$
60	0.9994	0.99±0.03	$0.07_2 \pm 0.08_3$
75	0.9985	1.03±0.07	$0.1_3 \pm 0.1_6$

[a] Units = 10^{-4} cm^{2}V^{-1}s^{-1}

4.3.1.1 Influence of Analyte Charge on Ionic Strength Effect

For both the anions and cations, the ionic strength effect generally increases with increasing analyte charge at all methanol contents. As seen in Figure 4.1 and Table 4.3, the Onsager slopes for the –3 anions are significantly larger than those for the –2 anions at the 95% confidence level, and the slopes for the –2 ions are statistically larger than those for the –1 ions. The one exception to this is phthalate, whose ionic strength behavior is consistently greater than the other –2 analytes in all buffers studied. One possible explanation for this is the unsymmetrical charge distribution on phthalate. One of the assumptions of the Pitts equation is that the analyte charge is evenly distributed over the entire ion surface. However, phthalate's two charged moieties are *ortho* to one another and so the ion charge is entirely located on one side of the molecule.

To investigate this phenomenom, the mobilities of the *meta* and *para* isomers of phthalate were also determined at 0% and 75% MeOH. The results from the corresponding regression analyses are in Table 4.6. The absolute mobilities of the

Table 4.6: Ionic Strength Effects on the Mobility of Phthalate Isomers[a]

Anion	Charge	Pitts Equation			
		N[b]	R^2	Onsager Slope[c]	Intercept[d], μ_o
0% MeOH					
Phthalate (*ortho*)	-2	5	0.9973	-11.4±0.3	5.94±0.04
Isophthalate (*meta*)	-2	6	0.9976	-10.7±0.3	5.92±0.03
Terephthalate (*para*)	-2	5	0.9975	-9.6±0.3	5.77±0.04
75% MeOH					
Phthalate (*ortho*)	-2	6	0.9935	-13.6±0.6	3.25±0.06
Isophthalate (*meta*)	-2	6	0.9992	-10.4±0.2	3.35±0.02
Terephthalate (*para*)	-2	6	0.9989	-9.6±0.2	3.31±0.02

[a] Uncertainties are one standard deviation. [b] Number of data points used in the regression analysis. [c] Units = $10^{-4}cm^2V^{-1}s^{-1}mol^{-0.5}L^{-0.5}$. [d] Units = $10^{-4}cm^2V^{-1}s^{-1}$.

different isomers in both solvent systems are not statistically different at the 95% confidence level, suggesting that charge distribution does not significantly influence absolute mobility. This justifies the treatment of all investigated analytes as having symmetrical charge distributions, as discussed in Section 3.4.3.2.2. In contrast, upon changing the isomers from *ortho* to *meta* to *para*, the Onsager slopes show a decreasing trend at both methanol contents. Similar trends are seen for the *meta* and *para* diammonium ions in Table 4.4. Furthermore, at the 95% confidence level, the Onsager slopes for terephthalate at 0% and 75% MeOH are not significantly different from those for 2,6-naphthalenedisulfonate and 2,6-naphthalenedicarboxylate, respectively. Therefore, in contrast to phthalate, the data for terephthalate is in good agreement with the results obtained for the other –2 analytes. This supports our theory that the anomalous behavior of phthalate may result from its unsymmetrical charge distribution. However, it is unclear why similar behavior for phthalate was not observed by Li et al. [48]. Further investigations are required in order to fully understand the influence of charge distribution on mobility.

In Figure 4.1 and Table 4.3, the Onsager slopes for the –4 carboxylates at 0% MeOH are significantly larger than those for the –3 ions at the 95% confidence level. At 30% and 60% MeOH, the ionic strength effect experienced by the –4 ions are greater than for the –3 ions, although the large uncertainties in the Onsager slopes for these anions prevents a statistical interpretation of the data. At 75% MeOH, although statistically equivalent, the Onsager slopes for the –4 ions appear to be smaller than those for the –3 ions. Thus, despite the discrepancies seen for phthalate and for the –4 carboxylates at 75% MeOH, the overall trend is that the ionic strength effect increases with increasing anion charge.

Similar conclusions can be drawn for the cations. As seen in Figure 4.2 and Table 4.4, cations of higher charge experience larger ionic strength effects. In each buffer composition studied, the Onsager slopes for the +2 ammonium ions are always significantly larger than those for the +1 ions at the 95% confidence level. Further, with the exception of 75% MeOH, the Onsager slope for the +3 ammonium ion is statistically larger than those for the +2 analytes at the 95% confidence level. At 75% MeOH, the ionic strength efffect experienced by the +3 ion is greater than for the +2 ions, although the large uncertainties in the Onsager slopes for these ammonium ions prevents a statistical interpretation of the data.

The increase in ionic strength effect with increasing anion and cation charge is consistent with theory, since both terms in the brackets of equations 3.39 and 3.40 depend on analyte charge (z_- or z_+, respectively). It is also consistent with the ionic strength effects observed for anions in aqueous media [48]. Since the Onsager slope depends on analyte charge, varying the ionic strength is a powerful tool for altering the relative mobility between ions that differ in charge. Selectivity changes arising from the charge-dependence of the ionic strength effect have been frequently documented in the literature [49-51].

In the presence of methanol, selectivity changes resulting from ionic strength effects become more dramatic. For example, at 70 mM ionic strength, the general order of the ion mobilities is $\mu_{e,-2} \approx \mu_{e,-3} > \mu_{e,-1} > \mu_{e,-4}$ at 75% MeOH, compared to $\mu_{e,-3} > \mu_{e,-4} > \mu_{e,-2} > \mu_{e,-1}$ at 0% MeOH. For the cations at 0% MeOH (Figure 4.2a), the relative mobilities of the +1, +2 and +3 ions are changed by varying the ionic strength, but their migration order is not altered (at least up to I=90 mM). On the other hand, a migration order reversal is observed between +2 and +3 analytes in 60% MeOH and I=30 mM, and between +1 and +3 ions in 75% MeOH and I=70 mM. The more dramatic selectivity changes in methanol-containing media result from the variation of the Onsager slopes with solvent $1/\eta\varepsilon^{1/2}$, and from the slowing of the ions by viscosity and dielectric friction effects. The influence of solvent parameters on the Onsager slope is discussed in Section 4.3.1.2, while the influence of dielectric friction on ion mobility is discussed in Section 4.3.2.

4.3.1.2 Dominance of the Electrophoretic Term in the Onsager Slope

For the anions and cations investigated herein, the electrophoretic effect in the Pitts equation (left-hand term in the brackets of eqns 3.39 and 3.40) is predicted to contribute 60-80% towards the overall Onsager slope. The electrophoretic effect is therefore the dominant term in the brackets of the Pitts equation, and it can thus be used to estimate the magnitude of the ionic strength effect. However, before this term can be used to predict Onsager slopes, its charge dependence must be clarified.

As discussed in Section 3.5.4, z is bracketed in eqns 3.39 and 3.40 to reflect the discrepancy in charge dependence between the Debye-Hückel-Onsager theory and the Pitts equation [48]. Using GraphPad Prism software (GraphPad Software, Inc., San Diego, CA) and the anion data presented herein, the power dependence of z_- in the electrophoretic effect was optimized by plotting (Onsager slope)$\times\eta\times\varepsilon^{1/2}$ versus z_-^a, where a was allowed to vary. The optimal power dependence of the charge was 0.9±0.2 at the 95% confidence level, which supports a charge dependence of z_-, not z_-^2, in the first term in the brackets of eqns 3.39 and 3.40. Therefore, the form of the Pitts equation that is consistent with our results is

$$\mu_- = \mu_{-,o} - \left(\frac{41.25}{\eta(\varepsilon T)^{1/2} F} z_- + \frac{1.40 \times 10^6}{(\varepsilon T)^{3/2}} \left| z_- z_+ \right| \frac{2g}{1+\sqrt{g}} \mu_{-,o} \right) \frac{\sqrt{I}}{1 + Ba\sqrt{I}} \qquad (4.3)$$

for the anions, and

$$\mu_+ = \mu_{+,o} - \left(\frac{41.25}{\eta(\varepsilon T)^{1/2} F} z_+ + \frac{1.40 \times 10^6}{(\varepsilon T)^{3/2}} \left| z_+ z_- \right| \frac{2g}{1+\sqrt{g}} \mu_{+,o} \right) \frac{\sqrt{I}}{1 + Ba\sqrt{I}} \qquad (4.4)$$

for the cations. The charge dependence in eqns 4.3 and 4.4 is consistent with that of the Debye-Hückel-Onsager theory [37, 52].

Figure 4.3 shows the plots of Onsager slope versus the $z/\eta\varepsilon^{1/2}$ dependence predicted by the electrophoretic effect (left-hand term in the brackets). For the anions (Figure 4.3a), the plot constructed using all data points shows fair correlation ($R^2 = 0.81$), although the data for phthalate and for the –4 analytes at 75% MeOH appear to be outliers. The anomalous behavior of these ions was discussed in Section 4.3.1.1. With these outliers removed, the correlation greatly improves ($R^2 = 0.96$), and the corresponding regression line is illustrated in Figure 4.3a. For the cations, the plot of Onsager slope versus $z/\eta\varepsilon^{1/2}$ (Figure 4.3b) also shows good correlation, with $R^2 = 0.92$. Therefore, the Onsager slopes for anions and cations in methanol-water media vary in a manner consistent with the electrophoretic effect. However, the importance of the relaxation effect should not be overlooked, especially when dealing with the mobilities of ions with similar charge. This is discussed in greater detail in Section 4.3.1.3. Also noteworthy is that in aqueous media, Li et al. [48] observed good agreement between Onsager slope and analyte charge up to a charge of –4. However, the more highly-charged –5 and –6 sulfonates experienced weaker ionic strength effects than predicted by the Pitts theory.

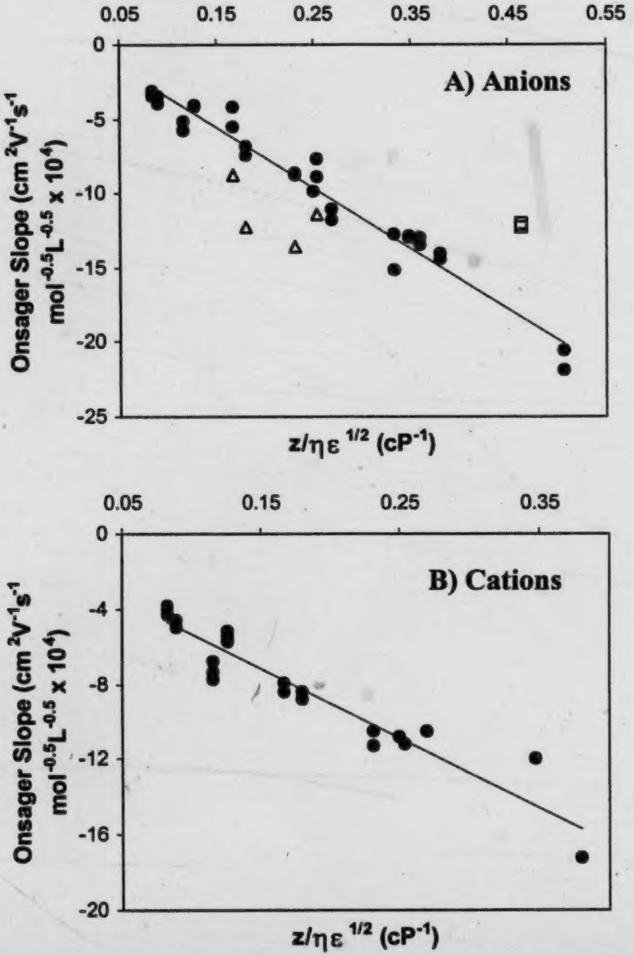

Figure 4.3: Dependence of Onsager slope on the electrophoretic effect for A) anions and B) cations in methanol-water media. In (A), the phthalate data is represented by Δ, and the –4 anions at 75% MeOH are represented by □. The regression line shown was constructed with these outliers removed.

4.3.1.3 Variations in Onsager Slope for Ions of Similar Charge: The Importance of the Relaxation Effect

It has previously been noted that the Onsager slopes for ions of similar charge are similar [41, 48], as would be predicted on the basis of the dominant electrophoretic term in eqns 4.3 and 4.4. For the anions and cations investigated herein, the plots in Figures 4.1 and 4.2 are approximately parallel for ions of like charge (with the exception of phthalate). As a result, changing the ionic strength is not an effective means to alter the selectivity between similarly charged ions. However, Mechref et al. [50] have demonstrated that changes in ionic strength can be used to alter the relative mobility between saccharides of similar charge. Indeed, although the plots in Figures 4.1 and 4.2 are nearly parallel for ions of like charge, there are several instances in which the slopes are not statistically equivalent at the 95% confidence level. Excluding phthalate, these include the –2 anions in 30% MeOH, the +1 ammonium ions in 0, 30 and 75% MeOH, and the +2 ions in 60% MeOH. Ionic strength-induced selectivity changes for ions of like charge are theoretically possible since the relaxation effect (right-hand term in the brackets of eqns 4.3 and 4.4) depends on both the analyte charge and the absolute mobility of the ion (μ_o). Although the electrophoretic effect is dominant, ionic strength-induced selectivity changes can occur between similarly charged ions if the absolute mobilities of the ions are significantly different.

In the present study, the relaxation effect can explain the differences between Onsager slopes for the –2 anions in 30% MeOH and the +2 cations in 60% MeOH. In both cases, the ion with the largest slope also has the largest absolute mobility. On the other hand, for the +1 ammonium ions, the solute with the lowest Onsager slope generally has the highest absolute mobility. Thus the relaxation effect cannot explain the small differences in Onsager slope observed for the +1 ions in 0, 30 and 75% MeOH. Furthermore, although phthalate's mobility is greater than that of the other two doubly charged anions studied herein (except at 75% MeOH), the relaxation effect cannot fully account for the large increase in phthalate's slope. As discussed in Section 4.3.1.1, phthalate's behavior may be partially explained by its unsymmetrical charge distribution.

In conclusion, the relaxation effect can account for some, but not all, of the ionic strength-induced selectivity changes observed between same-charge analytes in water-methanol media. Further investigations are required to fully understand the importance of additional factors, such as ion association and charge distribution.

4.3.2 Dielectric Friction

As shown in Table 4.1, increasing the methanol content causes a decrease in the dielectric constant and an increase in the dielectric relaxation time. Consequently, as predicted by eqn 3.27, the contribution of dielectric friction to the overall mobility of ions will increase as the % MeOH increases. For the anions and cations investigated herein, the influence of dielectric friction on ion mobility was investigated by plotting the Walden product ($\mu_o\eta$) versus %MeOH. The corresponding plots are in Figure 4.4. According to the Hückel equation (eqn 1.5), these plots will be horizontal if hydrodynamic friction is the only friction experienced by the ions. However, if additional frictional forces (i.e., dielectric friction) are present, the ions will migrate more slowly than predicted by the Hückel equation. This slower-than-expected migration will manifest itself as a negative deviation from the horizontal in plots of $\mu_o\eta$ versus solvent composition.

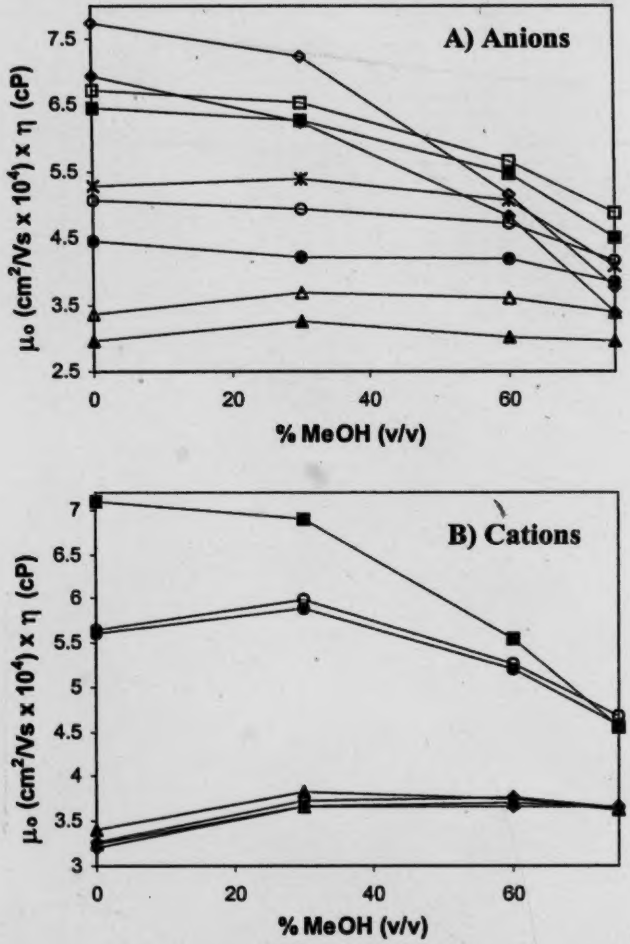

Figure 4.4: Dependence of the Walden product on the methanol content of the buffer for A) anions and B) cations. (A) Solutes: ▲, p-nitrobenzoate; Δ, benzenesulfonate; ●, 2,6-naphthalenedicarboxylate; ○, 2,6-naphthalenedisulfonate; ∗, phthalate; ■, 1,3,5-benzenetricarboxylate; □, 1,3,(6 or 7)-naphthalenetrisulfonate; ♦, 1,4,5,8-naphthalenetetracarboxylate; ◊, 1,2,4,5-benzenetetracarboxylate. Experimental conditions as in Figure 4.1. (B) Solutes: ▲, benzylammonium; Δ, N-benzylmethylammonium; ♦, N,N-dimethylbenzylammonium; ◊, benzyltrimethylammonium; ●, p-xylylenediammonium; ○, m-xylylenediammonium; ■, 1,3,5-triammoniummethylbenzene. Experimental conditions as in Figure 4.2.

According to van der Waals' volumes generated using Molecular Modeling Pro (WindowChem Software, Fairfield, CA; Version 1.44), the anions and cations range in size from 127-268 Å^3 and 109-166 Å^3, respectively. Therefore, the anion size approximately doubles as the charge is increased from –1 to –4, while the cation size increases by a factor of ~1.5 as the charge is increased from +1 to +3. However, over the same charge range, q^2 increases by a factor of 16 for the anions and 9 for the cations. Since dielectric friction is proportional to q^2/r^3, the effect of charge has a much larger impact on dielectric friction than analyte size. Thus, further discussion will refer to the 'charge' dependence, rather than the 'q^2/r^3' dependence, of dielectric friction.

In Figure 4.4, the negative deviation from ideal Hückel (horizontal) behavior for the anions and cations increases with increasing methanol content. This is consistent with the Hubbard-Onsager dielectric friction theory (eqn 3.27), which predicts that dielectric friction should be proportional to τ/ε. From Table 4.1, τ increases and ε decreases with increasing % MeOH, so that the ratio τ/ε increases. Therefore, dielectric friction should increase as the buffer methanol content increases.

The Walden products for the singly charged ions are approximately constant as the methanol content is varied (Figure 4.4). This suggests that the +1 and –1 ions experience very little dielectric friction, which is not surprising since dielectric friction is proportional to q^2/r^3. Indeed, Sarmini and Kenndler [28] have reported that viscosity effects can roughly account for the changes in mobility observed for a series of monocarboxylated organic anions (charge = –1). However, from 0-30% MeOH, an *increase* in mobility for the –1, +1 and +2 ions is evident. Therefore, these ions are experiencing *less* friction than that predicted solely by the Hückel equation (eqn 1.5). Similar behavior has been previously reported for anions in ethanol-water [34] and propanol-water [35], as well as for alkylammonium ions in aqueous, methanol-water, ethanol-water and nonaqueous media [53-57]. Nakahara and coworkers [58-61] have proposed the "passing-through-cavities" mechanism to explain this anomalous increase in mobility. The premise behind this mechanism is that an ion that is weakly interacting with solvent molecules passes through a series of larger unoccupied cavities in the open structure of the solvent [59]. These cavities result from the heterogeneity of the solvent structure. Further, Kay [62] has stated that the larger-than-expected Walden products observed for ions in mixed aqueous-organic media are likely due to the structure-breaking role of the ions. According to the Frank-Wen model [63] (Section 3.2.3), in the intermediate region between the solvation shell of the ion and the bulk solvent, the ionic charge interferes with the formation of the normal solvent structure. This structure-breaking effect increases with decreasing charge density of the ion, and results in a higher-than-expected ion mobility/conductivity.

As seen in Figure 4.4, the negative deviation from ideal Hückel behavior becomes more pronounced with increasing analyte charge. This is consistent with the dielectric friction theory of Hubbard and Onsager (eqn 3.27), which predicts that dielectric friction should increase with increasing analyte charge. Therefore, the selectivity changes observed in Figure 4.4 between anions and cations differing in charge can be attributed to dielectric friction. For example, a migration order reversal is observed between the –4 and –3 anions at 30% MeOH, and between the –4 and –2 anions at 75% MeOH. For the cations, the migration order between the +3 and +2 ions is reversed at 75% MeOH. These migration orders, which are contrary to the trends predicted by charge (eqn 1.5), result from the greater dielectric friction experienced by the more highly charged ions.

Dielectric friction may account for some of the anomalous mobility behavior that has been reported in the literature. For instance, Bowser et al. [3] studied the migration behavior of multiply charged porphyrins in nonaqueous CE using methanol as the solvent. They found that a porphyrin with a –2 charge had a higher mobility than a porphyrin of similar size with a –4 charge. This reversal in migration order could be explained on the basis of the greater dielectric friction expected for the highly charged porphyrin. In separate reports, Salimi-Moosavi et al. [4] and Yang et al. [5] studied the influence of methanol-water mixtures on the electrophoretic mobilities of small inorganic anions. In both accounts, the addition of methanol resulted in a preferential decrease in the mobilities of the –2-charged inorganic anions, as compared to the singly charged anions. In particular, the mobility of SO_4^{2-} dropped below that of NO_3^- as methanol was added to the buffer. This migration order may result from SO_4^{2-} experiencing more dielectric friction due to its higher charge-to-size ratio. Massart and coworkers [14] observed significant selectivity changes between singly and doubly charged inorganic cations upon varying the methanol content in the electrophoretic buffer. For example, they found that a migration order reversal between Na^+ and Ca^{2+} occurred when the methanol content was changed from 5% to 15%. Further, Tangen et al. [15] reported that upon addition of 25% (v/v) methanol to the electrophoretic media, the migration times of Ca^{2+}, Mg^{2+} and Sr^{2+} increased more than those for Na^+, K^+ and Ba^{2+}. These selectivity changes could be explained by the greater dielectric friction expected for cations with higher charge-to-size ratios.

4.3.3 Correlation Between Mobility and Solvent Parameters

According to the Hubbard-Onsager equation for ion mobility (eqn 3.27), the solvent parameters ε, η and τ are all important in regulating the mobility of ions. It is therefore of interest to determine whether changes in ionic mobility can be correlated to changes in solvent ε, η and τ. The Hubbard-Onsager equation can be easily rearranged into the following form:

$$\frac{1}{\mu_o \eta} = \frac{6\pi r}{q} + \left(\frac{17}{280}\right)\frac{\tau q}{r^3 \eta \varepsilon} \tag{4.5}$$

Plots of $1/\mu_o\eta$ versus $\tau/\eta\varepsilon$ should thus be linear, with intercepts proportional to *r*/*q* and slopes proportional to q/r^3. Figure 4.5 plots the absolute mobilities determined herein (Tables 4.3 and 4.4) in this manner. The corresponding correlation coefficients, slopes and intercepts are in Table 4.7.

For the singly-charged analytes (▲, Δ in Figure 4.5a; ▲, Δ, ◆, ◊ in Figure 4.5b), the plots of $1/\mu_o\eta$ versus $\tau/\varepsilon\eta$ are poorly correlated, and the slopes are not statistically different from zero. This is expected, since the +1 and –1 ions do not experience much dielectric friction (Figure 4.4) and have relatively uniform Walden products. The plots for the doubly-charged ions (●, ○, ✱ in Figure 4.5a; ●, ○ in Figure 4.5b) show better correlation (R^2>0.89), and with the exception of 2,6-naphthalenedicarboxylate, the slopes are significantly different from zero at the 95% confidence level. This reflects the onset of dielectric friction effects at 75% MeOH for the –2 ions and 60% MeOH for the +2 ions (Figure 4.4). For the +3, –3 and –4 ions, whose mobilities are strongly influenced by dielectric friction as early at 30% MeOH, the Hubbard-Onsager equation is successful in predicting the change in ion mobility with changing τ. ε and η. Plots of $1/\mu_o\eta$ versus

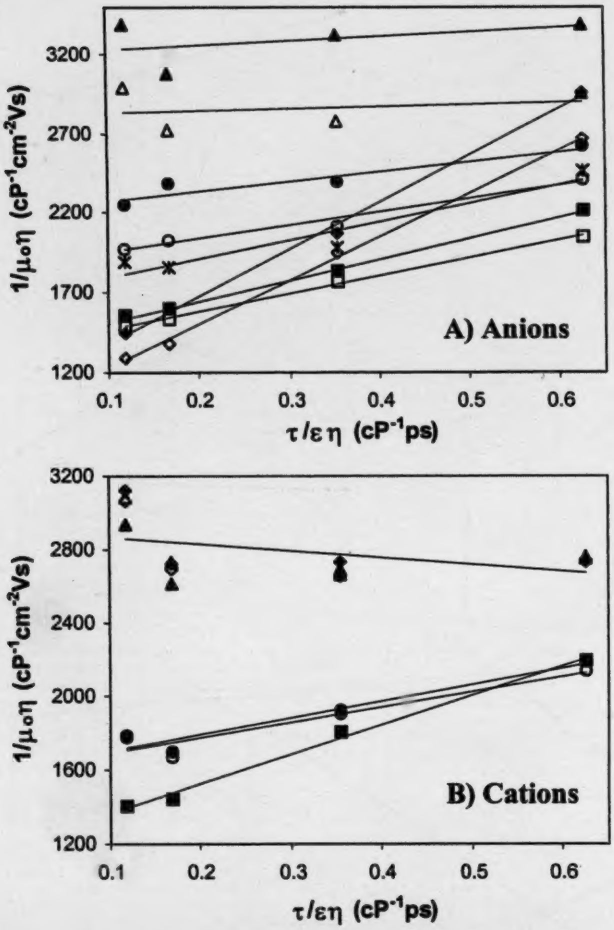

Figure 4.5: Correlation between change in ion mobility and solvent τ, ε and η for A) anions and B) cations in methanol-water media, according to the Hubbard-Onsager equation (eqn 3.27). For (A), legend and experimental conditions as in Figure 4.1. For (B), legend and experimental conditions as in Figure 4.2. For clarity, the regression line for only one of the +1 cations is shown.

$\tau/\varepsilon\eta$ for these highly-charged ions (■, □, ♦, ◊ in Figure 4.5a; ■ in Figure 4.5b) show excellent correlation, with $R^2 \geq 0.996$. The good correlation between ion mobility and solvent parameters supports the theory that dielectric friction plays an important role in the methanol-induced selectivity changes seen in Figure 4.4. To my knowledge, this is the first report relating ion mobility in CE to solvent τ, ε and η.

Table 4.7: Regression Data for the Plots of $1/\mu_o\eta$ versus $\tau/\varepsilon\eta$ (Figure 4.5) Constructed for the Anions and Cations in Methanol-Water Media[a]

Analyte	Charge	R^2	Slope[b]	Intercept[c]
ANIONS				
p-Nitrobenzoate	-1	0.209	310±420	3190±160
Benzenesulfonate	-1	0.072	160±400	2810±150
2,6-Naphthalenedicarboxylate	-2	0.895	630±150	2210±60
2,6-Naphthalenedisulfonate	-2	0.971	840±100	1870±40
Phthalate (*ortho*)	-2	0.911	1170±260	1680±100
1,3,5-Benzenetricarboxylate	-3	0.998	1330±50	1380±20
1,3,(6 or 7)-Naphthalenetrisulfonate	-3	0.999	1160±20	1348±9
1,4,5,8-Naphthalenetetracarboxylate	-4	0.997	2960±120	1080±50
1,2,4,5-Benzenetetracarboxylate	-4	0.999	2740±70	950±30
CATIONS				
Benzylammonium	+1	0.038	-120±430	2780±160
N-Benzylmethylammonium	+1	0.272	-410±480	2940±180
N,N-DimethylBenzylammonium	+1	0.311	-470±500	2980±190
Benzyltrimethylammonium	+1	0.215	-370±510	2900±190
p-Xylylenediammonium	+2	0.940	890±160	1610±60
m-Xylylenediammonium	+2	0.915	840±180	1600±70
1,3,5-Triammoniummethylbenzene	+3	0.996	1600±70	1210±30

[a] Uncertainties are one standard deviation. [b] Units = $10^{12}Vcm^{-2}$. [c] Units = $Vs(cm^{-2}cP^{-1})$.

In Figure 4.5 and Tables 4.7, the slopes and the intercepts vary with charge in a manner consistent with that predicted by eqn 4.5. The intercepts decrease with increasing analyte charge, and the slopes are generally steeper for analytes of higher charge. The anomalous behavior of phthalate has been previously noted in Section 4.3.1.1. Since the slope should be directly proportional to q/r^3, an increase in slope of ~33% should be observed on going from a –3 charged analyte to a –4 charged analyte (assuming a negligible change in size). However, the slope more than doubles! This anomaly may result from extending the use of the Hubbard-Onsager equation (eqn 3.27) beyond its limits. One of the simplifying assumptions used in deriving this equation was that the hydrodynamic friction accounted for >> 50% of the total friction (Section 3.4.3.2.2).

However, even at 0% MeOH, the hydrodynamic friction experienced by the –3 and –4 ions is only 57-70% and 45-53% of the total friction, respectively, as calculated on the basis of eqn 3.27. At 75% MeOH, the hydrodynamic friction contributes even less to the total friction, being only 21-33% for the –3 ions and 15-20% for the –4 ions. Thus, equation 3.27 might be too simplified to account for the significant dielectric friction experienced by the –3- and –4-charged analytes in mixed MeOH/H_2O media. Nonetheless, the Hubbard-Onsager model provides significant insight into the effect of such solvent systems on electrophoretic mobilities in CZE.

4.3.4 Comparison of Dielectric Friction Effects for Cations and Anions

The Hubbard-Onsager dielectric friction theory (eqn 3.27) does not predict a difference in behavior between anions and cations. However, it seems intuitive that solvent molecules will orient themselves differently depending on whether they are in the presence of a positive or a negative charge. It is therefore of interest to determine whether differences in dielectric friction between anions and cations can be experimentally observed. Figure 4.6 compares the plots of normalized $\mu_o\eta$ versus %MeOH for the +3 ammonium ion and the –3 carboxylate and sulfonate. The Walden product for each analyte at X% MeOH is normalized to its Walden product at 0% MeOH. As such, an increase in dielectric friction is expressed as a decrease in normalized $\mu_o\eta$.

At 60% and 75% MeOH, the +3 ammonium ion (■) experiences considerably more dielectric friction than both the –3 carboxylate (○) and the –3 sulfonate (Δ). This is not a result of size effects, since the +3 ammonium ion and the –3 carboxylate have almost identical van der Waals' volumes of 166 Å^3 and 170 Å^3, respectively (as determined using Molecular Modeling Pro). A larger size difference exists between the –

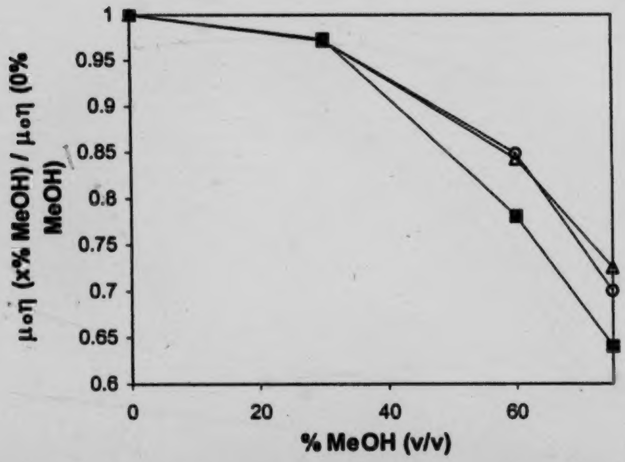

Figure 4.6: Comparison of dielectric friction effects experienced by cations and anions in methanol-water media. The Walden product for each analyte at X% MeOH is normalized to its Walden product at 0% MeOH. Solutes: ○, 1,3,5-benzenetricarboxylate; Δ, 1,3,(6 or 7)-naphthalenetrisulfonate; ■, 1,3,5-triammoniummethylbenzene.

3 carboxylate and the –3 sulfonate (170 Å^3 and 268 Å^3, respectively), yet these two anions experience almost identical dielectric friction. Thus the sign of the ion charge is apparently responsible for the variation in dielectric friction. Differences in behavior between anions and cations have been previously reported in the literature [64-69]. Depending on the nature of the solvent and analyte, the effect of dielectric fricton is greater for cations in some instances and greater for anions in others. The Hubbard-Onsager theory fails at predicting these differences because it is a continuum model, and as such, it does not consider ion-solvent interactions, solvent structure, or the nature of the solvent motion [70, 71]. Evans et al. [64] have stated that "*the different behaviors of cations and anions in a given solvent cannot be satisfactorily explained by a continuum theory since there is no direct way to account for cation-solvent or anion-solvent interactions*". Evidently, a molecular model would be more effective than a continuum

model at differentiating between anions and cations. Recently, a molecular dynamic simulation developed by Rasaiah and coworkers [65-68] has been able to reproduce the different behaviors observed for cations and anions in water. These differences were attributed to the charge asymmetry of the water molecules surrounding the ions [68]. Further, Chong and Hirata [69] have recently developed the first molecular theory capable of describing the difference in dynamics of positive and negative ions in aqueous solution. However, even though the Hubbard-Onsager continuum model cannot predict these differences, it is still successful at explaining the selectivity changes observed for aromatic anions and cations in mixed methanol-water media.

4.4 Concluding Remarks

In both aqueous and methanol-water media, the anions and cations investigated herein experience greater ionic strength effects with increasing analyte charge. Thus selectivity changes between ions differing in charge can be achieved by altering the ionic strength. Further, the ionic strength effects vary as a function of solvent $1/\eta\varepsilon^{1/2}$, as predicted by the electrophoretic term in the Pitts' equation.

The Hubbard-Onsager dielectric friction theory is successful at predicting the mobility behavior of aromatic anions and cations in media containing methanol. Consistent with the Hubbard-Onsager equation (eqn 3.27), an increase in dielectric friction is observed with increasing ion charge and with increasing methanol content. Further, changes in ion mobility correlate with the corresponding changes in solvent τ, ε and η. Therefore, the selectivity changes observed for both cations and anions in mixed methanol-water media can be accounted for by dielectric friction. To my knowledge, this is the first report demonstrating the importance of solvent τ to ion mobility.

Although the mobilities predicted by the Hubbard-Onsager theory are the same for both positive and negative ions, the +3 ammonium ion experiences greater dielectric friction than the –3 carboxylate and sulfonate. The inability of the Hubbard-Onsager model to predict these differences may be a result of its continuum nature, whereby ion-solvent interactions are not taken into account. Nonetheless, it remains a useful model for predicting solvent-dependent selectivity changes. Solvent systems other than methanol-water are investigated in Chapter 5.

4.5 References

(1) Salimi-Moosavi, H.; Cassidy, R. M. *Anal. Chem.* **1996,** *68*, 293-299.

(2) Bowser, M. T.; Sternberg, E. D.; Chen, D. D. Y. *Anal. Biochem.* **1996,** *241*, 143-150.

(3) Bowser, M. T.; Sternberg, E. D.; Chen, D. D. Y. *Electrophoresis* **1997,** *18*, 82-91.

(4) Salimi-Moosavi, H.; Cassidy, R. M. *Anal. Chem.* **1995,** *67*, 1067-1073.

(5) Yang, Y.; Liu, F.; Kang, J.; Ou, Q. *J. Chromatogr. A* **1999,** *834*, 393-399.

(6) Harrold, M. P.; Wojtusik, M. J.; Riviello, J.; Henson, P. *J. Chromatogr.* **1993,** *640*, 463-471.

(7) Lee, Y. J.; Price, W. E.; Sheil, M. M. *Analyst* **1995,** *120*, 2689-2694.

(8) Porras, S. P.; Wiedmer, S. K.; Strandman, S.; Tenhu, H.; Riekkola, M.-L. *Electrophoresis* **2001,** *22*, 3805-3812.

(9) Roldan-Assad, R.; Gareil, P. *J. Chromatogr. A* **1995,** *708*, 339-350.

(10) Vallejo-Cordoba, B.; Mazorra-Manzano, M. A.; Gonzalez-Cordova, A. F. *J. Capillary Electrop.* **1998,** *5*, 111-114.

(11) Mendonsa, S. D.; Hurtubise, R. J. *J. Liq. Chromatogr. Rel. Technol.* **1999,** *22*, 1027-1040.

(12) Wu, J.; Wong, M. K.; Lee, H. K.; Ong, C. N. *J. Chromatogr. Sci.* **1995,** *33*, 712-716.

(13) Galceran, M. T.; Carneiro, M. C.; Diez, M.; Puignou, L. *J. Chromatogr. A* **1997,** *782*, 289-295.

(14) Yang, Q.; Smeyers-Verbeke, J.; Wu, W.; Khots, M. S.; Massart, D. L. *J. Chromatogr. A* **1994,** *688*, 339-349.

(15) Tangen, A.; Lund, W.; Frederiksen, R. B. *J. Chromatogr. A* **1997,** *767*, 311-317.

(16) Geiser, L.; Cherkaoui, S.; Veuthey, J.-L. *J. Chromatogr. A* **2000,** *895*, 111-121.

(17) Porras, S. P.; Jyske, P.; Riekkola, M.-L.; Kenndler, E. *J. Microcolumn Sep.* **2001,** *13*, 149-155.

(18) Karbaum, A.; Jira, T. *Electrophoresis* **1999,** *20*, 3396-3401.

(19) Sahota, R. S.; Khaledi, M. G. *Anal. Chem.* **1994,** *66*, 1141-1146.

(20) Valkó, I. E.; Sirén, H.; Riekkola, M.-L. *LC-GC* **1997,** *15*, 560-567.

(21) Tjørnelund, J.; Bazzanella, A.; Lochmann, H.; Bächmann, K. *J. Chromatogr. A* **1998,** *811*, 211-217.

(22) Schwer, C.; Kenndler, E. *Anal. Chem.* **1991,** *63*, 1801-1807.

(23) Akhadov, Y. Y. *Dielectric Properties of Binary Solutions. A Data Handbook*; Pergamon Press: New York, 1980.

(24) Chekalin, N. V.; Shakhparonov, M. I. *Russ. J. Phys. Chem.* **1971,** *45*, 250-253.

(25) Daniel, V. V. *Dielectric Relaxation*; Academic Press: New York, 1967.

(26) *CRC Handbook of Chemistry and Physics*, 76th ed.; CRC Press: New York, 1995-1996.

(27) Perrin, D. D.; Dempsey, B. *Buffers for pH and Metal Ion Control*; Chapman and Hall Ltd: London, 1974.

(28) Sarmini, K.; Kenndler, E. *J. Chromatogr. A* **1998,** *806*, 325-335.

(29) Rived, F.; Canals, I.; Bosch, E.; Rosés, M. *Anal. Chim. Acta* **2001,** *439*, 315-333.

(30) Martell, A. E.; Smith, R. M. *Critical Stability Constants*; Plenum Press: New York, 1977, Vol. 3.

(31) Martell, A. E.; Smith, R. M. *Critical Stability Constants*; Plenum Press: New York, 1977, Vol. 5.

(32) Kortum, G.; Vogel, W.; Andrussow, K. *Dissociation Constants of Organic Acids in Aqueous Solution*; Butterworths: London, 1961.

(33) Weitl, F. L.; Raymond, K. N. *J. Am. Chem. Soc.* **1979,** *101*, 2728-2731.

(34) Sarmini, K.; Kenndler, E. *J. Chromatogr. A* **1998,** *811*, 201-209.

(35) Sarmini, K.; Kenndler, E. *J. Chromatogr. A* **1998,** *818*, 209-215.

(36) Williams, B. A.; Vigh, G. *Anal. Chem.* **1996,** *68*, 1174-1180.

(37) Erdey-Grúz, T. *Transport Phenomena in Aqueous Solutions*; John Wiley & Sons: New York, 1974, Chapter 4.

(38) Mussini, T.; Covington, A. K.; Longhi, P.; Rondinini, S. *Pure Appl. Chem.* **1985,** *57*, 865-876.

(39) Paabo, M.; Robinson, R. A.; Bates, R. G. *J. Am. Chem. Soc.* **1965,** *87*, 415-418.

(40) Barbosa, J.; Sanz-Nebot, V. *Anal. Chim. Acta* **1991,** *244*, 183-191.

(41) Porras, S. P.; Riekkola, M.-L.; Kenndler, E. *J. Chromatogr. A* **2001,** *924*, 31-42.

(42) McCormick, R. M. *Anal. Chem.* **1988,** *60*, 2322-2328.

(43) Gombotz, W. R.; Guanghui, W.; Horbett, T. A.; Hoffman, A. S. *J. Biomed. Mater. Res.* **1991,** *25*, 1547-1562.

(44) McPherson, T.; Kidane, A.; Szleifer, I.; Park, K. *Langmuir* **1998,** *14*, 176-186.

(45) Sofia, S. J.; Premnath, V.; Merrill, E. W. *Macromolecules* **1998,** *31*, 5059-5070.

(46) Ng, C. L.; Lee, H. K.; Li, S. F. Y. *J. Chromatogr. A* **1994,** *659*, 427-434.

(47) Miller, J. C.; Miller, J. N. *Statistics for Analytical Chemistry*, 2nd ed.; Ellis Horwood Limited: Chichester, 1988.

(48) Li, D.; Fu, S.; Lucy, C. A. *Anal. Chem.* **1999,** *71*, 687-699.

(49) Friedl, W.; Reijenga, J. C.; Kenndler, E. *J. Chromatogr. A* **1995,** *709*, 163-170.

(50) Mechref, Y.; Ostrander, G. K.; Rassi, Z. E. *J. Chromatogr. A* **1997,** *792*, 75-82.

(51) Carou, M. I. T.; Mahía, P. L.; Lorenzo, S. M.; Fernández, E. F.; Rodríguez, D. P. *J. Chromatogr. A* **2001,** *918*, 411-421.

(52) Bockris, J. O. M.; Reddy, A. K. N. *Modern Electrochemistry*; Plenum Press: New York, 1970, Vol. 1, pp 420-440.

(53) Ibuki, K.; Nakahara, M. *J. Chem. Phys.* **1986,** *84*, 2776-2782.

(54) Ibuki, K.; Nakahara, M. *J. Phys. Chem.* **1986,** *90*, 6362-6365.

(55) Ibuki, K.; Nakahara, M. *J. Phys. Chem.* **1987,** *91*, 1864-1867.

(56) Ibuki, K.; Nakahara, M. *J. Phys. Chem.* **1987,** *91*, 4411-4414.

(57) Kenndler, E.; Jenner, P. *J. Chromatogr.* **1987,** *390*, 185-197.

(58) Takisawa, N.; Osugi, J.; Nakahara, M. *J. Phys. Chem.* **1981,** *85*, 3582-3585.

(59) Takisawa, N.; Osugi, J.; Nakahara, M. *J. Chem. Phys.* **1982,** *77*, 4717-4722.

(60) Takisawa, N.; Osugi, J.; Nakahara, M. *J. Chem. Phys.* **1983,** *78*, 2591-2597.

(61) Nakahara, M.; Török, T.; Takisawa, N.; Osugi, J. *J. Chem. Phys.* **1982,** *76*, 5145-5149.

(62) Kay, R. L. In *Water. A Comprehensive Treatise*; Franks, F., Ed.; Plenum Press: New York, 1973; Vol. 3, pp 204-209.

(63) Frank, H. S.; Wen, W.-Y. *Disc. Faraday Soc.* **1957,** *24*, 133-140.

(64) Evans, D. F.; Tominaga, T.; Hubbard, J. B.; Wolynes, P. G. *J. Phys. Chem.* **1979,** *83*, 2669-2677.

(65) Koneshan, S.; Lynden-Bell, R. M.; Rasaiah, J. C. *J. Am. Chem. Soc.* **1998,** *120*, 12041-12050.

(66) Koneshan, S.; Rasaiah, J. C.; Lynden-Bell, R. M.; Lee, S. H. *J. Phys. Chem. B* **1998,** *102*, 4193-4204.

(67) Lee, S. H.; Rasaiah, J. C. *J. Phys. Chem.* **1996,** *100*, 1420-1425.

(68) Rasaiah, J. C.; Lynden-Bell, R. M. *Phil. Trans. R. Soc. Lond. A* **2001,** *359*, 1545-1574.

(69) Chong, S.-H.; Hirata, F. *J. Chem. Phys.* **1999,** *111*, 3654-3667.

(70) Biswas, R.; Bagchi, B. *J. Chem. Phys.* **1997,** *106*, 5587-5598.

(71) Wolynes, P. G. *J. Chem. Phys.* **1978,** *68*, 473-483.

CHAPTER FIVE. Mobility of Anions in Aqueous-Organic Media Containing Acetonitrile, Ethanol and 2-Propanol[‡]

5.1 Introduction

In Chapter 4, I demonstrated that dielectric friction could account for some of the observed selectivity changes in methanol-water media. The question that now arises is whether the Hubbard-Onsager dielectric friction model will be successful at predicting selectivity changes in solvent systems characterized by more or less dielectric friction. As detailed in Chapter 3, the Hubbard-Onsager equation (eqn 3.27) is derived with the simplifying assumption that hydrodynamic friction accounts for >> 50% of the total friction. However, the hydrodynamic friction experienced by the –3 and –4 ions in 75% methanol is already < 35% of the total friction (Section 4.3.3). In aqueous-organic media characterized by larger τ/ε ratios, the impact of hydrodynamic friction will be even less. It is therefore of interest to determine whether the use of the Hubbard-Onsager dielectric friction model can be extended to such solvent systems.

As seen in Table 5.1, aqueous-organic mixtures containing either ethanol or 2-propanol have greater τ/ε ratios than methanol-water media. According to the Hubbard-Onsager dielectric friction model (eqn 3.27), ion migration in these solvent systems should therefore be more strongly influenced by dielectric friction. Conversely, less dielectric friction should be experienced in acetonitrile-water mixtures than in methanol-water mixtures. The use of acetonitrile, ethanol and 2-propanol as organic modifiers in CE has been frequently reported. Among other applications, acetonitrile has been used as either organic modifier or as pure nonaqueous media for the analysis of quinolones [1], long-chain surfactants [2], inorganic anions [3], heterocyclic aromatic amines [4], substituted benzoic acids [5] and sulfonamides [6]. Aqueous-organic mixtures containing either ethanol or 2-propanol have been used for the capillary electrophoretic analysis of amino acids and peptides [7-9], erythromycin [10], enantiomers [11], pharmaceuticals [12] and aromatic sulfonates [13]. The use of these organic solvents has resulted in selectivity changes compared to aqueous media.

[‡] A version of this chapter has been published. a) Roy, K. I.; Lucy, C. A. *Electrophoresis* **2002**, 23, 383-392. b) Roy, K. I.; Lucy, C. A. *Journal of Chromatography A* **2002**, 964, 213-225.

Table 5.1: Effect of Buffer Organic Solvent Content on Solvent Parameters

% Organic Solvent (v/v)	η^a (cP)	ε^b	τ^c (ps)	τ/ε (ps)
0%	0.89^d	78.48^e	8.25^e	0.11
30% MeOH^f	1.46	67.61	16.6	0.25
60% MeOH^f	1.50	55.00	29.2	0.53
75% MeOH^f	1.25	47.78	37.4	0.78
30% ACN	0.95	65.5^e	9.1	0.14
60% ACN	0.73	51.0^e	7.8	0.15
75% ACN	0.57	44.72	6.5	0.15
30% EtOH	1.96	64.39	18.9	0.29
60% EtOH	2.28	47.91	36.8	0.77
75% EtOH	2.00	39.08	58.1	1.49
30% 2-PrOH	2.31	61.16	21.2	0.35
60% 2-PrOH	3.03	40.49	43.0	1.06
75% 2-PrOH	2.85	30.23	73.7	2.44

[a] Values calculated by multiplying the relative viscosities of the aqueous-organic mixtures (Section 5.2.4) and the viscosity of water. [b] Values obtained from interpolation of literature data [14]. To determine ε at 75% ACN and in EtOH/H_2O and 2-PrOH/H_2O media, a 3rd-order polynomial was fit to a plot of ε versus % organic solvent. [c] τ at 30%, 60% and 75% ACN was determined from a 3rd-order polynomial fit to a plot of τ versus % ACN. For the media containing EtOH and 2-PrOH, values for τ were obtained from Sato and coworkers' published [15] and unpublished results. [d] Literature value [16]. [e] Literature values [14]. [f] Reproduced from Table 4.1.

In this chapter, the effects of acetonitrile, ethanol and 2-propanol on the mobilities of organic anions are investigated. The Hubbard-Onsager dielectric friction model (eqn

3.27) is used to describe the changes in ion mobility and selectivity that occur upon varying the organic modifier content in the electrophoretic media. Changes in ion mobility are shown to correlate with the corresponding changes in solvent τ, ε and η. The success of the model at predicting the relative mobility trends between different solvents is also evaluated, revealing certain limitations of the Hubbard-Onsager model. Further, the effects of ion charge, solvent composition and solvent type on the ionic strength effects are studied.

5.2 Experimental

5.2.1 Apparatus

The CE instrument, data acquisition and control, and bare fused-silica capillaries were as described in Chapter 4. It has been reported [17] that the presence of acetonitrile in the electrophoretic media causes swelling of the polyimide capillary coating, thereby blocking the capillary ends. Therefore, for all studies involving acetonitrile-water media, ~5 mm of the polyimide coating was removed from both the inlet and outlet ends of the capillary by burning with a heating coil.

5.2.2 Chemicals

All solutions were prepared with Nanopure 10 MΩ water (Barnstead, Chicago, IL). Buffers were prepared from reagent-grade sodium hydroxide (BDH, Darmstadt, Germany), reagent-grade sodium chloride (BDH), HPLC-grade acetonitrile (ACN; Fisher, Fair Lawn, NJ), anhydrous ethanol (EtOH; Commercial Alcohols, Brampton, ON), and ACS certified 2-propanol (2-PrOH; Fisher). Solutions containing ACN were filtered through 0.22 μm Cameo 25N nylon syringe filters (Micron Separations, Westborough, MA), while all other solutions were filtered through 0.45 μm Millex syringe-driven filters (Millipore, Bedford, MA). As described in Chapter 4, all buffers consisted of 0.005 M NaOH, prepared by dilutions of a 0.1 M stock solution, and the ionic strength was adjusted from 0.005 M to 0.07 M by the addition of NaCl. Sodium hydroxide was used as a buffer in this study to ensure that all analytes were completely ionized, while avoiding the complicated task of measuring pH in mixed aqueous-organic solutions. Even though the pK_a of aromatic acids can increase by up to 2.5 units in the presence of some common alcohols [18-20] and by 1.5-2 units in the presence of ACN [21], the analytes used in this study are expected to be completely ionized in the high pH NaOH solutions.

Chemicals for sample solutions are as described in Chapter 4. The mobilities of the carboxylates and sulfonates listed in Table 4.3 were investigated in ACN/H_2O media, whereas only the mobilities of the sulfonates were studied in 2-PrOH/H_2O and EtOH/H_2O media.

5.2.3 Determination of Absolute Mobilities

Effective mobilities were determined according to the method of Williams and Vigh [22], as described in Section 4.2.3. Briefly, depending on the buffer viscosity, a sample plug consisting of analyte and mesityl oxide (EOF marker) was injected for 3-4 s at 0.4-1.5 psi, and was then transferred into the capillary using 0.4-2.5 psi for 3-5 min. The analyte was then separated from mesityl oxide by applying a voltage for a variable amount of time, depending on the mobility of the analyte. For ACN/H_2O, EtOH/H_2O and 2-PrOH/H_2O mixtures, the separation was performed at 6.0 kV for 3-6 min, 10.0 kV for 4-6 min, and 9.0 kV for 5.5-9 min, respectively. Finally, the three sample zones were mobilized past the detector by applying a pressure of 0.4-2.5 psi (again depending on solution viscosity). The voltages used herein were in the linear region of Ohm's plots and gave currents of 8.1-13.0 μA, 7.5-14.8 μA, and 3.8-12.1 μA for I=70 mM buffers containing acetonitrile, ethanol and 2-propanol, respectively. The field strengths are much less than 10^4 V/cm, so the measured mobilities are independent of voltage (i.e. the *Wien effect* is not significant) [23].

From the effective mobilities of the anions, the absolute ion mobilities (μ_o) at zero buffer ionic strength were determined by plotting μ_e versus $I^{1/2}/(1 + Ba \times I^{1/2})$ according to the Pitts equation (eqn 4.3). The number of ionic strengths used for each extrapolation ranged from 4-9, depending on the analyte and solvent system.

5.2.4 Measurement of Relative Viscosity

The viscosities of the ACN/H_2O, EtOH/H_2O and 2-PrOH/H_2O solvent mixtures were measured relative to that in pure water as described in Section 4.2.4.

5.3 Results and Discussion

5.3.1 Ionic Strength Effects

As with the methanol-water solvent systems investigated in Chapter 4, the absolute mobilities of the anions in ACN/H_2O, EtOH/H_2O and 2-PrOH/H_2O media were determined using the Pitts equation (eqn 4.3). For these aqueous-organic mixtures, the constant *Ba* was adjusted from 2.4 (aqueous value [24]) to reflect the change in *B* as a function of solvent dielectric constant, as per eqn 3.38. It was thus assumed that the ion size parameter (*a* in the constant *Ba*) remains unchanged as organic solvent is added to the buffer, which is consistent with the extended Bates-Guggenheim convention for solvent mixtures with water [25-27]. Using the values of ε in Table 5.1, *Ba* was determined to be 2.6, 3.0 and 3.2 for 30%, 60% and 75% ACN, 2.6, 3.1 and 3.4 for 30%, 60% and 75% EtOH, and 2.7, 3.3 and 3.9 for 30%, 60% and 75% 2-PrOH, respectively.

The corresponding Pitts' plots are in Figures 5.1-5.3, and the correlation coefficients, Onsager slopes and intercepts are in Table 5.2. The data for 0% organic solvent is the same as that presented in Chapter 4 (Table 4.3, Figure 4.1). However, it is re-presented herein in both Table 5.2 and Figures 5.1a-5.3a in order to facilitate the comparison. Ion pairing effects were not of concern, since extrapolation to zero buffer ionic strength should diminish such effects [28].

Good linearity is observed in the Pitts plots, suggesting that the Pitts equation with *Ba* values adjusted according to eqn 3.38 is appropriate for use with the present solvent systems. The p-values for all of the analytes in ACN/H_2O, EtOH/H_2O and 2-PrOH/H_2O media are less than 0.01, indicating that the data obey linear relationships at the 99% confidence level. The intercept and slope errors listed in Table 5.2 are the standard deviations obtained from the regression analysis. Therefore, the error in the intercept should reflect the long range over which extrapolation is performed (as illustrated in Figure 4.1a).

5.3.1.1 Influence of Analyte Charge on Ionic Strength Effect

For the buffers containing ethanol and 2-propanol, as well as that containing 30% acetonitrile, the Onsager slopes are greater for ions with higher charge (Table 5.2). The anomalous behavior of phthalate has been noted in Chapter 4, and so the behavior of this anion has been omitted in all further discussions. For these buffers, with the exception of 75% 2-PrOH, the ionic strength effect shows a statistically significant increase in

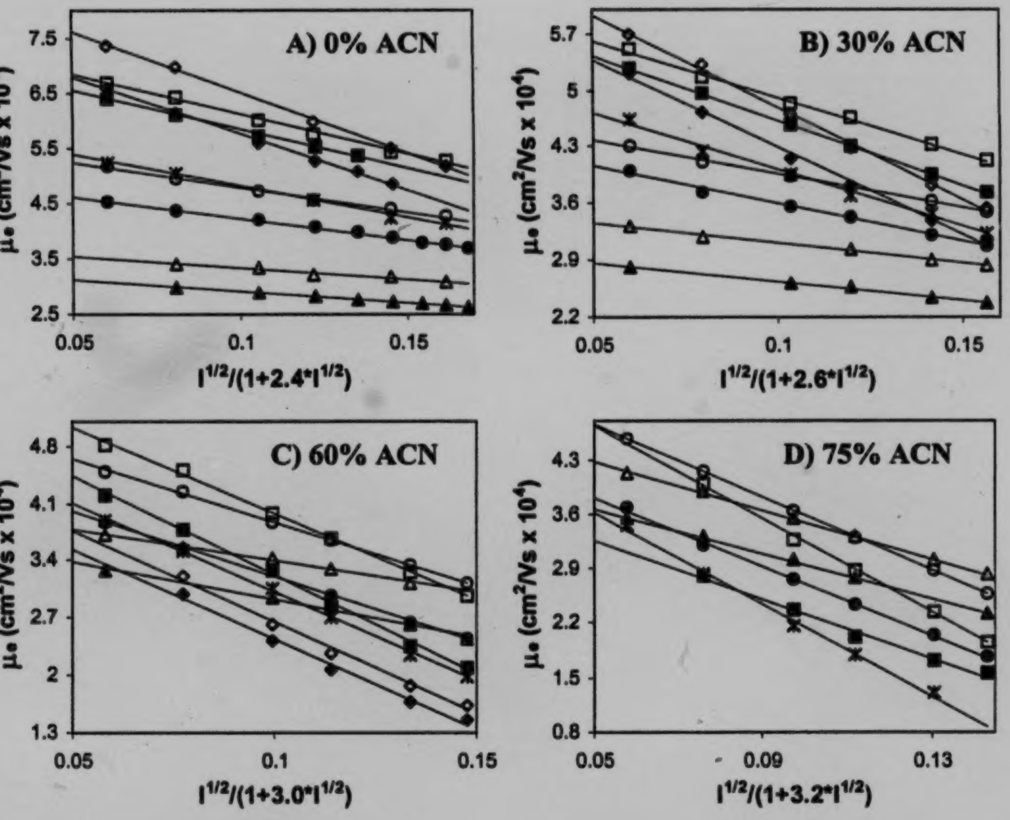

Figure 5.1: Ionic strength effects on the mobilities of organic anions for buffers containing (A) 0% ACN, (B) 30% ACN, (C) 60% ACN and (D) 75% ACN. Solutes: ▲, p-nitrobenzoate; Δ, benzenesulfonate; ●, 2,6-naphthalenedicarboxylate; O, 2,6-naphthalenedisulfonate; ∗, phthalate; ■, 1,3,5-benzenetricarboxylate; □, 1,3,(6 or 7)-naphthalenetrisulfonate; ♦, 1,4,5,8-naphthalenetetracarboxylate; ◊, 1,2,4,5-benzenetetracarboxylate. Experimental conditions: UV detection at 214 nm; 30-cm capillary (20 cm to detector) for (A), 60-cm capillary (50 cm to detector) for (B)-(D); 4.0 kV applied for (A), 6.0 kV applied for (B)-(D); 1 × 10^{-4} M sample concentration; 5 mM NaOH buffer, ionic strength adjusted using NaCl. Figure 5.1a is the same as Figure 4.3a.

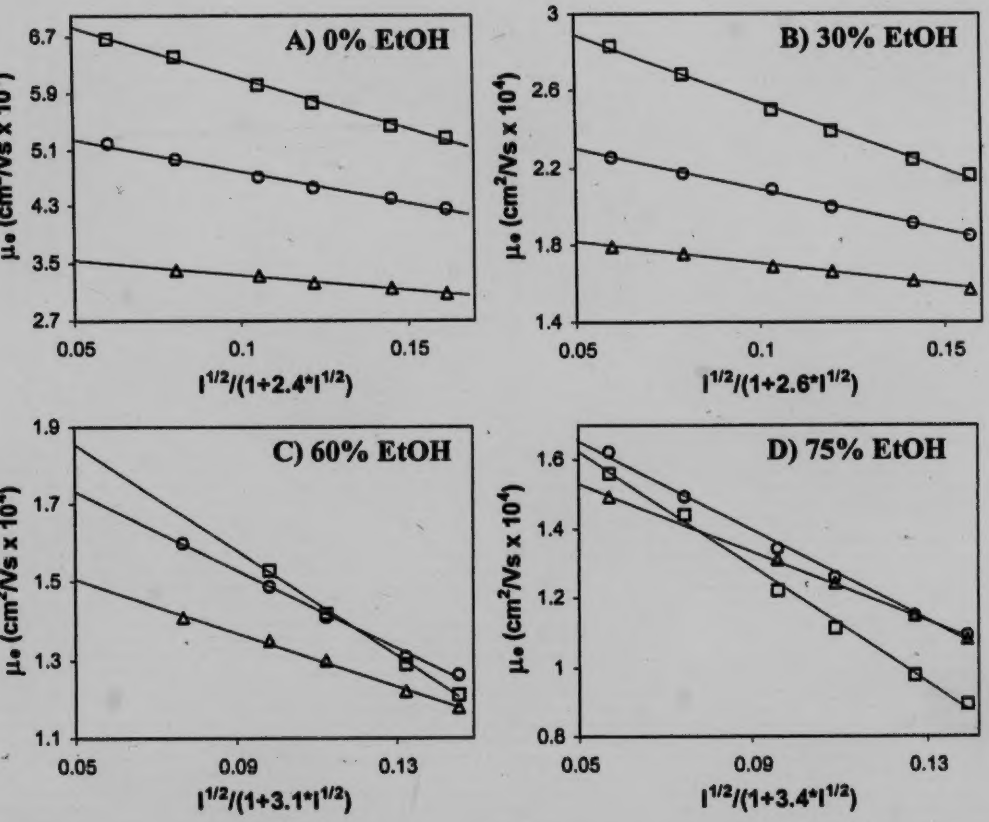

Figure 5.2: Ionic strength effects on the mobilities of organic anions for buffers containing (A) 0% EtOH, (B) 30% EtOH, (C) 60% EtOH and (D) 75% EtOH. Solutes: Δ, benzenesulfonate; ○, 2,6-naphthalenedisulfonate; □, 1,3,(6 or 7)naphthalenetrisulfonate. Experimental conditions: UV detection at 214 nm; 30-cm capillary (20 cm to detector) for (A), 60-cm capillary (50 cm to detector) for (B)-(D); 4.0 kV applied for (A), 10.0 kV applied for (B)-(D); 1 × 10^{-4} M sample concentration; 5 mM NaOH buffer, ionic strength adjusted using NaCl. Figure 5.2a is the same as Figure 4.3a.

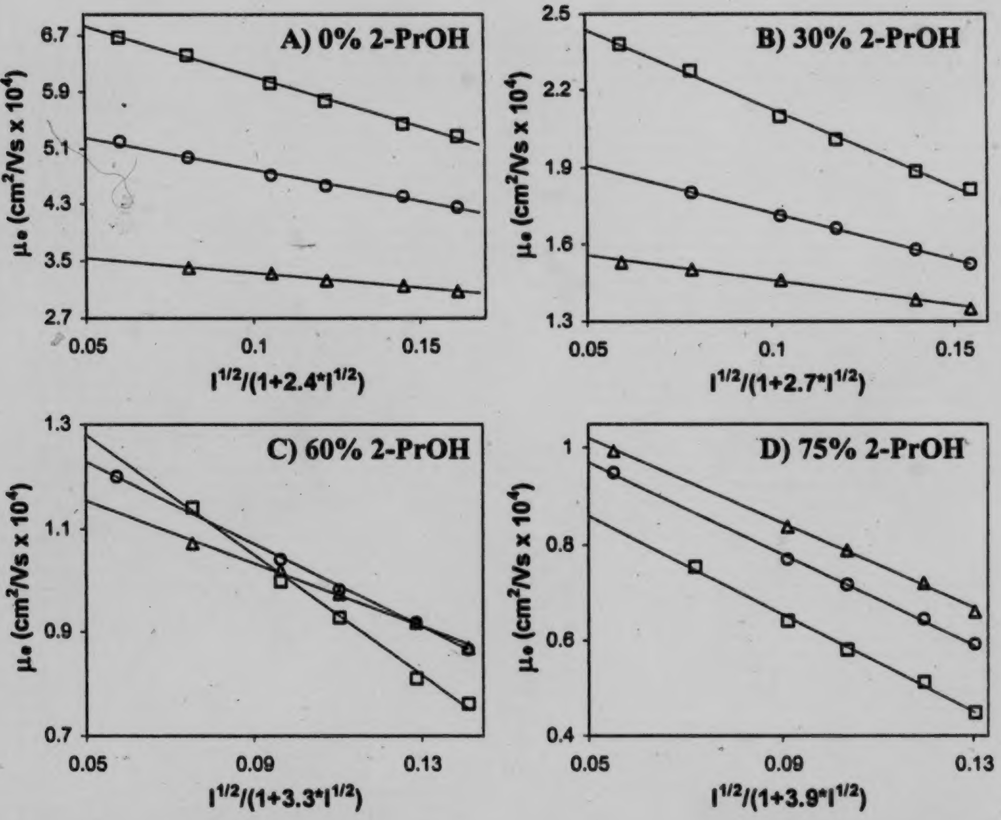

Figure 5.3: Ionic strength effects on the mobilities of organic anions for buffers containing (A) 0% 2-PrOH, (B) 30% 2-PrOH, (C) 60% 2-PrOH and (D) 75% 2-PrOH. Solutes: Δ, benzenesulfonate; O, 2,6-naphthalenedisulfonate; □, 1,3,(6 or 7)naphthalenetrisulfonate. Experimental conditions: UV detection at 214 nm; 30-cm capillary (20 cm to detector) for (A), 60-cm capillary (50 cm to detector) for (B)-(D); 4.0 kV applied for (A), 9.0 kV applied for (B)-(D); 1×10^{-4} M sample concentration; 5 mM NaOH buffer, ionic strength adjusted using NaCl. Figure 5.3a is the same as Figure 4.3a.

Table 5.2: Ionic Strength Effects on the Mobility of Anions in ACN/H_2O, EtOH/H_2O and 2-PrOH/H_2O Media[a]

Anion	Charge	Pitts Equation			
		N[b]	R^2	Onsager Slope[c]	Intercept[d], μ_o
0% Organic Solvent[e]					
p-Nitrobenzoate	-1	8	0.9980	-4.12±0.07	3.320±0.009
Benzenesulfonate	-1	5	0.9847	-4.2±0.3	3.76±0.04
2,6-Naphthalenedicarboxylate	-2	9	0.9995	-7.64±0.07	4.994±0.009
2,6-Naphthalenedisulfonate	-2	6	0.9905	-8.9±0.4	5.69±0.05
Phthalate	-2	5	0.9973	-11.4±0.3	5.94±0.04
1,3,5-Benzenetricarboxylate	-3	5	0.9989	-14.1±0.3	7.24±0.03
1,3,(6 or 7)-Naphthalenetrisulfonate	-3	6	0.9970	-14.4±0.4	7.55±0.05
1,4,5,8-Naphthalenetetracarboxylate	-4	6	0.9974	-20.5±0.5	7.80±0.06
1,2,4,5-Benzenetetracarboxylate	-4	5	0.9978	-21.9±0.6	8.70±0.07
30% ACN					
p-Nitrobenzoate	-1	5	0.9958	-4.6±0.2	3.10±0.02
Benzenesulfonate	-1	5	0.9956	-4.9±0.2	3.61±0.02
2,6-Naphthalenedicarboxylate	-2	6	0.9949	-9.3±0.3	4.52±0.04
2,6-Naphthalenedisulfonate	-2	6	0.9991	-8.3±0.1	4.80±0.02
Phthalate	-2	6	0.9930	-13.9±0.6	5.40±0.07
1,3,5-Benzenetricarboxylate	-3	6	0.9997	-16.0±0.1	6.22±0.02
1,3,(6 or 7)-Naphthalenetrisulfonate	-3	6	0.9974	-14.0±0.4	6.32±0.04
1,4,5,8-Naphthalenetetracarboxylate	-4	6	0.9944	-21.5±0.8	6.44±0.09
1,2,4,5-Benzenetetracarboxylate	-4	6	0.9966	-22.8±0.7	7.07±0.08
60% ACN					
p-Nitrobenzoate	-1	5	0.9920	-9.2±0.5	3.84±0.06
Benzenesulfonate	-1	5	0.9979	-7.7±0.2	4.17±0.02
2,6-Naphthalenedicarboxylate	-2	5	0.9997	-16.0±0.2	4.81±0.02
2,6-Naphthalenedisulfonate	-2	6	0.9987	-15.5±0.3	5.42±0.03
Phthalate	-2	6	0.9993	-21.7±0.3	5.18±0.03
1,3,5-Benzenetricarboxylate	-3	6	0.9979	-24.2±0.6	5.63±0.06
1,3,(6 or 7)-Naphthalenetrisulfonate	-3	6	0.9983	-21.1±0.4	6.08±0.05
1,4,5,8-Naphthalenetetracarboxylate	-4	5	0.9923	-22±1	4.6±0.1
1,2,4,5-Benzenetetracarboxylate	-4	5	0.9919	-22±1	4.9±0.1
75% ACN					
p-Nitrobenzoate	-1	5	0.9984	-14.4±0.3	4.39±0.03
Benzenesulfonate	-1	6	0.9989	-15.6±0.3	5.05±0.03
2,6-Naphthalenedicarboxylate	-2	6	0.9981	-22.0±0.5	4.91±0.05
2,6-Naphthalenedisulfonate	-2	6	0.9998	-23.4±0.2	5.92±0.02
Phthalate	-2	5	0.9956	-30±1	5.1±0.1
1,3,5-Benzenetricarboxylate	-3	5	0.9890	-19±1	4.2±0.1
1,3,(6 or 7)-Naphthalenetrisulfonate	-3	5	0.9985	-29.9±0.7	6.22±0.08
1,4,5,8-Naphthalenetetracarboxylate	-4	–	–	–	–
1,2,4,5-Benzenetetracarboxylate	-4	–	–	–	–

Table 5.2 (continued)

30% EtOH					
Benzenesulfonate	-1	6	0.9974	-2.32±0.06	1.934±0.007
2,6-Naphthalenedisulfonate	-2	6	0.9984	-4.27±0.09	2.51±0.01
1,3,(6 or 7)-Naphthalenetrisulfonate	-3	6	0.9975	-7.0±0.2	3.24±0.02
60% EtOH					
Benzenesulfonate	-1	5	0.9949	-3.4±0.1	1.68±0.02
2,6-Naphthalenedisulfonate	-2	5	0.9991	-5.06±0.09	1.99±0.01
1,3,(6 or 7)-Naphthalenetrisulfonate	-3	4	0.9963	-6.7±0.3	2.18±0.04
75% EtOH					
Benzenesulfonate	-1	5	0.9987	-5.0±0.1	1.78±0.01
2,6-Naphthalenedisulfonate	-2	6	0.9976	-6.5±0.2	1.98±0.02
1,3,(6 or 7)-Naphthalenetrisulfonate	-3	6	0.9959	-8.3±0.3	2.03±0.03
30% 2-PrOH					
Benzenesulfonate	-1	5	0.9981	-2.02±0.05	1.658±0.006
2,6-Naphthalenedisulfonate	-2	5	0.9974	-3.7±0.1	2.09±0.01
1,3,(6 or 7)-Naphthalenetrisulfonate	-3	6	0.9960	-6.2±0.2	2.75±0.02
60% 2-PrOH					
Benzenesulfonate	-1	5	0.9963	-3.1±0.1	1.31±0.01
2,6-Naphthalenedisulfonate	-2	5	0.9990	-4.02±0.08	1.432±0.008
1,3,(6 or 7)-Naphthalenetrisulfonate	-3	5	0.9957	-5.7±0.2	1.56±0.03
75% 2-PrOH					
Benzenesulfonate	-1	5	0.9990	-4.42±0.08	1.241±0.008
2,6-Naphthalenedisulfonate	-2	5	0.9993	-4.77±0.07	1.210±0.008
1,3,(6 or 7)-Naphthalenetrisulfonate	-3	5	0.9973	-5.1±0.2	1.12±0.02

[a] Uncertainties are one standard deviation. [b] Number of data points used in the regression analysis. [c] Units = 10^{-4}cm^{2}V^{-1}s^{-1}mol$^{-0.5}$L$^{-0.5}$. [d] Units = 10^{-4}cm^{2}V^{-1}s^{-1}. [e] As presented in Table 4.3. The –4 charged ions were insoluble in 75% ACN.

magnitude with increasing anion charge at the 95% confidence level. At 75% 2-PrOH, the Onsager slopes also increase with increasing analyte charge, although the large uncertainty in the –3 slope does not allow for a statistical interpretation of the data. The trend of increasing ionic strength effect with increasing analyte charge is consistent with theory, since both terms in the brackets of eqn 4.3 depend on the anion charge (z_-). Similar behavior was observed for methanol-water media in Chapter 4. The charge dependence of the ionic strength effect gives rise to the possibility of using ionic strength to alter the selectivity between ions that differ in charge. Such selectivity changes have been frequently documented in the literature [3, 29, 30].

In contrast, at 60% and 75% ACN, the observed charge dependence of the Onsager slope does not follow that predicted by eqn 4.3. At 60% ACN, the Onsager slope increases with analyte charge up to a charge of –3, but the slopes of the –4-charged anions are not significantly different from the –3-charged anions at the 95% confidence level. Similarly, at 75% ACN, the Onsager slope of the –3-charged carboxylate is not significantly different from that of the –2-charged naphthalenedicarboxylate. These deviations from the expected behavior may be explained by either incomplete anion ionization or ion-pair formation. Incomplete anion ionization would cause a decrease in Onsager slope as a result of the lower ion charge (eqn 4.3), while ion-pairing, which does not affect the y-intercepts (μ_o), would cause an increase in the Onsager slopes [28] due to the decreased effective mobility of the ion pairs. Either of these phenomena may account for the curvature in the Pitts' plots that is observed for the –4 anions at 60% ACN and the –3 carboxylate at 75% ACN. Further evidence supporting incomplete ionization of the anions, along with possible explanations for this incomplete ionization, are presented in Section 5.3.2. However, aside from these 'problem' anions, the observed charge dependence of the ionic strength effect in acetonitrile-water media is consistent with that predicted by eqn 4.3.

For any given ACN buffer content, with the exception of the –3-charged ions at 30% ACN and 75% ACN, anions of like charge have Onsager slopes that are statistically equivalent at the 95% confidence level (Table 5.2). Therefore, ionic strength is not a useful tool for altering the selectivity between similarly-charged ions. In Chapter 4, it was shown that the relaxation effect (right-hand term in the brackets of eqn 4.3) could account for some of the ionic strength-induced selectivity changes observed between ions of similar charge. However, the relaxation effect cannot account for the differences in Onsager slope observed herein between the –3-charged ions at 30% and 75% ACN. At 30% ACN, the ionic strength effect for the –3 carboxylate is greater than that for the –3 sulfonate, although it is the –3 sulfonate that has a slightly higher absolute mobility (Table 5.2). This behavior is contrary to that predicted by the relaxation effect (eqn 4.3). Furthermore, the difference in Onsager slopes between the –3-charged ions at 75% ACN may be explained by incomplete ionization of the –3 carboxylate (as discussed in Section 5.3.2).

5.3.1.2 Influence of Solvent Composition and Type on Ionic Strength Effects

In Chapter 4, the anion and cation Onsager slopes were shown to vary with buffer methanol content in a manner consistent with the $z/\eta\varepsilon^{1/2}$ dependence in the electrophoretic effect (left-hand term in the brackets of eqn 4.3). The large contribution of the electrophoretic term to the overall magnitude of the ionic strength effect is also observed herein with aqueous-organic media containing acetonitrile, ethanol or 2-propanol. Plots of Onsager slope versus $z/\eta\varepsilon^{1/2}$ (Figure 5.4) show good correlation, with R^2 values of 0.94, 0.95 and 0.92 for ACN/H_2O, EtOH/H_2O and 2-PrOH/H_2O media, respectively. For ACN/H_2O media, the data for phthalate and for the 'problem' anions discussed in Section 5.3.1.1 were neglected (these outliers are shown as open symbols in Figure 5.4a). Therefore, for a given solvent type, the relative magnitudes of the Onsager slopes vary with changing solvent content as a function of $z/\eta\varepsilon^{1/2}$.

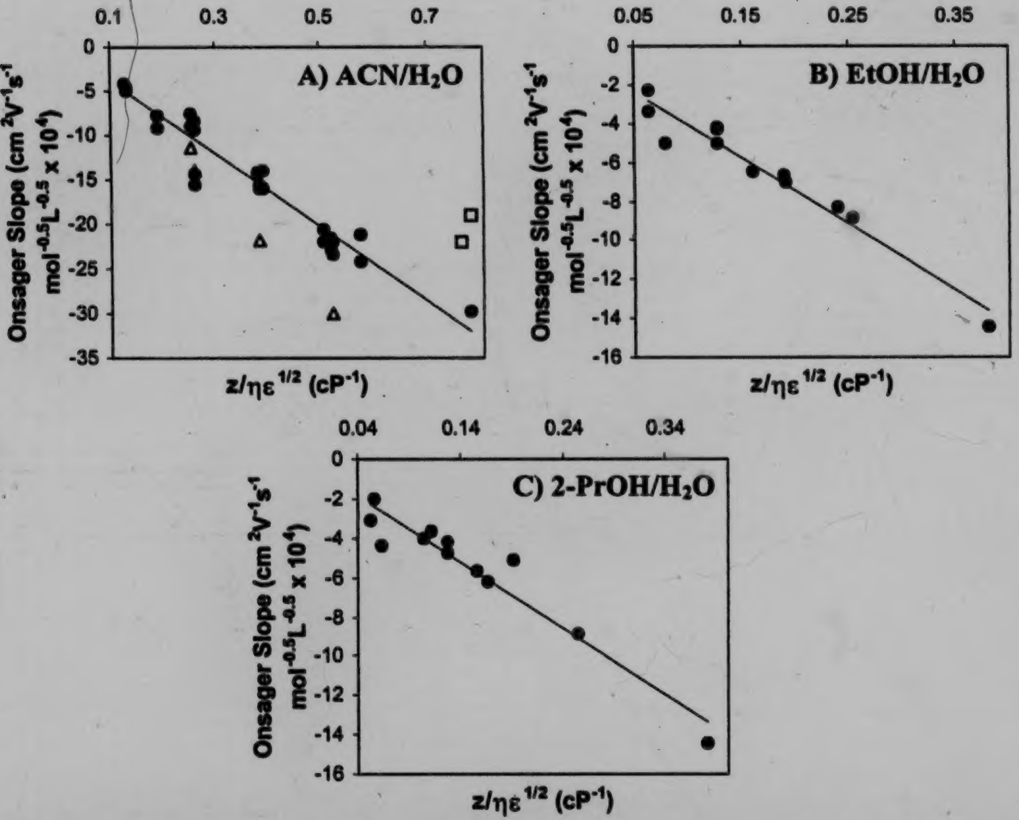

Figure 5.4: Dependence of Onsager slope on the electrophoretic effect for anions in A) ACN/H_2O, B) EtOH/H_2O and C) 2-PrOH/H_2O media. In (A), Δ represents the phthalate data, and □ represents the –4 ions in 60% ACN and the –3 carboxylate in 75% ACN. The regression line shown was constructed with these outliers removed.

Thus far, it has only been demonstrated that for a given organic solvent, the Onsager slope changes with solvent content in a manner consistent with the electrophoretic effect in the Pitts equation. However, the ionic strength effect also varies as a function of solvent type. Figure 5.5 illustrates the variation in ionic strength effect with changes in the solvent composition and type for the –3 sulfonate. The data for methanol-water media is from Chapter 4. For a buffer organic content of 30%, the Onsager slopes for all solvents are similar. In contrast, for the buffers containing 75%

organic solvent, the Onsager slope for the acetonitrile mixture is much larger than for all other solvents.

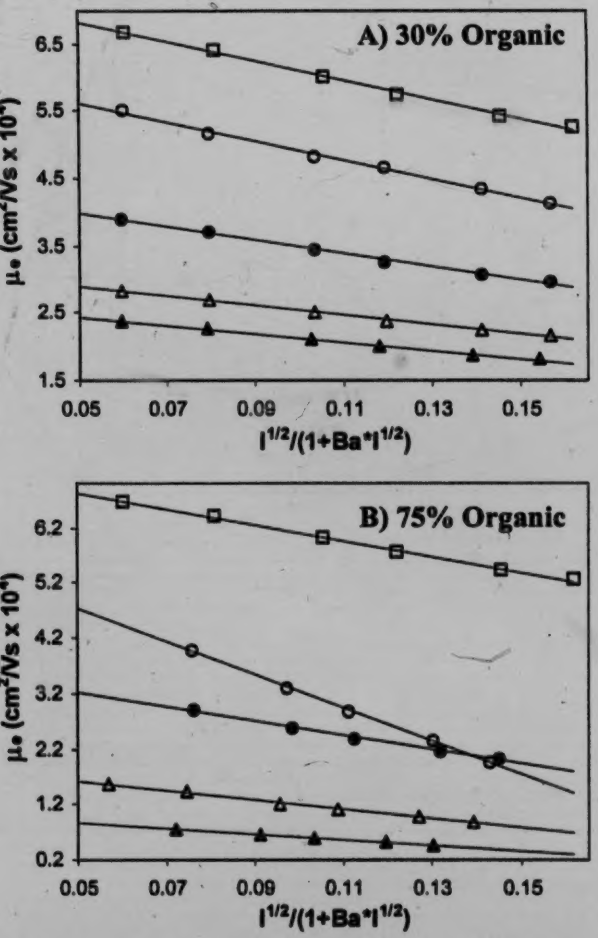

Figure 5.5: Ionic strength effects on 1,3,(6 or 7)-naphthalenetrisulfonate in media containing (A) 30% and (B) 75% organic solvent, as a function of organic modifier. The data for methanol-water media is from Chapter 4. Organic modifiers: □, purely aqueous media; ○, ACN; ●, MeOH; Δ, EtOH; ▲, 2-PrOH. Experimental conditions as in Chapter 4 and Figures 5.1-5.3.

The variation in Onsager slope with solvent type seen in Figure 5.5 can be explained based on the dominance of the electrophoretic effect in the Pitts equation (eqn 4.3). Just as the ionic strength effect varies with solvent *content* as a function of $z/\eta\varepsilon^{1/2}$, it also varies with solvent *type* as a function of $z/\eta\varepsilon^{1/2}$. Figure 5.6 is a plot of Onsager slope versus $z/\eta\varepsilon^{1/2}$ constructed for the –1, –2 and –3 sulfonates using the data for pure water and for aqueous mixtures of 30%, 60% and 75% methanol (Chapter 4), acetonitrile, ethanol and 2-propanol. The carboxylate data was not considered for two reasons. First,

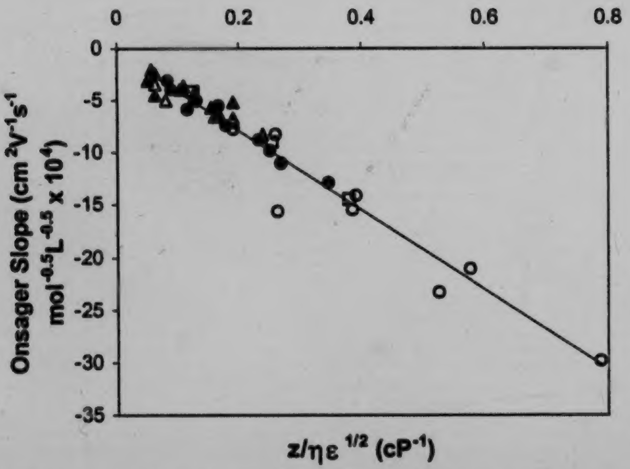

Figure 5.6: Correlation plot showing the influence of solvent content and type on the ionic strength effects for the –1, –2 and –3 sulfonates. The plot was constructed using the data for pure water and for aqueous mixtures of 30%, 60% and 75% methanol, acetonitrile, ethanol and 2-propanol. The data for the methanol-water mixtures is from Chapter 4. Organic modifiers: □, purely aqueous media; ○, ACN; ●, MeOH; △, EtOH; ▲, 2-PrOH.

only sulfonate mobilities were measured in ethanol-water and 2-propanol-water media. Second, there is evidence of incomplete carboxylate ionization in acetonitrile-water media, as will be discussed in Section 5.3.2. The plot shows good correlation, with a linear correlation coefficient (R^2) of 0.95. Therefore, upon changing the organic solvent content and type, the Onsager slope for a given ion will change as a function of the solvent parameter $1/\eta\varepsilon^{1/2}$. This explains the trends in Onsager slopes seen in Figure 5.5. For example, the large slope observed for the –3 sulfonate in 75% ACN (Figure 5.5b) can be attributed to the low viscosity of this solvent mixture, which leads to a large value of $1/\eta\varepsilon^{1/2}$ and consequently to a large Onsager slope. Indeed, the parameter $1/\eta\varepsilon^{1/2}$ in 75% ACN is 3.3 times greater than that in 75% EtOH, which is consistent with the 3.6-fold increase in Onsager slope between 75% EtOH and 75% ACN. At an organic content of 30%, the solvent parameter $1/\eta\varepsilon^{1/2}$ does not vary as dramatically between solvents, which accounts for the similar slopes observed in Figure 5.5a. Nonetheless, $1/\eta\varepsilon^{1/2}$ still increases by a factor of 2.1 between 30% EtOH and 30% ACN, which is consistent with the 2.0-fold increase in slope observed in Figure 5.5a.

In general, for the slopes that are significantly different at the 95% confidence level, the following order is always observed at any given organic solvent content: Onsager slope in ACN > MeOH > EtOH > 2-PrOH. This is in agreement with the relative sizes of the parameter $1/\eta\varepsilon^{1/2}$ predicted by the data in Tables 4.1 and 5.1.

5.3.2 Dielectric Friction

To investigate the influence of dielectric friction on mobility in acetonitrile-water, ethanol-water and 2-propanol-water media, the anion Walden products ($\mu_o\eta$) were plotted against % organic modifier. As described in Section 4.3.2, the Hückel equation (eqn 1.5) predicts that these Walden plots will be horizontal if hydrodynamic friction is the only friction experienced by the ion. However, if dielectric friction is important, a negative deviation from this horizontal behavior should be observed. The Walden plots for the anions and solvent systems investigated herein are in Figure 5.7. Since the effect of charge has a much larger impact on dielectric friction than analyte size (Section 4.3.2), all further discussion will refer to the 'charge' dependence of dielectric friction, rather than its 'q^2/r^3' dependence.

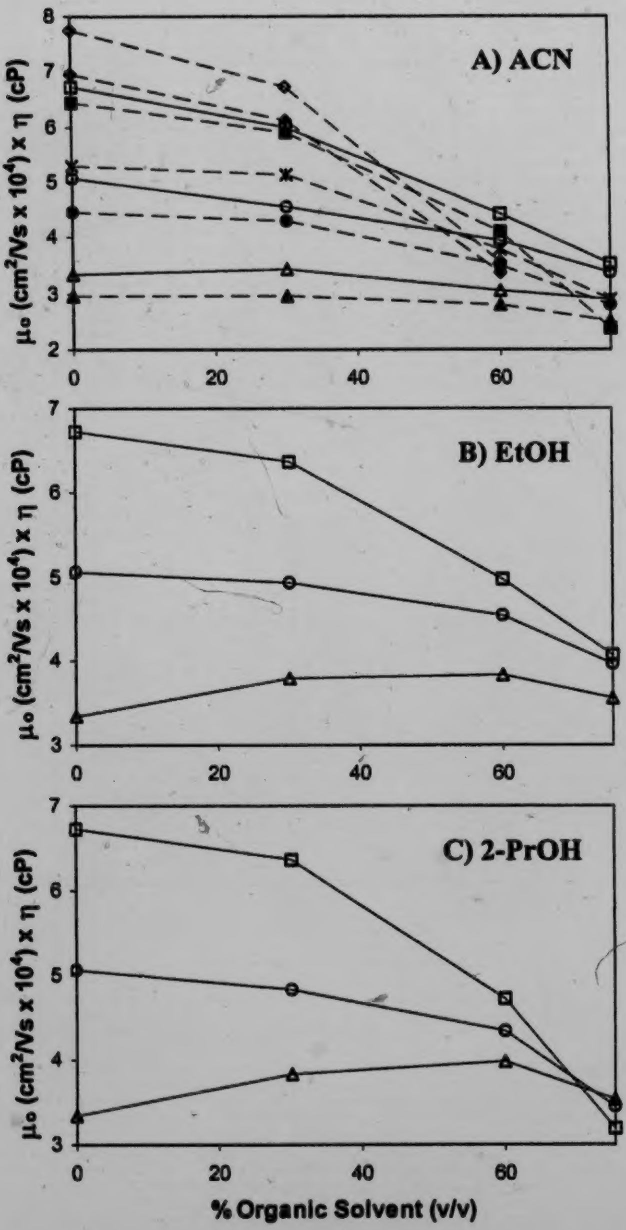

Figure 5.7: Dependence of Walden product on the organic content of the buffer for (A) ACN, (B) EtOH and (C) 2-PrOH. Solutes: ▲, p-nitrobenzoate; Δ, benzenesulfonate; ●, 2,6-naphthalenedicarboxylate; ○, 2,6-naphthalenedisulfonate; ∗, phthalate; ■, 1,3,5-benzenetricarboxylate; □, 1,3,(6 or 7)-naphthalenetrisulfonate; ♦, 1,4,5,8-naphthalenetetracarboxylate; ◊, 1,2,4,5-benzenetetracarboxylate. Solid lines, the sulfonates; dashed lines, the carboxylates. Experimental conditions as in Figures 5.1-5.3.

In Figure 5.7, the negative deviation from horizontal behavior becomes increasingly dramatic as the % ACN, % EtOH and % 2-PrOH increases. This is consistent with the Hubbard-Onsager theory of dielectric friction (eqn 3.27), which predicts that dielectric friction should increase with increasing τ/ε. As seen in Table 5.1, τ/ε generally increases with increasing ACN, EtOH or 2-PrOH content. The one exception to this is the acetonitrile solvent systems, in which τ/ε changes very little between 30% and 75% ACN. This results from the fact that τ and ε both decrease as the % ACN increases.

Also seen in Figure 5.7 for all solvent systems is a more dramatic deviation from Hückel behavior with increasing anion charge. This is also consistent with the Hubbard-Onsager theory (eqn 3.27), in which dielectric friction is proportional to the square of the analyte charge. In Figure 5.7a, the –1 anions in acetonitrile-water media exhibit fairly horizontal trends, indicating that these ions do not experience much dielectric friction. Similar behavior involving singly-charged nonhydroxy-substituted benzoates in ACN/H_2O mixtures has been previously reported by Sarmini and Kenndler [21]. Using effective mobilities, they found that the Walden products of these aromatic acids did not change significantly up to 60% ACN. However, the hydroxy-substituted benzoates did show a negative deviation from Hückel behavior upon increasing the buffer acetonitrile content.

In contrast, a positive deviation from the horizontal is observed in Figures 5.7b and 5.7c for the –1 sulfonate in ethanol-water and 2-propanol-water media. This suggests that this anion is experiencing *less* friction than that predicted solely by the Hückel equation. Similar behavior has been previously reported. In ethanol-water [19] and propanol-water [20] media, Sarmini and Kenndler observed that the product of *effective* mobility and viscosity for nonhydroxy-substituted singly-charged aromatic acids increased slightly with increasing organic content. Dutta and Lahiri [31] reported an initial increase in Walden product with buffer ethanol content for a series of cationic medicinal compounds. Similarly, Steel et al. [32] showed that in the presence of sucrose, mannitol or glycerol, the conductivity of small ions like H^+ follow the relation $\lambda_i^o \eta^x$ = constant, where $x<1$ [33]. Ibuki and Nakahara [34-37] have reported negative residual friction coefficients (total friction minus Stokes' friction) for alkylammonium ions and large halide ions in aqueous media, mixed $EtOH/H_2O$ media and nonaqueous media consisting of methanol, ethanol and 1-propanol. They proposed the "passing-through-cavities" mechanism to explain this anomalous increase in mobility [38-41]. Alternatively, Kay [42] has stated that the larger-than-expected Walden products observed for ions in mixed aqueous-organic media are likely due to the structure-breaking role of the ions. These two mechanisms were discussed in greater detail in Chapter 4 (Section 4.3.2).

Aside from the monocharged anions, the –2, –3 and –4 (ACN/H_2O only) ions in Figure 5.7 experience increasing amounts of dielectric friction with increasing analyte charge. The fact that dielectric friction preferentially slows down ions with higher charge (or higher q^2/r^3 for ions differing in size) can be used as a powerful tool to alter selectivity. Indeed, as early as 60% ACN, a migration order reversal is observed between the –4- and –2-charged anions. At 75% 2-PrOH, the migration order between the –1 and –3 sulfonate is reversed. Although migration order reversals are not apparent in $EtOH/H_2O$ media, the relative mobilities of the sulfonates are altered. Therefore, in mixed aqueous-organic media consisting of ACN, EtOH or 2-PrOH, dielectric friction can cause selectivity alterations between analytes that differ in charge. Dielectric friction may account for some of the anomalous behavior that has been reported in the literature. Carou et al. [3] found that in the presence of 15% ACN, NO_3^- migrated faster than CrO_4^{2-} and SCN^- migrated faster than $Fe(CN)_6^{4-}$. These reversals in migration order could be explained based on the greater dielectric friction expected for the more highly-charged anions.

As mentioned in Section 5.3.1.1, it is believed that incomplete anion ionization or ion-pair formation is responsible for the inconsistencies in the Onsager slope charge dependence for the –3 carboxylate at 75% ACN (■ in Figure 5.1d) and the –4 carboxylates at 60% ACN (♦ and ◊ in Figure 5.1c). The pK_a values for these analytes in water are listed in Table 4.2. These values are expected to increase by 1.5-2 units in media containing up to 80% ACN [21]. The argument of incomplete ionization is further supported by the results presented in Figure 5.7. As seen in this figure, at 0%, 30% and 60% ACN, the difference in absolute mobility between the –3-charged carboxylate (■) and sulfonate (□) is fairly constant. However, at 75% ACN the absolute mobility of the –3 carboxylate is much less than that of the –3 sulfonate. This cannot be explained by ion pairing, because interactions between the analyte ion and the buffer counter-ion cannot take place at infinite dilution [28]. However, this behavior is consistent with incomplete ionization of the carboxylate compared to the sulfonate, since sulfonate groups generally have lower pK_a's (pK_a of benzenesulfonic acid: 0.70 [16]) than do carboxylate groups (pK_a of benzoic acid: 4.19 [16]). Incomplete anion ionization may result from a combination of factors. First, it has been reported that the pK_a's of aromatic acids can increase by 1.5-2 units in the presence of 80% ACN [21]. Furthermore, since

ACN is a poor solvator and stabilizer of anions (i.e., OH^-) [43], the pH of the ACN-water solutions might not be as high as anticipated.

In light of these arguments, it seems reasonable that the –4-charged carboxylates would also be incompletely ionized at 60% ACN. This would account for the larger-than-expected decrease in absolute mobility for the –4 ions on going from 30% to 60% ACN (Table 5.2 and Figure 5.7). As calculated from the denominator of eqn 3.27, the total friction for the –4 carboxylates should increase by ~15% on going from 0 to 30% ACN, and should decrease by ~12% on going from 30 to 60% ACN. As predicted, the absolute mobilities of the –4 ions decrease by ~18% from 0 to 30% ACN. However, they *decrease* by ~30% on going from 30 to 60% ACN! Therefore, another important factor that must be considered when studying selectivity alterations in mixed aqueous-organic media is change in ion pK_a and solvent pH. Several reports in the literature have dealt with this topic [1, 18-21, 44-49].

5.3.3 Correlation Between Mobility and Solvent Parameters

Thus far, I have demonstrated that the selectivity changes observed in Figure 5.7 are consistent with Hubbard and Onsager's theory of dielectric friction. It is therefore of interest to determine whether the changes in ion mobility can be correlated with the changes in solvent viscosity, dielectric constant and dielectric relaxation time as predicted by eqn 3.27. It was shown in Chapter 4 that upon rearrangement of the Hubbard-Onsager equation (eqn 4.5), plots of $1/\mu_o\eta$ versus $\tau/\varepsilon\eta$ are expected to be linear, with slopes proportional to q/r^3 and intercepts proportional to r/q. The mobilities of the –1, –2 and –3 sulfonates in ACN/H_2O, $EtOH/H_2O$ and $2\text{-}PrOH/H_2O$ media are plotted in this manner in Figure 5.8. The carboxylate data in ACN/H_2O media was omitted to eliminate confusion concerning possible pK_a effects. The corresponding correlation coefficients, slopes and intercepts, along with their uncertainties, are in Table 5.3.

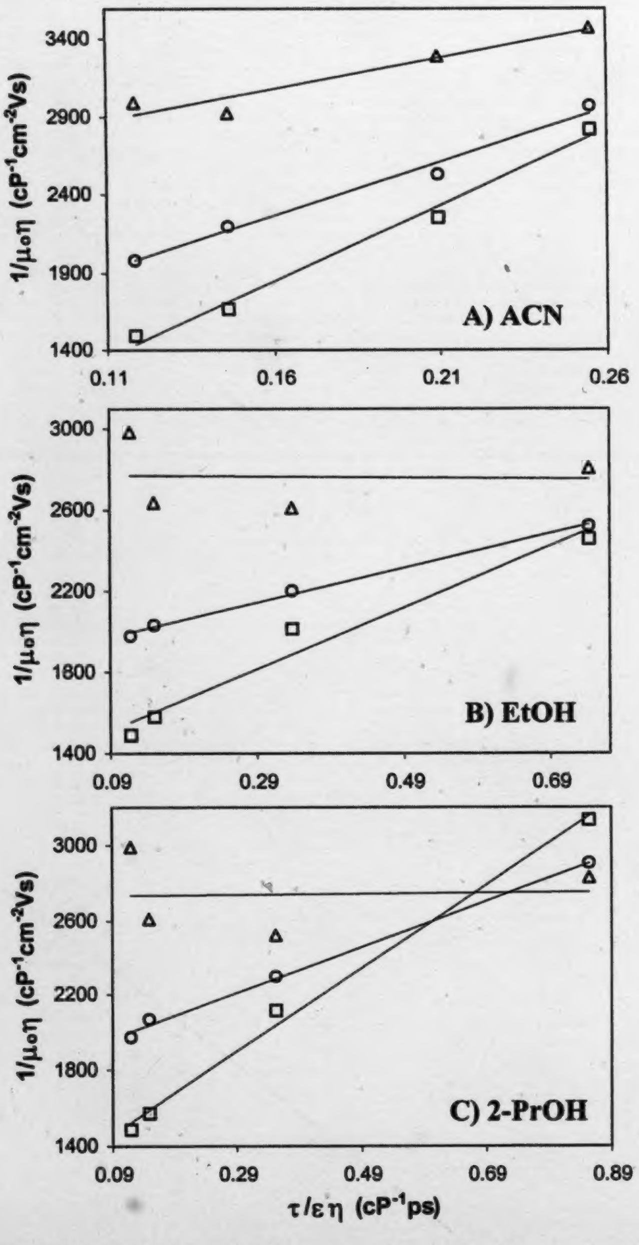

Figure 5.8: Correlation between change in ion mobility and solvent τ, ε and η for aqueous-organic media containing (A) ACN, (B) EtOH and (C) 2-PrOH. Solutes: Δ, benzenesulfonate; ○, 2,6-naphthalenedisulfonate; □, 1,3,(6 or 7)naphthalenetrisulfonate. Experimental conditions as in Figures 5.1-5.3.

Table 5.3: Regression Data for the Plots of $1/\mu_o\eta$ versus $\tau/\varepsilon\eta$ (Figure 5.8) Constructed for the Anions in Acetonitrile-Water, Ethanol-Water and 2-Propanol-Water Media[a]

Analyte	Charge	R^2	Slope[b]	Intercept[c]
ACN/H_2O				
Benzenesulfonate	-1	0.911	3770±830	2470±160
2,6-Naphthalenedisulfonate	-2	0.984	6730±610	1180±120
1,3,(6 or 7)-Naphthalenetrisulfonate	-3	0.988	9570±730	300±140
$EtOH/H_2O$				
Benzenesulfonate	-1	0.006	-50±420	2780±180
2,6-Naphthalenedisulfonate	-2	0.994	860±50	1900±20
1,3,(6 or 7)-Naphthalenetrisulfonate	-3	0.962	1520±220	1370±90
$2\text{-}PrOH/H_2O$				
Benzenesulfonate	-1	0.003	40±440	2720±210
2,6-Naphthalenedisulfonate	-2	0.996	1220±50	1870±30
1,3,(6 or 7)-Naphthalenetrisulfonate	-3	0.996	2230±100	1260±50

[a] Uncertainties are one standard deviation. [b] Units = 10^{12} Vcm^{-2}. [c] Units = Vs(cm^{-2}cP^{-1}).

In Figure 5.8 and Table 5.3, the slopes increase and the intercepts decrease with increasing analyte charge. This is consistent with eqn 4.5. For the –1 sulfonate, which does not experience much dielectric friction in aqueous-organic media consisting of either acetonitrile, ethanol or 2-propanol (Figure 5.7), the plots of $1/\mu_o\eta$ versus $\tau/\varepsilon\eta$ are poorly correlated in all solvent systems. Indeed, the slope for the –1 sulfonate is not statistically different from zero at the 95% confidence level in $EtOH/H_2O$ and 2-$PrOH/H_2O$ media, while in ACN/H_2O it is not significantly different from zero at the 99% confidence level. This is expected, since the –1 sulfonate has relatively uniform Walden products in the mixed aqueous-organic media investigated herein (Figure 5.7).

In contrast, the mobilities of the –2 and –3 sulfonates are more strongly influenced by dielectric friction (Figure 5.7). For these anions, the Hubbard-Onsager equation is successful in predicting the change in ion mobility with changing τ, ε and η. For ACN/H_2O media (Figure 5.8a), plots of $1/\mu_o\eta$ versus $\tau/\varepsilon\eta$ for the –2 and –3 sulfonates are reasonably correlated, with correlation coefficients of 0.984 and 0.988, respectively. Likewise, the plots for these anions in $EtOH/H_2O$ (Figure 5.8b) and 2-$PrOH/H_2O$ (Figure 5.8c) media generally show excellent correlation, with $R^2 \geq 0.994$. The one exception to this is the –3 sulfonate in ethanol-water mixtures, which has a correlation coefficient of 0.962. The overall good correlation between ion mobility and solvent parameters supports the theory that dielectric friction plays an important role in the acetonitrile-, ethanol- and 2-propanol-induced selectivity changes seen in Figure 5.7.

5.3.4 Influence of Solvent Type on Dielectric Friction

According to the Hubbard-Onsager equation (eqn 3.27), solvents with higher relaxation times (τ) and lower dielectric constants (ε) should experience greater dielectric friction effects. According to Tables 4.1 and 5.1, it is therefore expected that aqueous-organic media containing acetonitrile, methanol, ethanol or 2-propanol will experience increasing amounts of dielectric friction, respectively. Figure 5.9 plots the Walden product ($\mu_o\eta$) for the –2 and –3 sulfonates as a function of organic solvent content and type. The larger the dielectric friction effects, the more significant is the negative deviation from ideal Hückel (horizontal) behavior.

As seen in Figure 5.9, the observed trend for the alcohols is that the dielectric friction in 2-$PrOH/H_2O$ > $EtOH/H_2O$ > $MeOH/H_2O$. This is consistent with the trend predicted from the Hubbard-Onsager equation. Further, upon changing alcohol type, the magnitudes of the relative changes in dielectric friction observed in Figure 5.9 are consistent with theory. Recall from Chapter 4 that rearrangement of the Hubbard-Onsager equation leads to an equation (eqn 4.5) that predicts that plots of $1/\mu_o\eta$ versus $\tau/\varepsilon\eta$ should be linear, with slopes proportional to q/r^3 and intercepts proportional to r/q.

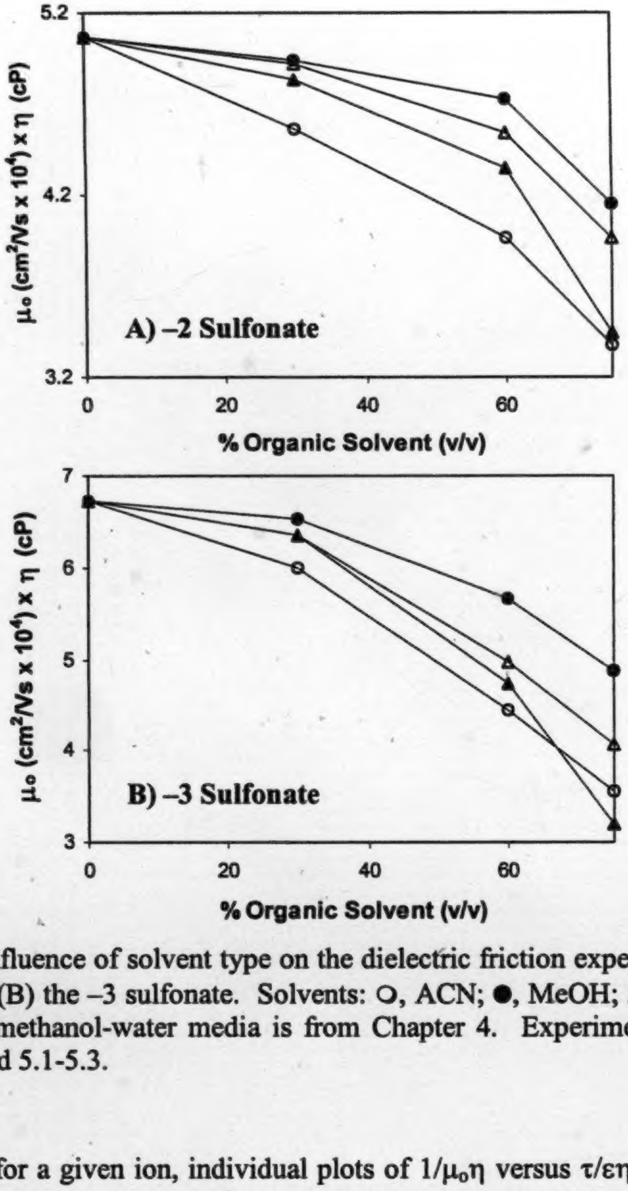

Figure 5.9: Influence of solvent type on the dielectric friction experienced by (A) the –2 sulfonate and (B) the –3 sulfonate. Solvents: ○, ACN; ●, MeOH; Δ, EtOH; ▲, 2-PrOH. The data for methanol-water media is from Chapter 4. Experimental conditions as in Figures 4.1 and 5.1-5.3.

Accordingly, for a given ion, individual plots of $1/\mu_o\eta$ versus $\tau/\varepsilon\eta$ constructed for each solvent type should all possess the same slope and intercept. Such plots have been constructed for the –1, –2 and –3 sulfonates in MeOH/H_2O media (Figure 4.5) and in EtOH/H_2O and 2-PrOH/H_2O media (Figure 5.8). The corresponding regression data is in Tables 4.7 and 5.3. For each anion, the intercepts of the correlation plots in MeOH/H_2O, EtOH/H_2O and 2-PrOH/H_2O media were not significantly different at the 95%

confidence level. The same statement can be made for the slopes, with the exception of the –3 sulfonate in MeOH/H_2O and 2-PrOH/H_2O media. For these two solvent systems, the slopes for the correlation plots of the –3 sulfonate were statistically equivalent at the 99% confidence level. Therefore, within a given class of organic solvents (i.e. alcohols), the Hubbard-Onsager model is successful at predicting the relative inter-solvent mobility trends in mixed aqueous-organic media.

In Sections 4.3.3 and 5.3.3, I demonstrated that the magnitude of the negative deviation from ideal Hückel behavior for MeOH/H_2O, ACN/H_2O, EtOH/H_2O and 2-PrOH/H_2O media was consistent with the Hubbard-Onsager model. This was evident by a strong linear correlation between $1/\mu_o\eta$ and $\tau/\varepsilon\eta$ for anions in these solvents. However, according to the Hubbard-Onsager equation (eqn 3.27) and the data in Tables 4.1 and 5.1, ions in ACN/H_2O media are expected to experience less dielectric friction than in alcohol-water media. This is contrary to what is observed in Figure 5.9, where the –2 and –3 sulfonates experience more dielectric friction in 30% and 60% ACN than in 30% and 60% 2-PrOH! Further, at 75% ACN, the –2 sulfonate is affected more by dielectric friction than in 75% 2-PrOH, while the –3 sulfonate is affected more by dielectric friction than in 75% EtOH. Therefore, it appears as though the –2 and –3 sulfonates are experiencing proportionally more dielectric friction in acetonitrile-water than would be predicted based on the observed behavior of the alcohols. As mentioned above, plots of $1/\mu_o\eta$ versus $\tau/\varepsilon\eta$ for the ACN/H_2O, MeOH/H_2O, EtOH/H_2O and 2-PrOH/H_2O solvent systems should have the same slopes and intercepts. However, at the 95% confidence level, the slopes and the intercepts for the multiply-charged sulfonates in ACN/H_2O media were statistically larger and smaller, respectively, than those for the MeOH/H_2O, EtOH/H_2O and 2-PrOH/H_2O media. This apparent failure of the Hubbard-Onsager model may result from the continuum nature of the model. As a continuum dielectric friction model, the Hubbard-Onsager theory does not allow for the microscopic nature of ion motion in terms of the solvent structure or the ion-solvent interactions [50, 51]. In other words, it considers only the bulk properties of the solvent (η, ε, τ) and does not differentiate between solvents with different microscopic properties (i.e. ion-solvent interactions).

The alcohols studied herein (methanol, ethanol, 2-propanol) and acetonitrile belong to two distinct classes of solvents. The alcohols are *protic* solvents, meaning that these solvents are hydrogen-bonded [43]. On the other hand, acetonitrile is *aprotic* and *dipolar* because it is a non-hydrogen-bonded solvent that has a high dielectric constant [43]. These two classes of solvents exhibit very different ion-solvent interactions. In protic solvents, hydrogen bonding and ion-dipole interactions are important, whereas in dipolar aprotic solvents, both ion-dipole interactions and interactions due to the mutual polarizability of the ion and solvent are important [52]. Since the Hubbard-Onsager dielectric friction model does not consider these differences in ion-solvent interactions, it will likely not predict the relative behavior of ions among these different classes of organic solvents. This is indeed the case in Figure 5.9, where the –2 and –3 sulfonates experience proportionally more dielectric friction in acetonitrile-water media than in alcohol-water media, which is contrary to what is expected based on the Hubbard-Onsager equation (eqn 3.27). However, within a given class of solvents (i.e. alcohol-water mixtures) in which the ion-solvent interactions are the same, the Hubbard-Onsager model successfully describes the relative behavior of ions in mixed aqueous-organic media. A molecular model, which takes into account solvent structure and ion-solvent interactions, would undoubtedly be more successful at predicting the relative mobility trends observed between different classes of solvents.

Hosoi and Masuda [53] have also observed that the frictional coefficients experienced by the perchlorate ion in alcohols are less than those predicted by the Hubbard-Onsager electrohydrodynamic model when the classical Debye dielectric relaxation times (as used herein) are used for the calculations. In contrast, they found good agreement between the observed and calculated frictional coefficients in other solvents, including acetonitrile. The smaller-than-expected friction in alcohol is consistent with the results presented herein (Figure 5.9), in which the –3 sulfonate experienced less dielectric friction in media containing alcohol than in media containing acetonitrile. Hosoi and Masuda explained that the anomalous behavior of the alcohols resulted from the shorter time scale of the translational motion of the perchlorate ion compared to the relaxation times of the alcohols [53]. As a result, the perchlorate ion did not feel the full dielectric friction predicted by the long relaxation times of the alcohols. Under these conditions, the contribution of local ion-solvent interactions to the overall ion motion becomes important [53]. Clearly, a molecular model would be more successful than a continuum model at predicting the behavior of ions in hydroorganic media containing alcohol.

It is important to note that the negative deviations from ideal Hückel behavior for MeOH/H_2O, ACN/H_2O, EtOH/H_2O and 2-PrOH/H_2O media are consistent with the dielectric friction model of Hubbard and Onsager. This is evident from the good linear correlation between $1/\mu_o\eta$ and $\tau/\varepsilon\eta$ for the sulfonates in these solvent systems (Figures

4.5 and 5.8). Therefore, the inability of the Hubbard-Onsager model at predicting the relative behavior of ions between different classes of solvents does not imply that the model is effective for one class of solvent (i.e. acetonitrile) and ineffective for another (i.e. alcohols). It simply reflects the fact that the model is limited by its continuum nature. For a given solvent type, the Hubbard-Onsager dielectric friction model remains a useful tool for explaining the selectivity changes that are observed upon going from aqueous to mixed aqueous-organic media.

5.4 Concluding Remarks

In hydroorganic CE using acetonitrile, ethanol or 2-propanol as cosolvent, several factors are involved in altering ion selectivity. Varying the buffer ionic strength can cause significant selectivity changes between ions that differ in charge. Upon changing the content and type of the organic solvent, the ionic strength effects vary as a function of solvent $1/\eta\varepsilon^{1/2}$. Dielectric friction can also account for some of the selectivity changes observed. Changes in sulfonate mobility correlate with changes in solvent τ, ε and η, as predicted by the Hubbard-Onsager dielectric friction model. Furthermore, changes in solvent pH and analyte pK_a must not be ignored when considering ion selectivity in mixed aqueous-organic CE. As seen in acetonitrile-water media, variations in the degree of ion ionization can cause dramatic changes in relative ion mobilities.

Within a given class of solvents (alcohol-water mixtures), the Hubbard-Onsager model successfully predicts the relative mobility trends upon changing solvent. However, the relative trends observed between acetonitrile-water and alcohol-water media are not consistent with the model. This limitation of the model may be explained by its continuum nature, whereby ion-solvent interactions are not taken into account. Nonetheless, for a given solvent type, the dielectric friction theory of Hubbard and Onsager remains a useful tool in predicting solvent-dependent selectivity changes.

5.5 References

(1) Barrón, D.; Jiménez-Lozano, E.; Irles, A.; Barbosa, J. *J. Chromatogr. A* **2000,** *871*, 381-389.

(2) Salimi-Moosavi, H.; Cassidy, R. M. *Anal. Chem.* **1996,** *68*, 293-299.

(3) Carou, M. I. T.; Mahía, P. L.; Lorenzo, S. M.; Fernández, E. F.; Rodríguez, D. P. *J. Chromatogr. A* **2001,** *918*, 411-421.

(4) Mendonsa, S. D.; Hurtubise, R. J. *J. Liq. Chromatogr. Rel. Technol.* **1999,** *22*, 1027-1040.

(5) Fujiwara, S.; Honda, S. *Anal. Chem.* **1987,** *59*, 487-490.

(6) Lin, C. E.; Lin, W. C.; Chiou, W. C.; Chong, C. C. *J. Chromatogr. A* **1996,** *755*, 261-269.

(7) Idei, M.; Mezó, I.; Vadász, Z.; Horváth, A.; Teplán, I.; Kéri, G. *J. Chromatogr.* **1993,** *648*, 251-256.

(8) Wan, H.; Engström, A.; Blomberg, L. G. *J. Chromatogr. A* **1996,** *731*, 283-292.

(9) Weinmann, W.; Parker, C. E.; Baumeister, K.; Maier, C.; Tomer, K. B.; Przybylski, M. *Electrophoresis* **1994,** *15*, 228-233.

(10) Lalloo, A. K.; Kanfer, I. *J. Chromatogr. B* **1997,** *704*, 343-350.

(11) Ahmed, A.; Lloyd, D. K. *J. Chromatogr. A* **1997,** *766*, 237-244.

(12) Valtcheva, L.; Mohammad, J.; Pettersson, G.; Hjertén, S. *J. Chromatogr.* **1993,** *638*, 263-267.

(13) Cugat, M. J.; Borrull, F.; Calull, M. *Analyst* **2000,** *125*, 2236-2240.

(14) Akhadov, Y. Y. *Dielectric Properties of Binary Solutions. A Data Handbook*; Pergamon Press: New York, 1980.

(15) Sato, T.; Chiba, A.; Nozaki, R. *J. Chem. Phys.* **1999,** *110*, 2508-2521.

(16) *CRC Handbook of Chemistry and Physics*, 76th ed.; CRC Press: New York, 1995-1996.

(17) Baeuml, F.; Welsch, T. *J. Chromatogr. A* **2002,** *961*, 35-44.

(18) Sarmini, K.; Kenndler, E. *J. Chromatogr. A* **1998,** *806*, 325-335.

(19) Sarmini, K.; Kenndler, E. *J. Chromatogr. A* **1998,** *811*, 201-209.

(20) Sarmini, K.; Kenndler, E. *J. Chromatogr. A* **1998,** *818*, 209-215.

(21) Sarmini, K.; Kenndler, E. *J. Chromatogr. A* **1999,** *833*, 245-259.

(22) Williams, B. A.; Vigh, G. *Anal. Chem.* **1996,** *68*, 1174-1180.

(23) Erdey-Grúz, T. *Transport Phenomena in Aqueous Solutions*; John Wiley & Sons: New York, 1974, Chapter 4.

(24) Li, D.; Fu, S.; Lucy, C. A. *Anal. Chem.* **1999,** *71*, 687-699.

(25) Mussini, T.; Covington, A. K.; Longhi, P.; Rondinini, S. *Pure Appl. Chem.* **1985,** *57*, 865-876.

(26) Paabo, M.; Robinson, R. A.; Bates, R. G. *J. Am. Chem. Soc.* **1965,** *87*, 415-418.

(27) Barbosa, J.; Sanz-Nebot, V. *Anal. Chim. Acta* **1991,** *244*, 183-191.

(28) Porras, S. P.; Riekkola, M.-L.; Kenndler, E. *J. Chromatogr. A* **2001,** *924*, 31-42.

(29) Friedl, W.; Reijenga, J. C.; Kenndler, E. *J. Chromatogr. A* **1995,** *709*, 163-170.

(30) Mechref, Y.; Ostrander, G. K.; Rassi, Z. E. *J. Chromatogr. A* **1997,** *792*, 75-82.

(31) Dutta, S. C.; Lahiri, S. C. *J. Indian Chem. Soc.* **1992,** *69*, 361-366.

(32) Steel, B. J.; Stokes, J. M.; Stokes, R. H. *J. Phys. Chem.* **1958,** *62*, 1514-1516.

(33) Sadek, H. *J. Electroanal. Chem.* **1983,** *144*, 11-32.

(34) Ibuki, K.; Nakahara, M. *J. Chem. Phys.* **1986,** *84*, 2776-2782.

(35) Ibuki, K.; Nakahara, M. *J. Phys. Chem.* **1986,** *90*, 6362-6365.

(36) Ibuki, K.; Nakahara, M. *J. Phys. Chem.* **1987,** *91*, 1864-1867.

(37) Ibuki, K.; Nakahara, M. *J. Phys. Chem.* **1987,** *91*, 4411-4414.

(38) Takisawa, N.; Osugi, J.; Nakahara, M. *J. Phys. Chem.* **1981,** *85*, 3582-3585.

(39) Takisawa, N.; Osugi, J.; Nakahara, M. *J. Chem. Phys.* **1982,** *77*, 4717-4722.

(40) Takisawa, N.; Osugi, J.; Nakahara, M. *J. Chem. Phys.* **1983,** *78*, 2591-2597.

(41) Nakahara, M.; Török, T.; Takisawa, N.; Osugi, J. *J. Chem. Phys.* **1982,** *76*, 5145-5149.

(42) Kay, R. L. In *Water. A Comprehensive Treatise*; Franks, F., Ed.; Plenum Press: New York, 1973; Vol. 3, pp 204-209.

(43) King, E. J. In *Physical Chemistry of Organic Solvent Systems*; Covington, A. K., Dickinson, T., Eds.; Plenum Press: New York, 1973, pp 331-393.

(44) Sarmini, K.; Kenndler, E. *J. Cap. Elec.* **1998,** *5*, 103-110.

(45) Barrón, D.; Jiménez-Lozano, E.; Barbosa, J. *Chromatographia* **2000,** *52*, 395-402.

(46) Chiari, M.; Kenndler, E. *J. Chromatogr. A* **1995,** *716*, 303-309.

(47) Kenndler, E.; Jenner, P. *J. Chromatogr.* **1987,** *390*, 169-183.

(48) Kenndler, E.; Schwer, C.; Jenner, P. *J. Chromatogr.* **1989,** *470*, 57-68.

(49) Miller, J. L.; Shea, D.; Khaledi, M. G. *J. Chromatogr. A* **2000,** *888*, 251-266.

(50) Biswas, R.; Bagchi, B. *J. Chem. Phys.* **1997,** *106*, 5587-5598.

(51) Wolynes, P. G. *J. Chem. Phys.* **1978,** *68*, 473-483.

(52) Price, E. In *The Chemistry of Non-Aqueous Solvents*; Lagowski, J. J., Ed.; Academic Press: New York, 1966; Vol. 1, pp 67-96.

(53) Hosoi, H.; Masuda, Y. *J. Phys. Chem. B* **1998,** *102*, 2995-3002.

CHAPTER SIX. Nonaqueous Capillary Electrophoresis

Chapters 4 and 5 have demonstrated that the selectivity changes observed in mixed aqueous-organic media can be attributed to dielectric friction. In this chapter, the influence of nonaqueous mixtures of methanol and acetonitrile on the mobilities of organic cations will be studied. The success of the Hubbard-Onsager dielectric friction model at predicting selectivity changes in nonaqueous media will be examined.

6.1 Introduction

Walbroehl and Jorgenson [1] were the first to use nonaqueous media in open-tubular capillary zone electrophoresis. Since then, the use of such media in capillary electrophoresis has gained popularity. Methanol, acetonitrile and their mixtures have been used for the analysis of polyaromatic hydrocarbons [2], alkali and alkaline earth metals [3], surfactants [4], amino acids [5], fatty acids [6], triazine herbicides [7], and most commonly, drugs and pharmaceuticals [8-14]. Methanol/acetonitrile solvent systems are also important for the rapidly growing field of CE coupled to mass spectrometry (MS). Detection by MS is favored when nonaqueous solvents are used because their low surface tension and high volatility enhance the sample ionization efficiency [15, 16]. The use of CE-MS with nonaqueous methanol/acetonitrile solvent systems for the analysis of drugs has been frequently reported in the literature [17-21]. In fact, mixtures of methanol and acetonitrile are the most common solvent systems used for the separation of basic compounds in CE [22].

The selectivity changes observed in methanol/acetonitrile media [3, 9, 18, 21, 22] have generally been attributed to solvation, ion association and/or pK_a effects. As illustrated in

Table 6.1, the solvent viscosity (η), dielectric constant (ε) and dielectric relaxation time (τ) also change with solvent content. The importance of ε/η to the electroosmotic and electrophoretic mobilities in methanol/acetonitrile media has been frequently cited in the literature [12, 23, 24]. The Hubbard-Onsager model (eqn 3.27) predicts that dielectric friction is proportional to τ/ε, and should therefore increase with decreasing acetonitrile content in the methanolic buffer. As a result, dielectric friction may also be responsible for solvent-induced selectivity changes in nonaqueous mixtures of methanol and acetonitrile. However, as observed in the previous chapter, ions experienced a considerably greater amount of dielectric friction in acetonitrile-water media than was predicted solely by the τ/ε values. If this behavior persists in nonaqueous media consisting of methanol and acetonitrile, the selectivity changes observed will be much less than predicted from the solvent parameters in Table 6.1.

Table 6.1: Variation of Solvent Parameters with MeOH/ACN content

% ACN in MeOH (v/v)	η (cP)	ε^b	τ^d (ps)	τ/ε (ps)
0	0.54^a	32.63^c	50.9	1.56
25	0.43	34.23	33.8	0.99
50	0.36	35.24	20.2	0.57
75	0.33	35.85	10.1	0.28
100	0.34	36.69^c	3.4	0.09

[a] Literature values [25]. [b] Values determined from interpolation of literature data, unless otherwise noted. ε at 25%, 50% and 75% ACN in MeOH were determined from a 3rd-order polynomial fit to a plot of ε versus molar percent ACN in MeOH. [c] Literature values [26]. [d] Data generously provided by T. Sato and coworkers at Waseda University in Tokyo, Japan. They fit the complex dielectric spectra of MeOH/ACN mixtures (determined by time domain reflectometry (TDR)) to various dielectric models in order to determine values for τ.

In this chapter, I will study the mobility behavior of +1, +2 and +3 ammonium ions in nonaqueous solvent systems consisting of methanol, acetonitrile and their mixtures. The effects of ion charge and solvent composition on the ionic strength effects are investigated, and the success of the Hubbard-Onsager dielectric friction model at predicting solvent-induced selectivity changes is examined. It will be seen that the changes in cation mobility between pure methanol and pure acetonitrile are indeed less than predicted by the values of τ/ε. Further, the data obtained herein in pure methanol will be compared to that obtained in methanol/water media in Chapter 4.

6.2 Experimental

6.2.1 Apparatus

A P/ACE 5000 capillary electrophoresis system (Beckman Instruments, Fullerton, CA) equipped with UV detection at 214 nm was used for all mobility measurements. The data acquisition and control were performed with P/ACE Station Software for Windows 95 (Beckman Instruments) on a 486 PC. The data acquisition rate was set at 4.0 Hz. The P/ACE MDQ system employed in Chapters 4 and 5 was not used for the nonaqueous studies presented herein due to evaporative loss of solution from the ends of the capillaries during vial transfer. This evaporation resulted in the introduction of air bubbles into the capillary, which appeared as large spikes in the electropherograms and altered the measured mobilities.

The untreated fused-silica capillaries (Polymicro Technologies, Phoenix, Az) had inner diameters of 50 μm, outer diameters of 365 μm, and total lengths of 57 cm (50 cm to detector). New capillaries were used for each new organic content, and their precise lengths were determined before discarding. Since the polyimide coating swells and blocks the capillary ends in the presence of acetonitrile [27], ~5 mm of the polyimide coating was removed from both the inlet and outlet ends of the capillary by burning with a heating coil. New capillaries were conditioned by rinsing at high pressure (20 psi) for 10 min with 0.1 M NaOH in methanol, 10 min with pure methanol, and 30 min with the background electrolyte (BGE). Between runs, the capillaries were rinsed at high pressure for 3 min with the BGE. At the end of the day, the capillaries were rinsed for 10 min with methanol and then dried with air.

6.2.2 Chemicals

All solutions were filtered through 0.2-µm Nalgene PTFE syringe-driven filters (Nalge Nunc International, Rochester, NY). Reagent-grade sodium hydroxide was obtained from BDH (Darmstadt, Germany), and HPLC-grade methanol (MeOH), HPLC-grade acetonitrile (ACN) and 70% perchloric acid were from Fisher (Fair Lawn, NJ). The precise $HClO_4$ concentration was determined to be 69.63% (w/w) by standardization with 0.1 M NaOH, which was itself standardized against potassium hydrogen phthalate (Fisher).

Buffers ranging in ionic strength from 0.005 M to 0.03 M were prepared daily by weighing the desired amount of $HClO_4$ into a volumetric flask, and then diluting to the mark with organic solvent. For the buffers containing 25%, 50% and 75% (v/v) ACN in MeOH, the required volume of ACN was first pipetted into the $HClO_4$-containing volumetric flask, and the volume was then adjusted to the mark using MeOH. Since the perchloric acid stock solution was 69.63% (w/w) in water, the final water content of the buffers ranged from 0.02-0.13% (v/v) for the 0.005-0.03 M solutions, respectively. This variation in water content had a negligible influence on ion mobility; regardless of whether the organic solvent composition was 100% MeOH, 100% ACN or 50% (v/v) ACN in MeOH, cation mobilities measured in 5 mM $HClO_4$ solutions with 0.02% and 0.13% (v/v) water were not significantly different at the 95% confidence level.

Perchloric acid is completely dissociated in both acetonitrile and methanol [7, 28-30]. It was used in this study to ensure that the cations were completely protonated while avoiding the complicated task of measuring pH in nonaqueous media. Porras et al. [30] used a similar buffer system for the study of anilinium ion mobilities in methanol-acetonitrile media. It has been reported that the pK_a of acidic amines can increase by 0.5-2.5 units [28, 31, 32] in methanolic media, and can increase by 6-8 units in acetonitrile [29, 33]. Therefore, the use of highly acidic $HClO_4$ solutions will ensure complete protonation of the analytes.

The cationic analytes are the same as those employed in Chapter 4. Sample solutions were prepared at concentrations of 5×10^{-3} M in methanol, and were diluted to 1×10^{-4} M in the corresponding buffer solution to eliminate sample stacking during electrophoresis. Mesityl oxide was used as the neutral electroosmotic flow (EOF) marker at a concentration of 0.75 mM.

6.2.3 Determination of Absolute Mobilities

Effective analyte mobilities were measured according to the method of Williams and Vigh [34], as described in Section 4.2.3. Briefly, injections were performed at 0.5 psi for 3 s with the 100% MeOH solutions and 2 s with all other solutions. Sample plugs were transferred into the capillary using 0.5 psi for 1 min, and the separation was carried out at 3.0 kV for 4 min. The sample zones were then mobilized past the detector by applying a pressure of 0.5 psi. For the I=30 mM buffer at 0%, 25%, 50%, 75% and 100% (v/v) ACN in MeOH, the voltage of 3.0 kV was in the linear region of an Ohm's plot and gave currents of 5.2, 6.0, 6.0, 5.6 and 4.8 μA, respectively. Fresh buffers and sample solutions were introduced in every run. Absolute ion mobilities (μ_o) were then determined at zero buffer ionic strength by plotting the effective mobilities versus $I^{1/2}/(1 + Ba \times I^{1/2})$ according to the Pitts equation (eqn 4.4).

6.2.4 Measurement of Relative Viscosity

The viscosities of the MeOH/ACN buffers and of the pure ACN buffers were measured relative to that of 100% MeOH as described in Section 4.2.4. The viscosities measured in this way (Table 6.1) are within 2.7% of previously reported values [30].

6.3 Results and Discussion

6.3.1 Ionic Strength Effects

For each solvent system investigated, the effective mobilities (μ_e) of the cations were plotted against $I^{1/2}/(1 + Ba \times I^{1/2})$ and extrapolated to zero ionic strength to yield absolute mobilities. The constant Ba was adjusted from its value of 2.4 in aqueous media to reflect the change in B as a function of dielectric constant, as per eqn 3.38. It was thus assumed that the ion size parameter (a) remains unchanged as the MeOH/ACN ratio is varied. Using the values of ε in Table 6.1, the adjusted Ba for 0, 25, 50, 75 and 100% (v/v) ACN in MeOH were calculated to be 3.7, 3.6, 3.6, 3.6 and 3.5, respectively. Figure 6.1 presents the Pitts' plots for the ammonium ions differing in charge, and Figure 6.2 presents the Pitts' plots for the singly-charged ammonium ions. The corresponding correlation coefficients, slopes and intercepts are in Table 6.2. As in Chapters 4 and 5,

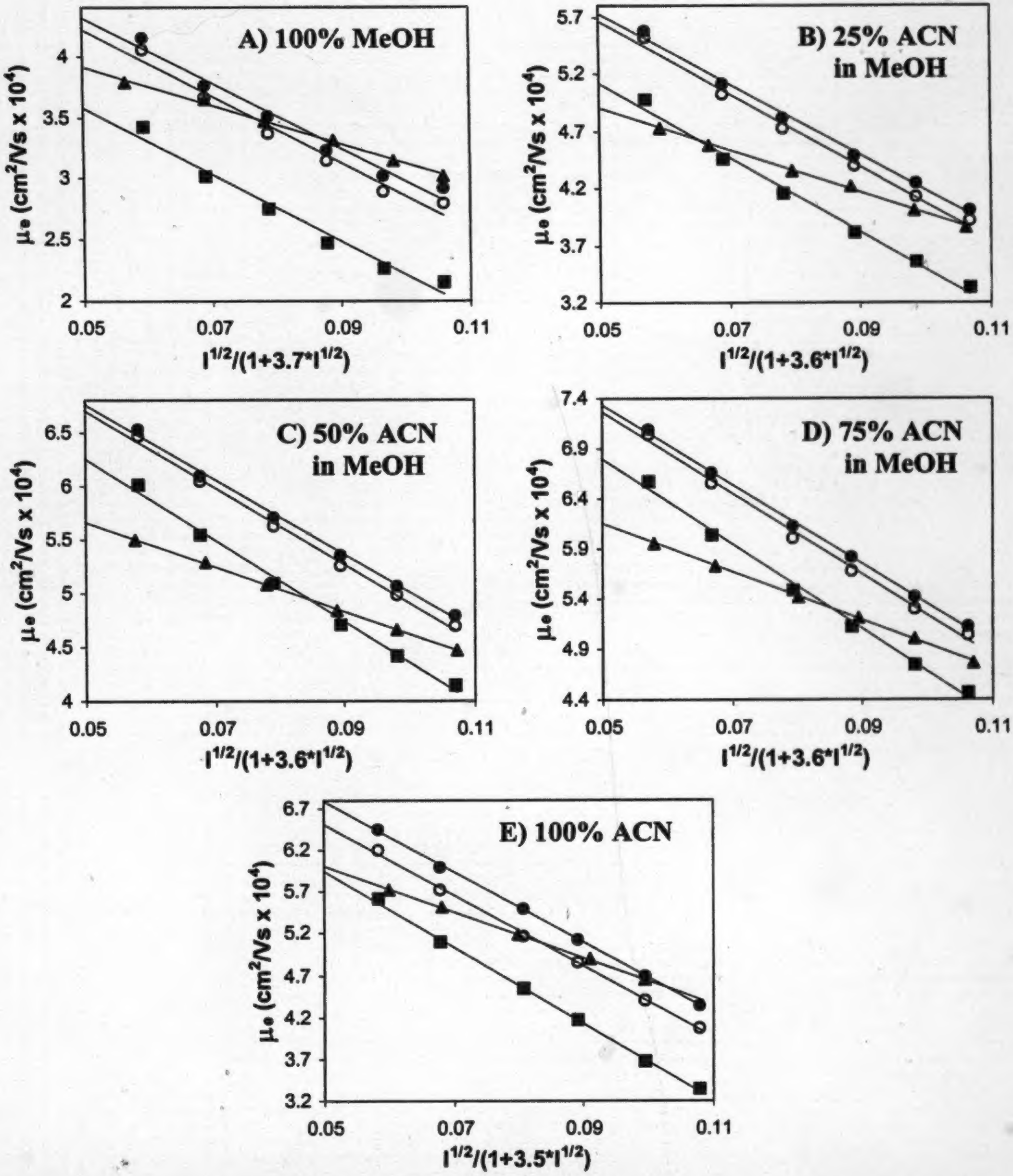

Figure 6.1: Ionic strength effects on the mobilities of organic cations differing in charge for nonaqueous buffers containing (A) 100% MeOH, (B) 25% (v/v) ACN in MeOH, (C) 50% (v/v) ACN in MeOH, (D) 75% (v/v) ACN in MeOH, and (E) 100% ACN. Solutes: ▲, benzylammonium; ●, p-xylylenediammonium; ○, m-xylylenediammonium; ■, 1,3,5-triammoniummethylbenzene. Experimental conditions: UV detection at 214 nm; bare fused-silica 57-cm capillary (50 cm to detector); 3.0 kV applied; 1 × 10^{-4} M sample concentration; 5-30 mM $HClO_4$ buffer.

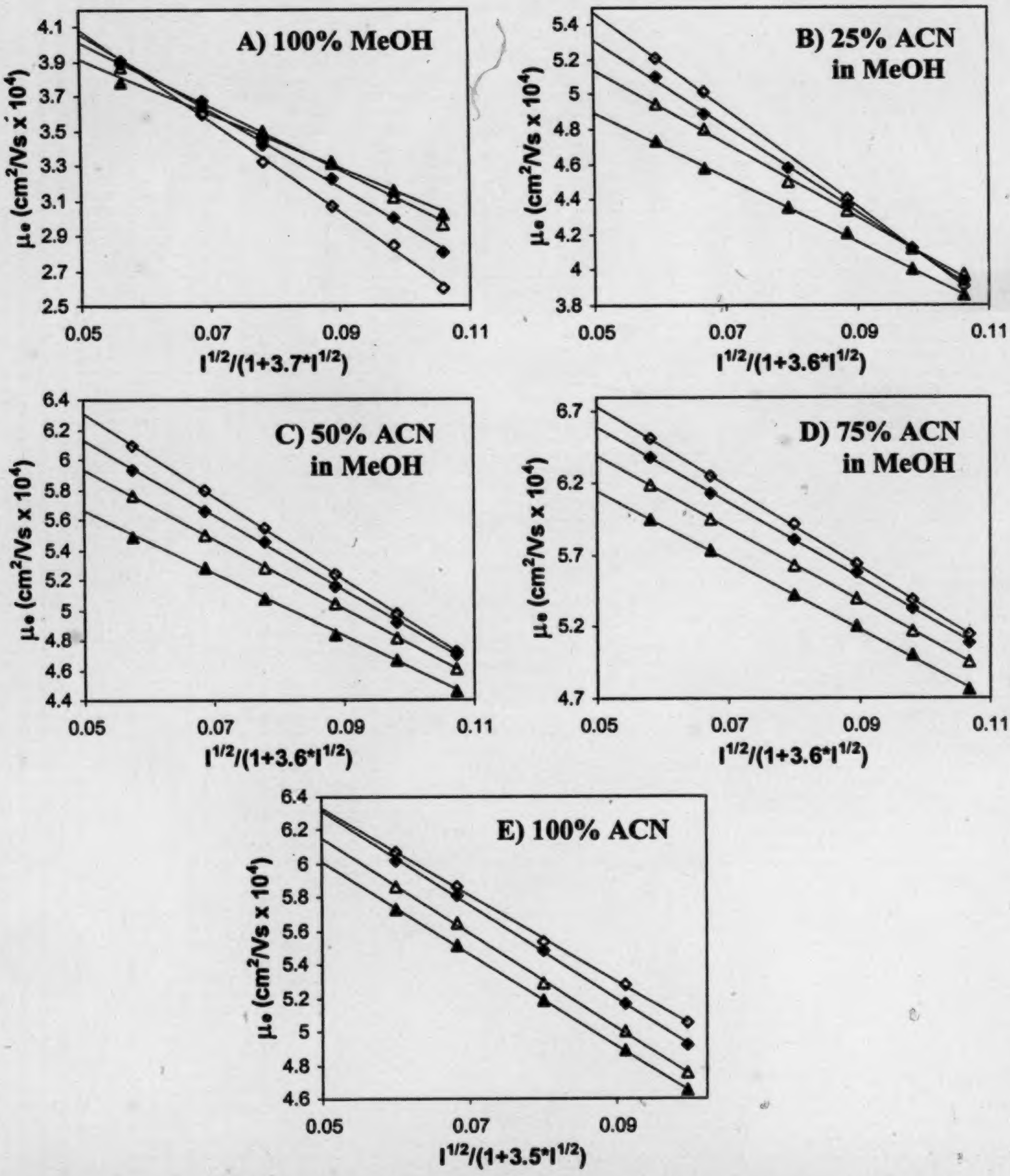

Figure 6.2: Ionic strength effects on the mobilities of singly-charged organic cations for buffers containing (A) 100% MeOH, (B) 25% (v/v) ACN in MeOH, (C) 50% (v/v) ACN in MeOH, (D) 75% (v/v) ACN in MeOH, and (E) 100% ACN. Solutes: ▲, benzylammonium; Δ N-benzylmethylammonium; ◆, N,N-dimethylbenzylammonium; ◊, benzyltrimethylammonium. Experimental conditions as in Figure 6.1.

Table 6.2: Ionic Strength Effects on the Mobility of Cations in Nonaqueous Media[a]

Cation	Charge	Pitts Equation			
		N[b]	R^2	Onsager Slope[c]	Intercept[d], μ_o
100% MeOH					
Benzylammonium	+1	6	0.9990	-16.7±0.3	4.78±0.02
N-Benzylmethylammonium	+1	6	0.9991	-19.7±0.3	5.04±0.02
N,N-Dimethylbenzylammonium	+1	6	0.9996	-23.5±0.2	5.28±0.02
Benzyltrimethylammonium	+1	6	0.9983	-27.9±0.6	5.54±0.05
p-Xylylenediammonium	+2	6	0.9887	-25±1	5.5±0.1
m-Xylylenediammonium	+2	6	0.9881	-26±1	5.4±0.1
1,3,5-Triammoniummethylbenzene	+3	6	0.9873	-26±1	4.8±0.1
25% ACN in MeOH					
Benzylammonium	+1	6	0.9991	-18.6±0.3	5.83±0.02
N-Benzylmethylammonium	+1	6	0.9990	-21.1±0.3	6.19±0.03
N,N-Dimethylbenzylammonium	+1	6	0.9994	-24.6±0.3	6.54±0.03
Benzyltrimethylammonium	+1	6	0.9999	-27.9±0.1	6.86±0.01
p-Xylylenediammonium	+2	6	0.9945	-31±1	7.3±0.1
m-Xylylenediammonium	+2	6	0.9923	-32±1	7.3±0.1
1,3,5-Triammoniummethylbenzene	+3	6	0.9897	-32±2	6.7±0.1
50% ACN in MeOH					
Benzylammonium	+1	6	0.9995	-20.8±0.2	6.69±0.02
N-Benzylmethylammonium	+1	6	0.9999	-23.0±0.1	7.08±0.01
N,N-Dimethylbenzylammonium	+1	6	0.9995	-25.0±0.3	7.38±0.02
Benzyltrimethylammonium	+1	6	0.9997	-27.7±0.2	7.69±0.02
p-Xylylenediammonium	+2	6	0.9962	-35±1	8.50±0.09
m-Xylylenediammonium	+2	6	0.9964	-36±1	8.50±0.09
1,3,5-Triammoniummethylbenzene	+3	6	0.9938	-38±2	8.1±0.1
75% ACN in MeOH					
Benzylammonium	+1	6	0.9995	-24.1±0.3	7.35±0.02
N-Benzylmethylammonium	+1	6	0.9999	-25.3±0.1	7.656±0.009
N,N-Dimethylbenzylammonium	+1	6	0.9998	-26.5±0.2	7.92±0.01
Benzyltrimethylammonium	+1	6	0.9998	-28.1±0.2	8.14±0.02
p-Xylylenediammonium	+2	6	0.9984	-39.7±0.8	9.33±0.07
m-Xylylenediammonium	+2	6	0.9958	-41±1	9.3±0.1
1,3,5-Triammoniummethylbenzene	+3	6	0.9943	-43±2	8.9±0.1
100% ACN					
Benzylammonium	+1	5	0.9997	-27.6±0.3	7.39±0.02
N-Benzylmethylammonium	+1	5	0.9994	-28.3±0.4	7.56±0.03
N,N-Dimethylbenzylammonium	+1	5	0.9995	-28.1±0.4	7.72±0.03
Benzyltrimethylammonium	+1	5	0.9996	-25.9±0.3	7.62±0.02
p-Xylylenediammonium	+2	6	0.9996	-42.3±0.4	8.90±0.04
m-Xylylenediammonium	+2	6	0.9990	-42.5±0.7	8.64±0.06
1,3,5-Triammoniummethylbenzene	+3	6	0.9982	-46±1	8.25±0.08

[a] Uncertainties are one standard deviation. [b] Number of data points used in the regression analysis. [c] Units = $10^{-4}cm^2V^{-1}s^{-1}mol^{-0.5}L^{-0.5}$. [d] Units = $10^{-4}cm^2V^{-1}s^{-1}$.

the p-values for all cations in MeOH/ACN media are less than 0.01, indicating that the data obey linear relationships at the 99% confidence level. Indeed, the correlation coefficients are 0.99 or better for all analytes and solvent systems (Table 6.2). However, some curvature of the Pitts' plots is evident, especially for the multiply-charged ions in 0-25% ACN in MeOH (Figure 6.1). This is discussed in detail in the following section.

6.3.1.1 Influence of Analyte Charge on Ionic Strength Effect

The Pitts equation (eqn 4.4) predicts that the ionic strength effect should increase with increasing cation charge. This is observed for the +2 ammonium ions at 25%, 50%, 75% and 100% ACN in MeOH, whose Onsager slopes are significantly larger at the 95% confidence level than those for the +1 ions. However, in 100% MeOH, the +1 and +2 ions experience ionic strength effects that are the same at the 95% confidence level. Further, the Onsager slope of the +3 ammonium ion is always statistically equivalent to those of the +2 cations. Possible explanations for these deviations from theory are discussed below.

In Figure 6.1, significant curvature of the Pitts' plots is apparent for the +2 and +3 ammonium ions in 100% MeOH and 25% ACN in MeOH. This may explain the observed trends in Onsager slope. Such curvature is possible if an unrealistic value for *Ba* is used. In assigning values to the constant *Ba*, I assumed that the ion size parameter '*a*' remains unchanged as the MeOH/ACN content is varied (Section 6.3.1). This is a reasonable assumption given that inorganic cations and anions show little variation in solvation number with solvent type [35-37]. Nonetheless, '*a*' is in reality an *adjustable* parameter whose value is varied to achieve optimal agreement between experiment and theory [38].

Using the Curve Fitter function of SlideWrite Plus (Version 2.0 for Windows, Advanced Graphics Software, Inc., Carlsbad, CA), *Ba* was optimized by fitting the experimental mobility data to an equation of the general form:

$$\mu_e = a_o + a_1 \times \left(\frac{\sqrt{I}}{1 + a_2\sqrt{I}} \right) \tag{6.1}$$

The constant *Ba* was one of the three constants (a_2) obtained from the fitting. Using these optimized *Ba* values, the Onsager slope of the +3 ammonium ion is always significantly larger than those for the +2 ammonium ions at the 95% confidence level. Further, the Onsager slopes for the +2 ions are always significantly greater than those for the +1 ions. This is consistent with the charge dependence of the Pitts equation.

However, the optimal *Ba* values calculated according to eqn 6.1 are often unrealistic. For example, the *Ba* values for m-xylylenediammonium, p-xylylenediammonium and 1,3,5-triammoniummethylbenzene in 100% MeOH were determined to be 19.2, 19.4 and 21.0, respectively. These correspond to ion size parameters of 38-41 Å in methanol, which are much larger than the 7 Å predicted for aqueous media using *Ba*=2.4. The value of 7 Å is consistent with literature values for the ionic size parameter in aqueous media [39]. The ion size parameter is the mean distance of closest approach for the ions. It seems unlikely that this distance would increase by a factor of ~6 upon going from aqueous to methanolic media, especially since inorganic cations and anions show little variation in solvation number with solvent type [35-37]. Indeed, personal communication with Dr. Mariusz Klobukowski at the University of Alberta has confirmed that such a large increase in ion size parameter is unrealistic.

Further, the optimal values of *Ba* determined using SlideWrite Plus show large variations for similar data sets. For example, *Ba* was determined to be 3.5 and 6.5 using two replicate data sets for benzylamine at 100% MeOH. With *Ba*=3.7, these two data sets produced intercepts and Onsager slopes that were not significantly different at the 95% confidence level. Evidently the fitted values of *Ba* are very sensitive to small changes in the experimental data. Although Li et al. [40] found that 2.4 was the optimal *Ba* value for aqueous media, they observed values ranging between 0.5 and 5.2 for singly-charged carboxylates. Therefore, owing to the large uncertainty and unrealistic nature of the optimized *Ba* values, the values calculated in Section 6.3.1 were retained.

Another possible explanation for the observed Onsager slope trends in Figure 6.1 and Table 6.2 is that ion-pairing is occurring. Ion association is more predominant in methanol and acetonitrile than in water because of the lower dielectric constants of these organic solvents [30, 41]. Ion-pairing would not affect the y-intercepts (μ_o), but would cause an increase in the Onsager slopes [30] due to the decreased mobility of the ion pairs. Depending on the degree of ion-pair formation for each analyte, the slopes in Figure 6.1 may be altered to different extents. This could explain the observed trends in Onsager slope. Furthermore, ion-pair formation may account for the curvature in the Pitts' plots observed for the +2 and +3 ammonium ions in 100% MeOH and 25% ACN in MeOH. However, no curvature is evident in the Pitts' plots for the +1 ammonium ions, yet evidence exists supporting ion-pair formation for these ions in MeOH/ACN media (see discussion in the next section). Further studies are required in order to better understand the influence of ion association on ionic strength effects.

6.3.1.2 Variations in Onsager Slope for Monocharged Ammonium Ions

The Pitts equation predicts that ions of similar charge will have similar Onsager slopes. This is observed for the +1 ammonium ions in 100% ACN, for which the ionic strength effects are not significantly different at the 95% confidence level. However, for all other MeOH/ACN buffer systems investigated, the +1 ammonium ions have Onsager slopes that increase in the following order: primary < secondary < tertiary < quaternary amine. As a result, migration order reversals between these ions can be observed in 100% MeOH and 25% ACN in MeOH (Figure 6.2). It has been reported that the migration order of primary, secondary and tertiary amines is reversed on going from pure methanol to pure acetonitrile media [22, 42]. This is observed in Figure 6.2, whereby at an ionic strength of 30 mM (highest x-axis value), the migration order is 3°<2°<1° in 100% MeOH and 1°<2°<3° in buffers containing at least 50% ACN.

Ion-pairing effects may account for the differing Onsager slopes between the +1 ammonium ions in MeOH/ACN media. To understand how ion-pairing varies with analyte and solvent type, one must consider the solvation of perchlorate and the H-bonding ability of the analytes in the various solvents. ClO_4^- is a relatively large polarizable anion, and it is therefore better solvated in acetonitrile than in methanol [3, 37, 43]. Whereas H-bonding of perchlorate is not favorable in methanol, it is preferentially solvated in acetonitrile by a combination of dispersion (mutual polarizability of anions and solvent) and ion-dipole interactions [3, 37]. As for the H-bonding properties of the cationic analytes, the 1°, 2° and 3° ammonium ions are H-bond donors while the 4° ammonium ion cannot participate in hydrogen-bonding. Since methanol and acetonitrile can both accept H-bonds, the H-bonding character of the analytes should increase in the order 4°<3°<2°<1° in all MeOH/ACN solvent systems. As the degree of H-bonding increases, the degree of solvation also increases.

The degree of ion-solvent interactions will influence the degree of ion-ion interactions[3, 44, 45]. Since ClO_4^- is not solvated well in MeOH, it will ion-associate to a greater extent with the cationic analytes that are less solvated. Therefore, ion-pairing in 100% MeOH should be greatest for the 4° amine and least for the 1° amine. Given that ion association results in an increase in the ionic strength effect[30], the trend in Onsager slopes observed for the +1 ammonium ions in 100% MeOH is consistent with the predicted ion-pairing trend.

As the % ACN in the methanolic media is increased from 25-75%, ClO_4^- becomes increasingly solvated. Therefore, its degree of ion association with the ammonium ions should decrease. Indeed, Barthel et al.[46, 47] have reported that the ion-pair formation of ammonium perchlorates is more pronounced in methanol than in acetronitrile. This is supported in Table 6.2 by an overall decrease in the difference between slopes for the 1° and 4° ammonium ions as the % ACN in increased. At 100% ACN, the perchlorate ion should be well solvated and should undergo minimal ion-pairing with the analytes. Consistent with this are the statistically equivalent slopes observed for the +1 ammonium ions in 100% ACN.

Another possible explanation for the trend in Onsager slopes in Figure 6.2 is that the relaxation effect for the singly-charged ammonium ions is important. According to the relaxation term in the Pitts equation (right-hand term in the brackets of eqn 4.4) the Onsager slopes of similarly-charged ions will be greater for ions with higher absolute mobilities. For the buffers investigated herein containing up to 75% ACN in MeOH, the ionic strength effects of the primary, secondary, tertiary and quaternary amines increase with increasing ion absolute mobility. Therefore, the trend in Onsager slopes and the resulting selectivity changes are consistent with the relaxation effect.

Whether relaxation effects or ion-pair formation are responsible for the observed trends in Onsager slopes, further investigations are required before a complete understanding can be achieved. Some ideas for future studies are proposed in Chapter 8.

6.3.1.3 Correlation Between Onsager Slope and $z/\eta\varepsilon^{1/2}$

In Chapters 4 and 5, I have shown that the Onsager slopes for ions in MeOH/H_2O, ACN/H_2O, EtOH/H_2O and 2-PrOH/H_2O are consistent with the electrophoretic effect (left-hand term in the brackets of eqn 4.4). For the ammonium ions investigated herein in methanol/acetonitrile media, the plot of Onsager slope versus $z/\eta\varepsilon^{1/2}$ is in Figure 6.3a. The correlation is only fair, with an R^2 value of 0.73.

The correlation is inferior to those in the aqueous-organic solvent systems (eg., Figures 4.3, 5.4 and 5.6) for two main reasons. First, as shown in the previous section, the relaxation effect may be important for the +1 ammonium ions. A good correlation will be achieved in Figure 6.3a only if the electrophoretic effect is dominant. Secondly, as discussed in Section 6.3.1.1, the Onsager slopes in Table 6.2 do not follow the charge dependence predicted by the Pitts equation (eqn 4.4). Since Figure 6.3a includes a charge term in the x-axis, the correlation of this plot will be poor unless the charge dependence in eqn 4.4 is obeyed. This problem can be overlooked by plotting Onsager slope versus $1/\eta\varepsilon^{1/2}$ for each analyte, as illustrated in Figure 6.3b. For clarity, the plots for only one representative analyte of each charge are shown. Considering all five MeOH/ACN buffer systems investigated, the correlation coefficients for the cations are fair, ranging between 0.68-0.93 (Table 6.3, neglecting benzyltrimethylammonium). With the exclusion of the

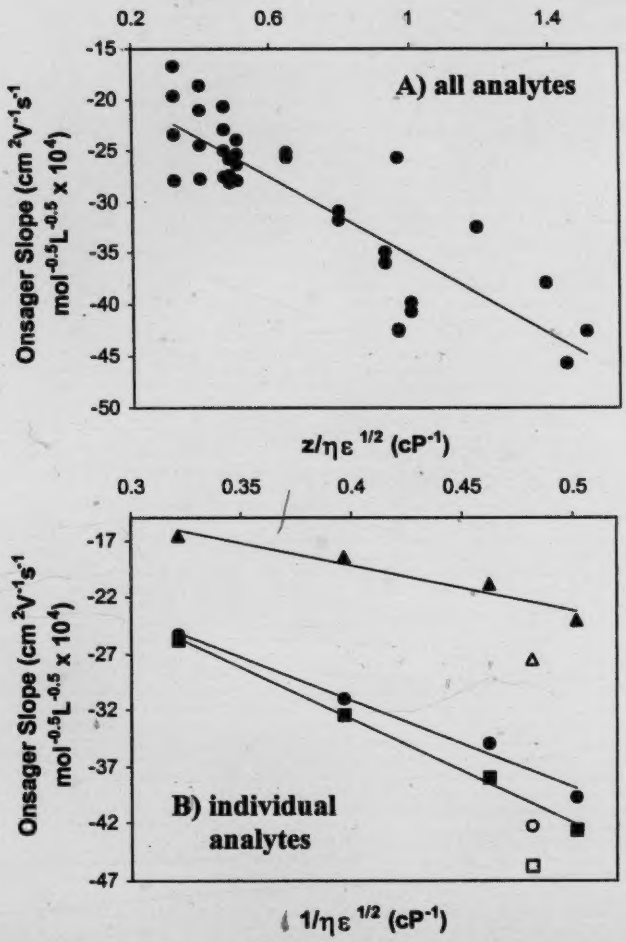

Figure 6.3: Dependence of the Onsager slope on the electrophoretic effect for cations in methanol-acetonitrile media. (A) All analytes are considered together. (B) Each analyte is considered individually. Legend for (B): triangles = benzylammonium; circles = p-xylylenediammonium; squares = 1,3,5-triammoniummethylbenzene. The open symbols represent the data at 100% ACN. The regression lines in (B) were constructed neglecting the data at 100% ACN. Experimental conditions as in Figure 6.1.

100% ACN data (open symbols in Figure 6.3b), which appear to be outliers, the correlation coefficients greatly improve. Indeed, $R^2 \geq 0.92$ for all cations except for benzyltrimethylammonium (Table 6.3). Therefore, for media consisting of 0-75% ACN in MeOH, the Onsager slopes for each analyte generally vary in a manner consistent with

Table 6.3: Correlation Coefficients (R^2) for the Plot of Onsager Slope versus $1/\eta\varepsilon^{1/2}$ (Figure 6.3b) Constructed for the Cations in Methanol-Acetonitrile Media

Cation	R^2	
	with 100% ACN	without 100% ACN
Benzylammonium	0.729	0.933
N-Benzylmethylammonium	0.724	0.945
N,N-Dimethylbenzylammonium	0.683	0.916
Benzyltrimethylammonium	0.128	0.004
p-Xylylenediammonium	0.902	0.985
m-Xylylenediammonium	0.928	0.989
1,3,5-Triammoniummethylbenzene	0.916	0.996

the $1/\eta\varepsilon^{1/2}$ dependence of the electrophoretic effect. The one exception to this is benzyltrimethylammonium, whose Onsager slope is invariant over this solvent range (Table 6.2). This may result from the greater degree of ion-pairing experienced by the quaternary ammonium ion in the investigated solvents (Section 6.3.1.2). Different degrees of ion association in ACN versus MeOH/ACN media may also explain why the data for 100% ACN in Figure 6.3b are outliers.

6.3.2 Dielectric Friction

As the % ACN in MeOH is increased, the dielectric constant increases and the relaxation time decreases (Table 6.1). However, the use of ε in the Hubbard-Onsager equation (eqn 3.27) is a simplification of the more complex term $\varepsilon^2/(\varepsilon-\varepsilon_\infty)$, as discussed in Section 3.4.3.2.2. For the MeOH/ACN solvent systems, the importance of ε_∞ should not be overlooked, since methanol and acetonitrile have similar dielectric constants. The values of ε_∞ for methanol and acetronitrile are 5.6 and 2, respectively [48]. Although no literature values exist for various MeOH/ACN mixtures, Sato et al. [49, 50] have observed that ε_∞ values vary approximately linearly with volume percent organic solvent in methanol-water and ethanol-water media. Using this linear approximation, values of $\varepsilon^2/(\varepsilon-\varepsilon_\infty)$ for 0%, 25%, 50%, 75% and 100% ACN in MeOH were determined to be 39.4, 39.7, 39.5, 39.0 and 38.8, respectively. These values are nearly invariant with MeOH/ACN content. On the other hand, τ shows a much larger variation with solvent content (Table 6.1), so τ/ε and $\tau(\varepsilon-\varepsilon_\infty)/\varepsilon^2$ both decrease with increasing %ACN in MeOH. Since only approximated values of ε_∞ are available, ε will be used in all further discussions instead of $\varepsilon^2/(\varepsilon-\varepsilon_\infty)$.

The Hubbard-Onsager model (eqn 3.27) predicts that dielectric friction is proportional to τ/ε, and should therefore increase with decreasing % ACN in MeOH. In plots of $\mu_o\eta$ versus solvent content, this increase in dielectric friction will manifest itself as a negative deviation from horizontal behavior at higher MeOH contents. Such a plot was constructed for the MeOH/ACN solvent systems investigated herein, and is presented in Figure 6.4. Ion-pairing effects are not of concern in this plot, since absolute mobilities (μ_o) are used. These mobilities were determined by extrapolating the Pitts' plots to zero ionic strength, which should correct for ion association effects [30]. Also, as discussed in Section 4.3.2, the effect of analyte charge has a much larger impact on dielectric friction than analyte size. Therefore, further discussion will refer to the 'charge' dependence, rather than the 'q^2/r^3' dependence, of dielectric friction.

For the +2 and +3 cations between 0 and 25% ACN in MeOH, the change in Walden product is consistent with dielectric friction. In this solvent range, $\mu_o\eta$ increases with increasing acetonitrile content. Further, the increase in Walden product is greater for the +3 ammonium ion than for the +2 ammonium ions, which is consistent with the

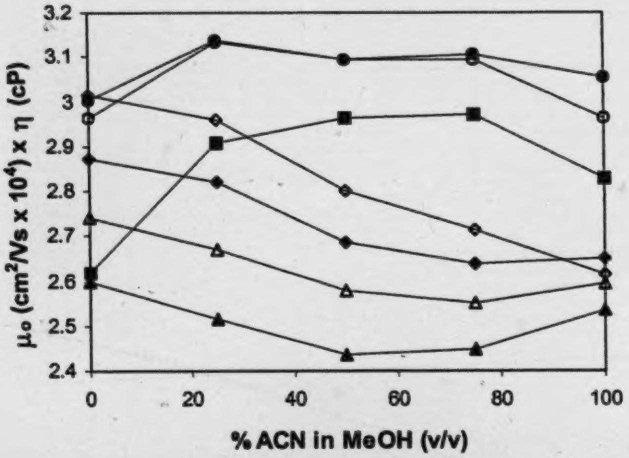

Figure 6.4: Dependence of the Walden product on the MeOH/ACN content of the buffer. Solutes: ▲, benzylammonium; Δ N-benzylmethylammonium; ♦, N,N-dimethylbenzylammonium; ◊, benzyltrimethylammonium; ●, p-xylylenediammonium; ○, m-xylylenediammonium; ■, 1,3,5-triammoniummethylbenzene. Experimental conditions as in Figure 6.1.

charge dependence of dielectric friction. Therefore, the selectivity changes seen in Figure 6.4 between 0 and 25% ACN in MeOH may be attributed to dielectric friction.

Although it appears as though dielectric friction may be responsible for some of the observed selectivity changes in Figure 6.4, its influence should not be over-interpreted. In fact, the change in dielectric friction observed between 0% ACN (100% MeOH) and 100% ACN in Figure 6.4 is much less than that predicted by the change in τ/ε with solvent content. In Chapter 4, τ/ε increased ~7-fold between 0% and 75% MeOH in water, resulting in a decrease in $\mu_o\eta$ of about 35% for the +3 cation. For the MeOH/ACN media investigated herein, τ/ε decreases by a factor of ~15 between 0 and 100% ACN in MeOH, while the Walden product for the +3 ion increases by only ~10%! Further, a decrease in $\mu_o\eta$ for the +2 and +3 ammonium ions is observed upon changing the organic content from 75% to 100% ACN, which is contrary to that predicted by the τ/ε values. These two behaviors suggest that the amount of dielectric friction experienced in acetonitrile is underestimated by its τ and ε values. In Chapter 5, a higher-than-predicted dielectric friction was observed in acetonitrile-water media compared to alcohol-water media. This was explained by the continuum nature of the Hubbard-Onsager model, which does not take into account the different ion-solvent interactions present in acetonitrile and the alcohols. This same reasoning can be used to explain the observed mobility behavior in MeOH/ACN media. The less-than-predicted change in dielectric friction between 100% MeOH and 100% ACN may be due to the neglect by the continuum mobility model of the different ion-solvent interactions present in acetonitrile and methanol.

With the exception of the quaternary ammonium ion, the singly-charged cations experience a minimum in $\mu_o\eta$ at ~75% ACN in MeOH. Therefore, the Walden product increases as the acetonitrile content is increased from 75-100%, which is consistent with dielectric friction. On the other hand, the Walden product increases with decreasing acetonitrile content between 0% and 75% ACN in MeOH, which is opposite to the trend predicted by dielectric friction. For the quaternary ammonium ion, $\mu_o\eta$ increases with decreasing acetonitrile content over the entire solvent range. As described in Chapter 4, the increase in $\mu_o\eta$ with decreasing acetonitrile content may be explained by Nakahara and coworkers' "passing-through-cavities" mechanism [51-54], or by the possible structure-breaking properties of the cations [55, 56]. In a recent paper, Kenndler and coworkers [30] observed similar behavior for anilinium ions in MeOH/ACN media. Figure 6.5 illustrates their results. If the mobilities at 10 mM are adjusted to zero ionic strength using the

Onsager slopes determined herein for the primary ammonium ion (Table 6.2), similar trends are obtained.

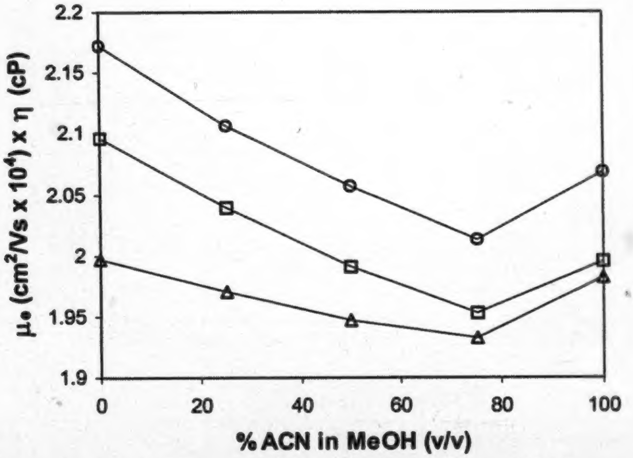

Figure 6.5: Dependence of Walden product on the MeOH/ACN content of the buffer for a series of anilinium ions, as determined by Kenndler and coworkers [30]. Solutes: ○, anilinium; □, 3-methylanilinium; Δ, 2,6-dimethylanilinium. BGE: 9 mM tetrapropylammonium perchlorate, 1 mM $HClO_4$.

Another feature evident in Figure 6.4 is that the selectivity between the +1 ammonium ions is not significantly altered by varying the solvent content. Indeed, the only migration order reversal observed is between the tertiary and quaternary ammonium ions at 100% ACN. This reinforces the belief that the selectivity changes previously observed between 1°, 2° and 3° amines in MeOH/ACN media [22, 42] likely result from differences in the apparent ionic strength effects due to ion pairing, and not from dielectric friction.

6.3.3 Correlation Between Mobility and Solvent Parameters

As described in Section 4.3.3, the Hubbard-Onsager equation (eqn 3.27) predicts that plots of $1/\mu_o\eta$ versus $\tau/\varepsilon\eta$ should be linear. Such plots were constructed for the amines investigated herein, and are presented in Figure 6.6. For clarity, only one cation of each charge is shown. The correlation is poor for all analytes since the only trends in Figure 6.4 consistent with dielectric friction are those between 0% and 25% ACN for the +2 and +3 ammonium ions. Therefore, the cation mobilities in MeOH/ACN media do not vary with solvent parameters in a manner consistent with the Hubbard-Onsager dielectric friction model.

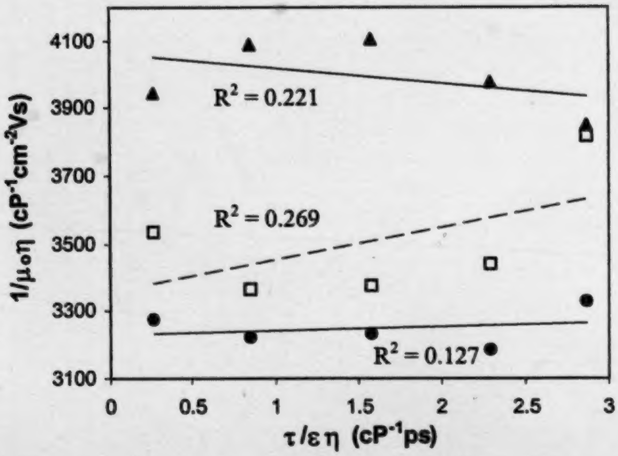

Figure 6.6: Correlation between change in cation mobility and solvent τ, ε and η in methanol-acetonitrile media. Solutes: ▲, benzylammonium; ●, p-xylylenediammonium; □, 1,3,5-triammoniummethylbenzene. Experimental conditions as in Figure 6.1. The dashed line is the regression line for the +3 ammonium ion.

6.3.4 Comparison of Cation Mobilities in 100% MeOH and MeOH/H_2O Media

In Chapter 4, I demonstrated how the cation Walden products vary with buffer methanol contents ranging between 0% and 75% (v/v) MeOH. The Walden products observed herein in 100% MeOH are compared to those in MeOH/H_2O media in Figure 6.7. For clarity, benzylammonium is the only +1 ion shown; the other +1 ammonium ions exhibit similar behavior. For all cations, $\mu_o\eta$ decreases on going from 75% MeOH

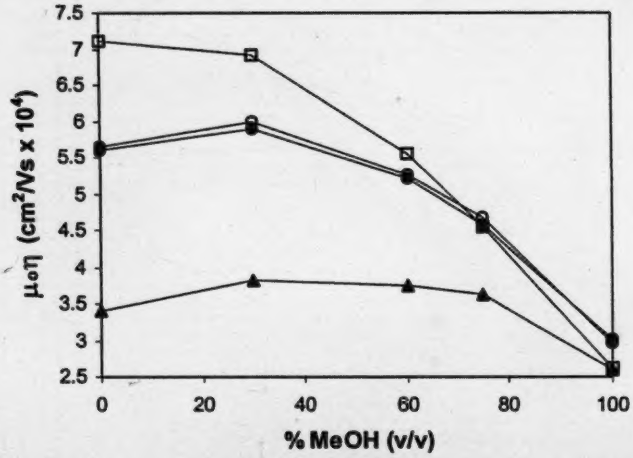

Figure 6.7: Variation of the Walden products of cations in media consisting of 0-100% (v/v) methanol. Solutes: ▲, benzylammonium; ●, p-xylylenediammonium; ○, m-xylylenediammonium; □, 1,3,5-triammoniummethylbenzene. Experimental conditions for 0-75% (v/v) MeOH as in Figure 4.2. Experimental conditions for 100% MeOH as in Figure 6.1.

to 100% MeOH. This suggests that dielectric friction increases as the methanolic buffer is changed from mixed aqueous-organic to nonaqueous media, which is consistent with the τ/ε values in Tables 4.1 and 6.1. Further, the decrease in $\mu_o\eta$ between 75% and 100% MeOH increases with analyte charge, as predicted by the charge dependence of dielectric friction in eqn 3.27. Therefore, the selectivity changes observed in Figure 6.7 are consistent with dielectric friction.

However, as seen in Figure 6.8 and Table 6.4, the correlation between $1/\mu_o\eta$ and $\tau/\varepsilon\eta$ is fairly poor for all analytes. The correlation coefficients in Table 6.4 are artificially high due to the large gap in data points between 75% MeOH and 100% MeOH. For the +2 and +3 ammonium ions, the correlation slopes obtained using data points for 0-75% MeOH (Table 4.7) are greater than those obtained herein when 100% MeOH is included. Therefore, the values of $1/\mu_o\eta$ at 100% MeOH ($\tau/\varepsilon\eta = 2.9$) lie below

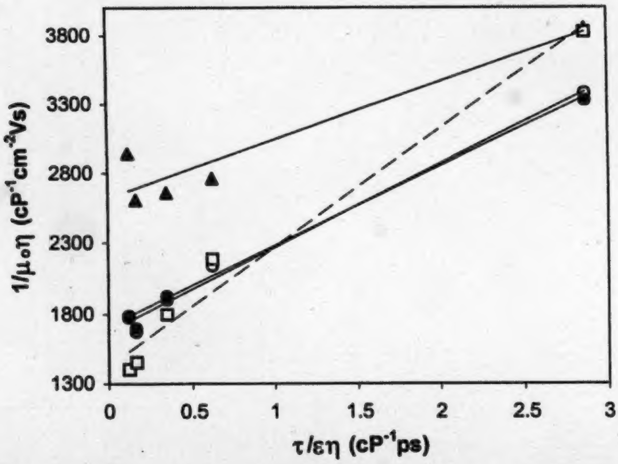

Figure 6.8: Correlation between change in cation mobility and solvent τ, ε and η for media consisting of 0-100% methanol in water. Solutes: ▲, benzylammonium; ●, p-xylylenediammonium; ○, m-xylylenediammonium; □, 1,3,5-triammoniummethylbenzene. Experimental conditions for 0-75% (v/v) MeOH as in Figure 4.2. Experimental conditions for 100% MeOH as in Figure 6.1. The dashed line is the regression line for the +3 cation.

Table 6.4: Regression Data for the Plots of $1/\mu_o\eta$ versus $\tau/\varepsilon\eta$ (Figure 6.8) Constructed for the Cations in Media Consisting of 0-100% Methanol in Water[a]

Cation	Charge	R^2	Slope[b]	Intercept[c]
Benzylammonium	+1	0.899	420±80	2620±110
N-Benzylmethylammonium	+1	0.762	310±100	2730±130
N,N-Dimethylbenzylammonium	+1	0.650	240±100	2760±130
Benzyltrimethylammonium	+1	0.596	190±90	2730±120
p-Xylylenediammonium	+2	0.986	570±40	1710±50
m-Xylylenediammonium	+2	0.990	600±40	1680±50
1,3,5-Triammoniummethylbenzene	+3	0.976	850±80	1430±100

[a] Uncertainties are one standard deviation. [b] Units = $10^{12}Vcm^{-2}$. [c] Units = $Vs(cm^{-2}cP^{-1})$.

the trendlines constructed for 0-75% MeOH. These higher-than-anticipated mobilities at 100% MeOH may result from extending the use of the Hubbard-Onsager equation (eqn 3.27) beyond its limits. As discussed in Chapter 3, one of the simplifying assumptions used in deriving this equation was that the hydrodynamic friction accounted for >> 50%

of the total friction. However, as calculated from eqn 3.27, the dielectric friction experienced by the +1, +2 and +3 cations in 100% MeOH ranges between 67-95% of the total friction. Thus, eqn 3.27 might be too simplified to account for the significant dielectric friction experienced by the cations in pure methanolic media. Nonetheless, although the magnitudes of the mobility changes between 75% and 100% methanol are less than predicted by the solvent parameters, the general trends are consistent with Hubbard and Onsager's dielectric friction model.

6.4 Concluding Remarks

The charge dependence of the Pitts equation (eqn 4.4) is generally not obeyed for cations in MeOH/ACN media. This may result from ion association, since the presence of ion-pairing effects will cause an increase in the apparent ionic strength effect. Indeed, the selectivity changes observed herein between primary, secondary, tertiary and quaternary amines are consistent with ion-pairing effects.

The mobility behavior of the cations in MeOH/ACN media is not effectively explained by Hubbard and Onsager's dielectric friction model. In addition, the change in dielectric friction observed between 0% ACN (100% MeOH) and 100% ACN is much less than that predicted by the corresponding change in τ/ε with solvent content. It appears as though acetonitrile's τ and ε values underestimate the amount of dielectric friction experienced in this solvent. Similar behavior was reported in Chapter 5 for ACN/H_2O media, and was attributed to the different ion-solvent interactions occurring in acetonitrile compared to the alcohols.

The decrease in $\mu_o\eta$ on going from methanol-water to pure methanol media is consistent with dielectric friction, but the magnitude of the change is less than that predicted by the corresponding solvent parameters. This is likely due to the fact that eqn 3.27, which was derived for the situation in which hydrodynamic friction is dominant, is too simplified to account for the large amount of dielectric friction experienced in methanol.

6.5 References

(1) Walbroehl, Y.; Jorgenson, J. W. *J. Chromatogr.* **1984,** *315*, 135-143.

(2) Miller, J. L.; Khaledi, M. G.; Shea, D. *Anal. Chem.* **1997,** *69*, 1223-1229.

(3) Salimi-Moosavi, H.; Cassidy, R. M. *J. Chromatogr. A* **1996,** *749*, 279-286.

(4) Salimi-Moosavi, H.; Cassidy, R. M. *Anal. Chem.* **1996,** *68*, 293-299.

(5) Piette, V.; Lammerhofer, M.; Lindner, W.; Crommen, J. *Chirality* **1999,** *11*, 622-630.

(6) Wang, T.; Wei, H.; Li, S. F. Y. *Electrophoresis* **1998,** *19*, 2187-2192.

(7) Carabias-Martínez, R.; Rodríguez-Gonzalo, E.; Domínguez-Alvarez, J.; Hernández-Méndez, J. *Anal. Chem.* **1997,** *69*, 4437-4444.

(8) Fillet, M.; Bechet, I.; Piette, V.; Crommen, J. *Electrophoresis* **1999,** *20*, 1907-1915.

(9) Cherkaoui, S.; Varesio, E.; Christen, P.; Veuthey, J.-L. *Electrophoresis* **1998,** *19*, 2900-2906.

(10) Porras, S. P.; Jussila, M.; Sinervo, K.; Riekkola, M.-L. *Electrophoresis* **1999,** *20*, 2510-2518.

(11) Sirén, H.; Hiissa, T.; Min, Y. *Analyst* **2000,** *125*, 1561-1568.

(12) Cherkaoui, S.; Veuthey, J.-L. *J. Chromatogr. A* **2000,** *874*, 121-129.

(13) Li, X.-F.; Liu, C.-S.; Roos, P.; Hansen Jr., E. B.; Cerniglia, C. E.; Dovichi, N. J. *Electrophoresis* **1998,** *19*, 3178-3182.

(14) Leung, G. N. W.; Tang, H. P. O.; Tso, T. S. C.; Wan, T. S. M. *J. Chromatogr. A* **1996,** *738*, 141-154.

(15) Valkó, I. E.; Sirén, H.; Riekkola, M.-L. *LC-GC* **1997,** *15*, 560-567.

(16) Steiner, F.; Hassel, M. *Electrophoresis* **2000,** *21*, 3994-4016.

(17) Cherkaoui, S.; Geiser, L.; Veuthey, J.-L. *Chromatographia* **2000,** *52*, 403-407.

(18) Cherkaoui, S.; Rudaz, S.; Veuthey, J.-L. *Electrophoresis* **2001,** *22*, 491-496.

(19) Geiser, L.; Cherkaoui, S.; Veuthey, J.-L. *J. Chromatogr. A* **2000,** *895*, 111-121.

(20) Li, X.-F.; Carter, S. J.; Dovichi, N. J. *J. Chromatogr. A* **2000,** *895*, 81-85.

(21) Cherkaoui, S.; Veuthey, J.-L. *Electrophoresis* **2002,** *23*, 442-448.

(22) Tjørnelund, J.; Hansen, S. H. *J. Biochem. Biophys. Methods* **1999,** *38*, 139-153.

(23) Cherkaoui, S.; Bekkouche, K.; Christen, P.; Veuthey, J.-L. *J. Chromatogr. A* **2001,** *922*, 321-328.

(24) Yang, Q.; Benson, L. M.; Johnson, K. L.; Naylor, S. *J. Biochem. Biophys. Methods* **1999,** *38*, 103-121.

(25) *CRC Handbook of Chemistry and Physics*, 76th ed.; CRC Press: New York, 1995-1996.

(26) Akhadov, Y. Y. *Dielectric Properties of Binary Solutions. A Data Handbook*; Pergamon Press: New York, 1980.

(27) Baeuml, F.; Welsch, T. *J. Chromatogr. A* **2002,** *961*, 35-44.

(28) Porras, S. P.; Jyske, P.; Riekkola, M.-L.; Kenndler, E. *J. Microcolumn Sep.* **2001,** *13*, 149-155.

(29) Porras, S. P.; Riekkola, M.-L.; Kenndler, E. *Chromatographia* **2001,** *53*, 290-294.

(30) Porras, S. P.; Riekkola, M.-L.; Kenndler, E. *J. Chromatogr. A* **2001,** *924*, 31-42.

(31) Rived, F.; Rosés, M.; Bosch, E. *Anal. Chim. Acta* **1998,** *374*, 309-324.

(32) Rived, F.; Canals, I.; Bosch, E.; Rosés, M. *Anal. Chim. Acta* **2001,** *439*, 315-333.

(33) Coetzee, J. F. *Prog. Phys. Org. Chem.* **1967,** *4*, 45-92.

(34) Williams, B. A.; Vigh, G. *Anal. Chem.* **1996,** *68*, 1174-1180.

(35) Ohtaki, H. *Monatsh. Chem.* **2001,** *132*, 1237-1268.

(36) Spiro, M. In *Physical Chemistry of Organic Solvent Systems*; Covington, A. K., Dickinson, T., Eds.; Plenum Press: New York, 1973, pp 635-680.

(37) Price, E. In *The Chemistry of Non-Aqueous Solvents*; Lagowski, J. J., Ed.; Academic Press: New York, 1966; Vol. 1, pp 67-96.

(38) Bockris, J. O. M.; Reddy, A. K. N. *Modern Electrochemistry*; Plenum Press: New York, 1970, Vol. 1, pp 224-230.

(39) Harris, D. C. *Quantitative Chemical Analysis*, 4th ed.; W. H. Freeman and Company: New York, 1995, Table 8.1.

(40) Li, D.; Fu, S.; Lucy, C. A. *Anal. Chem.* **1999,** *71*, 687-699.

(41) King, E. J. In *Physical Chemistry of Organic Solvent Systems*; Covington, A. K., Dickinson, T., Eds.; Plenum Press: New York, 1973, pp 331-393.

(42) Bjørnsdottir, I.; Hansen, S. H. *J. Chromatogr. A* **1995,** *711*, 313-322.

(43) Grob, M.; Steiner, F. *Electrophoresis* **2002,** *23*, 1853-1861.

(44) Salimi-Moosavi, H.; Cassidy, R. M. *Anal. Chem.* **1995,** *67*, 1067-1073.

(45) Kay, R. L.; Evans, D. F. *J. Phys. Chem.* **1966,** *70*, 2325-2335.

(46) Barthel, J.; Iberl, L.; Rossmaier, J.; Gores, H. J.; Kaukal, B. *J. Solution Chem.* **1990,** *19*, 321-337.

(47) Barthel, J.; Krell, M.; Iberl, L.; Feuerlein, F. *J. Electroanal. Chem.* **1986,** *214*, 485-505.

(48) Evans, D. F.; Tominaga, T.; Hubbard, J. B.; Wolynes, P. G. *J. Phys. Chem.* **1979,** *83*, 2669-2677.

(49) Sato, T.; Chiba, A.; Nozaki, R. *J. Chem. Phys.* **1999,** *110*, 2508-2521.

(50) Sato, T.; Chiba, A.; Nozaki, R. *J. Chem. Phys.* **2000,** *112*, 2924-2932.

(51) Takisawa, N.; Osugi, J.; Nakahara, M. *J. Phys. Chem.* **1981,** *85*, 3582-3585.

(52) Takisawa, N.; Osugi, J.; Nakahara, M. *J. Chem. Phys.* **1982,** *77*, 4717-4722.

(53) Takisawa, N.; Osugi, J.; Nakahara, M. *J. Chem. Phys.* **1983,** *78*, 2591-2597.

(54) Nakahara, M.; Török, T.; Takisawa, N.; Osugi, J. *J. Chem. Phys.* **1982,** *76*, 5145-5149.

(55) Kay, R. L. In *Water. A Comprehensive Treatise*; Franks, F., Ed.; Plenum Press: New York, 1973; Vol. 3, pp 204-209.

(56) Frank, H. S.; Wen, W.-Y. *Disc. Faraday Soc.* **1957,** *24*, 133-140.

CHAPTER SEVEN. The Influence of Temperature on Selectivity in Capillary Electrophoresis

In the previous three chapters, dielectric friction was altered by changing the solvent composition of the electrophoretic media. In this chapter, varying the capillary temperature is investigated as a means to alter ion selectivity in aqueous CE. Since solvent parameters are dependent upon temperature, dielectric friction may be able to account for temperature-induced selectivity changes.

7.1 Introduction

Temperature is an independent variable that can be used to alter the separation in capillary electrophoresis [1]. This is useful because temperature is an easily-controlled variable. Numerous literature reports exist documenting temperature-induced selectivity changes in CE. Gil et al. [2, 3] used temperature to optimize the separation between metacycline, doxycycline and their related substances. They found that the resolution decreased as the temperature increased. Migration order reversals between inorganic anions upon changing the capillary temperature were observed by Harrold et al. [4] and François et al. [5]. Further, Nielen [6] reported that the resolution between positional isomers of substituted benzoic acids increased as the temperature was increased. In this instance, the selectivity changes were attributed to shifts in pK_a and chemical equilibria with temperature. On the other hand, Wang and coworkers [7] reported that changes in peptide migration with temperature were predominantly due to changes in the solvent viscosity. As a result, temperature-induced selectivity changes between the peptides were not observed.

It is of interest to see whether dielectric friction can account for temperature-induced selectivity changes in CE, especially those between the inorganic anions mentioned above. Table 7.1 shows how η, ε and τ change with temperature. Since the Hubbard-Onsager model (eqn 3.27) predicts that dielectric friction is proportional to τ/ε, dielectric friction should increase with decreasing capillary temperature. However, the variation in τ/ε with temperature is small compared to its variation with solvent content seen in Chapters 4, 5 and 6. Therefore, the effect of dielectric friction on ion mobility is expected to be much less herein than in the studies involving aqueous-organic and nonaqueous media.

Table 7.1: Effect of Buffer Temperature on Solvent Parameters

Temperature (°C)	η^a (cP)	ε^a	τ^b (ps)	τ/ε (ps)
15.0±0.1	1.15	82.05	10.89	0.133
20.0±0.1	1.01	80.19	9.54	0.119
25.0±0.1	0.89^c	78.48^d	8.25^d	0.105
30.0±0.1	0.79	76.59	7.42	0.097
35.0±0.1	0.72	74.85	6.58	0.088
40.0±0.1	0.65	73.15	5.86	0.080

[a] Values obtained from interpolation of literature data [8]. Values for η were determined at various temperatures by fitting a 4th-order polynomial to a plot of η versus T (K). Similarly, values for ε were determined using a 3rd-order polynomial [8]. [b] Values obtained from interpolation of literature data [9]. For each temperature, values of τ were determined using the relationship [10] $\tau = Ae^{(w/kT)}$. [c] Literature value [8]. [d] Literature values [9].

In this chapter, the mobilities of a –3- and a –4-charged organic anion are investigated in aqueous media at temperatures ranging between 15°C and 40°C. Dielectric friction and ionic strength effects are evaluated as to their success at predicting temperature-induced selectivity changes.

7.2 Experimental

7.2.1 Apparatus

A P/ACE MDQ capillary electrophoresis system (Beckman Instruments, Fullerton, CA) equipped with UV detection at 214 nm was used for all mobility measurements. Data acquisition and control, as well as bare fused-silica capillary length, diameter and rinsing, were as described in Section 4.2.1. The capillary was thermostatted to a desired temperature (±0.1°C) using a cooling cartridge filled with a liquid coolant. Separations were performed at 15.0, 20.0, 25.0, 30.0, 35.0 and 40.0°C.

7.2.2 Chemicals

All of the solutions were prepared with Nanopure 18 MΩ water (Barnstead, Chicago, IL) and were filtered through 0.45-μm syringe-driven filters (Millipore, Bedford, MA). The buffers consisted of 2.3-81.9 mM boric acid (BDH, Darmstadt, Germany), with the pH adjusted to 10.00 (25°C) using reagent-grade sodium hydroxide (BDH). These concentrations corresponded to ionic strengths of ~2-70 mM. The pH values were measured at 25°C using a Corning digital pH meter model 445 (Corning, Acton, MA) calibrated immediately prior to use.

The ionic strengths of the buffers were calculated from the concentrations of all ionic species present in solution. Boric acid (H_3BO_3) has two acid dissociation contants, $pK_{a1}=9.24$ and $pK_{a2}=12.74$ (at 25°C) [11]. The amount of NaOH needed to reach a pH of 10.00 was calculated using pK_{a1} and the Henderson-Hasselbach equation:

$$pH = pK_{a(1)} + \log\frac{[H_2BO_3^-]}{[H_3BO_3]} \tag{7.1}$$

Eqn 7.1 predicts that for an initial H_3BO_3 concentration of C at 25°C, $0.852C$ of NaOH is required to adjust the pH to 10.00. The amounts of H_3BO_3, $H_2BO_3^-$ and HBO_3^{2-} in solution at pH 10.00 were determined by [11]

$$\left[H_3BO_3\right] = \alpha_o C_{H_3BO_3} \tag{7.2}$$

$$\left[H_2BO_3^-\right] = \alpha_1 C_{H_3BO_3} \tag{7.3}$$

$$\left[HBO_3^{2-}\right] = \alpha_2 C_{H_3BO_3} \tag{7.4}$$

where $C_{H_3BO_3}$ is the initial added concentration of boric acid and

$$\alpha_o = \frac{\left[H^+\right]^2}{\left[H^+\right]^2 + K_{a1}\left[H^+\right] + K_{a1}K_{a2}} \tag{7.5}$$

$$\alpha_1 = \frac{K_{a1}\left[H^+\right]}{\left[H^+\right]^2 + K_{a1}\left[H^+\right] + K_{a1}K_{a2}} \tag{7.6}$$

$$\alpha_2 = \frac{K_{a1}K_{a2}}{\left[H^+\right]^2 + K_{a1}\left[H^+\right] + K_{a1}K_{a2}} \tag{7.7}$$

Therefore, for a boric acid buffer at pH=10.00 and 25°C, the ionic strength was calculated as follows:

$$\begin{aligned} I &= \tfrac{1}{2}\ \{\Sigma z_i^2 c_i\} \\ &= \tfrac{1}{2}\ \{(-1)^2[H_2BO_3^-] + (-2)^2[HBO_3^{2-}] + (+1)^2[Na^+] + (-1)^2[OH^-]\} \\ &= \tfrac{1}{2}\ \{0.851C + 0.006C + 0.852C + 1\times10^{-4}\ M\} \end{aligned} \tag{7.8}$$

For the studies performed at temperatures other than 25°C, the ionic strength was adjusted to account for the changes in pH and pK_a with temperature. The pK_a of boric acid decreases by ~0.006 units for every 1°C increase in temperature [12, 13]. Using this general rule for pK_{a2} and tabulated values [13] for pK_{a1}, the concentrations of HBO_3^{2-}, $H_2BO_3^-$, H_3BO_3, H^+ and OH^- at various temperatures were calculated according to eqns

7.1-7.7. Since the buffers were always prepared at 25°C, the concentration of Na^+ was independent of temperature.

The sample analytes 1,3,(6 or 7)-naphthalenetrisulfonic acid and 1,2,4,5-benzenetetracarboxylic acid were purchased from Aldrich (Milwaukee, WI) and were used without any further purification. Sample anion solutions were prepared at concentrations of 2×10^{-3} M in waterand were diluted to 1×10^{-4} M in the corresponding buffer solution to eliminate sample stacking during electrophoresis. The neutral electroosmotic flow marker was 4 mM mesityl oxide (Aldrich). The sample analytes should be completely ionized at all temperatures investigated. As the temperature was increased from 15°C to 40°C, the pH of the boric acid buffer decreased from 10.09 to 9.89 (eqn 7.1). With a pK_{a4} of 6.23 [14] at 25°C, 1,2,4,5-benzenetetracarboxylic acid should be completely ionized even if its pK_{a4} increases by 1 in the temperature range studied. However, such a large increase in pK_a is highly unlikely, given that both the pK_{a1} and pK_{a2} of phthalic acid change by only 0.04 units in the temperature range 15-40°C [15].

7.2.3 Determination of Mobility

Effective analyte mobilities were measured according to the method of Williams and Vigh [16], as described in Section 4.2.3. This method was employed to ensure that the separation occurred in the thermostatted region of the capillary. Briefly, depending on the buffer viscosity, a sample plug consisting of analyte and EOF marker was injected for 3-4 s at 0.5 psi, and was then transferred into the thermostatted region of the capillary using 0.5 psi for 2.7-5 min. A voltage of 6.0 kV was subsequently applied for 3 min, followed by a second injection of the EOF marker. Finally, the three sample zones were mobilized past the detector by applying a pressure of 0.5 psi. For the I=70 mM buffer at 15-40°C, a voltage of 6.0 kV was within the linear region of an Ohm's plot and gave currents of 8.4-13.5 μA. Effective mobilities were calculated using eqn 4.2. Absolute ion mobilities (μ_o) at zero buffer ionic strength were determined by plotting the effective mobilities versus $I^{1/2}/(1 + Ba \times I^{1/2})$ according to the Pitts equation (eqn 4.3).

7.3 Results and Discussion

7.3.1 Ionic Strength Effects

For each temperature investigated, the effective mobilities (μ_e) were plotted against $I^{1/2}/(1+Ba\times I^{1/2})$ and extrapolated to zero ionic strength to yield absolute mobilities. Equation 3.38 suggests that B depends on temperature both directly and indirectly through ε. However, $1/(\varepsilon T)^{1/2}$ decreases by only 2% as the temperature is increased from 15 to 40°C. Assuming that a is independent of temperature, this results in a minimal change in Ba from 2.39 to 2.43 over the entire temperature range studied. Therefore, a value of 2.4 for Ba was used at all temperatures. Figure 7.1 shows the Pitts' plots obtained for the –3 sulfonate and the –4 carboxylate at 15, 20, 25, 30, 35 and 40°C. The corresponding correlation coefficients, Onsager slopes and intercepts (absolute mobilities, μ_o) are in Table 7.2. Good linearity is observed in the Pitts' plots ($R^2 \geq 0.996$ for both anions), suggesting that eqn 4.3 is applicable at various temperatures. Indeed, the p-values for both anions at all temperatures are less than 0.01, indicating that the data obey linear relationships at the 99% confidence level.

At 25°C, the absolute mobilities of the –3 and –4 ions in Table 7.2 are not significantly different at the 95% confidence level from those in Table 4.3 for aqueous

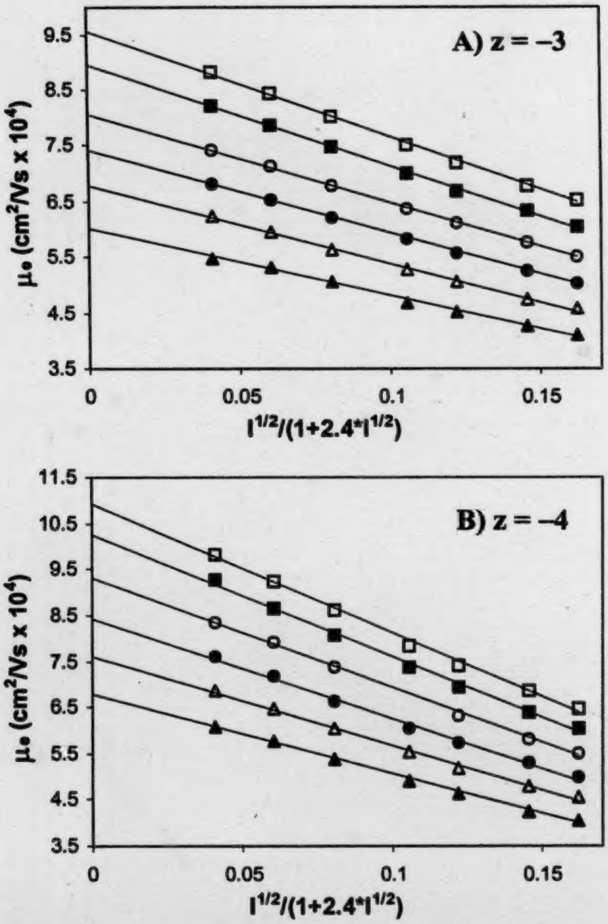

Figure 7.1: Influence of temperature on ionic strength effects for (A) 1,3,(6 or 7)-naphthalenetrisulfonate and (B) 1,2,4,5-benzenetetracarboxylate. Temperatures: ▲, 15°C; Δ, 20°C; ●, 25°C; ○, 30°C; ■, 35°C; □, 40°C. Experimental conditions: UV detection at 214 nm; 60-cm capillary (50 cm to detector); 6 kV applied; 1×10^{-4} M sample concentration; boric acid buffer (pH ~ 10).

media. The same can be said for the Onsager slopes. Thus, whether the buffer consists of boric acid or a mixture of NaOH and NaCl, the absolute mobilities and ionic strength effects are not affected. The invariance of μ_o is to be expected, since extrapolation to zero buffer ionic strength should diminish any electrolyte effects. The Onsager slopes are also expected to be the same. Different electrolytes can alter the ionic strength effect

Table 7.2: Ionic Strength Effects as a Function of Temperature[a]

			Pitts Equation	
Anion and Temperature (°C)	N[b]	R^2	Onsager Slope[c]	Intercept[d], μ_o
1,3,(6 or 7)-Naphthalenetrisulfonate (z=–3)				
15.0±0.1	7	0.9959	-12.0±0.3	6.00±0.04
20.0±0.1	7	0.9979	-13.9±0.3	6.77±0.03
25.0±0.1	7	0.9993	-14.8±0.2	7.42±0.02
30.0±0.1	7	0.9995	-16.0±0.2	8.07±0.02
35.0±0.1	7	0.9991	-18.1±0.2	8.95±0.03
40.0±0.1	7	0.9988	-19.1±0.3	9.57±0.03
1,2,4,5-Benzenetetracarboxylate (z=–4)				
15.0±0.1	7	0.9975	-17.1±0.4	6.77±0.04
20.0±0.1	7	0.9975	-19.3±0.4	7.61±0.05
25.0±0.1	7	0.9961	-21.7±0.6	8.43±0.07
30.0±0.1	6	0.9986	-24.0±0.4	9.32±0.05
35.0±0.1	7	0.9957	-26.7±0.8	10.27±0.09
40.0±0.1	7	0.9959	-28.0±0.8	10.91±0.09

[a] Uncertainties are one standard deviation according to the regression analysis. [b] Number of data points used in the regression analysis. [c] Units = $10^{-4}cm^2V^{-1}s^{-1}mol^{-0.5}L^{-0.5}$. [d] Units = $10^{-4}cm^2V^{-1}s^{-1}$.

through ion association and/or changes in the electrolyte-dependent parameter *q* in eqn 4.3. However, Na^+ is the counterion in both electrolyte systems, so ion association effects should be the same in both buffers. Also, both electrolyte systems consist of 1:1 electrolytes, since at pH~10 less than 0.2% of boric acid is present as HBO_3^{2-}. Therefore, *q* is 0.5 for both electrolytes. The Onsager slopes are thus expected to be the same in both buffer systems.

At any given temperature, the Onsager slope for the –4 carboxylate is always significantly larger than for the –3 sulfonate at the 95% confidence level. This is consistent with the Pitts equation, since both terms in the brackets of eqn 4.3 depend on analyte charge. Similar behavior was observed in Chapters 4 and 5 for anions in aqueous and mixed aqueous-organic media. Further, the Onsager slopes vary with temperature, viscosity and dielectric constant in a manner consistent with the electrophoretic term in the Pitts equation (left-hand term in the brackets of eqn 4.3). Plots of Onsager slope as a function of $1/\eta(\varepsilon T)^{1/2}$ for the –3 and –4 ions (Figure 7.2) show good correlation, with R^2 values of 0.988 and 0.993, respectively.

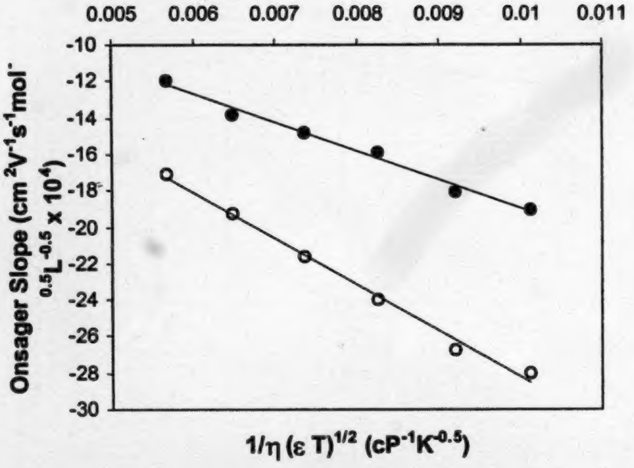

Figure 7.2: Dependence of Onsager slope on temperature, viscosity and dielectric constant. Solutes: ●, 1,3,(6 or 7)-naphthalenetrisulfonate; ○, 1,2,4,5-benzenetetracarboxylate. Experimental conditions as in Figure 7.1.

One possible explanation for temperature-induced selectivity changes in CE is that the relative ionic strength effects of different ions change as a function of temperature. It has already been established that for all temperatures investigated, the Onsager slope for the –4 carboxylate is always greater than that for the –3 sulfonate (Table 7.2). As a result, at any given temperature, there exists an ionic strength (I_C) at which a migration order reversal will occur between the –3 and –4 ions. For example, at 25.0°C, the regression data predicts that this migration order reversal will occur at I_C=52.7 mM. If I_C changes with temperature, then temperature-induced selectivity changes may be observed. This was investigated by plotting I_C versus temperature (Figure 7.3), whereby I_C was determined by solving simultaneous equations obtained from the regression data (Table 7.2). As seen in Figure 7.3, no clear trend is observed between I_C and temperature, and the values of I_C over the investigated temperature range are not statistically different. This is consistent with the observation that the slopes and intercepts in Table 7.2 all increase at the same rate with increasing temperature. Due to the large uncertainties in I_C as calculated from the regression data, it is impossible to deduce from Figure 7.3 whether I_C changes with temperature. However, *experimental* mobilities show that I_C is approximately 50 mM at 15°C and 70 mM at 35°C. Therefore, if the right ionic strength is selected, it may be possible to see temperature-induced migration order reversals in CE.

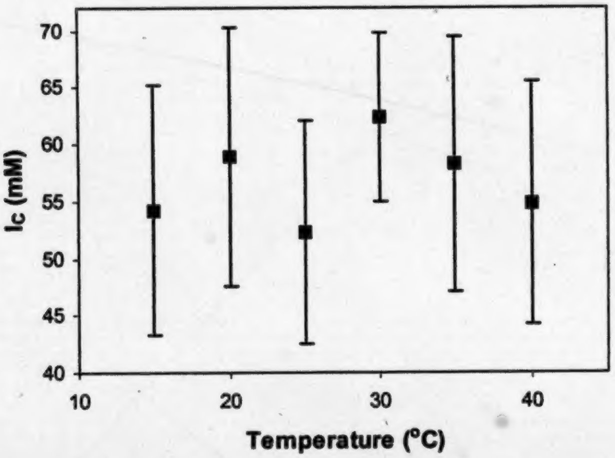

Figure 7.3: Influence of temperature on the ionic strength (I_c) at which a migration order reversal occurs between the –3 and –4 ions. The error bars represent ± 1 standard deviation as calculated from the regression data in Table 7.2. Experimental conditions as in Figure 7.1.

7.3.2 Influence of Dielectric Friction

According to Table 7.1 and the Hubbard-Onsager equation (eqn 3.27), dielectric friction should increase with decreasing temperature. Therefore, if dielectric friction is responsible for temperature-induced selectivity changes, a negative deviation from horizontal (Hückel) behavior with decreasing temperature should be observed in plots of $\mu_o\eta$ versus temperature. Figure 7.4a plots $\mu_o\eta$ as a function of temperature for the –3 and –4 ions investigated herein, constructed using literature viscosity values (Table 7.1). For both anions, the Walden products decrease with increasing temperature at roughly the same rate. As a result, temperature-induced selectivity changes are not observed. Further, the decrease in $\mu_o\eta$ with increasing temperature is opposite to the trend predicted by dielectric friction, since τ/ε *decreases* with increasing temperature. It therefore does not appear as though dielectric friction is responsible for temperature-induced selectivity changes in this system. This can be reasoned from the relatively small change in τ/ε with temperature (Table 7.1). The effects of dielectric friction are likely to be more pronounced in mixed aqueous-organic media, since τ/ε generally varies to a greater extent with % organic content than with temperature (Tables 4.1 and 5.1).

A decrease in Walden product with increasing temperature, as observed in Figure 7.4a, has been previously reported [17-23]. Nakahara and coworkers [19, 22] have explained this behavior using the 'passing-through-cavities' mechanism, whereby an ion that is weakly interacting with water molecules passes through a series of larger unoccupied cavities in the open structure of water [24]. They reason that this mechanism must be more pronounced at lower temperatures. Further, the concept of ***structure-breaking*** ions has been applied [18] to account for the decrease in $\mu_o\eta$ with increasing temperature.

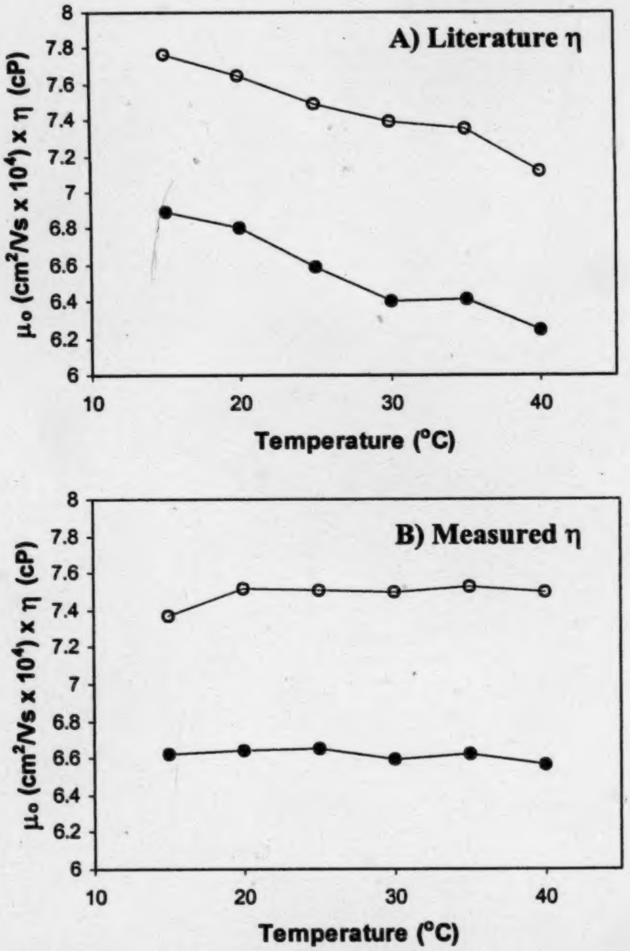

Figure 7.4: Walden plots as a function of temperature using (A) literature viscosities (Table 7.1) and (B) measured viscosities. In (B), the viscosities at X°C were measured relative to that at 25°C according to the procedure described in Section 4.2.4. Solutes: ●, 1,3,(6 or 7)-naphthalenetrisulfonate; ○, 1,2,4,5-benzenetetracarboxylate. Experimental conditions as in Figure 7.1.

According to the Frank-Wen model [25] (Section 3.2.3), in the intermediate region between the solvation shell of the ion and the bulk solvent, the ionic charge interferes with the formation of the normal solvent structure. This structure-breaking effect increases with decreasing charge density of the ion, and results in a higher-than-expected ion mobility/conductivity. For structure-breaking ions, a decrease in Walden product with increased temperature is anticipated due to the fact that there is less structure to break at higher temperatures [18]. Indeed, the –3 sulfonate and the –4 carboxylate may be structure-breaking ions, since their charge density is less than that for Cl^-, which is a structure-breaking ion [18, 26].

In our present system, another possible explanation exists for the decrease in $\mu_o\eta$ with increasing temperature. If the capillary thermostatting is inadequate, then the actual viscosities within the capillary will not correspond to the literature viscosities (Table 7.1). According to the cartridge design, ~5 cm at both ends of the capillary lie outside the thermostatted region and are at room temperature (approx. 25°C). Inadequate temperature control within the cartridge will therefore result in the actual temperatures being less than or greater than the predicted temperatures for temperature settings above or below 25°C, respectively. As such, within the thermostatted region, the actual viscosities for temperature settings above or below 25°C will be higher or lower, respectively, than the literature viscosities. Corrections for such effects would shift the Walden products in Figure 7.4a to lower values at 15 and 20°C, and to higher values at 30, 35 and 40°C. This would eliminate the decrease in $\mu_o\eta$ with temperature observed in Figure 7.4a.

To investigate whether inadequate thermostatting was a real phenomenon in our system, the viscosities at all temperatures were measured relative to that at 25°C according to the procedure described in Section 4.2.4. Actual viscosities were then calculated by multiplying the relative viscosities by the viscosity of water at 25°C (0.89 cP) [8]. Since the capillary ends are always at the same ambient temperature, the viscosities calculated in this manner reflect the actual changes in thermostatted-region viscosity with temperature. Figure 7.4b plots the Walden products as a function of temperature using the measured viscosities. The plots for both ions are fairly horizontal, suggesting that insufficient temperature control may be the cause of the negative deviations seen in Figure 7.4a. Further, except for perhaps the –4 ion at 15°C, dielectric friction effects are not observed. It should be noted that although these measured viscosities correct for inefficiencies in thermostatting, they are unrealistic in that their measurement is biased by the viscosity of the unthermostatted regions of the capillary. Since all mobility measurements were performed in the temperature-controlled region of the capillary, I feel more justified in using literature viscosity values. For this reason, with the exception of Figure 7.4b, all data is treated using literature viscosities.

As illustrated above, variations in dielectric friction with temperature appear to have a negligible effect on the mobilities of the –3 sulfonate and the –4 carboxylate. It has been reported that changes in migration time with temperature are mainly due to the temperature-induced viscosity changes of the solvent [7, 19, 23, 27]. As such, the Hückel equation (eqn 1.5) predicts that plots of μ_o versus $1/\eta$ will be linear, with slopes proportional to q/r. These plots were constructed for the –3 and –4 ions investigated herein, and are shown in Figure 7.5. Excellent linear correlation is obtained, with $R^2=0.998$ for both ions. Therefore, the absolute mobilities vary with temperature in a manner consistent with the Hückel equation. The influence of temperature on viscosity appears to be the predominant factor governing ion mobility in the present system.

Although dielectric friction is not responsible for temperature-induced selectivity changes in the present system, this does not imply that it cannot account for some of the

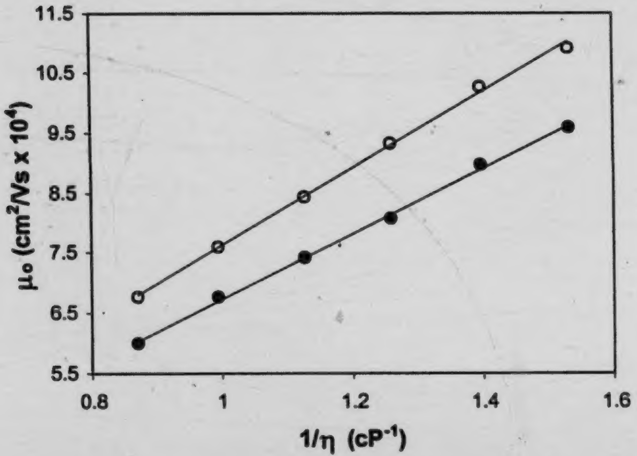

Figure 7.5: Correlation between absolute mobility and viscosity according to the Hückel equation. Solutes: ●, 1,3,(6 or 7)-naphthalenetrisulfonate; ○, 1,2,4,5-benzenetetracarboxylate. Experimental conditions as in Figure 7.1.

selectivity changes that have been observed in the literature. Harrold et al. [4] reported a migration order reversal between F^- and PO_4^{3-} and between Cl^- and SO_4^{2-} upon decreasing the capillary temperature. In both cases, the higher-charged anion migrated slower than the –1 inorganic ion at lower temperatures. Further, temperature-induced selectivity changes between SO_4^{2-}, NO_3^- and NO_2^- were reported by Morin and coworkers [5]. These changes in relative migration may be explained by the increase in dielectric friction with decreasing temperature. The reason why these selectivity changes may be attributed to dielectric friction while no such effects were observed herein is because the inorganic anions have higher charge densities than the aromatic organic anions that I used. According to the Hubbard-Onsager model (eqn 3.27), dielectric friction is proportional to $q^2\tau/r^3\varepsilon$, so ions with larger q^2/r^3 will experience more dielectric friction. Since the variation in τ/ε with temperature is small, changes in dielectric friction with temperature will only be noticeable for ions with higher charge densities.

7.4 Concluding Remarks

The selectivity between the organic anions investigated herein is not significantly altered by temperature. In fact, the influence of temperature on viscosity is the predominant factor governing the mobility of these ions. Therefore, neither ionic strength effects nor dielectric friction are conclusively shown to account for temperature-induced selectivity changes in CE. However, experimental evidence exists suggesting that small changes in the ionic strength effect with temperature may result in selectivity changes. Further, although dielectric friction effects are not seen here, dielectric friction may still account for the temperature-induced selectivity changes observed in the literature between inorganic anions of high charge density. A systematic study of the variation of inorganic anion mobility with temperature is required in order to confirm whether temperature-induced selectivity changes can result from dielectric friction.

7.5 References

(1) Oda, R. P.; Landers, J. P. In *Handbook of Capillary Electrophoresis*; Landers, J. P., Ed.; CRC Press: Boca Raton, 1994, pp 9-42.

(2) Gil, E. C.; Dehouck, P.; van Schepdael, A.; Roets, E.; Hoogmartens, J. *Electrophoresis* **2001,** *22*, 497-502.

(3) Gil, E. C.; Van Schepdael, A.; Roets, E.; Hoogmartens, J. *J. Chromatogr. A* **2000,** *895*, 43-49.

(4) Harrold, M.; Stillian, J.; Bao, L.; Rocklin, R.; Avdalovic, N. *J. Chromatogr. A* **1995,** *717*, 371-383.

(5) François, C.; Morin, P.; Dreux, M. *J. High Resol. Chromatogr.* **1996,** *19*, 5-16.

(6) Nielen, M. W. F. *J. Chromatogr.* **1991,** *542*, 173-183.

(7) Zhang, Y. K.; Chen, N.; Wang, L. *J. Liq. Chromatogr.* **1993,** *16*, 3689-3697.

(8) *CRC Handbook of Chemistry and Physics*, 76th ed.; CRC Press: New York, 1995-1996.

(9) Akhadov, Y. Y. *Dielectric Properties of Binary Solutions. A Data Handbook*; Pergamon Press: New York, 1980.

(10) Daniel, V. V. *Dielectric Relaxation*; Academic Press: New York, 1967.

(11) Harris, D. C. *Quantitative Chemical Analysis*, 4th ed.; W, H. Freeman and Company: New York, 1995.

(12) Albert, A.; Serjeant, E. P. *Ionization Constants of Acids and Bases*; John Wiley & Sons Inc.: New York, 1962.

(13) Perrin, D. D. *Ionisation Constants of Inorganic Acids and Bases in Aqueous Solution*, 2nd ed.; Pergamon Press: New York, 1982.

(14) Martell, A. E.; Smith, R. M. *Critical Stability Constants*; Plenum Press: New York, 1977, Vol. 3.

(15) Kortüm, G.; Vogel, W.; Andrussow, K. *Dissociation Constants of Organic Acids in Aqueous Solution*; Butterworths: London, 1961.

(16) Williams, B. A.; Vigh, G. *Anal. Chem.* **1996,** *68*, 1174-1180.

(17) Kenausis, L. C.; Evers, E. C.; Kraus, C. A. *Proc. Nat. Acad. Sci.* **1963,** *49*, 141-146.

(18) Kay, R. L.; Evans, D. F. *J. Phys. Chem.* **1966,** *70*, 2325-2335.

(19) Ibuki, K.; Nakahara, M. *J. Phys. Chem.* **1987,** *91*, 4411-4414.

(20) Bhat, J. I.; Bindu, P. *J. Indian Chem. Soc.* **1995,** *72*, 783-789.

(21) Islam, N.; Kochi, I.; Ali, A. *Indian J. Chem.* **1980,** *19A*, 254-256.

(22) Takisawa, N.; Osugi, J.; Nakahara, M. *J. Phys. Chem.* **1981,** *85*, 3582-3585.

(23) Nakahara, M.; Ibuki, K. *J. Chem. Phys.* **1986,** *85*, 4654-4659.

(24) Takisawa, N.; Osugi, J.; Nakahara, M. *J. Chem. Phys.* **1982,** *77*, 4717-4722.

(25) Frank, H. S.; Wen, W.-Y. *Disc. Faraday Soc.* **1957,** *24*, 133-140.

(26) Stuart, S. J.; Berne, B. J. *J. Phys. Chem. A* **1999,** *103*, 10300-10307.

(27) Ibuki, K.; Nakahara, M. *J. Chem. Phys.* **1988,** *89*, 5015-5019.

CHAPTER EIGHT. Conclusions and Future Work

8.1 Conclusions

This thesis has demonstrated both applications and fundamentals of capillary electrophoresis (CE). In Chapter 2, micellar electrokinetic chromatography (MEKC) was applied to the sensitive and selective determination of derivatized polyamines. The focus of my research then shifted to fundamental mobility studies. A theoretical charge-induced friction mobility model introduced in Chapter 3 was investigated as a mechanism for solvent- and temperature-induced selectivity changes in Chapters 4-7.

Putrescine, spermidine, spermine and cadaveraine are biologically-important polyamines present in the human body. However, they do not exhibit any structural features that enable their direct detection in a sensitive manner. In Chapter 2, derivatization of the polyamines with 1-pyrenebutanoic acid succinimidyl ester (PSE) enabled their sensitive and selective detection by laser-induced fluorescence. Separation of the labeled polyamines was achieved using MEKC with cholate as surfactant and acetonitrile as organic modifier. Detection limits for PSE-labeled putrescine, cadaverine, spermidine and spermine were 2, 2, 4 and 5 nM, respectively, which are comparable or superior to those previously reported in the literature using fluorescence detection. To my knowledge, this is the first use of PSE with a capillary electrophoretic technique.

The Hückel equation, which is the most commonly used mobility model in CE, fails at predicting the mobilities of small inorganic anions (Figure 3.1) and cannot explain solvent- or temperature-induced selectivity changes. A main limitation of this model is that it only considers hydrodynamic friction and neglects charge-induced friction. The Hubbard-Onsager dielectric friction mobility model (eqn 3.27), which was introduced in

Chapter 3, accounts for both hydrodynamic friction and dielectric (charge-induced) friction. This model was investigated in Chapters 4-7 as a mechanism for both solvent- and temperature-induced selectivity changes.

The Hubbard-Onsager dielectric friction model successfully predicted the mobility behavior of organic anions and cations in methanol-water media (Chapter 4), as well as that of organic anions in acetonitrile-water, ethanol-water and 2-propanol-water media (Chapter 5). As predicted by this model, dielectric friction increased with increasing analyte charge and with increasing organic modifier content. Further, the changes in ion mobility correlated with the corresponding changes in solvent viscosity (η), dielectric constant (ε) and dielectric relaxation time (τ). To my knowledge, this is the first report relating ion mobility in CE to solvent τ. The resulting selectivity changes observed for ions in aqueous-organic media consisting of methanol, acetonitrile, ethanol and 2-propanol could thus be attributed to dielectric friction. The mechanism of dielectric friction can account for some of the anomalous mobility behavior observed in the literature, such as the migration order reversal between SO_4^{2-} and NO_3^- upon addition of methanol to the electrophoretic media [1].

The Hubbard-Onsager dielectric friction theory does suffer some limitations due to its continuum nature. It was shown in Chapter 4 that a +3 cation experienced more dielectric friction than –3 anions of similar size. However, the Hubbard-Onsager equation predicts that ions with similar charge-to-size ratios will experience similar amounts of dielectric friction, regardless of the sign of the ion charge. This results from the continuum nature of the model, whereby differences between anion-solvent and cation-solvent interactions are not considered. Further, in Chapter 5, the Hubbard-

Onsager model was successful at predicting the relative mobility trends upon changing alcohol type. In contrast, the relative trends observed between acetonitrile-water and alcohol-water media were not consistent with the model. Indeed, the –2 and –3 ions experienced proportionally more dielectric friction in acetonitrile-water media than in alcohol-water media, which is contrary to the trend predicted by the solvent parameters. This may also be explained by the continuum nature of the model, whereby the different ion-solvent interactions characteristic to each solvent class are not taken into account. Nonetheless, for a given solvent type, the dielectric friction theory of Hubbard and Onsager remains a useful tool in predicting solvent-dependent selectivity changes.

For the nonaqueous methanol-acetonitrile solvent systems investigated in Chapter 6, the overall selectivity changes were not consistent with dielectric friction. Moreover, the changes in mobility observed between 100% methanol and 100% acetonitrile were much less than predicted by the Hubbard-Onsager model and the corresponding solvent parameters. The amount of dielectric friction experienced in acetonitrile was apparently underestimated by its τ and ε values, which is consistent with the results obtained in Chapter 5 for acetonitrile-water media. This was attributed to the different ion-solvent interactions occurring in acetonitrile compared to the alcohols.

In aqueous media and in aqueous-organic media consisting of methanol, acetonitrile, ethanol and 2-propanol, the ionic strength effects increased with increasing analyte charge (Chapters 4 and 5). This is consistent with the Pitts equation. As such, selectivity could be altered by changing the ionic strength. Further, upon varying the content and type of the organic modifier, the ionic strength effect varied as a function of solvent $1/\eta\varepsilon^{1/2}$. In contrast, the charge dependence of the Pitts equation was generally not obeyed by the cations in methanol-acetonitrile media (Chapter 6). This may have resulted from ion association. Ion-pairing effects could also explain the reversal in migration order between primary, secondary, tertiary and quaternary amines on going from methanol to acetonitrile. These ion association effects are discussed in greater detail in the Future Work Section.

Varying the temperature did not significantly alter the selectivity between organic anions (Chapter 7). Indeed, the predominant influence of temperature was on the solution viscosity. Therefore, neither ionic strength effects nor dielectric friction could be shown to account for temperature-induced selectivity changes in CE.

Overall, the dielectric friction model of Hubbard and Onsager is quite successful at explaining solvent-induced selectivity changes in CE. As CE matures, a more fundamental understanding of the factors affecting analyte migration is essential. Indeed, before the full potential of the technique can be exploited, insight must be gained into what variables affect mobility, and how they interrelate with one another to govern the overall ion mobility. DryLab™ is a marvelous software package that allows the prediction of chromatograms in HPLC. My studies on the influence of dielectric friction on mobility bring us one step closer to having equivalent software for CE.

8.2 Future Work

8.2.1 Measurement of Conductivity Spectra

According to the Hubbard-Onsager dielectric friction model (eqn 3.27), which has been discussed in detail in Chapters 3-7, different ions will respond differently to changes in solvent composition. The degree to which their mobility/conductivity changes will depend largely on their charge-to-size ratios. This leads to the possibility of using the characteristic conductivity spectrum of an ion (measured as a function of solvent composition) for species identification and quantification.

The proposed future project involves the measurement of conductivity spectra for common inorganic anions (eg., Cl^-, Br^-, NO_3^-, SO_4^{2-}). These ions have high charge densities and will thus experience significant changes in mobility/conductivity in the presence of organic solvents (eqn 3.27). A simple approach for obtaining conductivity spectra is to use flow injection analysis. The sample is mixed on-line with a solvent whose organic content (eg., methanol) is gradually varied, and is then continuously detected in a conductivity cell as a function of solvent composition. If several ions are present in the sample, the overall conductivity profile is deconvoluted to give the characteristic conductivity spectrum (signature) of each ion. Chemometrics methods can be used for this deconvolution, provided that no unknown compounds are in the sample. From the resulting ion signatures, the sample species may be identified and quantified. This is ideal for quality control, since a time-consuming separation step is not required.

8.2.2 Determination of Peptide Charge by Ionic Strength Effects

Charge ladders are used in CE to estimate the effective charges of proteins and peptides in solution [2, 3]. A protein charge ladder is a series of protein derivatives that have similar viscous drag but that differ by integral units of charge. It is generated by sequentially acetylating the protein's lysine residues. The charge of the native protein ($Z_{x=0}$) can be determined from:

$$\Delta Z_x = Z_{x=0}(\mu_x / \mu_{x=0} - 1) \qquad (8.1)$$

where ΔZ_x is the charge difference between the native protein and the protein with x derivatives, and $\mu_{x=0}$ and μ_x are the mobilities of the proteins with 0 or x derivatives, respectively. The native protein charge can be determined from the slope of a plot of ΔZ_x versus $(\mu_x/\mu_{x=0}-1)$. One of the assumptions in using eqn 8.1 is that ΔZ_x is exactly equal to the number of charge units modified by the derivatization [3]. However, charge regulation results in the first element of the charge ladder being slightly less than one electronic charge from the unmodified protein [3].

Since ionic strength effects depend on ion charge (eqn 3.39), it may be possible to use the magnitude of these effects to predict peptide charge. To investigate this, the Onsager slopes can be determined for a series of peptides of similar size but with varying charge. The peptide charge can be altered by varying the number of amino acids containing ionizable groups in their side chains, such as lysine or aspartic acid [4]. Using these peptides, a plot of Onsager slope versus peptide charge can be constructed. This plot can then be used to estimate the charge of an unknown peptide once its Onsager slope is experimentally determined. If time is an issue, the Onsager slopes can be determined from a minimum of two ionic strengths.

Some factors will have to be considered before this technique can be used to predict peptide charge. The first issue to consider is whether the model will be effective if the unknown peptide has a different size than the peptides used in the model set. If size effects are significant, then different correlation plots will have to be constructed for each peptide size. This would be very tedious and time consuming. Another issue to consider is that ion association between the peptides and buffer counterions will influence the ionic strength effects. The buffer electrolyte must therefore be selected with care to avoid ion-pairing.

8.2.3 Ion-Ion and Ion-Solvent Interactions

Ion mobility is influenced by four main processes: ion-solvent interactions, ion-dipole interactions (dielectric friction), ion-ion interactions (ion association or ion-pairing), and electrostatic interactions with the counterions (ionic strengths effects) [5]. In Chapter 6, the migration order of primary, secondary, tertiary and quaternary ammonium ions was reversed upon changing the nonaqueous media from methanol to acetonitrile (Figure 6.2). Specifically, different ionic strength effects were observed for these singly-charged cations in media consisting of 0-75% ACN in MeOH. This was attributed to different degrees of ion-solvent and ion-ion interactions in each solvent. Further studies to investigate these effects are proposed here.

Ion association between the analyte and the buffer counterions will have a significant influence on mobility and selectivity, especially in nonaqueous solvents with low dielectric constants. For a 1:1 ion association between a cation C^{n+} and an anion A^-, the apparent mobility of the cation ($\mu'_{C^{n+}}$) is [6,7]:

$$\mu'_{C^{n+}} = \frac{1}{1+\left[A^-\right]K_A}\mu_{C^{n+}} + \frac{\left[A^-\right]K_A}{1+\left[A^-\right]K_A}\mu_{CA^{n-1}} \tag{8.2}$$

where $\mu_{C^{n+}}$ is the effective mobility of the unassociated cation, $\mu_{CA^{n-1}}$ is the mobility of the ion-pair, and K_A is the ion association constant. For a neutral ion-pair, the right-hand term in eqn 8.2 is zero. Ion association therefore results in a reduction of the apparent mobility of the ion of interest.

Ion-pairing effects are not accounted for in the ionic strength theory developed by Pitts (eqn 3.37). The conductance theory of Fuoss and coworkers, modified to include ion association, can account for such effects [8, 9]:

$$\mu_i = \mu_{i,o} - S\sqrt{\alpha_{IP}c} + E(\alpha_{IP}c)\ln(\alpha_{IP}c) + J_1(\alpha_{IP}c) - J_2(\alpha_{IP}c)^{3/2} - K_A\mu_i y_{\pm}^2(\alpha_{IP}c) \qquad (8.3)$$

where c is the initial total ion concentration, α_{IP} is the degree of dissociation of the ion-pair, K_A is the ion association constant, $y_{\pm}$ is the mean activity coefficient, and S, E, J_1, and J_2 are parameters that depend on the effects of the ionic atmosphere on mobility. Unfortunately, literature K_A values are scarce for many salts (including ammonium perchlorates) in methanol, acetonitrile and their mixtures. Therefore, the following studies proposed for investigating the ion-association and solvation effects in Figure 6.2 will adopt a systematic rather than a theoretical approach.

As discussed in Chapter 6, the different ionic strength effects observed for the 1°, 2°, 3° and 4° amines in 100% methanol were attributed to a combination of both ion-ion and ion-solvent interactions. It was suggested that the combined effects of poor solvation of ClO_4^- by methanol and lack of H-bonding between the 4° ammonium ion and methanol led to a higher degree of ion association between these two ions (Figure 6.2). In contrast, the well-solvated perchlorate ion in 100% ACN did not appreciably ion-pair with the ammonium ions. These conclusions can be investigated by systematically varying the buffer electrolyte counterion. In a protic solvent such as methanol, hydrogen-bonding is strongest for the smallest anions and those with localized charge such as acetate and chloride [10]. Therefore, contrary to ClO_4^-, acetate and chloride ions are favorably solvated in methanol. If counterion solvation limits the degree of ion association, then replacing the perchloric acid background electrolyte in 100% MeOH by either acetic acid or hydrochloric acid should result in a less dramatic variation in ionic strength effects between the different +1 ammonium ions. Indeed, Porras et al. [8] have recently studied the influence of cationic counterions on the electrophoretic mobilities of benzoates in methanol. They reported that ion-pairing effects followed the counterion sequence $Li^+ < Na^+ < K^+ < Rb^+$. The greater solvation of Li^+ compared to the other cations may explain its lesser degree of ion association.

A second approach to these investigations is to systematically vary the hydrogen bonding properties of the analytes. As discussed above, the increased ion association between perchlorate and the 4° ammonium ion in 100% MeOH was attributed in part to the absence of hydrogen bonding between the ammonium ion and methanol. This can be verified by studying a series of benzylamine derivatives whose hydrogen bonding character is gradually changed through addition of various substituents (eg., –OH, $-NO_2$, etc…). As the analyte H-bonding character is increased, ion-pairing effects between ClO_4^- and the analyte in 100% MeOH should decrease.

An interesting possibility for further studies is to investigate whether ion-ion and ion-solvent interactions can be modeled according to solvatochromic parameters. The π^*, α and β scales developed by Kamlet, Taft and coworkers [11-13] can be used to evaluate the solvent or solute dipolarity/polarizability, hydrogen bond donor acidity, and hydrogen bond acceptor basicity, respectively. These parameters are available in the literature for a wide variety of solvents [14], and have been successfully used to study retention in HPLC [15-17]. Further, Barrón et al. [18] have demonstrated that the pK_a values of quinolones in tetrahydrofuran-water media, as determined by CE, are correlated to the solvent polarity/polarizability π^*. It would be interesting to determine whether ion-solvent and ion-ion interactions can be described by these parameters. Instead of using methanol-acetonitrile solvent systems, acetonitrile-water media should be used in the initial studies since solvatochromic parameters are readily available for these solvent mixtures [17].

8.3 References

(1) Yang, Y.; Liu, F.; Kang, J.; Ou, Q. *J. Chromatogr. A* **1999,** *834*, 393-399.

(2) Gao, J.; Whitesides, G. M. *Anal. Chem.* **1997,** *69*, 575-580.

(3) Menon, M. K.; Zydney, A. L. *Anal. Chem.* **2000,** *72*, 5714-5717.

(4) Harris, D. C. *Quantitative Chemical Analysis*, 4th ed.; W, H. Freeman and Company: New York, 1995.

(5) Porras, S. P.; Riekkola, M.-L.; Kenndler, E. *J. Chromatogr. A* **2001,** *924*, 31-42.

(6) Takayanagi, T.; Wada, E.; Motomizu, S. *Analyst* **1997,** *122*, 57-62.

(7) Takayanagi, T.; Wada, E.; Motomizu, S. *Analyst* **1997,** *122*, 1387-1391.

(8) Porras, S. P.; Riekkola, M.-L.; Kenndler, E. *Electrophoresis* **2002,** *23*, 367-374.

(9) Fernández-Prini, R.; Spiro, M. In *Physical Chemistry of Organic Solvent Systems*; Covington, A. K., Dickinson, T., Eds.; Plenum Press: New York, 1973, pp 525-680.

(10) Salimi-Moosavi, H.; Cassidy, R. M. *J. Chromatogr. A* **1996,** *749*, 279-286.

(11) Kamlet, M. J.; Taft, R. W. *J. Am. Chem. Soc.* **1976,** *98*, 377-383.

(12) Kamlet, M. J.; Taft, R. W. *J. Am. Chem. Soc.* **1976,** *98*, 2886-2894.

(13) Kamlet, M. J.; Abboud, J. L.; Taft, R. W. *J. Am. Chem. Soc.* **1977,** *99*, 6027-6038.

(14) Kamlet, M. J.; Abboud, J.-L. M.; Abraham, M. H.; Taft, R. W. *J. Org. Chem.* **1983,** *48*, 2877-2887.

(15) Sadek, P. C.; Carr, P. W.; Doherty, R. M.; Kamlet, M. J.; Taft, R. W.; Abraham, M. H. *Anal. Chem.* **1985,** *57*, 2971-2978.

(16) Carr, P. W.; Doherty, R. M.; Kamlet, M. J.; Taft, R. W.; Melander, W.; Horvath, C. *Anal. Chem.* **1986,** *58*, 2674-2680.

(17) Barbosa, J.; Sanz-Nebot, V.; Toro, I. *J. Chromatogr. A* **1996,** *725*, 249-260.

(18) Barrón, D.; Jiménez-Lozano, E.; Barbosa, J. *Chromatographia* **2000,** *52*, 395-402.